Doctoral theses at NTNU, 2018:386

Konstantin Pandakov

Improvements in protection of medium voltage resonant grounded networks with distributed sources

Doctoral thesis

Konstantin Pandakov

ISBN 978-82-326-3560-3 (printed ver.)
ISBN 978-82-326-3561-0 (electronic ver.)
ISSN 1503-8181

NTNU
Norwegian University of
Science and Technology

NTNU
Norwegian University of Science and Technology
Thesis for the Degree of
Philosophiae Doctor
Faculty of Information Technology and Electrical
Engineering
Department of Electric Power Engineering

Doctoral theses at NTNU, 2018:386

NTNU
Norwegian University of
Science and Technology

Konstantin Pandakov

Improvements in protection of medium voltage resonant grounded networks with distributed sources

Thesis for the Degree of Philosophiae Doctor

Trondheim, December 2018

Norwegian University of Science and Technology
Faculty of Information Technology and Electrical Engineering
Department of Electric Power Engineering

NTNU
Norwegian University of
Science and Technology

NTNU
Norwegian University of Science and Technology

Thesis for the Degree of Philosophiae Doctor

Faculty of Information Technology and Electrical Engineering
Department of Electric Power Engineering

ISBN 978-82-326-3560-3 (printed ver.)
ISBN 978-82-326-3561-0 (electronic ver.)
ISSN 1503-8181

Doctoral theses at NTNU, 2018:386

Printed by NTNU Grafisk senter

Acknowledgments

I would like to express my gratitude to my supervisor, Professor Hans Kristian Høidalen, for his guidance and support during the work on my PhD-project. I would also like to thank my co-supervisor, Doctor Jorun Irene Marvik, because her study served as a starting point for my research work, and my mentor, Professor Bruce A. Mork, for knowledge and assistance in the initial stages.

I consider myself very fortunate to be part of the ProSmart project at NTNU because it involves numerous people from different industries and provided excellent collaboration with them. The sharing of experience allowed me to improve the quality of my research work and I would like to thank all of them for their valuable help and discussions.

I also wish to express my gratitude to the Finnish department of ABB in Vaasa, namely Petri Hovila and Ari Wahlroos, for their experience and useful comments regarding my research work, as well as for granting equipment for the development of our laboratory. Associate Professor Murari Mohan Saha deserves a special acknowledgment for establishing this collaboration.

My special thanks go to my friends, colleagues and staff at the Department of Electric Power Engineering at NTNU where I spent three fruitful years.

Finally, I wish to thank my family for their continuous love and support.

Abstract

The increasing penetration of distributed generation into medium voltage networks creates challenges for traditional protective schemes developed for conventional radial systems with unidirectional power flows. Moreover, the internal protection of embedded generators must guarantee necessary decoupling in case of abnormal events in the network or prevent from unnecessary disconnection. This becomes especially important during earth faults in resonant grounded networks because the reliable identification of damaged feeders or sections is a challenge. Dependability enhancement of feeder and ground protection to overcome adverse effects from distributed generation, and the improvement of generator protection are important tasks in ensuring reliable and secure network operation.

The current PhD research work focuses on developing new protective schemes and algorithms for application in distribution networks with embedded dispersed generation in order to resolve these issues. Since the Smart Grid concept is inseparable from the involvement of communication networks in future power system operation and protection, the thesis actively utilises this benefit.

The research method includes: electromagnetic transient program simulations of various faulty scenarios in a medium voltage network; processing of acquired data, analysis and development of protective algorithms; laboratory verifications utilising real-time simulations with hardware in the loop (commercially available relays and self-developed prototypes).

Firstly, the work employs impedance protection against phase-to-phase faults as an alternative to the standard overcurrent relays and proposes a new communication-assisted method for its dependability improvement as impedance measurements are affected by remote infeed currents from local generations and non-zero fault resistances. The method compensates for

both these negative impacts by using multi-point synchrophasor measurements. Impedance measurements with error compensations can be further utilised for fault location.

Secondly, the research work develops new algorithms for the identification of the faulty feeder (or section on the feeder) during earth faults in resonant grounded networks. Two methods are proposed: the utilisation of two-end measurements and one-end measurements. The two-end method is universal since it works independently of network configuration and is suitable for any earth fault type. It also provides possibilities for exact faulty point location, suitable for persistent and permanent earth faults. The one-end method is based on system transients and is especially useful for intermittent faults in mixed networks with cable sections.

The results of impedance protection laboratory tests demonstrate improved relay dependability with application of the compensation method. Accuracy of fault location estimation based on reactance is also investigated and it is acceptable for fault discrimination. Imperfections in communication channels (jitters and data losses) have negative influence on the method; however, it is still better than relay performance without the compensation.

Tests of the two-end method for earth fault location are conducted offline on simulated fault records and show good dependability and security for various fault and network parameters. Laboratory verification of the one-end method is done on a prototype with simulated and real fault records, and shows improved dependability compared to the standard steady-state approach. Both methods are capable of handling adverse effects arising from the large capacitive imbalance of phases, cable penetration, high fault impedances and insufficient natural watt-metric contribution (the parallel resistor can be excluded). Protective schemes for fast anti-islanding protection of embedded generators or prevention of their unintentional decoupling based on these methods are designed with communication links.

The application of the developed method allows increased reliability of power supply in future distribution networks with large penetration of renewable sources, and improves their security.

Contents

List of Tables

List of Figures

List of Symbols

AVR	Automatic Voltage Regulator
CCVT	Capacitive Coupled Voltage Transformer
CIREPP	Converter-Interfaced Renewable Energy Power Plants
CNN	Convolutional Neural Network
CT	Current Transformer
CTI	Coordination Time Interval
CWT	Continuous Wavelet Transform
DFT	Discrete Fourier Transform
DG	Distributed Generation
ELA	Equivalent Line Approach
EMTP	Electromagnetic Transients Program
ENA	Equivalent Network Approach
FRT	Fault Ride Through
GF	Ground Fault
GOOSE	Generic Object Oriented Substation Events
HIF	High Impedance Fault
HIL	Hardware In The Loop
HL	High Load
IIDG	Inverter-Interfaced DG
LF	Low-Pass Filter
LL	Low Load

LOF	Low-Ohmic Fault
MU	Merging Unit
MV	Medium Voltage
OC	Overcurrent
PMU	Phasor Measurement Unit
RT	Real Time
SV	Sample Values
TCP/IP	Transmission Control Protocol/Internet Protocol
TVC	Transient Variation Component
UDP	User Datagram Protocol
USART	Universal Asynchronous Receiver Transmitter
VT	Voltage Transformer

Chapter 1

Introduction

Distributed generation (DG) technology has become more widespread in medium voltage (MV) networks, increasing the diversification and reliability of power supply, and allowing efficient utilisation of local resources. At present, DG in Norway is mainly small hydro stations with synchronous or induction generators. Normally, the penetration level of DG into distribution networks is not large (about 10% of the total power of the main distribution transformer); therefore, generators are embedded without significant precautions. The main type of feeder protection against short circuit faults in MV distribution networks is typically non-directional overcurrent relays with constant-time characteristics [1]. Selectivity is achieved through the application of coordination time intervals (CTI), delaying tripping.

Nevertheless, with the increase of DG rating and penetration level, impact on protection rises due to the appearance of significant bi-directional power flows in the system, as is summarised in [2]. DG proliferation creates challenges for traditional protective schemes and aspects such as blinding [3], sympathetic tripping [4], islanding detection [5], and re-closing procedure violation [6] are very important to consider. Unnecessary disconnection of DG or nuisance tripping is not desirable because DG should help support and restore power supply instead of decoupling.

Many studies are dedicated to enhancements of overcurrent protection dependability in the presence of DG. Usually methods are focused on adaptive overcurrent protection [7] and very often involve communication networks for better performance [8]. Alternatively, the application of directional overcurrent relays [9], new methods based on local current measurements [10] or fault current limiters [11] are also introduced in the literature. Alternative reliable solutions are schemes based on differential protection [12].

However, current-based fault detection schemes do not always have fault location capabilities, which are an important aspect in improving the overall reliability of power supply. Hence, methods based on impedance measurements, for instance [13], become more attractive since they can provide information about fault location [14]. Distance or impedance relaying is mainly utilised in transmission systems. Nevertheless, it additionally has two inherent advantages that can be useful in distribution networks with DG: independence of fault current level and directionality. Moreover, settings require information about network configuration and do not depend on current. This is useful for self-healing systems with variable topology or microgrids [15]. The main disadvantage of this type of protection is its susceptibility to negative effects of load currents, large fault impedances and remote infeed currents usually caused by DG.

The importance of fault location arises especially during earth faults in distribution networks with DG. The main challenges are discussed, for instance, in [16] in case of loss-of-main situations; including sustained overvoltages (touch voltage), cross-country faults, increased fault currents, difficulties for reclosing operations; requiring the development of fast anti-islanding protection. In the opposite case, if the damaged feeder has a complex topology and fault can be isolated by local breakers, DG disconnection is not desired. Thus, rapid earth fault location is of interest.

In Norway, a common grounding type for distribution networks involves suppressing coils where the main advantage is small fault current [17]. However, it introduces challenges for correct tripping of a faulty feeder or a damaged section on the feeder (ground fault protection selectivity). The standard methods are based on steady-state zero sequence voltage (used for detection of an abnormal event) and current (provides location information). The connection of a parallel resistor [18] at the neutral point of the main distribution transformer in parallel to the suppressing coil is often required to improve selectivity. This approach is not always adequate or reliable for earth fault location, let alone protection speed. Therefore, earth fault location procedures on the faulty feeder are performed manually by consecutively opening breakers, affecting numerous customers. On feeders with DG, such procedures are accomplished with disconnected generators to avoid fault current being maintained by them, whereas decoupling reduces the cost effectiveness of DG utilisation.

The above-mentioned challenges show the motivations behind this PhD thesis, which aims to develop new protection methods and schemes for application in distribution networks with DG.

1.1 Objectives and scope of the work

The current PhD thesis has two main research directions, determined by two types of faults: short circuit faults (phase-to-phase) and earth faults (phase-to-the-ground). The MV (22 kV) distribution network is considered for analysis with resonance grounding (through the suppressing or Petersen coil). For both fault types, aspects of DG presence in the distribution network are considered.

The first objective focuses on the application of impedance relaying against phase-to-phase faults and for assistance to DG internal protection to minimise unnecessary disconnections. Special attention is paid to the malfunctioning of distance relays due to high impedance faults and remote infeed currents caused by DG. Elimination of these adverse effects tends to increase the reliability of this protection type for application in distribution networks with large penetration of DG in case of arcing and possible high impedance faults. Location of short circuit faults is not a primary goal of the research work. However, it is analysed because it is an obvious way to quantify distance protection accuracy.

Impedance measurements are not applicable for earth fault protection in resonant (high impedance) grounding systems due to the significant adverse impact of load currents. At the same time, application of the standard methods can also be problematic. This is especially so in future systems where underground cable share will increase, complicating earth fault location [19]. Moreover, short protection operation time becomes an important target in the presence of DG for the realisation of fast anti-islanding schemes or to avoid unnecessary disconnections.

Thus, the second objective is earth fault location in mixed (both cables and overhead lines) resonant grounded systems with DG. Firstly, to provide fast decoupling of DG for the initiation of a reclosing procedure (if the fault is not self-extinguishing), avoiding a complex logic with synchronisation checks and, vice versa, to avert unnecessary DG decoupling if a faulty section can be isolated. Secondly, to improve quality of power supply, minimising the number of affected customers. The detection of high impedance earth faults is beyond the scope of the current thesis.

The proposed new protection schemes and methods are based on the availability of communication technologies assumed to be part of the future Smart Grid.

1.2 Structure of the thesis

This PhD thesis is organised into two parts. The first part contains an introduction to the research work, a literature overview, research methods,

summary and discussions of the scientific contributions. The second part consists of 6 papers presenting the major and minor contributions, simulations and experimental results, an analysis and discussions.

The thesis is divided into 6 chapters, and short descriptions are given below.

Chapter 2 contains a literature review related to two main areas of the thesis: impedance relaying in distribution networks with DG and earth fault location in compensated systems. This chapter provides insight into previous works, developed methods, algorithms, protective schemes and establishes a niche for the given work.

Chapter 3 presents descriptions of the research methods, tools and models used extensively in this thesis. They mainly include PSCAD/EMTDC simulations, data processing and programming in MATLAB, and real-time hardware-in-the-loop simulations for laboratory verifications with the help of OPAL-RT and commercially available or self-developed intelligent electrical devices.

Chapter 4 discusses and supplements the work presented in the published papers, as well as providing additional explanatory analyses and examinations not presented in the papers.

Chapter 5 concludes the PhD thesis and proposes directions for future research.

The papers reporting the main core of the present work are enclosed at the end of this PhD thesis in Appendix B. A complete list of the scientific contributions of each is given below.

1.3 Scientific contributions

The scientific contributions are divided into two categories according to the presented scope. The main contributions are found in [Papers II,V,VI] and are highlighted by font which is italicised and emboldened. The papers' contributions are listed as follows:

- Impedance relaying in distribution networks with DG:
  - [Paper I], in general, studies the feasibility of impedance relaying with the standard settings (based on line impedances without a power swing blocking logic) in an actual distribution network with DG of two types (a synchronous and an induction generator) under different conditions: commutation operations, production and load variation. Moreover, it proposes utilising Zone 3 to

improve the fault-ride-through capability of the generators. Finally, it reveals the main issues associated with impedance measurements: underreaching due to remote currents and non-zero fault impedances, overreaching during ground faults, and miscoordination with downstream devices in the lateral branches. The disclosed underreaching problems served as a motivation for the development of a solution, which is presented in the next paper.

- [Paper II] presents ***a new compensation method consisting of two approaches*** aiming to eliminate underreaching errors during impedance measurements caused by remote currents and/or large fault resistances (contact with extraneous objects that might occur in medium voltage networks).

  The first is referred to as an equivalent line approach and is dedicated to compensating for fault resistance in a passive network. The second is referred to as an equivalent network approach and improves impedance measurement precision in an active network. The method requires a minimum of two points to be measured (at a substation and DG). The current paper considers synchronised phasor measurements as the main information for exchange between protective devices.

- [Paper III] presents thorough laboratory validation of the developed method in [Paper II] using a co-simulation test platform. It includes a real-time hardware-in-the-loop test setup and a communication network emulator to simulate the realistic behaviour of links. The test method is based on the Monte Carlo approach with a large number of simulated fault incidents using a realistic model: variable load profile with phase imbalance in different phases and phase-to-phase faults at arbitrary locations, as well as the presence of different distortions in the communication network. Finally, the paper examines the impact of the method on fault location accuracy.

- Earth fault location in compensated networks:

  - [Paper IV] presents a malfunctioning analysis of earth fault location algorithms available in the literature or implemented in real products. The paper suggests a theory for analysis of earth fault characteristics in frequency (steady-state signals) and time domain (low-frequency transients). It demonstrates the importance of considering mixed networks (overhead lines and cables) with

insufficient natural watt-metric contribution (line-to-the-ground conductance) and inclusion of electrostatic imbalance between phases (that take place in reality) to reveal negative influence on the steady-state and transient methods. Several methods have been selected for analysis, which constitute a basis for the development of various algorithms presented in section 2.2 of this thesis. The inadequacy of the presented methods in a few scenarios served as a motivation for the development of new approaches.

– [Paper V] presents ***a new indicator for faulty feeder or section selection*** during earth faults in compensated systems and is based on two-end measurements. The indicator is used for rapid earth fault location to avoid islanding or unnecessary tripping of DG.

  Furthermore, the paper proposes ***a new method for exact earth fault location*** in compensated systems based on the same measurements as the indicator above. Ways to enhance locator precision are also given.

– [Paper VI] presents ***a new transient-based algorithm for faulty feeder or section selection*** during earth faults in compensated systems. This algorithm only utilises one-end measurements. The paper proposes using it as an additional criterion in modern devices to improve selectivity. The paper also demonstrates hardware-in-the-loop tests of the prototype developed on a microprocessor board. Moreover, the paper develops a theoretical method (different from that used in [Paper IV]) that can be used in sensitivity assessments of the developed transient algorithm in real applications.

1.4 List of publications

[Paper I] K. Pandakov, H. Kr. Høidalen, J. I. Marvik. (2016) Implementation of distance relaying in distribution network with distributed generation, *13th International Conference on Development in Power System Protection (DPSP 2016)*, p. 1-7.

[Paper II] K. Pandakov, H. Kr. Høidalen. (2017) Distance protection with fault impedance compensation for distribution network with DG, *IEEE PES Innovative Smart Grid Technologies Conference Europe (ISGT-Europe 2017)*, p. 1-6.

[Paper III] K. Pandakov, C. M. Adrah, H. Kr. Høidalen, Ø. Kure. Experimental validation of a new impedance based protection for networks

with distributed generation using co-simulation test platform, *Journal to be decided*.

[Paper IV] K. Pandakov , H. Kr. Høidalen, J. I. Marvik. (2017) Misoperation analysis of steady-state and transient methods on earth fault locating in compensated distribution networks, *Sustainable Energy, Grids and Networks*. Available at: https://doi.org/10.1016/j.segan.2017.12.001 (accessed: 15 December 2017).

[Paper V] K. Pandakov, H. Kr. Høidalen, J. I. Marvik. (2017) Fast protection against islanding and unwanted tripping of distributed generation caused by ground faults, *CIRED - Open Access Proceedings Journal*, 2017(1), pp. 1126 - 1130.

[Paper VI] K. Pandakov, H. Kr. Høidalen, S. Trætteberg. (2018) An additional criterion for faulty feeder selection during ground faults in compensated distribution networks, *IEEE Transactions on Power Delivery*, 33(6), pp. 2930 - 2937.

The following papers accomplished during PhD work and presented at international conferences are not included in the thesis because either they extended to a journal publication or are out of the scope:

[Paper VII] K. Pandakov, C. M. Adrah, Z. Liu, H. Kr. Høidalen, Ø. Kure. (2018) Hardware-in-the-loop testing of impedance protection with compensation of fault impedance and DG infeed current, *The Journal of Engineering*. Available at: http://digital-library.theiet.org/content/journals/10.1049/joe.2018.0189 (accessed: 19 July 2018).

[Paper VIII] K. Pandakov, E. Tedeschi, H. Kr. Høidalen. (2017) Analysis of D-STATCOM Impact on Protection of Distribution Network, *International Conference on Power Systems Transients (IPST 2017)*, p. 1 - 6.

Chapter 2

Literature review

The current chapter encompasses two research directions: different studies previously conducted on impedance-based protection for distribution networks with DG and various earth fault locating algorithms and methods developed for resonant grounding systems with or without DG. The presented overview provides thorough insights into state-of-the-art methods and algorithms of these research directions and indicates the motivations behind the present study.

2.1 Impedance relaying in distribution networks with DG

The application of impedance measurements in distribution networks with DG is studied in [20] where it is used as the main type of protection and as a monitoring tool. Paper [21] discusses the coordination of this type of protection with downstream fuses. The combination of directional overcurrent and distance protection in networks with renewable energy sources is presented in [22]. These simple studies demonstrate the effectiveness of impedance relaying in networks with uncomplicated topologies due to simpler settings and better reliability. More advanced studies involving application examples in real networks are presented in [13, 23, 24].

[13] illustrates specific challenges arising from traditional overcurrent protection schemes due to relatively high levels of DG in the distribution system. This paper presents the use of distance relays to solve such associated issues as anti-islanding protection, variable nature of DG, temporary over- voltages, and loss of sensitivity of overcurrent relays on long feeders. The paper provides real-world event report data and cost analysis in order to demonstrate distance protection effectiveness.

[23] performs protection of medium voltage system with embedded generators. The work proposes the use of distributed distance relays in non-communicating environments to enhance reliability, service quality and grid stability. The algorithm implements detection (overcurrent based) and discrimination (impedance based). The method is verified for mixed networks (overhead lines and cables) with different grounding types.

[24] describes design and evaluation of distance relaying (primary and backup functions) in a particular 11 kV system with DG. The scheme proposes utilising voltage measurements at the second side of distribution step-down load transformers to decrease cost. In the proposed method, impedance relays are located at regular intervals in a ring-operated system to improve the operating performance. Communication involvement is not considered due to its assumed unavailability.

The papers above do not thoroughly examine the adverse effect of DG on impedance measurements, but [25] does. The work illustrates how DG, its size, location and power factor together with maximum fault resistance affect the relay settings. The main fault type is single-phase-to-ground in the solidly grounded system. [26] extends the previous study with a consideration of phase-to-phase faults, illustrating the considerable impact of DG on relay characteristics. The influence of different DG type, DG number and size, transformer configuration and earthing type, load flow, capacitive coupled voltage transformer (CCVT) transients, current transformer (CT) saturation, power swings, and sub-synchronous resonance are described in [27]. Additionally, the impact of DG as a source of intermediate/remote infeed current on relay settings is discussed in [28].

Basically, the main approach proposed in the literature to overcome DG adverse effects is settings modification in accordance with the simulation and theoretical analysis as presented, for example, in [29]. Furthermore, time intervals are often required for coordination with downstream protective devices (fuses). Paper [30] also demonstrates the application of impedance protection in a microgrid operated in different modes. In this study, impedance errors caused by infeed currents are eliminated by introducing branch coefficients depending on current ratios (branch to main feeder) and topology.

The previous references rely on standard impedance measurements only and do not propose new approaches to improve the performance of distance protection in distribution networks with DG. In contrast, [31] presents the utilisation of impedance relays in the system with intermittent wind generation. The work illustrates the adverse impact of System Impedance Ratio (it affects voltage reference and directionality capability) on protection

dependability and proposes a method for improving relay performance – polarisation voltage is dynamically changed according to variations of wind power source impedance. [32] solves a similar problem, proposing adaptive distance protection: the algorithm assumes that faults in Zone 1 (it reaches DG) do not affect relay performance due to small fault resistance and limited infeed fault current from inverter-interfaced DG (IIDG); Zone 2 must have adaptive settings depending on DG output power (automatically determined without communication) to avoid underreaching. Paper [33] introduces fault current limiters to eliminate the miscoordination of the relays and to preserve constant relay settings.

Nevertheless, the application of these methods is limited by a maximum fault resistance (about 100 Ohm). Moreover, the studies presented above consider impedance relaying without the involvement of communication technologies using only one-end measurements, whereas telecommunication can significantly improve distance protection performance in presence of DG in MV networks [34].

Hence, papers [15, 35–45] present new protective schemes utilising communication links. References [15, 35] discuss the application of impedance relays in networks including converter-based DGs with limited fault current and propose adaptive settings for island and grid-connected modes. In the schemes, the relays communicate with each other in order to obtain crucial information on changes in network conditions. Similarly, [36] focuses on a meshed system with interconnected full-scale converter-interfaced renewable energy power plants (CIREPPs) and reveals impedance relay malfunction cases. [37] proposes a pilot protection scheme to handle them. A novel pilot protection scheme applicable to distribution networks with IIDG is also introduced in [38], and a noticeable difference here is that there are no requirements for synchronised communication.

Multiple-point measurements allow the development of completely new impedance-based protection approaches. Thus, [39] presents the differential method and the inverse-time low-impedance method. The first employs a communication link for fast fault isolation: for out-of-zone faults, differential impedance is zero; for in-zone faults, impedance rises rapidly. The method is also suitable for high impedance faults. The second method provides adaptive protection, combining inverse-time current characteristics with impedance measurements. The methods have been verified in islanding mode as well. The similar impedance differential method is proposed in [40], requiring two-end, non-synchronised measurements for fault detection. [41] introduces a new scheme using information about currents injected into the zone in order to compensate for impedance errors. The advantage of such

an approach is that the impedance relay does not require standard reach settings to be adjusted.

References [42–45] consider communication-assisted impedance protection in microgrids with dispersed renewable sources. Such a situation is challenging because it requires a protection scheme that is capable of operating in two modes: grid-connected and islanding (stand-alone). [42] develops a protection scheme based on positive sequence components using phasor measurements. Communication is used to switch relay settings groups. Similarly, [43] presents a strategy using phasor measurements and consists of off-line pre-calculation of setting groups; their restoration and selection are determined by current topology. The strategy also uses the permissive underreach transfer tripping scheme to clear faults on weak lines (such situations can arise due to the intermittent nature of DG). [44] introduces a new scheme utilising permissive and blocking signals between two adjacent relays to locate faults (low bandwidth communication is needed). [45] develops a new adaptive distance protection algorithm based on an improved wavelet algorithm for digital filtering (it solves issues connected with a constant frequency Fourier algorithm). The paper builds a coordination optimisation model and calculates the relay setting using an ant colony algorithm.

Application of the presented new schemes and methods might be limited by high impedance faults, which introduce significant impedance calculation errors. Moreover, DGs with inverter interfaces are mainly examined that implies limited fault currents and insignificant influence on impedance measurements. The same is valid for small scale renewable sources. Furthermore, simple network topologies resembling multi-terminal transmission grids without presence of numerous load outfeeds are typically considered. Studies of impedance protection in microgrids do not involve strong fault currents from utility networks and their impact. Therefore, proper research work on error compensations during impedance measurements caused by high fault impedances, large remote or intermediate currents and complex topology is lacking in the literature.

Nevertheless, the vast majority of studies dedicated to eliminating underreaching errors were done for transmission systems where impedance protection is the main type and references [46–57] present different methods developed for this purpose. Hence, [46–52] introduce protective schemes for a two-terminal transmission system utilising one-end measurements. They propose adaptive settings [46–48], fault impedance calculation [49, 50], calculation distance to fault [51], fault resistance calculation [52], which can compensate adverse effect of fault resistance, and remote infeed current. The methods in [53–56] utilise two-point measurements in a two-terminal

transmission system. [53] describes an adaptive distance relaying scheme: it evaluates fault resistance and uses it for compensation. [54] develops impedance-differential protection suitable for pilot schemes. The algorithm in [55] is based on third harmonic appearance due to non-linear nature of an arc and in [56] on phase coordinates taking into account unbalanced loads and line asymmetries. The method in [57] is dedicated to a three-terminal system and utilises three-point measurements. The methods require synchronised measurements from remote terminals.

Performance of the described methods, developed for transmission systems, in distribution networks can be considerably affected by the following factors: the resistive part of line impedance is comparable with the reactive; arc resistance can be higher due to smaller fault current [58]; fault resistance can be very large due to contact of power lines with a tree [59]; a line under protection can have numerous load outfeeds; heavily branched and dynamic topology.

Regarding the latter point, references [60–62] present methods developed for the transmission systems with complex topology; these methods can be adopted for distribution networks. [60] presents a new algorithm that corrects distance element impedance measurements under infeed conditions. It requires synchronised measurements that are utilised for correction. [61] proposes the modification of relay settings coordinated with infeed using a fuzzy-set-based scheme. It requires statuses of circuit breakers. [62] develops a new algorithm based on synchrophasors sent to the system protection centre for analysis (active power calculations for fault resistance determination and location) and following fault clearance.

To summarise, a lack of research dedicated to impedance error compensation in distribution networks with DG is observed. The methods used in transmission systems can be inadequate in MV networks and require thorough investigation. The introduced approaches for distribution grids, such as new settings [28,29], known corrective coefficients [30], adaptive settings [31,32], fault current limiters [33], and communication based [39–41] have their own limitations depending on network configuration, DG type and capacity, as well as fault nature. Therefore, the first main focus of the current PhD thesis is to fill the gap in this area, focusing on the communication-based approach as the most robust approach, and aiming to find effective ways of utilising multi-point measurements.

2.2 Earth fault location in compensated systems

The methods and approaches presented in literature, dedicated to faulty feeder or section selection, can be divided conditionally into two groups. The

first utilises the steady-state period of faulty signals, where reliable location cannot be guaranteed during earth faults with unstable characteristics (intermittent nature); while the second extracts information from the transient period after fault inception.

References [63–75] describe steady-state methods for faulty feeder selection in compensated MV networks. The approaches presented in references [63–65] are mainly based on calculations of zero sequence admittance (or phase-to-the-ground) for each feeder and subsequent comparisons in order to reveal the faulty feeder. Hence, [63] focuses on the detection of high impedance faults; however, the approach can be used for feeder selection as well. The paper proposes comparing the relative change of admittance in pre- and post-fault conditions. Similar approaches are described in [64, 65]. References [63–65] differ by algorithms for indications of admittance change in a faulty feeder. A complex algorithm involving a special type of mathematical graph (referred to as the small-world network theory) is introduced in [66]. It requires zero sequence voltages and currents. Utilisation of phase voltage and current measurements (not zero sequence as in all previous) is presented in [67], which proposes a novel approach calculating fault resistance (it serves as an indicator) for every feeder.

These methods are passive and use only locally available measurements. In contrast to this, an active approach is defined when additional signals are injected into the network. Hence, [68] presents a newly developed methodology that proposes superimposing a voltage of a certain frequency (higher than the fundamental) at the neutral point. A fault resistance is calculated for each feeder and phase utilising phasors at the given frequency, and is then used in a fault identification procedure. For method security, natural feeder imbalance is taken into account.

In order to affect as few customers as possible, location of a faulty section along a feeder is necessary. Such procedures are addressed in references [69–75]. The main approach here is to utilise information exchange through the communication network. Thus, [69–71] consider the possibility of utilising smart meters (in the frame of Smart Grid concept) for earth fault location. [69] suggests using negative sequence voltages and locating faulty sections by applying a clustering approach. The method is immune to DG and partial loss of communication between units (synchronised signals are not required). A similar method is proposed in [70]. The approach in [71] utilises temporary zero sequence voltage sags (at the secondary low side of load transformers) which appear during the connection of an auxiliary resistor. The methods in [72, 73] exploit the variability of the grounding suppression coil: it can be adjusted to a certain range to minimise fault

current and for retuning after the disconnection of a network part. [72] uses zero sequence admittance to reveal faulty feeders during the adjustment process. The method is also suitable for faulty section identification if data is collected along the faulty feeder. [73] uses zero sequence current variation for the same purposes. Finally, active methods for faulty section identification are presented in [74, 75]. [74] proposes injecting additional current of a non-grid-frequency (183 Hz is tested) into transformer neutral point and locating faults using distributed sensors which measure magnetic fields. [75] describes a similar approach, but current pulses are injected.

The steady-state methods above are most applicable to permanent earth faults mainly because they require stable signals for extraction of phasors (typically only the first main harmonic is used) for further calculations. Nevertheless, the vast majority of earth faults in distribution networks have an intermittent nature (especially in underground cables) [76], producing signals with low- and high-frequency transients without the steady-state period. In such cases, steady-state methods might not be suitable for the extraction of information on transient characteristics. Furthermore, they can lose sensitivity and directionality during high impedance faults, as [77] demonstrates. Therefore, numerous transient methods are proposed in the literature [78–105]. Moreover, transient methods are preferable to fast earth fault location due to their short operation times. They are divided into two groups: methods based on low-frequency transients and those based on high-frequency transients. The first group requires a sampling frequency of 2-10 kHz according to the Nyquist sampling theorem, the second - 0.01-1 MHz.

Many algorithms utilising low-frequency transients have been developed [78–97]. In fact, they have one common physical principle as a basis: right after fault inception, capacitive current to the ground in the faulty feeder has a discharging nature, whereas in all healthy feeders it has a charging nature. This leads, for example, to situations where the polarity of zero sequence currents in faulty feeders differs from that in healthy feeders. This is demonstrated in [78] where the time derivative of a zero sequence current is used to establish settings and thresholds. Charging and discharging processes are visible with the application of methods based on the calculation of zero sequence active power [79] or energy [80, 81] because they have a different sign for the faulty feeder. The proposed algorithms accomplish integration during the fault (integration time is not limited) and start time is typically determined by the zero sequence over-voltage function. Such algorithms are broadly used in modern fault passage indicators. In contrast, [82] presents an algorithm which calculates zero sequence active power during the first quarter of the period. A short integration time window can be beneficial be-

cause processes taking place in the following steady-state period can corrupt algorithm performance. More complex algorithms with the same physical principle are presented in [83–85]. [83] uses the observation that similarity between transient zero sequence current in the faulty and a healthy feeder is lower than between currents in only healthy feeders. The main mathematical tool here is the grey relation degree, which can be used to characterise the similarity between curves. [84] exploits the cluster approach for transient zero sequence currents and [85] suggests utilising correlation coefficients computed for two different data windows (the first and the second quarter of the period). Since a zero sequence current has a mainly capacitive nature (the active part is typically much smaller), several algorithms are based on calculation of capacitances or charges. Hence, the algorithm in [86] integrates instantaneous zero sequence current during two periods to estimate capacitance. It is compared with the calculated capacitance for assumed purely capacitive network and an error deviation is used as a selection criterion. [87, 88] offer to use charge-voltage characteristics determined during the first few cycles. Variability of the suppressing coil is also used, as in the transient methods. For instance, [89] derives transient variation components (TVCs) of feeder zero sequence currents and bus voltage before and after fault. For healthy feeders, TVC is around zero, whereas for the faulty feeder, considerable variations can be registered. [90] evolves an algorithm that uses the derivative of the zero sequence current over the inductance derivative of the Petersen coil. Apart from zero sequence current, phase currents can also be used, as proposed in [91]. All these algorithms utilise instantaneous signals, whereas few algorithms involve phasors. Thus, [92] proposes a novel algorithm which checks phase displacement between a fundamental frequency component of zero sequence current and voltage after fault inception: phase displacement is different for the faulty feeder compared to the healthy feeder. Higher frequency components are used in the algorithm presented in [93]. The main operation principle here is based on multi-frequency neutral admittance measurements together with a cumulative phasor summing technique. Finally, analysis of frequency spectrum is proposed in [94].

Selection of a faulty section along the feeder is discussed in [93, 95–97]. Thus, [95] proposes a new algorithm for faulty feeder/section selection based on transient estimation of the earth capacitance of the background network during the first one-eighth of the power frequency period. A more complex approach is used in [96], utilising hierarchical clustering for transient capacitive components from the zero sequence current. As can be seen, all the above algorithms exploit the same physical principle and in contrast to

them, [97] presents a fundamentally new approach: measurements of electrical and magnetic fields produced by the power line right after an earth fault. It is used in commercially available fault passage indicators which are capable of faulty section identification. They are installed on the poles and send information remotely to the central controller.

Methods utilising high-frequency transients are not so widely presented in the literature [98–105]. The main mathematical tool in such algorithms is the wavelet analysis of zero sequence currents. Hence, [98] uses waveband energy during the first quarter of the period, [99] suggests utilising wavelet transform for the first half of the period, [100] proposes utilising discrete wavelet packet transform and machine learning, [101] applies continuous wavelet transform (CWT) and convolutional neural network (CNN), [102, 103] introduce the S-transform (a reversible local time-frequency analysing method) of travelling waves, [104] presents the Hilbert-Huang transform, and [105] uses the Morlet's wavelet transform and fuzzy logic for decision making.

The practical application of high-frequency transients is complicated due to high sampling rate and a need for special filters that are capable of abnormal transient extraction (sometimes it is not possible because of significant noise). Therefore, such an approach is not considered in the current thesis. Moreover, the active methods are also beyond the scope of the current work because they require additional equipment and investments. Thus, utilisation of low-frequency transients are of interest. The low-frequency transient methods presented above might be inadequate for high impedance faults filtering out harmonics, in networks with highly unequal earth capacitive currents of feeders (uneven penetration of cables or short lines) or with capacitive imbalance among line phases (nearly ideal models with equal feeders are typically used in the studies). The latter is discussed in [106] and adverse effects on energy function are shown. The impact of other factors must also be verified. Disadvantages of the fundamental method proposed in [78] are discussed in [87]. Methods which work with the computation of feeder capacitances or charges require pre-fault measurements or information about background networks. Finally, settings diversification depending on network configuration can be considered as a shortcoming. Thus, comparative analysis of the presented methods and exploration of misoperation scenarios are required.

The previously presented steady-state and transient methods are not applicable when locating the exact point in a section where an earth fault takes place. However, such information is extremely useful for reduction of outage time; therefore, the work done in this direction needs to be reviewed. Refer-

ences [107–115] address this issue. In general, the steady-state approaches are presented based on calculations using network data: [107] utilises network transmission matrices, [108] suggests involving multiple measurements resembling the two-end method for a transmission line, [109] studies short-term additional earthing of unaffected (healthy) phases in the faulty feeder with further impedance-based calculations, [110] applies an equivalent circuit requiring information about line shunt admittances and introduces a set of equations with solutions containing a distance to the faulty point. References [111,112] use the active methods with the steady-state signals of inter-harmonic frequencies. As mentioned above, intermittent earth faults require transient methods. Hence, [113] examines fault current frequency spectrum characteristics for exact fault location, and [114] analyses the frequency spectrum of zero sequence currents. Finally, the high- frequency-transient-based approach is presented in [115]. To summarise, a limited amount of methods is present in the literature, presenting opportunities for further study.

DG presence aspects are discussed in [69, 70] where immunity of the algorithm to infeed currents is claimed. Few additional references on this issue can be made. Papers [116–119] discuss steady-state methods in presence of DG: [116] introduces a binary particle swarm optimisation and a genetic algorithm used for earth fault location, [117] proposes a new impedance-based algorithm based on a nodal admittance matrix of the network and available measurements at nodes, [118] utilises a ratio of negative and positive sequence current (voltage measurements are not needed), and [119] suggests a new protection framework where fault location is based on comparisons with clustered historical or pre-simulated data. Low-frequency transients are utilised in [120,121]: [120] considers an MV microgrid with IIDG and earth fault location in such a system, [121] proposes cross correlation coefficients to detect the faulty line in the system with DG. Application of high-frequency transients in distribution networks with DG is considered in [122, 123]: the algorithm in [122] compares wavelet coefficients of currents at the interconnection points (busbars) and determines the direction of currents (polarity) during fault (as well as the distance to the faulty point), [123] proposes using wavelet transform for the decomposition of zero sequence currents and Back Propagation neural networks for extraction of fault characteristics. To summarise, little consideration has been given to DG presence in the network during development of earth fault location algorithms. The reason is that the impact of DG on zero sequence network characteristics is absent if an embedded generator is connected to the grid by means of a YD transformer (as is typical in Norway [124]). This is demonstrated, for instance,

in [116, 123].

Summarising this section, the methods based on low-frequency transients are of significant interest because they are a promising solution for fast earth fault location (an alternative to the steady-state methods) and due to the simplicity of their practical realisation (unlike the high-frequency-transient-based or active methods). Therefore, analysis of the existing approaches, revealing drawbacks and development of new methods, is the second main focus of the current PhD thesis. Moreover, exact faulty point location (in case of a permanent earth fault) is also included in the scope. These methods should become a basis for designing fast, selective and robust protective schemes which can resolve the afore mentioned issues associated with resonant grounding and presence of DG in the system.

Chapter 3

Research methods and tools

The current chapter describes different tools, methods and models used in the current PhD thesis. The main process of the research method includes the following steps:

- Development and construction of power system models (MV networks) utilising PSCAD/EMTDC [125]. This software allows analysis of transient processes in power systems that is utilized in the next steps.
- Simulation of various fault scenarios with the help of the developed models and data collection for further processing.
- Signal processing, analysis and development of algorithms using MATLAB/M-FILES [126] for programming. The main innovative contributions summarised in the current thesis were done at this stage.
- Laboratory verification of the developed algorithms. This step, with reference to [Paper III], consists of:
  - development of power system dynamic models in MATLAB/SIMULINK [127].
  - conversion of the developed models into C-code using RT-LAB [128].
  - real-time hardware-in-the-loop simulations by means of OPAL-RT [129] (using the generated code) and commercially available ABB feeder relay RED670 that has impedance protection functions [130].

  With reference to [Paper VI]:

- creation of a prototype based on microprocessor card STM32F407VGT6 [131] with the implemented algorithm and its programming in MATLAB/SIMULINK.
- real-time hardware-in-the-loop simulations by means of OPAL-RT and the prototype. Here, the simulated or real fault records are played back in the simulator.
- performance comparison with a commercially available relay that is tested with the help of OMICRON CMC356 [132].

The rest of the chapter provides details on the laboratory test setups and development of the model presented in [Papers I,II,V]. The models used in [Papers III,IV,VI] are fully described within the corresponding papers and are not given in this chapter.

3.1 Modelling of an actual distribution network with DG

[Papers I,II,V] have a test case network based on a real distribution system with DG operated by Norwegian distribution network operator EIDSIVA NETT. Development of the model having actual data provided by the operator (network parameters and measurements) is given below.

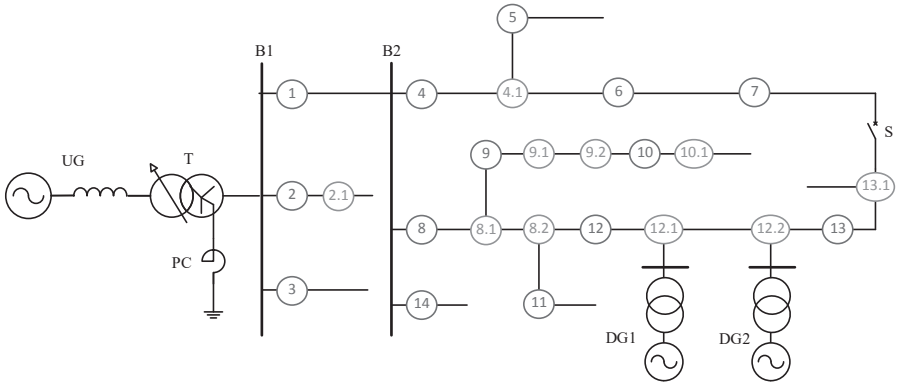

Figure 3.1: An actual 22 kV distribution network with DG for modelling.

Fig.3.1 shows the single line diagram of a part of the network chosen for modelling (voltage level is 22 kV). It has two busbars, B1, B2, with CTs and VTs (measuring points 1-3,4,8,14 marked with blue colour), remote substations with own local CTs and VTs (measuring points 5-7, 9-13), two interconnected generators (hydro plants) DG1, DG2, and switch S for ring

operation. The network is connected to the utility grid UG (voltage level is 66 kV) by means of a distribution transformer T which is grounded through a Petersen coil PC. Additional points marked with green colour enumerate side branches, cables or DG connecting lines.

In the real network, numerous line sections with different cross-sections exist; moreover, there are many short lateral outfeeds (mainly load taps). In order to simplify the model, these outfeeds are not taken into account and numerous unequal lines between marked points in Fig.3.1 are merged into one equivalent, which is modelled as a Π-section. Loads are combined and connected at both sides of each Π-section.

This representation with lumped parameters is reasonable because wave travelling time in an equivalent line is less than simulation time step (50 μs); moreover, only signals of the fundamental frequency are exploited and Π-section can be used for slow frequency phenomena (up to 1 kHz) [133].

The following approach is used for merging:

- each short line is represented by lumped parameters: series impedance Z_s and shunt admittance Y_{sh}, Fig.3.2. These parameters are calculated as:

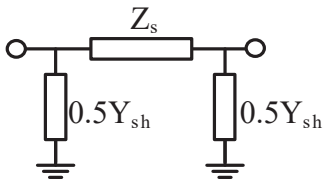

Figure 3.2: Π-equivalent of a line.

$$Z_{s1} = R_1 + jX_{L1} \tag{3.1}$$

$$Y_{sh1} = j100\pi C_d \tag{3.2}$$

$$Z_{s0} = R_1 + 3R_g + j(X_{L1} + 3M) \tag{3.3}$$

$$Y_{sh0} = j100\pi C_g, \tag{3.4}$$

where index 1 denotes positive sequence, 0 - zero sequence, R and X_L are resistance and reluctance of a section, C_d is drift capacitance, R_g is ground resistance, M is mutual inductance, C_g is capacitance to the ground. All parameters, except R_g and M, are provided by the network operator.

Ground resistance (in Ohms) is calculated using the first order approximation [14, 133]:

$$\mathrm{R_g} = 0.25\mu_r\mu_0 f\pi l_s = 0.25 \cdot 1 \cdot 4\pi \cdot 10^{-7} \cdot 50\pi l_s = 0.049 l_s \cdot 10^{-3}, \quad (3.5)$$

where l_s is the length of a short line in meters.

Mutual inductance (in Ohms) is calculated with the assumption that the distance between conductors is $D = 1.5$ m (typical geometry for 22 kV networks), and earth resistivity $\rho = 200$ Ωm [14]:

$$\mathrm{M} = \mu_0 f \ln\left(\frac{660\sqrt{\frac{\rho}{f}}}{D\sqrt[3]{2}}\right) l_s = 4.11 l_s \cdot 10^{-4} \quad (3.6)$$

- Since numerous short lines are connected in series, parameters of an equivalent Π-section can be found using the abcd-matrix theory [134]:

$$\begin{bmatrix} A_e & B_e \\ C_e & D_e \end{bmatrix} = \prod_i \begin{bmatrix} A & B \\ C & D \end{bmatrix}_i, \quad (3.7)$$

where i denotes a short line number and

$$A = 1 + \mathrm{Z_s} \cdot 0.5\mathrm{Y_{sh}} \quad (3.8)$$
$$B = \mathrm{Z_s} \quad (3.9)$$
$$C = \mathrm{Y_{sh}} + \mathrm{Z_s} \cdot 0.25\mathrm{Y_{sh}^2} \quad (3.10)$$
$$D = A \quad (3.11)$$

Thus, $\mathrm{Z_{se}} = B_e$ and $\mathrm{Y_{she}} = 2(A_e - 1)/\mathrm{Z_{se}}$ of an equivalent Π-section substituting all short lines can be found for positive and zero sequence networks. An equivalent length l_e is the sum of all short lines' lengths.

Table 3.1 contains data on all the equivalent Π-sections used in the model. Parameters are calculated as:

Table 3.1: Positive and zero sequence line parameters.

From	To	l_e, m	R_1, Ω/m $\cdot 10^{-4}$	X_{L1}, Ω/m $\cdot 10^{-4}$	X_{C1}, M$\Omega\cdot$m $\cdot 10^{2}$	R_0, Ω/m $\cdot 10^{-4}$	X_{L0}, Ω/m $\cdot 10^{-3}$	X_{C0}, M$\Omega\cdot$m $\cdot 10^{2}$
1	B2	3472	3.42	3.56	1.31	5.00	1.60	1.59
2	2.1	938	1.91	3.51	3.06	3.00	1.60	6.37
2.1[1]	-[2]	10183	2.67	1.48	0.145	4.00	1.40	0.136
3	-	100	3.42	3.56	1.31	5.00	1.60	1.59
4	4.1	14529	4.34	3.73	2.98	6.00	1.60	6.47
4.1	5	433	3.59	3.73	3.25	5.00	1.60	6.57
5	-	7798	4.08	3.77	3.46	6.00	1.60	6.66
4.1	6	1854	3.59	3.73	3.25	5.00	1.60	6.56
6	7	9573	5.07	3.84	3.37	7.00	1.60	6.67
7	S	10808	6.47	3.91	3.64	8.00	1.60	6.83
8	8.1	15015	3.59	3.66	3.14	5.00	1.60	6.64
8.1[1]	9	492	5.35	3.20	0.187	7.00	1.60	0.187
9[1]	9.1	933	5.35	3.20	0.067	7.00	1.60	0.067
9.1	9.2	505	2.57	3.62	3.15	4.00	1.60	6.46
9.2[1]	10	4336	5.35	3.20	0.067	7.00	1.60	0.067
10[1]	10.1	3412	5.35	3.20	1.20	7.00	1.60	1.20
10.1	-	6201	11	4.00	3.58	13	1.60	6.89
8.1	8.2	4820	3.59	3.73	3.25	5.00	1.60	6.56
8.2	11	1398	5.05	3.82	3.66	7.00	1.60	6.78
11	-	4094	6.87	3.93	3.57	8.00	1.60	6.81
8.2	12	644	5.12	3.84	3.56	7.00	1.60	6.66
12	12.1	8930	5.11	3.84	3.51	7.00	1.60	6.66
12.1	DG1	91	7.25	3.97	6.72	9.00	1.60	3.43
12.1	12.2	193	5.12	3.84	3.35	7.00	1.60	6.65
12.2	DG2	1643	7.21	3.95	6.76	9.00	1.60	3.45
12.2	13	1619	5.43	3.86	3.50	7.00	1.60	6.73
13	13.1	6967	7.21	3.95	3.45	9.00	1.60	6.76
13.1	-	8738	7.21	3.95	3.45	9.00	1.60	6.76
13	S	676	7.21	3.95	3.45	9.00	1.60	6.76
14	-	100	3.59	3.66	3.14	5.00	1.60	6.64

[1]cable, [2] dash denotes unenumerated line end.

$$\mathrm{R}_{1,0} = \frac{\mathrm{real}(\mathrm{Z}_{\mathrm{se1,0}})}{l_e} \tag{3.12}$$

$$\mathrm{X}_{\mathrm{L1,0}} = \frac{\mathrm{imag}(\mathrm{Z}_{\mathrm{se1,0}})}{l_e} \tag{3.13}$$

$$\mathrm{X}_{\mathrm{C1,0}} = \frac{l_e}{\mathrm{imag}(\mathrm{Y}_{\mathrm{she1,0}})} \tag{3.14}$$

3.1.1 Modelling of network non-idealities

Line modelling with Π-section is sufficient for studying of phase-to-phase faults and even transposition can be neglected. Nevertheless, Π-section does not reflect two main effects presenting in the real network and which are extremely important for studying earth faults: lines have resistive losses to the ground; lines have electrostatic asymmetry (capacitance to the ground is different for different phases).

In order to take these aspects into account, at both ends of each Π-section in the model the following additional elements are connected:

- Shunt resistor in each phase is calculated as:

$$\mathrm{R}_{\mathrm{sh}} = \frac{2\mathrm{X}_{\mathrm{C0}}}{k_r} l_e \tag{3.15}$$

  The resistor models watt-metric losses of lines; that is resistive current to ground that typically constitutes 1-10% from capacitive [18]; therefore, k_r is varied in the model between 0.01 and 0.1.

- Additional shunt capacitor in phase B is calculated as:

$$\mathrm{C}_{\mathrm{sh}} = k_c \frac{3\mathrm{X}_{\mathrm{C0}}}{200\pi} l_e \tag{3.16}$$

  The capacitor models electrostatic asymmetry of overhead lines (it is absent in cable Π-sections, marked in Table 3.1) taking place in the middle phase. In fact, it can be located in any phase due to line transposition. The value can vary as much as 1-5% from the total capacitance to the ground [18]; therefore, k_r is changed in the model between 0.01 and 0.05.

3.1.2 Modelling of short load cables

In the real network, loads are connected to the main trunks by means of short cables that were left out of the diagram above in order to simplify the model, as was stated above. Nevertheless, their accumulated contribution to capacitive and resistive current to the ground must be taken into account to get the model as close to reality as possible.

For this purpose, the network operator provided information about zero sequence current $|I_0|$ (magnitude) measured at various substations in back direction (i.e. during a low-ohmic earth fault at bus B2), Table 3.2.

Table 3.2: Backward zero sequence fault current measured at a substation.

Substation	$\|I_0\|$ backward, A
6	1.8
7	0.5
9	10.9
10	0.5
11	2.5
12	3.1
13	1.5

On the basis of this data, lack of capacitance to the ground was revealed in some locations in the initial model. For correction, additional shunt capacitors C_{ad} to the ground are added to the model at both line ends in each phase of the lines specified in Table 3.3.

Table 3.3: Additional capacitance replacing uncounted short cables.

From	To	C_{ad}, μF
5	-	0.05
6	7	0.144
7	S	0.0325
11	-	0.3
12	12.1	0.175
13	13.1	0.1425

Since the neglected cables also have resistive losses, they are represented as shunt resistors R_{ad} at both line ends in each phase of the lines given in Table 3.3. The values are calculated as:

$$R_{ad} = \frac{1}{k_r 100\pi C_{ad}} \tag{3.17}$$

3.1.3 Modelling of loads

Loads are modelled as constant impedances. Such representation is valid for the study of faults in distribution networks when voltage dependency of load becomes quadratic. In order to estimate loads, the network operator provided information about total power $P+jQ$ and positive sequence current $|I_1|$ measurements (the highest load in the network) at each substation given in Table 3.4.

Table 3.4: Load current and power flow measured at a substation.

Substation	$\|I_1\|$, A	P, MW	Q, MVAr
1	173	6.548	1.174
2	150	5.534	1.523
3	207	7.745	1.839
4	104	1.63	0.427
5	16	0.56	0.119
6	27	0.96	0.219
7	6	0.139	0.035
8	45	3.9	0.5
9	14	0.51	-0.014
10	2	0.086	0.008
11	7	0.254	0.036
12	23	-0.838	0.049
13	7	0.26	0.039
14	10	0.368	0.063
DG1	11	0.408	-0.013
DG2	26	0.976	0.061

In the real network, loads are decoupled from the feeders by ungrounded YD transformers (excluded from modelling); therefore, in the model, load impedances are connected in an ungrounded star to avoid impact on zero sequence currents. Impedance per phase connected at both ends of each line is approximately (line losses are neglected) evaluated as

$$Z_{ld,i} = 2\frac{P_i + jQ_i - (P_k + jQ_k)}{3|I_{1,i}\angle\phi_i - I_{1,k}\angle\phi_k|^2}, \tag{3.18}$$

where i is the upstream substation, and k is downstream. Current angle $\phi = \arctan(Q/P)$. For i=2,3,5,10,11,13,14, P_k+j$Q_k = 0$ and $I_k = 0$.

If there are several lines between adjacent substations, load is evenly divided for each line:

$$Z_{ld,i} = 2N_l \frac{P_i + jQ_i - \sum_{k=1}^{N_s}(P_k + jQ_k)}{3|I_{1,i}\angle\phi_i - \sum_{k=1}^{N_s} I_{1,k}\angle\phi_k|^2}, \tag{3.19}$$

where N_l is number of lines, N_s is number of adjacent substations (e.g. for i=4, k=5,6).

A particular case is the load between substation 12 and 13 because the DG must be included:

$$Z_{ld,12} = \frac{10(P_{12} + P_{DG1} + P_{DG2} - P_{13}) + j10(Q_{12} + Q_{DG1} + Q_{DG2} - Q_{13})}{3|I_{1,12}\angle\phi_{12} + I_{1,DG1}\angle\phi_{DG1} + I_{1,DG2}\angle\phi_{DG2} - I_{1,13}\angle\phi_{13}|^2} \tag{3.20}$$

The calculated load impedances using the information in Table 3.4 are considered high load in the system. In such cases, tap changer of the main distribution T transformer is set to 0.93. Low load in the system is modelled as 25% from the high load, then tap is 0.98.

The balanced load model is suitable for the development of algorithms against phase-to phase faults as is the case in [Paper II]; however, laboratory tests in [Paper III] are conducted in presence of load imbalance. The impact of loads on earth fault algorithms is negligible.

3.1.4 Petersen coil size

For normal operation of the network, a resonance curve can be plotted: it is a dependency of voltage over the Petersen coil (U_{PC}) on its size in amperes ($I_{PC} = 22\text{ kV}/(100\sqrt{3}\pi L_{PC})$, where L_{PC} is variable inductance of the coil). From this curve, size of the coil can be chosen.

Fig.3.3 shows several curves for different k_r and k_c. It is possible to see that the total uncompensated capacitive ground fault current produced by the network is around 87 A (the resonance point). Operation point of the Petersen coil is chosen in the overcompensation region as $I_{PC} = 87 + 3 = 90$ A according to Norwegian regulations [18].

Coefficients k_r and k_c are varied in the model to get $U_{PC} \approx 500$ V, which corresponds to the real measurements.

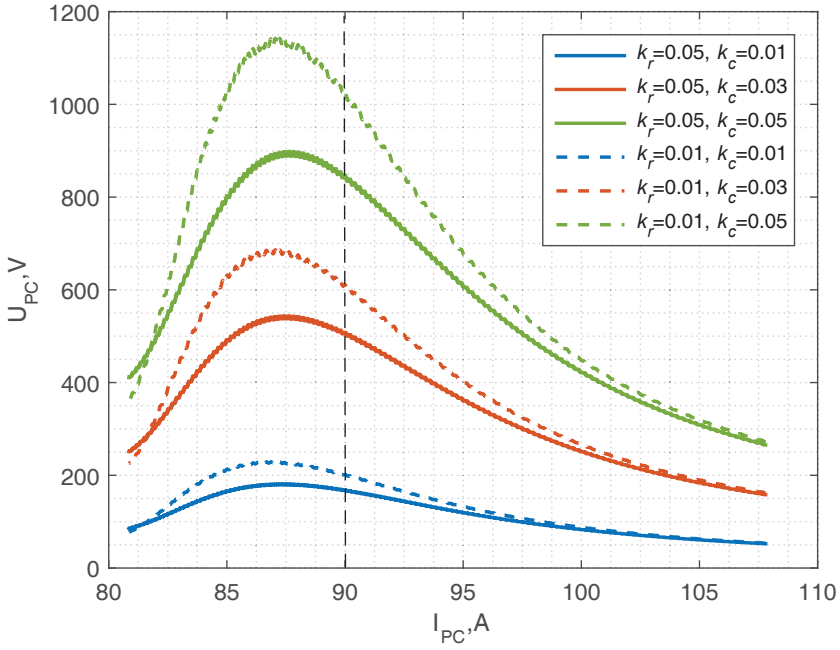

Figure 3.3: Simulated resonant characteristics of the network for different k_r, k_c.

3.1.5 Modelling of DG

DG in the network is represented by two electrical machines: an induction generator (DG1) and a synchronous (DG2). Each generator is governed by a small hydro turbine. Parameters of the prime movers are not available and they are not modelled. Such an assumption is valid because response time during phase-to-phase faults is large due to high inertia and, therefore, the prime movers can be replaced by constant torque. For earth faults, impact of DG is negligible, mainly due to the YD-connected step-up transformers.

The induction generator is operated in torque control mode. The input torque is set to -0.66 pu (generator mode) to produce active power 0.976 MW (see Table 3.4). Normally, the machine is started in speed control mode (rated speed 1 pu), before it is switched over to torque control in the steady-state period. Table 3.5 provides the parameters used in the standard model from the PSCAD library.

The synchronous generator is also controlled by constant torque input, set as 0.75. Machine parameters are given in Table 3.6; the model is also taken from the PSCAD library.

Table 3.5: Parameters of the induction generator (DG1).

Rated power	0.623 MVA
Rated line voltage	0.38 kV
Base angular frequency	314.16 rad/s
Stator/rotor turns ratio	2.638
Angular moment of inertia	0.727 s
Mechanical damping	0.01 pu
Stator winding neutral	Grounded
Squirrel cage	No
Mutual saturation	No
Leakage saturation	No
Stator resistance	0.01 pu
Wound rotor resistance	0.01 pu
Magnetising inductance	4 pu
Stator leakage inductance	0.1 pu
Wound rotor leakage inductance	0.1 pu
Reactive power of compensating capacitors	0.21 MVAr

Table 3.6: Parameters of the synchronous generator (DG2).

Rotor type	round
d-axis saturation	No
Rated line voltage	0.381 kV
Rated line current	1.22 kA
Base angular frequency	314.16 rad/s
Inertia constant	1 s
Mechanical friction and windage	0.04 pu
Neutral resistance	1e4 pu
Neutral reactance	0 pu
Iron loss resistance	300 pu
Armature time constant	0.05 s
Potier reactance	0.1 pu
Unsaturated reactance (d-axis)	1.5 pu
Unsaturated transient reactance (d-axis)	0.25 pu
Unsaturated transient time (open, d-axis)	4 s

Unsaturated sub-transient reactance (d-axis)	0.15 pu
Unsaturated sub-transient time (open, d-axis)	0.03 s
Unsaturated reactance (q-axis)	1.5 pu
Unsaturated transient reactance (q-axis)	0.4 pu
Unsaturated transient time (open, q-axis)	1 s
Unsaturated sub-transient reactance (q-axis)	0.15 pu
Unsaturated sub-transient time (open, q-axis)	0.03 s
Air gap factor	1

Automatic voltage regulator (AVR) of the synchronous machine does not compensate load current and does not have input for system stabiliser [135]. AVR is used in the model to keep output reactive power at 0 (both generators run at unit power factor). It has a PI-controller with proportional gain 0.1, integral time constant 1 s, and output limits ±0.1 (reference voltage is regulated in the range 0.9–1.1) [14].

Exciter and regulator parameters of the synchronous machine are given in Table 3.7. The model is taken from the PSCAD library.

Table 3.7: Parameters of the exciter and regulator of the synchronous generator.

AC Exciter Type	AC8B
PID proportional gain	100 pu
PID integral gain	0.1 pu
PID derivative gain	100 pu
PID derivative time constant	0.09 s
Regulator gain	1 pu
Regulator time constant	0 s
Maximum regulator output	10 pu
Minimum regulator output	0 pu
Field limiter loop reference	0.79
Field current limiter	15
Exciter time constant	1 s
Exciter constant related to field	1 pu
Field circuit commutating reactance	0.55
Demagnetising factor	1.1

Saturation at Efd1	1.5 pu
Exciter voltage for SE1	4.5 pu
Saturation at Efd2	1.36 pu
Exciter voltage for SE2	3.38 pu

Transformer parameters included in the model are given in Table 3.8.

Table 3.8: Parameters of the transformers.

Transformer	T	DG1	DG2
Total power	20 MVA	0.6 MVA	1.6 MVA
Frequency	50 Hz	50 Hz	50 Hz
HV	66 kV	22 kV	22 kV
LV	22 kV	0.38 kV	0.66 kV
Winding HV	D	Y	Y
Winding LV	Y	D	D
D lags/leads Y	Lags	Lags	Lags
x_1^1	0.09739 pu	0.04919 pu	0.06336 pu
Ideal model	No	No	No
No load losses	0 pu	0 pu	0 pu
Copper losses	0.0045 pu	0.0084 pu	0.0066 pu
Tap changer on winding	HV	None	None
Saturation	No	No	No

[1]positive sequence reactance.

The utility grid UG has short circuit capacity 250 MVA and is modelled as an ideal voltage source with an internal inductance value which is calculated per phase as $(66\text{ kV})^2/(250\text{ MVA} \cdot 100\pi) = 0.055$ H.

Finally, the developed model can be considered sufficiently close to the real network because:

- The simulated steady-state healthy currents and power flows at the substations coincide (with error less than 3%) with the real measurements (Table 3.4).
- The simulated steady-state faulty (phase-to-phase and phase-to-ground) voltages and currents at the substations can be detected with the given real settings provided by the system operator.

- The simulated zero sequence currents at the substations listed in Table 3.2 during ground fault at busbar B2 coincide (error is less than 1.5%) with the real measurements.

- The derived size of the Petersen coil (90 A in section 3.1.4) is in the range of the real coil that has variable size 10-100 A. Lower values (below 90 A) are needed when a part of the network is disconnected.

3.2 Laboratory test setups

3.2.1 Setup 1

Fig.3.4 shows a general view of the laboratory test setup used in [Paper III]. It is used for real-time hardware-in-the-loop tests of commercially available products. The real-time eMEGAsim simulator OP5600 (OPAL-RT for short) runs a power system model (initially constructed in MATLAB/SIMULINK, then the model is converted into C-code in RT-LAB that is uploaded to the simulator). The simulator communicates with the relay through the network: it sends sample values (SV) with 4 kHz sampling rate to the relay and receives GOOSE messages containing tripping signals. Communication standard in the test setup is IEC 61850 [136].

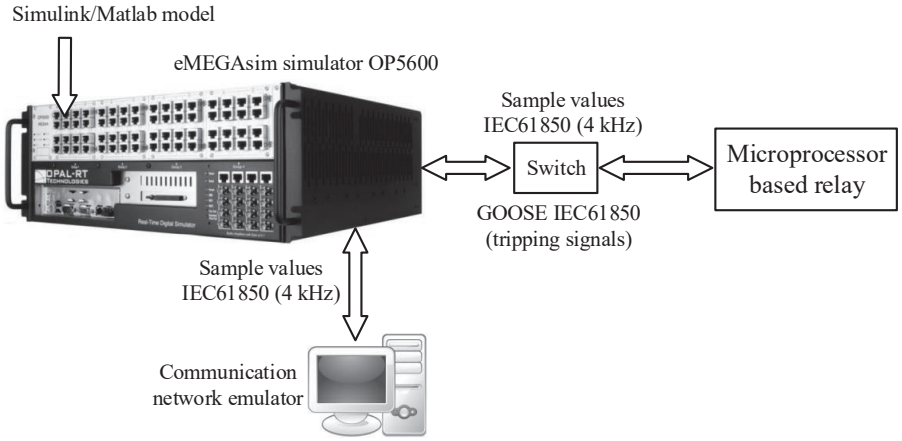

Figure 3.4: Test setup 1: co-simulation platform for real-time hardware-in-the-loop tests.

The protection method proposed in [Paper II] requires remote measurements that in reality would be sent through a network. In order to mirror behaviour of this network during tests, a communication network

emulator [137] is included in the testbed. Its main purpose is to model communication network impairments such as delays, jitters, data losses. The full list of functions is given in [Paper III]. The simulator and the emulator also exchange SV at 4 kHz sampling rate.

The advantages of such a testbed are: reliable results due to the availability of an actual protection relay; fast and flexible model of a power system that enables the researches to conduct many test scenarios; taking into account communication links' imperfections; presence of actual environmental conditions (communication networks with the relay) and hidden or neglected factors that might be concealed in off-line simulations; possibility to replicate experiments and to identify influencing factors; compare different algorithms and products under the same conditions.

3.2.1.1 Power system model for real-time simulations

An example of the model used for real-time hardware-in-the-loop simulations realised in MATLAB/SIMULINK is presented in Fig.3.5. Subsystem representation is used by RT-LAB software for C-code generation and further uploading it on the OPAL-RT simulator. Subsystems' names must start with 'SC' (always one control subsystem), 'SM' (always one master subsystem), and 'SS' (several supplementary subsystems). Each subsystem uses one core of the simulator. The model has the following elements and signals:

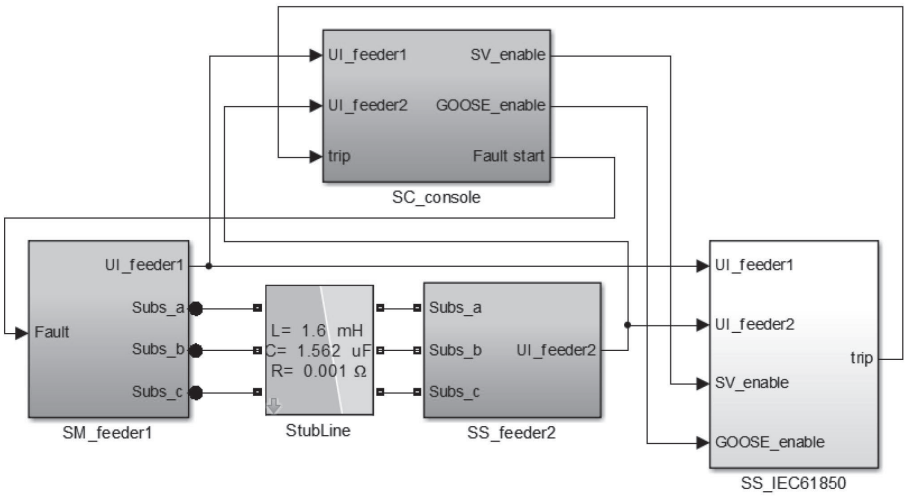

Figure 3.5: General view of the model for real-time simulations.

- 'SC_console' is the control panel of the model. It sends permissive signals to initiate SV and GOOSE streams with hardware in the loop

(the relay). Faults are also applied from this panel. At the same time, it collects measurements from the simulated network and trip signals from the relay for further (e.g. off-line) analysis.

- 'SM_feeder1' is the master subsystem containing a dynamic model of a part of the network (e.g. one feeder). It produces voltage and current measurements (instantaneous quantities with time step 50 μs) that are sent to 'SC_console' (for visualisation or further processing) and to communication subsystem 'SS_IEC61850' (connection with the external hardware).

- 'SS_feeder2' has the same functions as 'SM_feeder1'. It is separate from the main model and uses a different simulator core in order to decrease computation load and avoid overruns in the simulator (the situation where calculations have not been completed before the next time step, leading to errors and falling of test confidence level).

- 'StubLine' is a line (can be lossless) with wave traveling time equal to the simulation time step. It is used for connection of different parts of the power network model situating in separate subsystems.

- 'SS_IEC61850' is the subsystem containing models of the merging unit (conversion of voltages and currents into SV according to the IEC61850 standard) and the GOOSE subscriber (the tripping signal from the relay is sent as a GOOSE message).

The dynamic models of the feeders are built using elements from the SIMULINK library 'Simscape/SimPowerSystems'. The stub-line model is taken from the pre-installed 'ARTEMIS' library. The merging unit and the GOOSE subscriber are part of the pre-installed library 'RT-LAB I/O'.

3.2.2 Setup 2

Fig.3.6 shows a general view of the laboratory test setup used in [Paper VI]. It is used for real-time hardware-in-the-loop tests of a prototype developed using the microprocessor STM32F407VGT6. This testbed is used to play back pre-simulated signals (in PSCAD/EMTDC) or, as in the previous case, to run the power system model. Here, communication with the microprocessor is done through TCP/IP protocol [138] at 4 kHz sampling rate. The board has an embedded universal asynchronous receiver transmitter (USART) [139]; therefore, an interface converter is used [140]. The algorithm is run on the microprocessor (C-code), which produces the analogue tripping signal which is sent to the simulator.

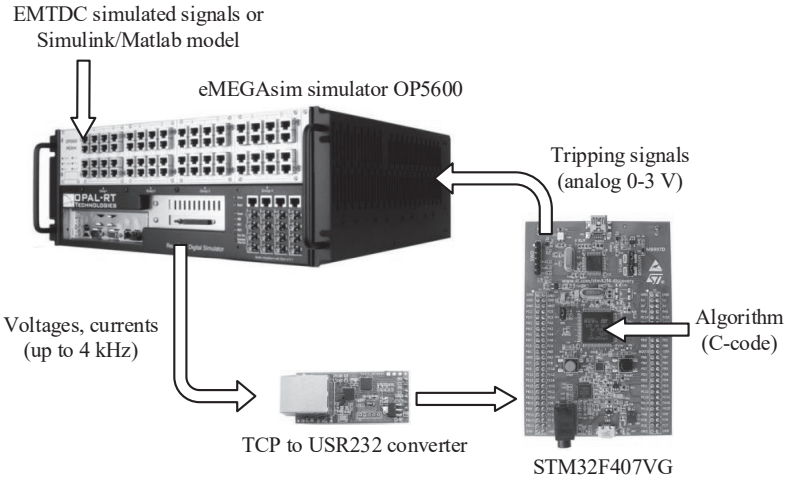

Figure 3.6: Test setup 2: platform for real-time hardware-in-the-loop tests of the prototype.

The SIMULINK model used in [Paper VI] to reproduce pre-simulated signals and program the microprocessor is given below.

3.2.2.1 Signal reproducing model for real-time simulations

The model realised in MATLAB/SIMULINK and used to play back the voltages and currents pre-simulated in PSCAD/EMTDC is demonstrated in Fig.3.7.

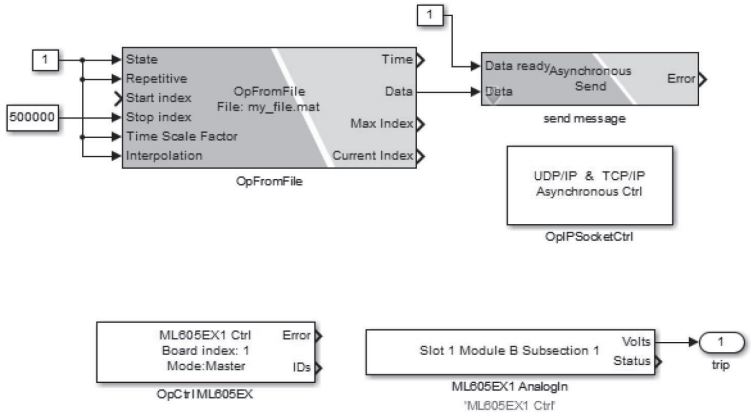

Figure 3.7: General view of the model used to reproduce fault records in real-time.

The model includes the following blocks:

- 'OpFromFile' reads values from the prepared .mat-file with the simulated electrical quantities and reproduces them in real time.
- 'Asynchronous send' sends data to an asynchronous external hardware (the interface converter in Fig.3.6).
- 'OpIPSocketCtrl' defines communication protocol for the sent data. In the given test setup, the TCP/IP protocol is used. The block requires remote IP address, local and port belonging to the converter.
- 'ML605EX1 AnalogIn' captures analogue input signals. For the given test setup, it is the tripping signal from the microprocessor.
- 'OpCtrl ML605EX' controls programming of one OPAL-RT ML605 card.

All blocks can be found in the 'RT-LAB' and 'RT-LAB I/O' library.

3.2.2.2 C-code generation for microprocessor programming

Programming of the microprocessor STM32F407VGT6 is done using C-code, which can be generated by the means of MATLAB/SIMULINK. It has an embedded coder and is fully compatible with the board. Fig.3.8 illustrates an example of a model for further C-code generation.

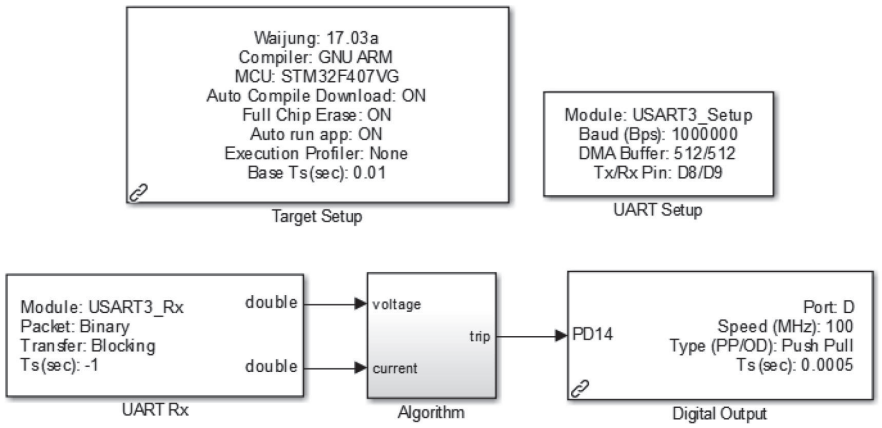

Figure 3.8: General view of the model for microprocessor programming.

The 'Target Setup' block specifies the embedded compiler, the microprocessor settings and uploading settings; 'UART Setup' block specifies settings of the serial interface USART realised on the board and connecting pins; 'UART Rx' block receives data (double format); 'Digital Output' block

sends a digital signal (0 or 3 V) to a specific pin (it is the tripping signal from the algorithm); 'Algorithm' subsystem contains calculation blocks according to a developed algorithm.

All blocks can be found in the pre-installed SIMULINK library 'Waijung Blockset' [141]. Code compilation in the MATLAB is accomplished with the standard embedded function *rtwbuild*.

3.2.3 Setup 3

The test setup in Fig.3.9 is used to test protection functions of commercially available products. This configuration is used in [Paper VI] for performance investigation of the standard steady-state method for earth fault location.

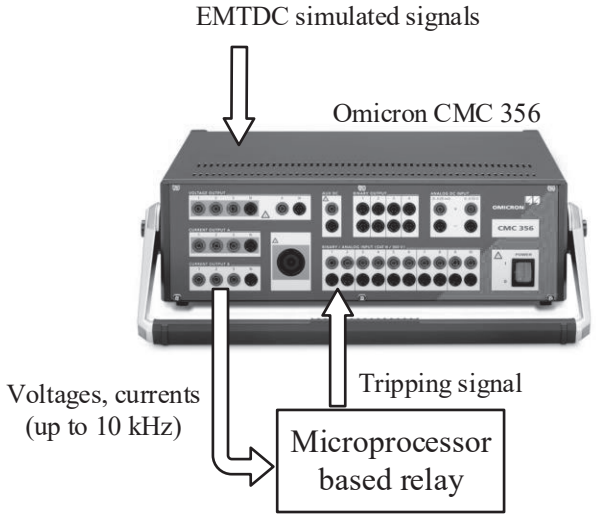

Figure 3.9: Test setup 3: tests of relay protection functions with reproduced fault records.

The test tool OMICRON [132] allows the play back of voltages and currents simulated in PSCAD/EMTDC with sampling frequencies of up to 10 kHz (maximum is 5 A and 250 V). Binary inputs are used to register tripping signals, and operation time of a relay can be measured.

3.2.4 Signal processing

For analysis and development of the protection algorithms and methods presented in the current PhD thesis, the approach depicted in Fig.3.10 is used.

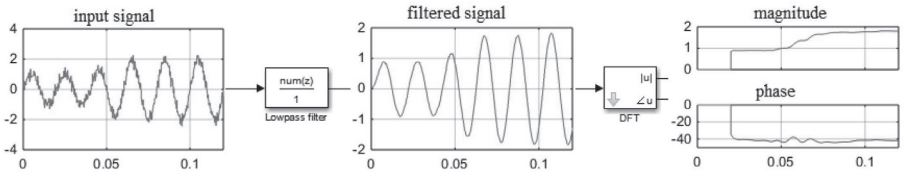

Figure 3.10: Algorithm for phasor extraction from instantaneous signal.

Firstly, a distorted periodic input signal (simulated in PSCAD/EMTDC samples) is exposed to a low-pass filter (cut-off frequency is 2 kHz). It is a discrete finite impulse response filter that is based on a feed-forward difference equation (computes a weighted finite term sum of past, present, and future values of the filter input) [142].

Secondly, the filtered signal is processed in the discrete Fourier transform block: it performs a Fourier analysis of the input signal over a constant sliding window of one cycle of the fundamental frequency of the signal (no frequency-tracking algorithms) [143]. The first main harmonic is typically utilised.

Finally, as a result, the input signal is decomposed into its magnitude (root mean square values) and phase (degree). Such 50-Hz-phasors are utilized substantially in the current work.

Chapter 4

Summary of research results and discussion

This chapter presents a summary of the major research results. Detailed analysis, discussions and other study outcomes are presented in the appended papers [Papers I–VI]. The current chapter also supplements the work presented in the papers providing additional analyses and discussions. Hence, it outlines: motivations for development of new protective methods, using simulations to demonstrate possible challenges for the existing relays; a theoretical base and numerical analyses of the presented algorithms and methods conducted for simple networks to provide explanations of their work flow; possible improvements, applications and other comments.

4.1 Protection challenges

Here, possible challenges for the existing protection in the actual network are shown. The network is secured against phase-to-phase faults by definite time overcurrent (OC) feeder relays with coordination time intervals (CTI) to achieve protection selectivity. Earth faults are detected with zero sequence overvoltage and OC functions of a ground relay, and zero sequence current direction is determined by its active component (i.e. $|\mathrm{I}_0|\cos(\phi_0)$ is measured, where ϕ_0 is an angle between zero sequence current I_0 and voltage U_0 phasors) for selective tripping.

Fault scenarios are simulated in PSCAD/EMTDC for the model described in section 3.1.

4.1.1 Impact of DG presence on feeder protection

This section studies the impact of the generators on OC feeder relays during high and low load in the system discussed in 3.1.3. Fig.4.1 illustrates

phase currents measured at substations (denoted as 'Subst' in the figure) 8, 12 and 13 during phase-to-phase fault with different resistances applied at the end of the feeder with the DG (next to point 13.1 in Fig.3.1). Plots show the ratio between maximum phase current $|I_p|$ and pick-up current I_{trip} of a feeder relay at this substation as a function of fault resistance.

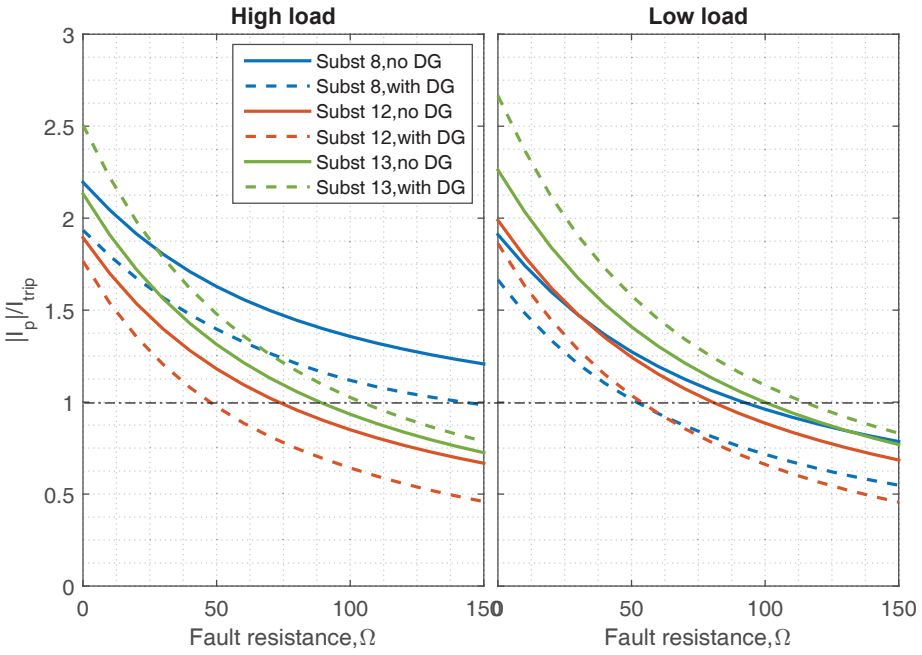

Figure 4.1: Simulated normalised phase currents at substations 8, 12 and 13 for different fault resistances with and without DG during phase-to-phase faults at the end of the DG feeder (point 13.1).

If the measured current is below settings (i.e. $|I_p|/I_{trip} < 1$), a feeder relay is blinded (fault is not detected). It is possible to see that for high or low load in the system, protection blinding does not occur for fault resistances below 50 Ohm (contact with an extraneous object [59]); however it is possible for higher values (expected value of arc resistance is 7.5 Ohm for the given fault level according to [58]). Comparing situations with DG and without, it can be observed that DG reduces fault current through substation 8 and 12 because protection blinding always starts for lower fault resistances if DG injects current (curve 'with DG' is under 'no DG'). The opposite is true for substation 13.

Fig.4.2 demonstrates the same analysis for smaller short circuit capacity of the utility grid (S_{SC} = 50 MVA, 250 MVA is the initial) and higher rated

power of the DG (S_{DG} = 4.4 MVA, 2.2 MVA is the initial). It is possible to see that the weak grid and high DG production leads to the same effect as above: fault current at substations 8 and 12 is reduced and protection blinding begins for lower fault impedances (curves with S_{SC} = 50 MVA and S_{DG} = 4.4 are under the initial solid). Moreover, the week grid has a bigger impact than the increased DG capacity (the dotted curves are above the dashed curves). For substation 13, the high DG capacity increases fault current and the week grid decreases.

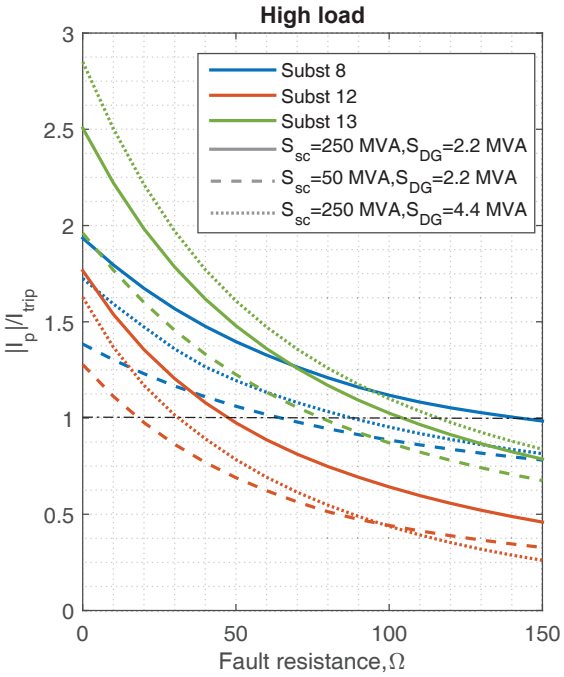

Figure 4.2: Simulated normalised phase currents at substations 8, 12 and 13 for different network short circuit and DG capacities during phase-to-phase faults at the end of the DG feeder (point 13.1).

Thus, DG changes fault current levels in the system (decrease for upstream substations and increase for downstream). As a result, OC protection misoperation can be observed; moreover, it might lead to problems with coordination between relays (and downstream fuses), that require higher CTI for upstream devices and, consequently, prolonged faults.

4.1.1.1 Sympathetic tripping

The feeder protection at point 8 (see Fig.3.1) is secured against sympathetic tripping during faults in the upper feeder (next to point 4.1) or

in the lower (point 14) by application of higher CTI than CTIs of relays at points 4 and 14. Nevertheless, sympathetic tripping of the DG feeder cannot happen for the given S_{SC} and S_{DG} and, therefore, study is omitted in the current work (thorough analysis can be found in [4]). Though unintentional islanding caused by upstream faults can take place in the actual network that is demonstrated below.

Fig.4.3 shows an analysis of this effect for fault at location close to point 8.2: protection at substation 12 cannot detect this fault (it is upstream) because $|I_p|/I_{trip} < 1$ for high load, but the ratio becomes closer to 1 for low fault resistances and, finally, exceeds 1 in the case of low load. In other words, the feeder relay at substation 12 can initiate tripping during upstream faults with DG presence.

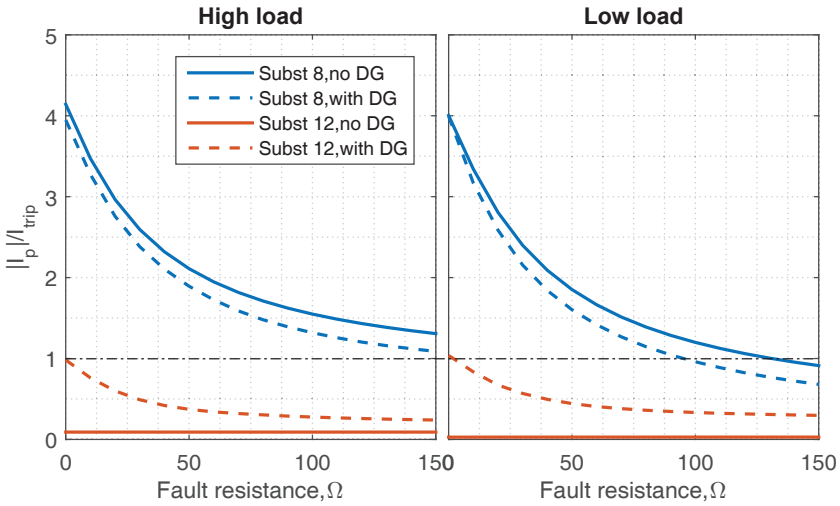

Figure 4.3: Sympathetic tripping effect at substation 12 with presence of DG during phase-to-phase faults upstream from DG and substation 12 but downstream from substation 8 (point 8.2).

Fig.4.4 demonstrates that this situation can happen even for high load and higher fault resistances if DG rated power is doubled ($S_{DG} = 4.4$ MVA, 2.2 MVA is the initial): the red dotted curve is above 1 for fault resistances 0-25 Ohm that means tripping at substation 12 during the upstream fault and formation of a healthy islanding.

Application of directional OC protection at substation 12 in order to resolve this issue might lead to unnecessary disconnection of the DG (because its undervoltage protection acts faster than the relay at substation 8), whereas it can be connected to the upper feeder during upstream faults.

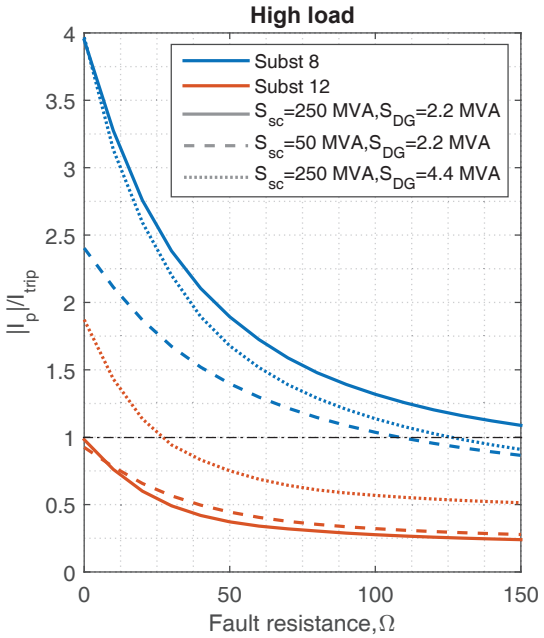

Figure 4.4: Sympathetic tripping effect at substation 12 for different network short circuits and DG capacities.

Without a directional relay, formation of a healthy islanding is possible and is undesirable in case of temporary faults.

4.1.2 Nuisance tripping of DG

Nuisance tripping of the DG implies unnecessary disconnection of the generator, typically by its undervoltage protection during fault in the system, faster than it is cleared by a local breaker (especially if fault location is in the adjacent feeders). Decrease of such instances is an important goal during network operation because of power supply reliability, stability and economic reasons.

Fig.4.5 demonstrates voltage dips (the minimum steady-state phase voltage in p.u. during faults) measured at the DG location during low-ohmic (7.5 Ohm) phase-to-phase faults in different locations ('S' stands for substation/measuring point, e.g. S4 denotes a fault in front of and close to measuring point 4 in Fig.3.1). The figure also shows the typical settings of DG undervoltage protection (the red horizontal lines) according to requirements [124]: if voltage falls below 50%, the tripping signal is initiated after 200 ms; if it is higher (but lower than 88%), then the time delay is 2 s.

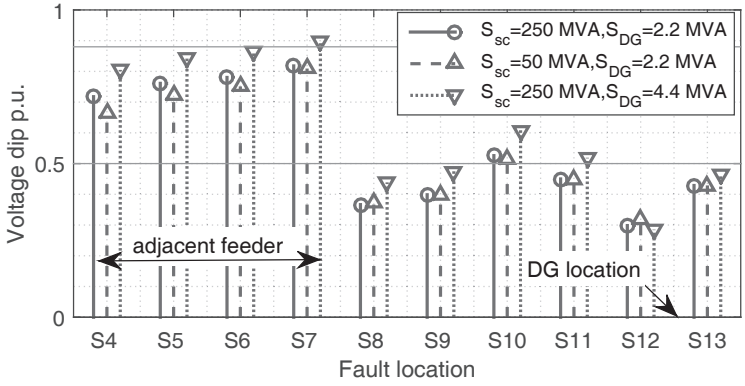

Figure 4.5: Voltage dips measured at DG during low-ohmic (7.5 Ohm) phase-to-phase faults at different locations in the network with high load.

As it is possible to see, there is a risk of accidental disconnection of the DG if fault clearance is delayed (by more than 200 ms) due to application of CTIs and breaking operations (typically about 5 cycles) at locations S9, S11 and S13, whereas these faults can be cleared by the local breakers and DG decoupling is unnecessary.

4.1.3 Disruption of ground fault protection

Problems with detection of earth faults with impedances up to 3 kOhm (Norwegian requirements for ground fault protection sensitivity [145]) have not been revealed for the actual network (zero sequence overvoltage function is utilised). The main approach to discriminate fault locations (a feeder/section selection task) in compensated systems, as mentioned above, is to measure an active component of zero sequence current, i.e. $|\mathrm{I}_0|\cos(\phi_0)$.

Fig.4.6 illustrates the ratio between $|\mathrm{I}_0|\cos(\phi_0)$ and the set pick-up active current component $\mathrm{I}_{0\text{a-trip}}$ at the corresponding substation for earth fault in the system at different locations ('Sm' means in front of and close to a specific measuring point 'm'). The ratio is measured for one specific high impedance (3 kOhm) fault location at different substations ('Subst') for comparison. A value of $\mathrm{I}_{0\text{a-trip}}$ is chosen to recognise 3 kOhm fault in the system with $k_r = 0.1$, $k_c = 0.05$ (coefficients of line resistive losses and capacitive asymmetry are discussed in 3.1.1).

The plot shows that earth current during a fault in front of measuring point 4 (S4) is correctly seen by the ground relay at substation 4 in the forward direction ($|\mathrm{I}_0|\cos(\phi_0)/\mathrm{I}_{0\text{a-trip}} > 1$). Similarly, S6 is correctly recognised by relays 4 and 6, S8 by relay 8, S9 by relays 8 and 9, S12 by relays 8 and 12 (see Fig.3.1). It can be seen that active current during faults at S4

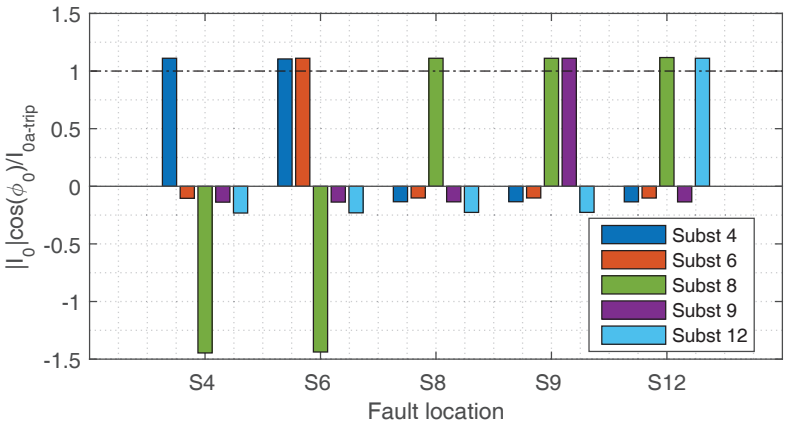

Figure 4.6: Normalised $|\mathrm{I_0}|\cos(\phi_0)$ measured at substations 4,6,8,9,12 during high impedance (3 kOhm) earth faults at different locations in the network with $k_r = 0.1$, $k_c = 0.05$.

or S6 exceeds the settings of the relay at substation 8 (greater than 1), but in the backward direction (the ratio is negative) and the tripping signal is not initiated (correct selective operation). In the other cases, the measured value is also negative and below the thresholds. Low-ohmic faults are not demonstrated because the ratio is much higher than 1.

As can be seen from Fig.4.6, recognition of fault current in correct direction is important for security and selective tripping because zero sequence current magnitude $|\mathrm{I_0}|$ is not a reliable indicator, especially if detection of high impedance faults (higher than 3 kOhm) is required (more sensitive settings).

Very often insufficient natural watt-metric contribution of the network can be present [144] (low phase-to-ground conductance typically appearing in dry/clean physical conditions). Fig.4.7 shows the same faults as before for the system with $k_r = 0.01$.

As can be seen in the figure, all measured $|\mathrm{I_0}|\cos(\phi_0)/\mathrm{I_{0a\text{-}trip}} < 1$. Moreover, earth current direction in a few cases is recognised as forward, whereas faults are behind the corresponding substations. The variable nature of natural active earth fault currents makes it difficult to find the correct settings for a ground relay. However, this situation is not observed for low-ohmic faults.

Besides variable nature of line conductances, electrostatic imbalance in the network can also vary. Fig.4.8 illustrates the same faults as above for the system with $k_r = 0.01$, $k_c = 0.1$. Strong capacitive asymmetry leads to

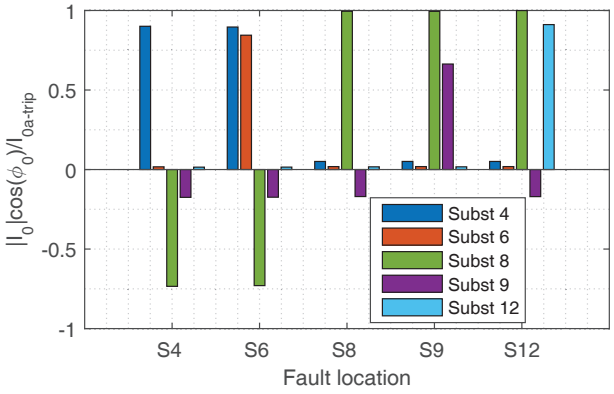

Figure 4.7: Impact of insufficient natural watt-metric contribution of the network ($k_r = 0.01$) on normalised $|\mathrm{I}_0|\cos(\phi_0)$.

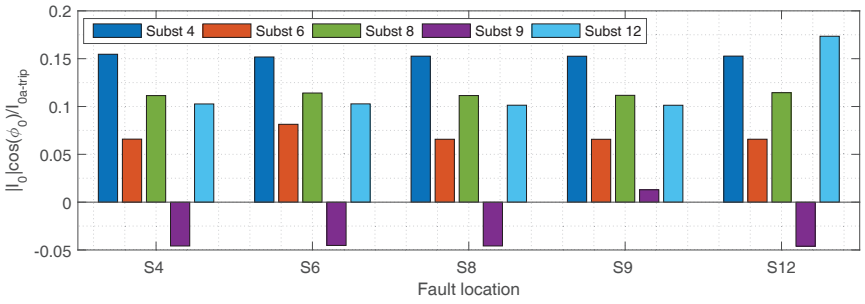

Figure 4.8: Impact of insufficient natural watt-metric contribution ($k_r = 0.01$) and strong capacitive asymmetry in the network ($k_c = 0.1$) on normalised $|\mathrm{I}_0|\cos(\phi_0)$.

larger overcompensation to avoid overvoltages on the neutral; therefore, suppressing coil current becomes 110 A. It is seen from the figure that directions of earth currents are now detected in forward directions regardless of fault location (except at substation 9); moreover, all ratios $|\mathrm{I}_0|\cos(\phi_0)/\mathrm{I}_{0\text{a-trip}}$ are high and comparable. This completely corrupts ground fault protection performance (the situation is better for low-ohmic faults).

Typically in practice, in order to improve performance of ground fault protection and to eliminate its dependency on variable network parameters, a parallel resistor is connected to the Petersen coil. The parallel resistor resolves these issues: Fig.4.9 demonstrates the same faults and measurements illustrated in Fig.4.7 and Fig.4.8 with application of a parallel resistor (value 530 Ohm is chosen according to the Norwegian requirements in [18]). In such a case, $|\mathrm{I}_0|\cos(\phi_0)$ is mainly determined by the value of the parallel resistor

(all faults are correctly recognised by the protection because $|\mathrm{I}_0|\cos(\phi_0)$ exceeds the settings and has the preset sign) and stays almost the same regardless of fault resistance, k_r or k_c.

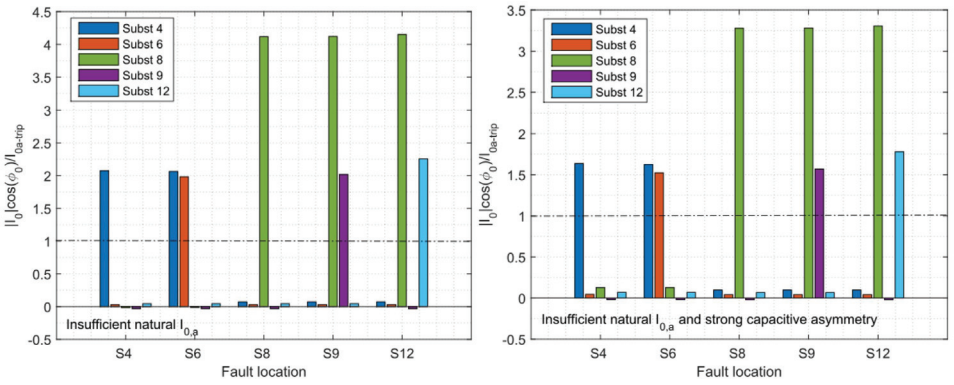

Figure 4.9: Normalised $|\mathrm{I}_0|\cos(\phi_0)$ measured with the parallel resistor in the network with insufficient natural watt-metric contribution ($\mathrm{I}_{0,\mathrm{a}}$) and strong capacitive asymmetry.

4.1.4 Summary

The presented examples of phase-to-phase faults show a motivation for the application of impedance protection in the distribution network with the DG since its operation principle does not depend on fault current level in the system; moreover, it has inherent directional capability.

Additionally, a measured impedance can provide information about fault location. It is an advantage for minimisation of the restoration time and, with respect to the DG, for discrimination of far-end faults to prevent nuisance tripping of the generator.

A study dedicated to the feasibility of impedance relaying in the current network and its application for assistance of DG undervoltage protection is presented in [Paper I].

The illustrated issues for earth fault location and the remedial measure indicate the dependency of ground protection on additional equipment (a parallel resistor). Normally, the Petersen coil is used alone to suppress capacitive current and to decrease overall fault current to make an arc self-extinguishing. If the fault is persistent, a parallel resistor is connected to facilitate a location procedure. Such operations require time and lead to fault current increase (and touch voltage that corrupts safety), as well as decrease of zero sequence voltage that requires smaller settings (might cause

insecure operations). Furthermore, its connection can fail because of actuators that can considerably deteriorate ground fault protection performance.

These disadvantages serve as a motivation for development of new earth fault location indicators which do not depend on additional equipment. Speed is especially important in the case of DG presence: if the fault is in a zone implying DG disconnection (e.g. S12), its location must be identified in a fast manner in order to disconnect the generator and initiate a reclosing procedure (in which case rapid anti-islanding protection is not required); if fault is outside such a zone (e.g. S9), nuisance tripping of the generator can be prevented (clearing time might exceed seconds with the standard approach).

Studies dedicated to the development of such indicators are presented in [Papers V,VI]. They introduce two different approaches: two-end (communication assisted) and one-end (transient-based).

4.2 Impedance relaying in distribution networks with DG

4.2.1 Implementation [Paper I]

The paper demonstrates the feasibility of distance protection (without involvement of telecommunication) to solve potential problems illustrated in section 4.1. For calculation of relay settings, the same approach is used as for transmission systems. The standard quadrilateral tripping zones are better to utilise for feeder relays to avoid the underreaching caused by arc resistance. Additionally, using CTI for Zone 1 for coordination with downstream devices is proposed: fuses and relays in the lateral branches. *Fig.3c* (hereafter, italicised font denotes figures or tables in the enclosed papers) shows DG impact: infeed current increases the reactive part of the impedance measured on the feeder (especially for ground faults) causing relay underreach. *Fig.6a* illustrates that faults in the side branch with its own relay (the adjacent protection zone) can cause nonselective tripping of the main feeder if CTI is not applied. Finally, impedance measurements can be used to discriminate faults. *Fig.5a* demonstrates that impedance loci (measured at DG location) of faults in the adjacent feeder do not fall into Zone 1 or 2. This can help to prevent nuisance tripping of the generators.

The main issues revealed in the paper are as follows: 1) application of impedance relays for ground faults is not reliable. For example, *Fig.6b* shows that the feeder relay cannot distinguish ground faults during high load in the system because all impedance loci are in Zone 1 regardless of fault location (relay overreach). The reason of this selectivity loss is significant

impact of load currents on impedance measurements (in contrast, the low load case, illustrated in *Fig.6c*, leads to better selectivity; 2) non-zero fault impedances and strong remote infeed currents lead to relay underreach. *Fig.4a* demonstrates that impedance measured at DG location has a big error during fault on the feeder and, consequently, generator relay blinding occurs due to arc resistance and large current from the utility grid.

4.2.2 Method for impedance error compensation [Paper II]

The previous paper indicated the negative influence of non-zero fault impedance and remote infeed currents on impedance measurements. The current paper proposes a method for eliminating these issues. It consists of two approaches: 1) two-point measurements are required to compensate for the impact of fault impedance in a passive network. This is referred to as the equivalent line approach because the network is wrapped into a line with lumped parameters (such an approach is valid for short lines in distribution networks); 2) multi-point measurements are utilised to compensate both fault impedance and adverse effects from remote infeed currents in an active network. This approach is called as the equivalent network because the actual network is wrapped into several equivalent lines. The required measurements are differences of current and voltage phasors in affected phases. The paper develops the method for synchronised measurements and it is tested for non-synchronised measurements in [Paper III] (impact of communication network imperfections).

A simple numerical analysis of the method providing reasoning and details is presented below since it is omitted in the paper.

4.2.3 Numerical analysis of the method

4.2.3.1 Equivalent line approach

Fig.4.10 shows a simple network for the analysis of two cases: network (a) represents a situation where load impedance Z_L is not present in the loop of impedance calculation taking place at node 2; network (b) represents the opposite situation - load impedance is present in the loop. In both cases, fault impedance Z_f splits a line such that the impedance of each part can be expressed through parameter k and line impedance Z_1 or Z_2. The utility grid is presented as an ideal voltage source E_g with internal reactance x_g, and remote infeed current from DG is an ideal current source I_{dg}.

In order to apply the equivalent line approach for impedance calculation at node 2 and to compensate Z_f and I_{dg}, voltages at nodes 2, 5 and grid current I_g must be found. To find the solution, the node-voltage method

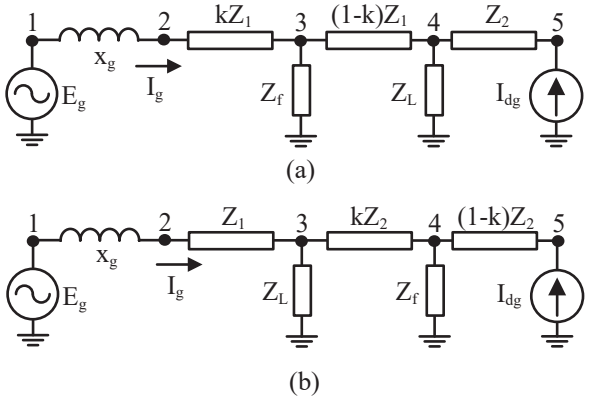

Figure 4.10: Network for equivalent line approach analysis with load impedance (a) out of the measuring loop and (b) in the loop.

is used – it allows the researcher to write the following matrix equation for networks (a) and (b):

$$\begin{bmatrix} Y_{11} & -Y_{12} & 0 & 0 & 0 \\ -Y_{12} & Y_{22} & -Y_{23} & 0 & 0 \\ 0 & -Y_{23} & Y_{33} & -Y_{34} & 0 \\ 0 & 0 & -Y_{34} & Y_{44} & -Y_{45} \\ 0 & 0 & 0 & -Y_{45} & Y_{55} \end{bmatrix} \begin{bmatrix} \mathrm{E_g} \\ V_2 \\ V_3 \\ V_4 \\ V_5 \end{bmatrix} = \begin{bmatrix} \mathrm{I_g} \\ 0 \\ 0 \\ 0 \\ \mathrm{I_{dg}} \end{bmatrix}, \tag{4.1}$$

where vector of nodal voltages $[V_2\ V_3\ V_4\ V_5]^T$ are unknown, and the elements of the nodal admittance matrix for networks (a) and (b) are:

$$\text{(a)} \begin{cases} Y_{12} = 1/(j\mathrm{x_g}) \\ Y_{23} = 1/(\mathrm{kZ_1}) \\ Y_{34} = 1/((1-\mathrm{k})\mathrm{Z_1}) \\ Y_{45} = 1/\mathrm{Z_2} \\ Y_{11} = Y_{12} \\ Y_{22} = Y_{12} + Y_{23} \\ Y_{33} = Y_{23} + Y_{34} + 1/\mathrm{Z_f} \\ Y_{44} = Y_{34} + Y_{45} + 1/\mathrm{Z_L} \\ Y_{55} = Y_{45} \end{cases} \qquad \text{(b)} \begin{cases} Y_{12} = 1/(j\mathrm{x_g}) \\ Y_{23} = 1/\mathrm{Z_1} \\ Y_{34} = 1/\mathrm{kZ_2} \\ Y_{45} = 1/((1-\mathrm{k})\mathrm{Z_2}) \\ Y_{11} = Y_{12} \\ Y_{22} = Y_{12} + Y_{23} \\ Y_{33} = Y_{23} + Y_{34} + 1/\mathrm{Z_L} \\ Y_{44} = Y_{34} + Y_{45} + 1/\mathrm{Z_f} \\ Y_{55} = Y_{45} \end{cases} \tag{4.2}$$

For numerical analysis, the following parameters are used: $E_g = 12.7$ kV, $x_g = 17.3\ \Omega$, $Z_1 = Z_2 = (1+j)\ \Omega$, k = 0.5, $Z_L = 100e^{j\pi/18}$ (high load), $Z_L = 200e^{j\pi/18}$ (low load), $I_{dg} = 0.25$ MVA/12.7 kV or $I_{dg} = 0.5$ MVA/12.7 kV.

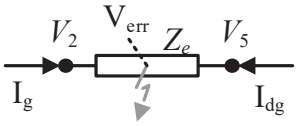

Figure 4.11: Equivalent line replacing passive network with fault.

According to the equivalent line approach in [Paper II], both networks in Fig.4.10 are replaced by an equivalent line Fig.4.11 and the following steps are accomplished: 1) equation (4.1) is solved for $Z_f = \infty$ (pre-fault conditions); 2) equivalent impedance is calculated as

$$Z_e = \frac{V_2 - V_5}{I_g}; \tag{4.3}$$

3) equation (4.1) is solved for $Z_f \neq \infty$ (fault conditions); 4) voltage error is calculated as

$$V_{err} = \frac{V_2 I_{dg} + V_5 I_g - Z_e I_{dg} I_g}{I_{dg} + I_g}; \tag{4.4}$$

5) compensated impedance is calculated as

$$Z_{cps} = \frac{V_2 - V_{err}}{I_g}. \tag{4.5}$$

The computed compensated impedance Z_{cps} can be compared with the actual impedance from node 2 to the fault: network (a) – $Z_{act} = kZ_1$; network (b) – $Z_{act} = Z_1 + kZ_2$. Fig.4.12 presents relative error (a real and imaginary part) computed for different fault resistances in the range 0.1-100 Ohm as

$$\frac{\text{real}(Z_{cps} - Z_{act})}{\text{real}(Z_{act})} \cdot 100\% \text{ and } \frac{\text{imag}(Z_{cps} - Z_{act})}{\text{imag}(Z_{act})} \cdot 100\% \tag{4.6}$$

As can be seen from the plots for network (a) (Z_L out of loop, the solid curves), the real part of the error is positive, indicating relay underreach. For network (b) (Z_L in loop, the solid curves), the real and imaginary parts of the error are negative, indicating relay overreach. In both cases, the errors are increased if the fault impedance rises. The method does not

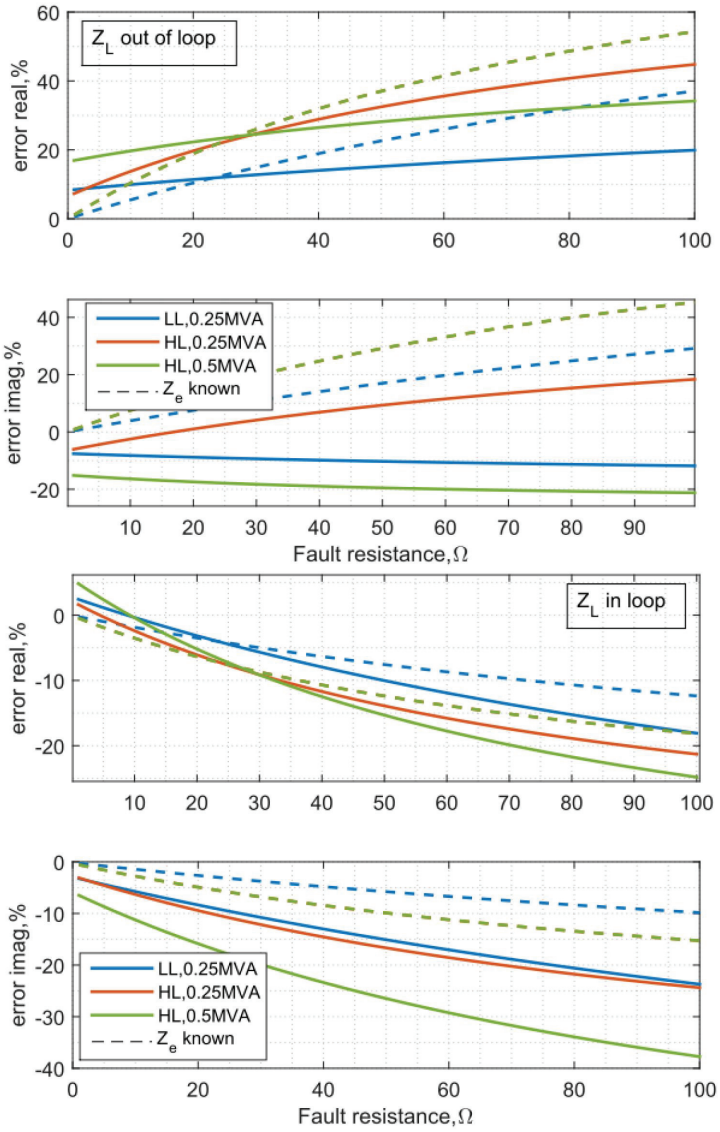

Figure 4.12: Fault location errors for equivalent line approach application for different fault resistances, load impedance and DG capacity.

fully compensate load currents using pre-fault measurements; therefore, the absolute errors for high load (HL) are bigger than for low load (LL). Increase of DG production also leads to error rise in general.

The compensation can also be accomplished for the known equivalent

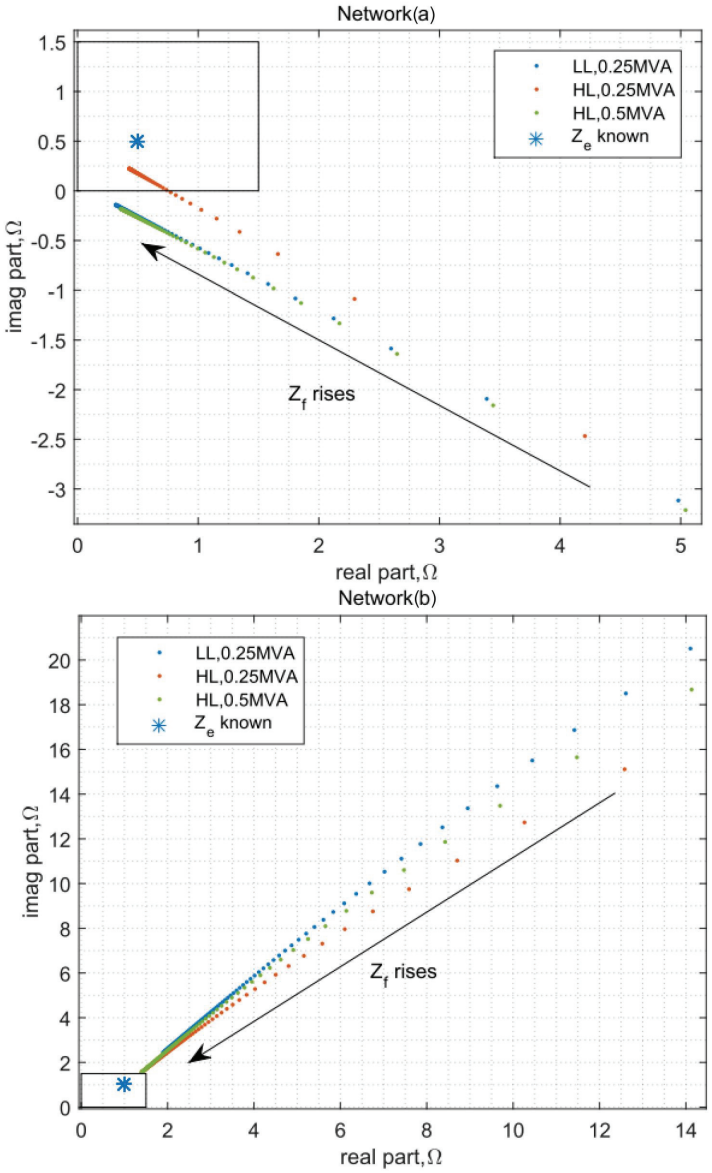

Figure 4.13: Compensated impedances calculated using the equivalent line approach and different fault resistances taking place outside of the monitoring zone.

impedance calculated using the line impedances as $Z_e = \mathrm{Z}_1 + \mathrm{Z}_2$ instead of pre-fault measurements as above. The dashed curves in Fig.4.12 ('Z_e known') demonstrate the errors calculated for this case. It can be seen that

in such a case the difference is not significant, but the known Z_e leads to better precision for network (b). Moreover, the errors do not depend on I_{dg} (the dashed red and green curves coincide). Nevertheless, application of Z_e based on line impedances does not always give positive effect (e.g. network (a) and forthcoming examples), therefore the method always uses measurements that make it universal (free from topology).

It is worth noting that errors without compensation can exceed 1000% in this analysis and are not presented. In the next analyses, the situation with Z_L out of loop is not considered since a path from a measuring point to a fault in a distribution network normally includes load outfeeds.

Fig.4.13 illustrates Z_{cps} in the impedance plane for a situation where Z_f is out of the monitoring zone: in network (a) measurements of nodes 3 and 5 are taken for calculations; in network (b) – nodes 2 and 4. It is seen from the plots that with the increase of fault impedance, Z_{cps} falls into the tripping region (the black rectangle reflects actual line impedance). If Z_e is calculated on the basis of the known line impedances, Z_{cps} is inside the tripping region irrespective of the fault impedance. Since false tripping might occur, utilisation of only pre-fault measurements for Z_e calculations is more secure (it is an additional reason to what is specified above).

In order to avoid initialisation of the compensation and, consequently, to improve security, [Paper III] proposes using three criteria: 1) a measured impedance falls below a certain threshold; 2) falling rate is high; 3) fault current has forward direction.

4.2.3.2 Equivalent network approach

Fig.4.14 demonstrates two simple networks for analysis of the equivalent network approach. Here, the monitoring zone is bounded by nodes 2 and 5, and infeed current is injected at node 6 (an additional measuring point). Network (a) presents a situation where the DG is not included in the faulty loop, and network (b) presents the opposite situation. Impedance measurements take place at node 2 and are affected in advance by the load. An additional line appears in these networks (with variable Z_3), connecting the DG to the main trunk.

A matrix equation similar to (4.1) can be written for these networks and solved to find voltages and currents at nodes 2, 5 and 6 required for the equivalent network approach (a particular case for one infeed source) described in [Paper II]. Both networks in Fig.4.14 are replaced by two equivalent lines Fig.4.15 and the following steps are accomplished: 1) a derived equation (not shown here) is solved for $Z_f = \infty$ and impedances of two equivalent

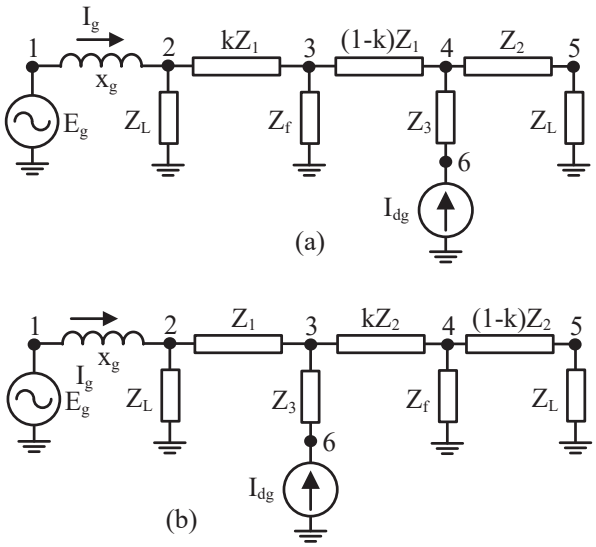

Figure 4.14: System for equivalent network approach analysis with DG a) out of the measuring loop, b) in the loop.

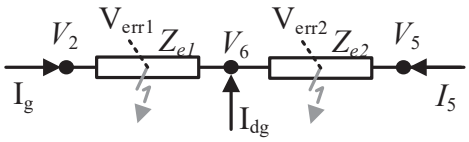

Figure 4.15: Two equivalent lines replacing active network with fault.

lines are calculated as

$$Z_{e1} = \frac{V_2 - V_6}{\mathrm{I_g}} \text{ and } Z_{e2} = \frac{V_5 - V_6}{I_5}, \tag{4.7}$$

where

$$I_5 = -\frac{V_5}{\mathrm{Z_L}}; \tag{4.8}$$

2) solution for $\mathrm{Z_f} \neq \infty$ is found and voltage errors are calculated as

$$\mathrm{V_{err1}} = \frac{V_2(\mathrm{I_{dg}} + I_5) + V_6\mathrm{I_g} - Z_{e1}(\mathrm{I_{dg}} + I_5)\mathrm{I_g}}{\mathrm{I_{dg}} + I_5 + \mathrm{I_g}}, \tag{4.9}$$

$$\mathrm{V_{err2}} = \frac{V_5(\mathrm{I_{dg}} + \mathrm{I_g}) + V_6\mathrm{I_5} - Z_{e2}(\mathrm{I_{dg}} + \mathrm{I_g})I_5}{\mathrm{I_{dg}} + I_5 + \mathrm{I_g}}; \tag{4.10}$$

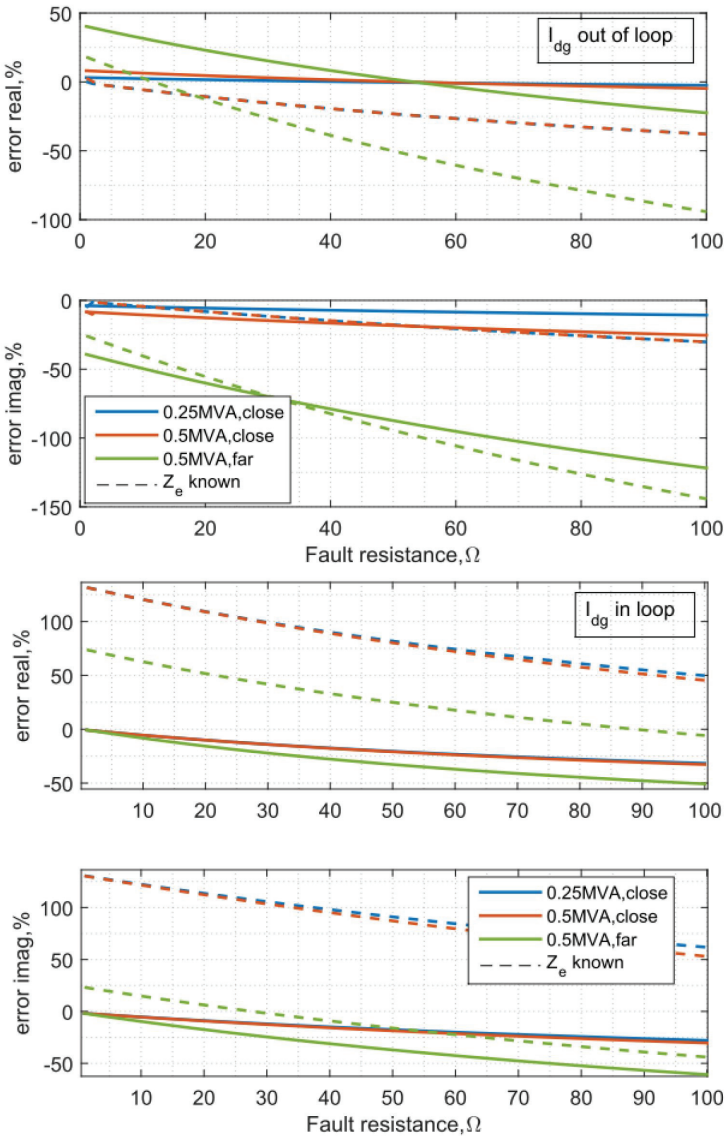

Figure 4.16: Fault location errors for equivalent network approach application for different fault resistances, DG capacity and its location.

3) a voltage drop on equivalent line Z_{e1} caused by infeed current is $\mathrm{V_{DG1}} = 0$, and on Z_{e2} is

$$\mathrm{V_{DG2}} = V_6 - \mathrm{V_{err2}} - \frac{\mathrm{I_g}}{I_5}(\mathrm{V_{err2}} - V_5 + I_5 Z_{e2}); \tag{4.11}$$

4) Equitation (4.5) is also used to calculate the compensated impedance Z_{cps}, where voltage error is determined as the minimum between $V_{err1} + V_{DG1}$ and $V_{err2} + V_{DG2}$, that is

$$V_{err} = \min[V_{err1} + V_{DG1},\ V_{err2} + V_{DG2}]. \tag{4.12}$$

Such selection conditions, firstly, allow the method to avoid large overreaching errors during compensation, and secondly, it determines a correct faulty equivalent line. In these exemplary networks, one infeed current source is present, dividing the network into two equivalent lines; [Paper II] describes a general case with several sources.

For numerical analysis, the same parameters as in the previous case are used and $Z_L = 200e^{j\pi/18}$, and Z_3 is 1% (close DG location) and 200% (the DG is located far from the main trunk) of Z_1.

Fig.4.16 demonstrates errors (calculated using the same expressions (4.6)) for actual impedances $Z_{act} = kZ_1$ in network (a) and $Z_{act} = Z_1 + kZ_2$ in network (b). For comparison, known equivalent impedances are determined as $Z_{e1} = Z_1 + Z_3$, $Z_{e2} = Z_2 + Z_3$.

As can be seen from Fig.4.16, the errors are mainly negative (overreaching due to Z_L in the loop) and are increased with fault impedance rise as in the previous analysis. The impact of DG production is not significant if it is located close to the main trunk; however, it is significant for distant location (especially for network (a)). Additionally, it is seen that the known equivalent impedances lead to the biggest errors (underreaching for network (b), overreaching for network (a)). Thus, performance of the approach for fault location is better for short DG connecting lines (seen from the results presented in [Paper III]).

As in the previous analysis, errors without compensation are much higher. Analysis of a situation where fault impedance is out of the monitoring zone is not presented because its results are similar to previous results.

4.2.3.3 Fault in side branch

Fig.4.17 illustrates faults in side branches: network a is used for analysis of the equivalent line approach (measuring points 2 and 4), network b - for the equivalent network approach (measuring points 2, 4 and 5). Fig.4.18 presents calculated fault location errors in these networks applying the approaches. All parameters are as specified above.

Here, $Z_{act} = Z_1 + Z_3$ ($Z_1 = Z_2 = Z_3$) for network a and $Z_{act} = Z_1 + Z_4$ ($Z_1 = Z_2 = Z_4$, Z_3 is varied) for network b. For comparison, curves for $Z_{act} = Z_1$ are also given, reflecting a distance to outfeed point 3.

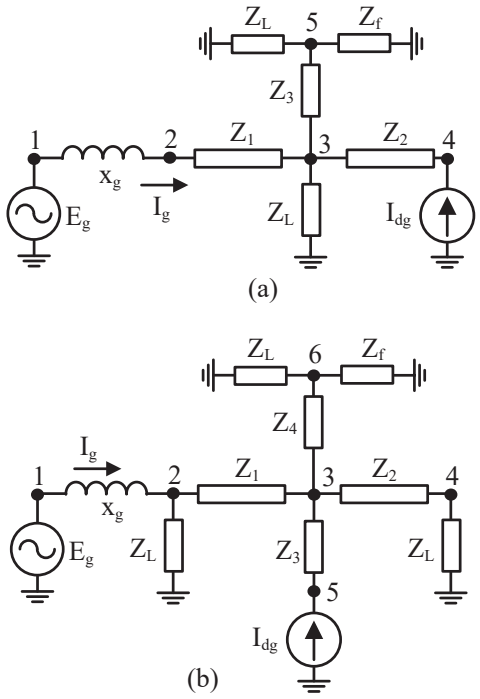

Figure 4.17: Systems with fault in side branches for equivalent line (a) and network (b) approach analysis.

As can be seen, in both cases, the fault is seen as if it is located in node 3 because the errors are about -50%; therefore, $Z_{act} = Z_1$ leads to better precision (the dashed curves).

This is the special peculiarity of the presented approaches that requires additional measurements in side branches for accurate fault location. Hence, in order to determine fault location correctly when faced with multiple measuring points, the maximum among all provided compensated impedances (corresponds to a number of measuring points) is selected because it gives higher accuracy (seen from Table I in [Paper II], and thoroughly analysed in [Paper III]).

4.2.4 PSCAD/EMTDC tests of the method [Paper II]

The paper presents tests of the compensation method using fault records (three-phase high impedance faults) obtained with the help of the PSCAD/EMTDC model described in section 3.1. *Fig.4b* shows the results of an equivalent line approach application (the feeder without DG). It demonstrates that faults at the end of the feeder can be recognised on the in-

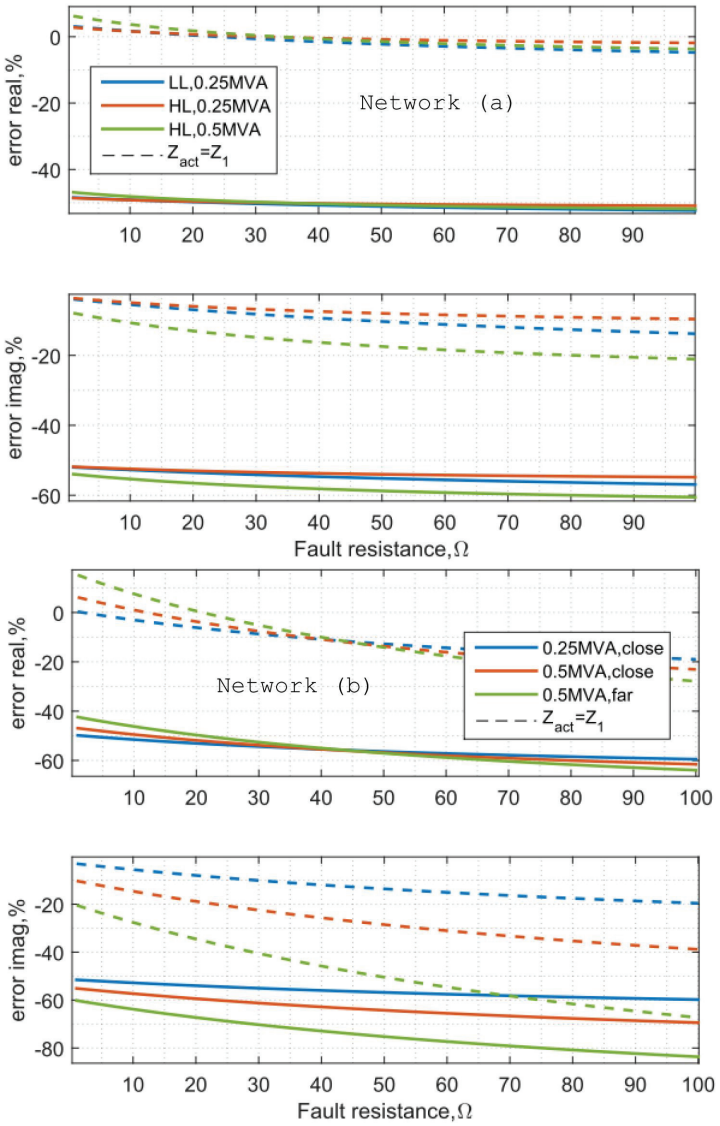

Figure 4.18: Fault location errors for equivalent line and network approach application for different fault resistances in side branch.

tersection point of the side branch and the feeder if measurements of the relay in the side branch are utilised for compensation (the issue is discussed in 4.2.3.3). In contrast, if the relay on the feeder is used, fault location is correctly determined. Calculation errors in this case are negligible (the compensated impedance coincides with the actual). *Fig.6* illustrates that

impedance errors for equivalent network approach application are more considerable due to load currents and the distant DG location. As was discussed in 4.2.3.2, these errors are negative; therefore, the relay overreaches. At the same time, the fault in the side branch has the compensated impedance such that it is recognised at a closer location than it really is (due to the issues discussed in 4.2.3.3). *Fig.8* illustrates that fault location precision becomes better if measurements of the relays closer to the DG are utilised. Finally, compensation of impedance measurements during faults taking place outside the primary protection zone does not provoke unintentional tripping (discussed in 4.2.3.1). *Fig.7* shows that impedance loci do not fall into Zone 1 in case of faults in the adjacent feeder or other remote locations. As can be seen, the presented study is in agreement with the analysis in section 4.2.3.

4.2.5 Laboratory verification of the method [Paper III]

[Paper III] studies the performance of the method for more complex fault scenarios (phase-to-phase, low-ohmic and high impedance faults in presence of load imbalance) in laboratory conditions (hardware-in-the-loop tests of the impedance relay with setting of two tripping zones). The test method uses the Monte Carlo approach [147] to calculate the dependability of an impedance relay with the compensation method.

Firstly, the method is tested for communication links without significant distortions (known latencies are compensated during calculations, no data losses). *Table II* shows dependability indices for tests of the equivalent network approach. It significantly improves the dependability of the relay, especially for high impedance faults. Nevertheless, Zone 1 misses few faults due to impedance errors. They are demonstrated in *Fig.7* in terms of fault location errors. The analysis mainly shows that faults in the side branch are detected with large negative impedance errors (they are identified as being closer to the relay than they really are), but then relay dependability is high. Moreover, unbalanced load currents and DG remoteness lead to a deterioration of precision. *Table III* demonstrates dependability indices for the equivalent line approach and *Fig.8* illustrates fault location errors. Here, the same outcome associated with the side branch is valid. Thus, the presented results are confirmed by the analysis in section 4.2.3.

The compensation method preserves impedance-based fault location capability and it is an advantage compared to differential protection (it also uses multi-point measurements). Comparing fault location errors, it is possible to see that the equivalent line approach demonstrates better precision than the equivalent network approach. Finally, to improve

security, a blocking logic for the compensation is proposed when fault is out of the zone under protection.

Due to the inherent overreaching error of the method, loads and DG location do not have a negative impact on relay dependability, unlike the communication network impairments. *Tables IV, V, VI* demonstrate test results with applied jitters and data losses in communication links. The main conclusion is that such impairments significantly deteriorate the dependability of both approaches, and to a lesser degree, of the equivalent line approach because it requires only one link with DG.

Finally, impact of background traffic is tested (channel bandwidth is occupied by other data): it leads to an increase of communication latencies and packet losses with the same consequences for protection as previously described.

4.3 Earth fault location in compensated systems

4.3.1 Theoretical approach for transient and steady-state analysis [Papers IV,VI]

Theoretical calculation of steady-state zero sequence currents and voltages during earth faults in the system is used for finding/checking ground relay settings, assessment sensitivity, protection malfunction and other analyses. It is presented in [Paper IV], as well as in the presented literature, e.g. [67, 110]. At the same time, the developed low-frequency-transient-based methods might require their own theoretical approach for the same purposes to obtain transient signals without simulations in an EMTP (electromagnetic transient program) software; however, such approach is not present in the literature.

The current section demonstrates the validity of the theoretical approach based on the solution of differential equations compared to results with PSCAD/EMTDC simulations. It is briefly presented in [Paper IV] for a three-phase system (analysed below) and in [Paper VI] for a system decomposed into positive, negative and zero sequence networks (not inspected because, as will be shown, decomposition is not necessary and complicates analysis).

Fig.4.19 shows an equivalent scheme that can model the faulty feeder/section (denoted with 'f') and the background healthy network (denoted with 'h'). This model neglects series impedances of lines (as well as effects of mutual couplings between phases) since they are typically much less than the shunt parameters; therefore, the fault location is not important for the analysis. For networks with large cable sections, it must be revised because such an assumption is not valid anymore. The earth

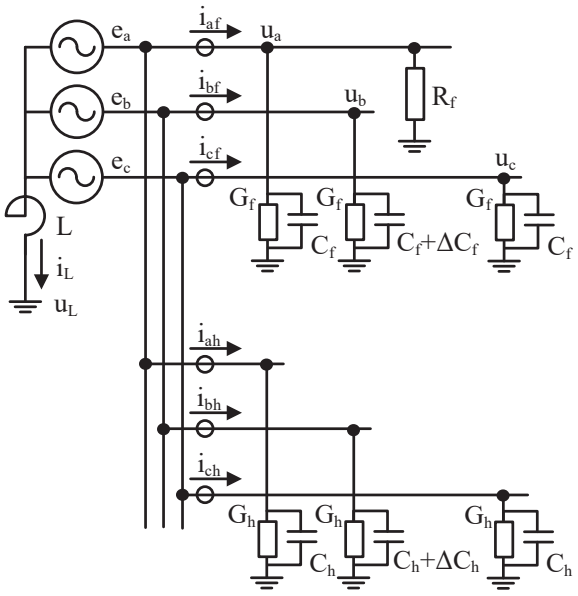

Figure 4.19: Network for earth fault transient analysis.

fault with resistance R_f occurs in phase a. Electrostatic asymmetry takes place in phase b. For the given network, the following system of equations can be written:

$$\begin{cases} i_{af} = u_a G_f + C_f \frac{du_a}{dt} + u_a/R_f \\ i_{bf} = u_b G_f + (C_f + \Delta C_f) \frac{du_b}{dt} \\ i_{cf} = u_c G_f + C_f \frac{du_c}{dt} \\ i_{ah} = u_a G_h + C_h \frac{du_a}{dt} \\ i_{bh} = u_b G_h + (C_h + \Delta C_h) \frac{du_b}{dt} \\ i_{ch} = u_c G_h + C_h \frac{du_c}{dt} \\ i_{af} + i_{bf} + i_{cf} + i_{ah} + i_{bh} + i_{ch} + i_L = 0 \\ u_L = L \frac{di_L}{dt} \\ e_a = u_a - u_L \\ e_b = u_b - u_L \\ e_c = u_c - u_L \end{cases} \tag{4.13}$$

where i_{af} is the instantaneous current in phase a of the faulty feeder/section; similarly i_{bf} and i_{cf} are the instantaneous currents in phases

b and c; analogously, i_{ah}, i_{bh}, i_{ch} are the phase currents in the background healthy network; u_a, u_b, u_c are the instantaneous voltages at the common busbar; G_f, C_f are the shunt conductances and capacitances respectively of each phase in the faulty feeder/section, and capacitive imbalance is expressed through ΔC_f; analogously, parameters G_h, C_h, ΔC_h are used to describe the background healthy network; i_L and u_L are the instantaneous current and voltage correspondingly in the Petersen coil with inductance L; the network is supplied by the ideal symmetrical voltage source with phase voltages e_a, e_b, e_c. Time is t.

$u_0 = u_L$ since

$$e_a + e_b + e_c = u_a + u_b + u_c - 3u_L = 3u_0 - 3u_L = 0 \tag{4.14}$$

Zero sequence currents in each part of the network (i_{0f} in the faulty feeder/section and i_{0b} in the background healthy network) can be found as follows:

$$\begin{aligned} 3i_{0f} &= i_{af} + i_{bf} + i_{bf} = \\ G_f(u_a + u_b + u_c) + C_f\frac{d(u_a + u_b + u_c)}{dt} &+ \Delta C_f\frac{du_b}{dt} + \frac{u_a}{R_f} = \\ 3G_f u_0 + 3C_f\frac{du_0}{dt} &+ \Delta C_f\frac{d(e_b + u_0)}{dt} + \frac{e_a + u_0}{R_f} \end{aligned} \tag{4.15}$$

$$3i_{0h} = 3G_h u_0 + 3C_h\frac{du_0}{dt} + \Delta C_h\frac{d(e_b + u_0)}{dt} \tag{4.16}$$

Having zero sequence current in the faulty feeder and in the background healthy network, it is possible to determine coil current as

$$i_L = -3i_{0f} - 3i_{0h}, \tag{4.17}$$

allowing u_0 to be calculated as $u_0 = u_L$.

The described solution approach is accomplished numerically with the help of the MATLAB solver, utilising the Runge-Kutta method [146] with the time step equal to 0.1 ms. The model of the solver is demonstrated in Fig.4.20. The inputs are the network parameters, the fault resistance and a fault inception time. The outputs are instantaneous zero sequence voltage (tag 2) and current in the faulty (tag 1) feeder/section utilised for dependability (the fault in front of a measuring point) analysis of a protection transient method. In this model, capacitive imbalance is calculated through coefficients and shunt capacitances:

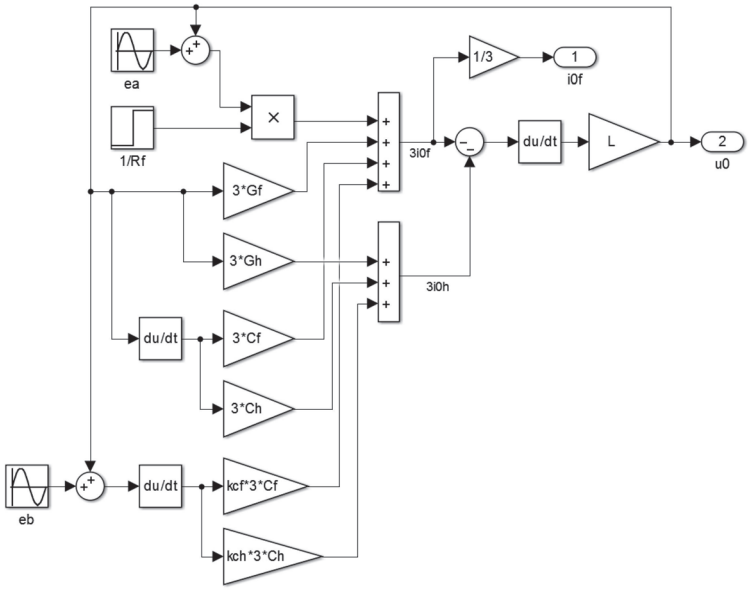

Figure 4.20: Model of the earth fault transient analysis solver.

$$\Delta C_f = 3k_{cf}C_f \tag{4.18}$$

$$\Delta C_h = 3k_{ch}C_h \tag{4.19}$$

The same approach can also be used for security analysis when the fault is behind the measuring point (in the background healthy network). In this case, phase current i_a in the faulty and healthy feeders is rewritten in system (4.13) as follows:

$$i_{af} = u_a G_f + C_f \frac{du_a}{dt} \tag{4.20}$$

$$i_{ah} = u_a G_h + C_h \frac{du_a}{dt} + \frac{u_a}{R_f}, \tag{4.21}$$

and the solver in Fig.4.20 is modified correspondingly (now $3i_{0h}$ contains the faulty component $(e_a + u_0)/R_f$).

The described approach is verified comparing i_{0f} and u_0 obtained with the help of the solver and PSCAD/EMTDC. As an example, fault records of relay 4 during earth faults at locations 4.1 and 8.1 in the network in Fig.3.1 are taken from PSCAD/EMTDC simulations. Since simulations are used as

a reference point, the network parameters required for the solver must also be given for the model. Their calculation using the known model parameters given in section 3.1 is complicated; therefore, calculation from fault records is utilised. The approach is described in Appendix A. Moreover, this approach can be used for a real system when network parameters are generally unknown, but fault records are available. The solver parameters used in the current example are: $G_f = 8.2\ \mu S$, $C_f = 0.7\ \mu F$, $G_h = 97.5\ \mu S$, $C_h = 7\ \mu F$, $k_{cf} = 0.0178$, $k_{ch} = 0.0029$. L has the same value as used during PSCAD/EMTDC simulations, 0.4492 H. The source has $e_a = 18\sin(100\pi t)$ kV, $e_b = 18\sin(100\pi t - 2\pi/3)$ kV (adjustable to obtain more precise results if needed).

Fig.4.21 shows the phasor magnitude of zero sequence current $|I_{0f}|$ (measured by relay 4), voltage $|U_0|$ (at busbar B2) and cosine of the angle between them $\cos(\phi_0)$ for low-ohmic fault (10 Ohm) in front of and behind relay 4. Signals are processed according to the approach presented in section 3.2.4.

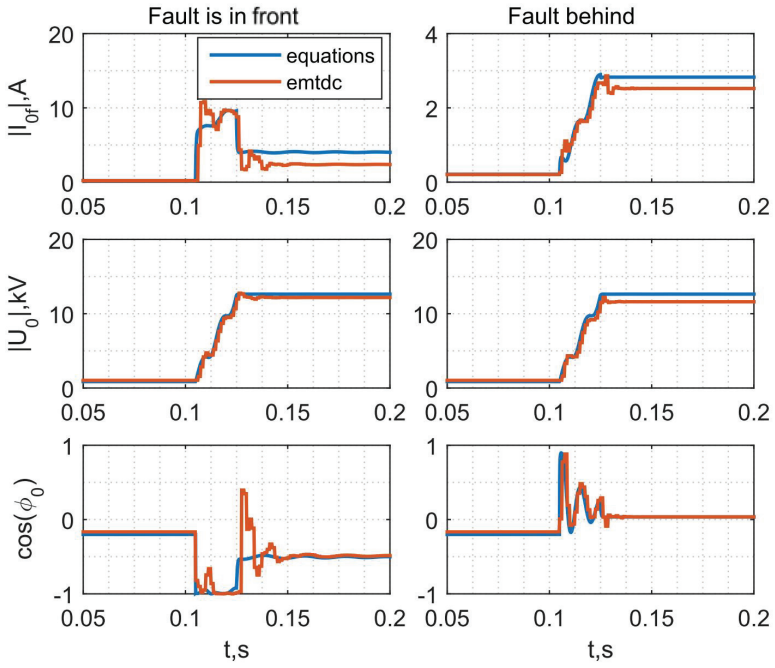

Figure 4.21: Zero sequence current, voltage and angle for low-ohmic faults at different locations.

During low-ohmic faults, higher harmonics in the faulty signals are present that are not taken into account by the equations in system (4.13) (only 50 Hz components are considered); therefore, discrepancies in the

transient periods are observed (especially for faults in the front section). There are magnitude divergences in the faulty steady-state periods (especially for currents). Nevertheless, accuracy is sufficient for initial evaluation of protection methods.

For high impedance faults (3 kOhm) in Fig.4.22, better precision in the transient period is achieved (compared to the previous low-ohmic fault) because higher harmonics in the faulty signals are filtered out by the fault resistance. Magnitude differences in the faulty steady-state period can be compensated for by adjusting e_a, e_b, e_c.

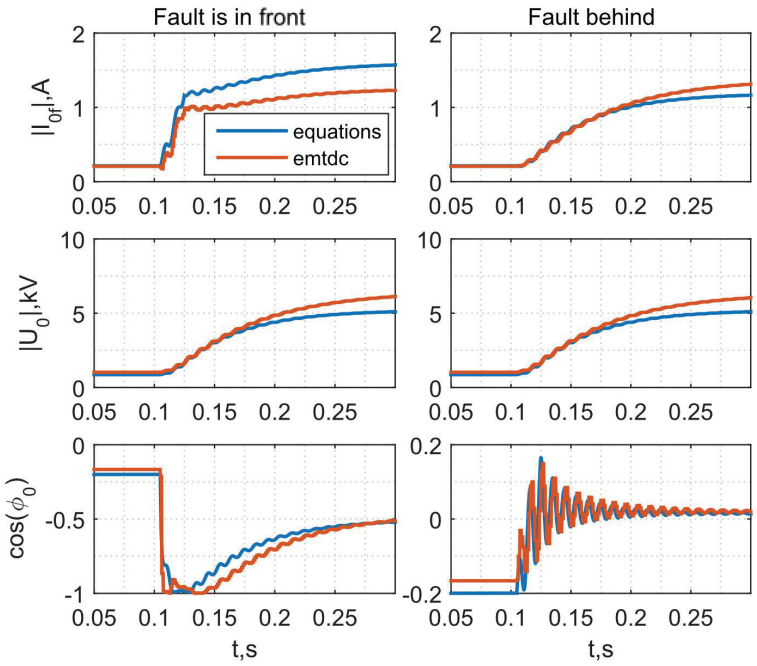

Figure 4.22: Zero sequence current, voltage and angle for high impedance faults at different locations.

Thus, this approach can be used for sensitivity analysis and verification of method security in real systems, avoiding comprehensive EMTP simulations because the parameters required for the solver can be calculated from records of real (or artificially organised) earth faults. Since there is sufficient coincidence of simulated and calculated i_{0f} and u_0 in the steady-state period, the same equivalent scheme can be utilised for analysis of steady-state methods. In this case, the equations must be written in the frequency domain. This is done in [Paper IV] and it will be used further for numerical analysis of the method presented in [Paper V].

4.3.2 Maloperation of the existing methods for earth fault location [Paper IV]

The paper demonstrates possible scenarios when the existing steady-state and low-frequency transient methods can prove inadequate for reliable earth fault location. Firstly, it shows that $\cos(\phi_0)$ in the healthy or faulty feeders can change the prescribed sign (*Fig.2*) that leads to misoperation due to directionality disruption of the ground fault protection discussed in section 4.1.3. Here, the theoretical approach for the steady-state analysis in the frequency domain is used. *Fig.3* demonstrates that the main reasons for this are insufficient natural watt-metric contribution of the network and significant capacitive imbalance of lines. Moreover, large overcompensation (low inductance of the suppressing coil) can also be a negative factor; as seen in *Fig.4*. Analysis of the steady-state methods also includes a method based on zero sequence admittance with pre-fault measurements (e.g. [110]), *Fig.7*. Its performance can be affected by the same factors as above plus highly unequal feeders (in terms of uncompensated capacitive earth current), leading to blinding or sympathetic tripping.

The second part of the paper is focusing on analyses of methods based on transient $\cos(\phi_0)$ (e.g. [92]), transient zero sequence active power/energy (e.g. [79]), instantaneous zero sequence current (e.g. [78]), and transient zero sequence admittance (e.g. [93]). Analysis is conducted with the help of PSCAD/EMTDC simulations. *Fig.8* demonstrates that $\cos(\phi_0)$ in the healthy feeder can cross the threshold set for detection of the faulty feeder (accidental sympathetic tripping). *Fig.9a* illustrates that zero sequence active power/energy can change the sign during integration, and *Fig.9b* shows that the sign can be the same for the faulty and healthy feeder or the opposite to the expected. The main affecting factor here is capacitive imbalance of the lines. Impact of cables (large earth capacitive current in one feeder compared to another) is demonstrated in *Fig.10*: polarity of instantaneous zero sequence current for the faulty and healthy feeder is the same. Finally, cable presence can lead to pre-fault displacement of $\cos(\phi_0)$, *Fig.11*. In turn, this has negative influence on the method based on zero sequence admittance, *Fig.12*. The presented analysis is summarised in *Table I*.

The paper indicates motivations for the development of new approaches independent of fault and network parameters, and complex simple settings.

4.3.3 A new indicator for faulty feeder or section selection [Paper V]

The paper proposes a new method for faulty feeder or section selection based on a universal indicator that is referred to as the k-indicator.

The method requires two-point measurements (zero sequence current and voltage) to identify fault position: inside the monitoring zone (downstream for one and upstream for another) or outside (downstream or upstream for both). The method replaces a network between two measuring points with an equivalent line with lumped parameters (this type of approach is valid for short lines in distribution networks; the long line effect is not considered in the current PhD thesis) and provides a quadratic equation with unknown parameter k that is used for indication of earth fault location. This parameter expresses the per unit distance to the fault on the equivalent line.

The k-indicator has simple universal settings not depending on network parameters (zero sequence current is not used for operation) and variable topology, immunity to fault nature (transient, permanent, high impedance faults), and it does not require pre-fault information. Moreover, its application is possible without the parallel resistor. The paper develops the algorithm using synchronised measurements. Laboratory tests and impact of unsynchronised measurements are not presented in the thesis.

A simple numerical analysis of the method providing reasoning and details is presented below since it is omitted from the paper.

4.3.4 Numerical analysis of the k-indicator

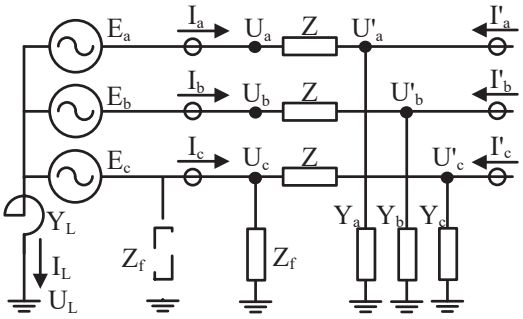

Figure 4.23: Network for analysis of the k-indicator.

Fig.4.23 shows a simple network for analysis of the k-indicator. In contrast to Fig.4.19, the series impedance of the line Z is not neglected (normally, it is much less than the shunt impedance) to avoid infinite solutions of equations. As was discussed in section 4.3.1, the steady-state faulty conditions can be described in the frequency domain using phase quantities as follows (the earth fault with impedance Z_f is inside the monitoring zone):

$$\begin{cases} I_a = U_a(Z + 1/Y_a)^{-1} \\ I_b = U_b(Z + 1/Y_b)^{-1} \\ I_c = U_c(Z + 1/Y_c)^{-1} + U_c/Z_f \\ I_a + I_b + I_c + I_L = 0 \\ I_L = U_L Y_L \\ E_a = U_a - U_L \\ E_b = U_b - U_L \\ E_c = U_c - U_L \\ U'_a = U_a - ZI_a \\ U'_b = U_b - ZI_b \\ U'_c = U_c - Z(I_c - U_c/Z_f) \end{cases} \tag{4.22}$$

where I_a, I_b, I_c are the phase currents at the sending end and $I'_a = 0$, $I'_b = 0$, $I'_c = 0$ at the receiving end; U_a, U_b, U_c are the phase voltages at the sending end and U'_a, U'_b, U'_c at the receiving end; Y_a, Y_b, Y_c are the phase shunt admittances of the line; I_L, U_L, Y_L are the current, voltage and admittance of the Petersen coil respectively. The network is supplied by the ideal voltage source with E_a, E_b, E_c.

As previously, $U_L = U_0$ because

$$E_a + E_a + E_a = U_a + U_b + U_c - 3U_L = 3U_0 - 3U_L = 0 \tag{4.23}$$

Taking into account that

$$U_{a,b,c} = E_{a,b,c} + U_0 \tag{4.24}$$

$$I_a + I_b + I_c + U_0 Y_L = 0, \tag{4.25}$$

it is possible to obtain an expression for U_0 (the sending end):

$$U_0 = -\frac{\frac{E_a}{Z+1/Y_a} + \frac{E_b}{Z+1/Y_b} + \frac{E_c}{Z+1/Y_c} + \frac{E_c}{Z_f}}{\frac{1}{Z+1/Y_a} + \frac{1}{Z+1/Y_b} + \frac{1}{Z+1/Y_c} + \frac{1}{Z_f} + Y_L} \tag{4.26}$$

As $I_a + I_b + I_c = 3I_0$, then zero sequence current at the sending end and voltage at the receiving end are:

$$\mathrm{I}_0 = -\frac{\mathrm{I}_\mathrm{L}}{3} = -\frac{\mathrm{U}_0 \mathrm{Y}_\mathrm{L}}{3} \tag{4.27}$$

$$\mathrm{U'}_0 = \mathrm{U}_0 - \mathrm{ZI}_0 + \frac{\mathrm{Z}}{3\mathrm{Z}_\mathrm{f}}(\mathrm{E}_\mathrm{c} + \mathrm{U}_0) \tag{4.28}$$

Finally, zero sequence current at the receiving end is $\mathrm{I'}_0 = 0$. Having zero sequence measurements at both ends, it is possible to find parameter k according to the method in [Paper V]: 1) equivalent zero sequence impedance and admittance are calculated as

$$Z_{0e} = \frac{\mathrm{U}_0^2 - \mathrm{U'}_0^2}{\mathrm{U'}_0 \mathrm{I}_0 - \mathrm{U}_0 \mathrm{I'}_0} \tag{4.29}$$

$$Y_{0e} = 2\frac{\mathrm{I}_0 + \mathrm{I'}_0}{\mathrm{U}_0 + \mathrm{U'}_0} \tag{4.30}$$

Because of this fault, the real part of Y_{0e} is normally negative; therefore, it is updated as $Y'_{0e} = \mathrm{real}(Y_{0e}) + j \cdot \mathrm{imag}(Y_{0e})$; 2) the following quadratic equation containing the k parameter (conditional distance to a faulty point) is solved for k:

$$\mathrm{k}^2 Z_{0e}\frac{Y'_{0e}}{2}(\mathrm{U}_0 - \mathrm{U'}_0) - \mathrm{k}Z_{0e}(\mathrm{I}_0 + \mathrm{I'}_0 - \mathrm{U'}_0 Y'_{0e}) + \\ + \mathrm{U}_0 - \mathrm{U'}_0 + Z_{0e}(\mathrm{I'}_0 - \mathrm{U'}_0\frac{Y'_{0e}}{2}) = 0 \tag{4.31}$$

If the earth fault is not in the monitoring zone (behind the sending end in Fig.4.23), then zero sequence current at the sending end and voltage at the receiving end are modified as

$$3\mathrm{I}_0 = -\mathrm{U}_0 \mathrm{Y}_\mathrm{L} - \frac{\mathrm{E}_\mathrm{c} + \mathrm{U}_0}{\mathrm{Z}_\mathrm{f}} \tag{4.32}$$

$$\mathrm{U'}_0 = \mathrm{U}_0 - \mathrm{ZI}_0 \tag{4.33}$$

The following parameters are used for the numerical analysis: $\mathrm{E}_\mathrm{a} = 12.7$ kV, $\mathrm{E}_\mathrm{b} = 12.7\mathrm{e}^{-j2\pi/3}$ kV, $\mathrm{E}_\mathrm{c} = 12.7\mathrm{e}^{j2\pi/3}$ kV, $\mathrm{Y}_\mathrm{a} = \mathrm{Y}_\mathrm{c} = 8.2 + j217.1$ μS, $\mathrm{Y}_\mathrm{b} = \mathrm{Y}_\mathrm{a} + \Delta\mathrm{Y}$, $\Delta\mathrm{Y} = j3k_c \cdot \mathrm{imag}(\mathrm{Y}_\mathrm{a})$, $\mathrm{Y}_\mathrm{L} = -j905.5$ μS, $\mathrm{Z} = 0.1 + j0.1$ Ω.

Fig.4.24 demonstrates parameter k (two roots of the quadratic equation) for different fault impedances and electrostatic asymmetry k_c. It is possible to see that if the fault is in front of the sending end (inside the monitoring zone), the roots take values between 0 and 1 or higher than 1; at the same time, if the fault is behind the sending end (outside the monitoring zone),

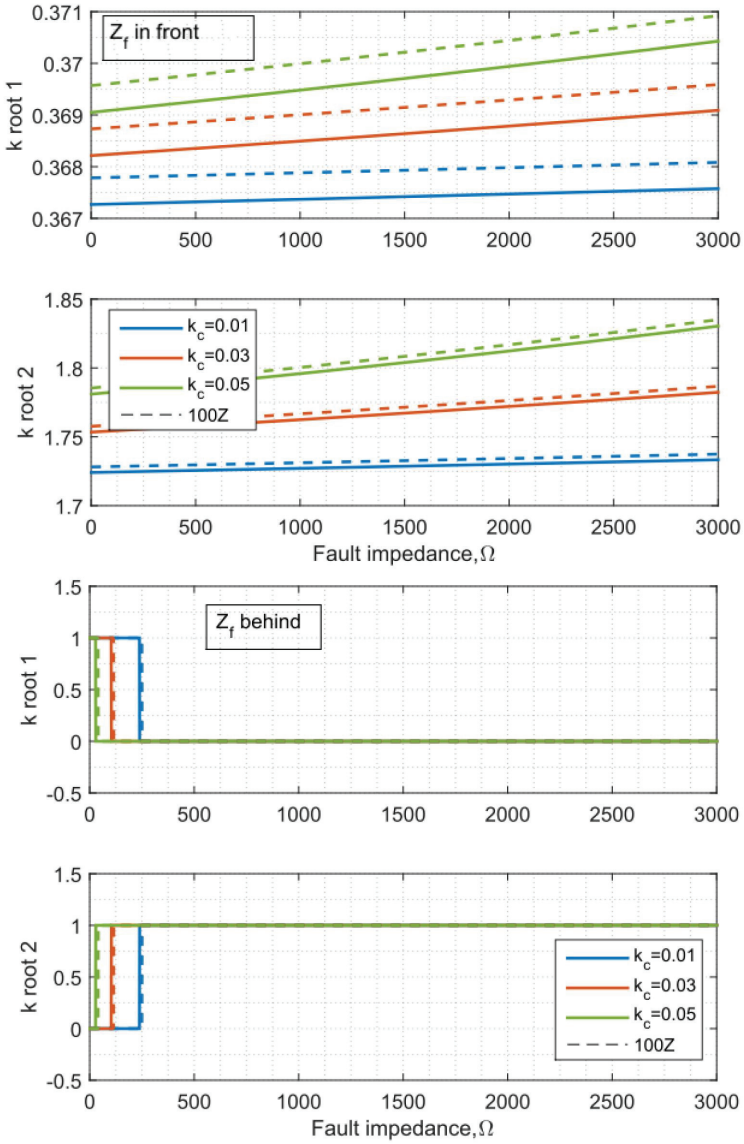

Figure 4.24: The k-indicator for different fault resistances and their locations.

the roots are equal to 0 or 1. This peculiarity is used to discriminate fault location in [Paper V]. Finally, dependency on fault impedance, electrostatic imbalance and line series impedance (the dashed lines show the k-indicator for $100\mathrm{Z} = 10 + j10\ \Omega$) are not significant.

4.3.5 PSCAD/EMTDC tests of the k-indicator [Paper V]

The paper demonstrates the application of the k-indicator for discrimination of earth fault locations without the parallel resistor in the system with the DG, Fig.3.1. *Fig.5* demonstrates dynamic performance of the k-indicator. It can be seen that decisions (discrimination of faults in feeders using measurements at the substation and at DG location) are made within several cycles that can be used for fast anti-islanding protection or to avoid unnecessary tripping of the generators. For complex topology, several pairs of measuring points are involved. *Fig.8* shows values for the k-indicator for faults in different lines in the systems, phases, low and high fault impedances utilising different pairs of relays. As a result, taking k=0.5 as logical one and k=0 as logical zero, it is possible to identify faults taking place in the zone of primary protection on the basis of *and* logic:

$$k_{s\text{-}r1} \;\&\; k_{s\text{-}r2} \;\&\; ... \;\&\; k_{s\text{-}rN} = 1 \rightarrow \text{fault is inside the monitoring zone}$$
$$k_{s\text{-}r1} \;\&\; k_{s\text{-}r2} \;\&\; ... \;\&\; k_{s\text{-}rN} = 0 \rightarrow \text{fault is outside the monitoring zone}$$

where $k_{s\text{-}r}$ denotes k calculated using measurements from the substation (s) and remote relay (r). Total number of relays in the feeder is N.

Finally, the analysis shows that performance of the k-indicator is independent of fault or network parameters.

4.3.6 A new method for exact fault location [Paper V]

The paper describes a new method for exact earth fault location in the compensated system. The locator is based on the matrix equation $Z^0 I^0 = V^0$, where I^0 and V^0 are the vectors of zero sequence currents and voltages containing measured values in different nodes, and Z^0 is the zero sequence impedance matrix of the network with unknown position of the earth fault (lumped parameters are used since the long line effect is not present). Solving this non-linear equation is done using an iterative scanning procedure with a minimal error condition (difference between the measured voltage and calculated voltage). The algorithm requires synchronised zero sequence remote measurements. Laboratory tests and impact of unsynchronised measurements are not presented in the thesis.

The similar locator is presented, for example, in [117]; however, the proposed method in [Paper V] introduces a new approach to enhance accuracy. The reasoning is not discussed in the paper, and therefore the approach is analysed below.

4.3.7 Numerical analysis of the exact fault location method

For analysis, a simple network depicted to the left in Fig.4.25 is used. The earth fault with impedance Z_f takes place in line 2. The network is supplied by an ideal voltage source with phase voltage E and grounded through the Petersen coil with inductance L. The exact fault location method presented in [Paper V] requires information about the zero sequence network, currents and voltages in some nodes (ideally in all). The network is decomposed into the positive (denoted with '+'), the negative (denoted with '-') and the zero (denoted with '0') sequence network (each line is represented by its π-equivalent) connected in series as is shown to the right in Fig.4.25 and the solution approach presented in section 4.2.3 is used (omitted here) to find zero sequence voltages and currents in nodes.

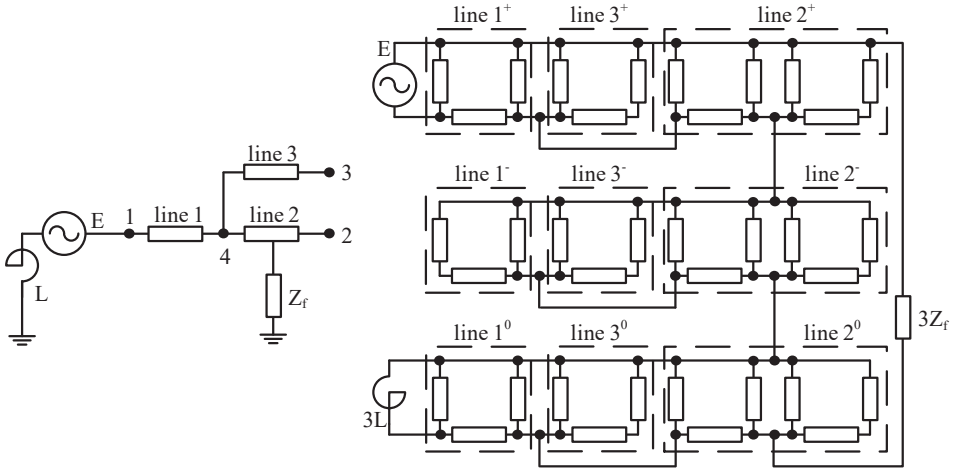

Figure 4.25: System for analysis of the earth fault locator (left) and its decomposition into sequence networks (right) for calculations.

The following parameters are used: line lengths $l = 10$ km, E=12.7 kV, L=0.2 H, positive sequence series resistance and reactance $R_1 = X_{L1} = 3.5 \cdot 10^{-4}$ Ω/m, positive sequence shunt reactance $X_{C1} = 300$ M$\Omega \cdot$ m, and zero sequence parameters $R_0 = 5 \cdot 10^{-4}$ Ω/m, $X_{L0} = 16 \cdot 10^{-4}$ Ω/m, $X_{C0} = 6.5$ M$\Omega \cdot$ m. Fault impedance $Z_f = 10$ Ω.

The locator in [Paper V] requires the zero sequence nodal admittance matrix constructed for the faulty system as input:

$$Y^0 = \begin{bmatrix} Y^0_{11} & 0 & 0 & -Y^0_{14} & -Y^0_{1\mathrm{f}} \\ 0 & Y^0_{22} & 0 & -Y^0_{24} & -Y^0_{2\mathrm{f}} \\ 0 & 0 & Y^0_{33} & -Y^0_{34} & -Y^0_{3\mathrm{f}} \\ -Y^0_{14} & -Y^0_{24} & -Y^0_{34} & Y^0_{44} & -Y^0_{4\mathrm{f}} \\ -Y^0_{1\mathrm{f}} & -Y^0_{2\mathrm{f}} & -Y^0_{3\mathrm{f}} & -Y^0_{4\mathrm{f}} & -Y^0_{\mathrm{ff}} \end{bmatrix}, \tag{4.34}$$

In real-life situations, the position of a faulty node (denoted as 'f') would be unknown. Therefore, the scanning procedure is applied. It is assumed that the faulty node is present in a certain line at a specific distance from the line end (node 1, 2 or 3 depending on a chosen line) on distance l_f. Thus, parameter k is defined as $k = l_\mathrm{f}/l$. To check the whole line, k takes values between 0 and 1 with a discrete step dk. Then, the next line is taken. Consequently, the scanning algorithm has two loops: one changes line (denoted by letter n below) and the second selects the faulty node on this line (denoted by letter i). Thus, matrix Y^0 is updated for each n and at each i incrementation. Matrix elements can be expressed in general form as

$$\begin{cases} Y^0_{nn} = \frac{1}{\mathrm{Z}_0 \cdot i \cdot dk} + \frac{\mathrm{Y}_0}{2} \cdot i \cdot dk \\ Y^0_{pp} = \frac{1}{\mathrm{Z}_0} + \frac{\mathrm{Y}_0}{2} \\ Y^0_{n4} = 0 \\ Y^0_{p4} = \frac{1}{\mathrm{Z}_0} \\ Y^0_{p5} = 0 \\ Y^0_{n5} = \frac{1}{\mathrm{Z}_0 \cdot i \cdot dk} \\ Y^0_{45} = \frac{1}{\mathrm{Z}_0(1 - i \cdot dk)} \\ Y^0_{44} = 2(\frac{1}{\mathrm{Z}_0} + \frac{\mathrm{Y}_0}{2}) + Y^0_{45} + \frac{\mathrm{Y}_0}{2}(1 - i \cdot dk) \\ Y^0_{55} = Y^0_{nn} + Y^0_{44} - 2(\frac{1}{\mathrm{Z}_0} + \frac{\mathrm{Y}_0}{2}), \end{cases} \tag{4.35}$$

where $\mathrm{Z}_0 = \mathrm{R}_0 l + j\mathrm{X}_{\mathrm{L}0} l$ and $\mathrm{Y}_0 = jl/\mathrm{X}_{\mathrm{C}0}$. $n = 1...3$ and for each n, $p = 1...3$ and $p \neq n$. $i = 0...1/dk$.

For each n and at each i incrementation, the following matrix equation is solved:

$$Z^0 \cdot \begin{bmatrix} I_1^0 \\ 0 \\ 0 \\ 0 \\ I_\mathrm{f}^0 \end{bmatrix} = \begin{bmatrix} V_1^0 \\ V_2^0 \\ V_3^0 \\ V_4^0 \\ V_\mathrm{f}^0 \end{bmatrix}, \tag{4.36}$$

where $Z^0 = (Y^0)^{-1}$, the current vector contains zero sequence currents injected into each corresponding node and the voltage vector contains zero sequence voltages at each corresponding node.

Assuming that measurements from node 1 and 2 are available (two points is a minimum requirement as stated in [Paper V]), it is possible to calculate fault current and voltage error V^{err}:

$$I_\mathrm{f}^0 = \frac{V_1^0 - Z_{11}^0 I_1^0}{Z_{15}^0} \tag{4.37}$$

$$V_{in}^{err} = \frac{|V_2^0 - Z_{21}^0 I_1^0 - Z_{25}^0 I_\mathrm{f}^0|}{|V_2^0|} \cdot 100\% \tag{4.38}$$

Here, subscript notation in means an element in row i and column n of a matrix. Thus, voltage error V_{in}^{err} for each n and at each i incrementation is stored in a matrix. Finally, after the scanning procedure (changing of network impedance matrix Z^0), matrix of voltage errors $\mathbb{V}^{err}$ is formed:

$$\mathbb{V}^{err} = \begin{bmatrix} V_{11}^{err} & V_{12}^{err} & V_{13}^{err} \\ V_{21}^{err} & V_{22}^{err} & V_{23}^{err} \\ \dots & \dots & \dots \\ V_{(1/dk+1)1}^{err} & V_{(1/dk+1)2}^{err} & V_{(1/dk+1)3}^{err} \end{bmatrix} \tag{4.39}$$

Elements of this matrix can be depicted. For this purpose, the actual fault is placed in the middle of line 2, i.e. 15 km from node 1 (equal to $1.5l$). Discrete step dk ($i = 0...1/dk$) is chosen 0.001 that corresponds to 10 km·0.001 = 10 m. Fig.4.26 shows the voltage error in each line (for each n) with respect to the distance error. The distance error is calculated as

$$\begin{cases} \frac{l \cdot i \cdot dk - 1.5l}{1.5l} \cdot 100\% \text{ for } n = 1 \\ \frac{l + (1 - i \cdot dk)l - 1.5l}{1.5l} \cdot 100\% \text{ for } n = 2, 3 \end{cases} \tag{4.40}$$

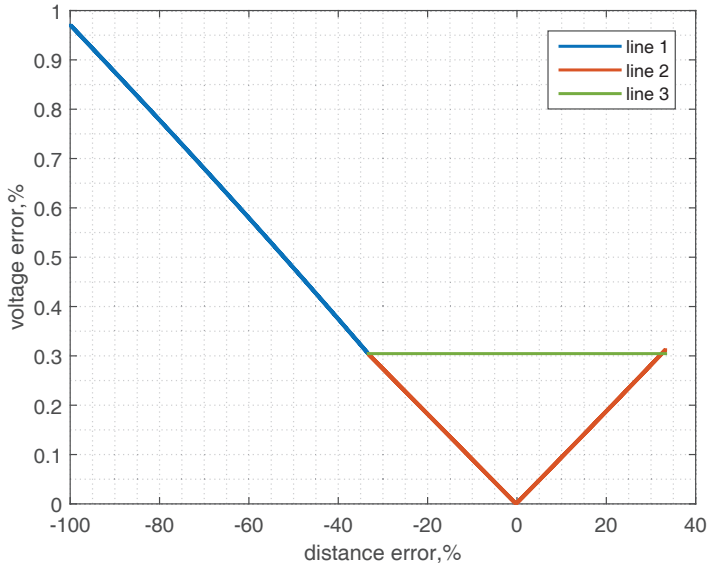

Figure 4.26: Dependency of voltage error on distance error in case of fault in line 2 and available measurements at points 1 and 2.

As can be seen, if $n = 2$, it gives fewer voltage errors at each i incrementation compared to $n = 1, 3$. Moreover, the minimum voltage error coincides with the minimum distance error for $n = 2$ (line 2); therefore, it is used as a criterion for the selection of a faulty line and exact fault location on the line.

The global minimum of matrix $\mathbb{V}^{err}$ is referred to as the first minimum and denoted as $\min(\mathbb{V}^{err})_1$. Its position in the matrix (corresponding to row i and column n) indicates the faulty line and exact fault location on it. Besides the first minimum, there is the second, determined as $\min(\mathbb{V}^{err})_1 < \min(\mathbb{V}^{err})_2 <$ all other elements in $\mathbb{V}^{err}$, the third and so on. Each of these can indicate its own faulty line and faulty point on it. The first ten minima can be used for approximate fault location when an earth fault occurs in the side branch and additional measurements are not available (this is demonstrated in [Paper V]).

To illustrate this, it is assumed that measurements from point 1 and 3 are available and fault is still in line 2. Next, voltage error is calculated using the third row:

$$V_{in}^{err} = \frac{|V_3^0 - Z_{31}^0 I_1^0 - Z_{35}^0 I_f^0|}{|V_3^0|} \cdot 100\% \tag{4.41}$$

Fig.4.27 shows the first ten minimum voltage errors $\min(\mathbb{V}^{err})_{1-10}$, and the lines and distance errors associated with them. As can be seen, the first voltage minimum incorrectly determines the faulty line (unlike the previous case in Fig.4.26): it is line 1, whereas the true faulty line is 2. The same for the second voltage minimum, the third and the forth voltage minimum, whereas the rest voltage minima can correctly indicate faulty line 2. The distance errors are also high and the fault is mistakenly identified as being close to node 4.

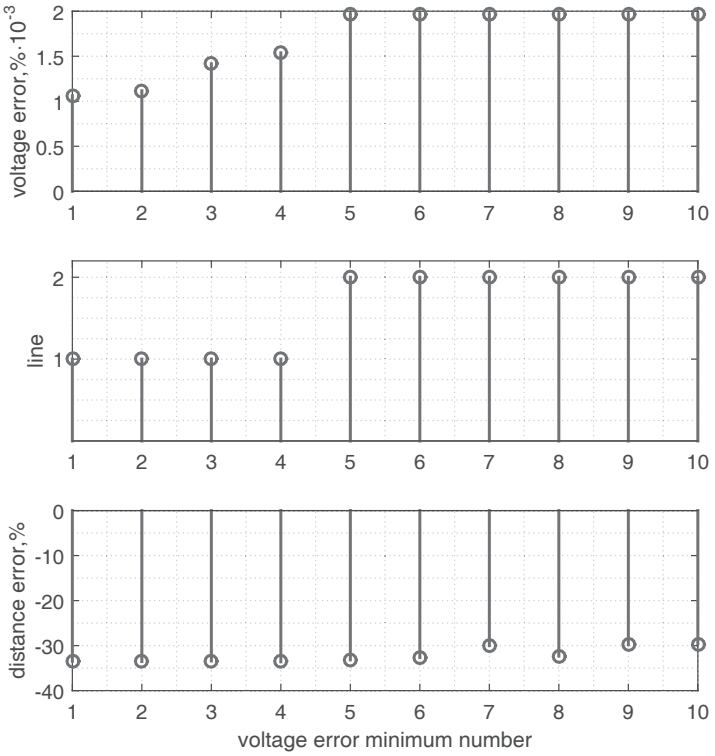

Figure 4.27: Identified faulty lines and distance errors for the first ten voltage error minima in case of actual fault in line 2 and available measurements at points 1 and 3.

This analysis demonstrates that application of a group of voltage error minima can correctly indicate the faulty side branch: the most frequently appearing line in the group (line 2 in the example above appears 6 times from 10). The same is illustrated in [Paper V], Fig.7b. Nevertheless, such an approach can produce significant errors when the number of side branches increases. When there is a large number of side branches, increasing the

number of measuring points is recommended.

In the next example, measurements taken from all three points are utilised. Then, fault current can be calculated using voltage at points 1, 2 or 3 (denoted by m below) and voltage error is determined using matrix norm:

$$I_{\mathrm{f}}^{0} = \frac{V_{m}^{0} - Z_{m1}^{0} I_{1}^{0}}{Z_{m5}^{0}} \tag{4.42}$$

$$V_{in}^{err} = \left|\left| \frac{|[V_1^{0*}\ V_2^{0*}\ V_3^{0*}]^T - Z_{(1:3)1}^{0} I_1^0 - Z_{(1:3)5}^{0} I_{\mathrm{f}}^{0}|}{|[V_1^{0*}\ V_2^{0*}\ V_3^{0*}]^T|} \right|\right| \cdot 100\% \tag{4.43}$$

Division in equation (4.43) is elementwise. Notation $Z_{(1:3)5}^{0}$ means that rows from 1 to 3 are selected in column 5. Here, matrix of voltage errors $\mathbb{V}^{err}$ is separately formed for each m, and, consequently, the first minimum $\min(\mathbb{V}^{err})_1$ in this matrix (a faulty line and a point) is also determined for each m.

Fig.4.28 shows the distance errors based on the first voltage error minimum $\min(\mathbb{V}^{err})_1$ calculated for different reference measuring points m (a faulty line is correctly determined for any m).

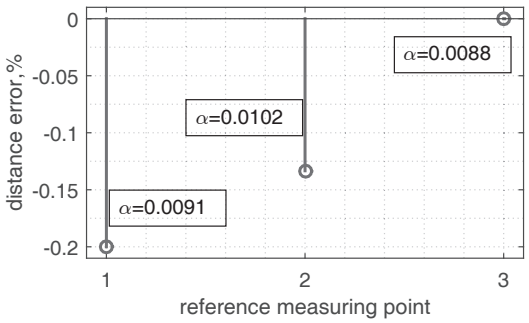

Figure 4.28: Distance errors for different reference measuring points in case of fault in line 2 and available measurements at points 1,2,3.

It is seen that $m = 3$ provides the best accuracy. In order to decide what reference measuring point to use in practice to achieve the minimal distance error, parameter α is introduced (given on the plot for each m): it is computed as matrix norm from the first ten voltage error minima, that is $\alpha = ||[\min(\mathbb{V}^{err})_1\ \min(\mathbb{V}^{err})_2\ ...\ \min(\mathbb{V}^{err})_{10}]||$ for each m. As can be seen, the minimum α coincides with the minimum distance error.

Fig.4.29 summarises the explained calculation steps and illustrates a final algorithm with precision enhancement (selection of reference measuring

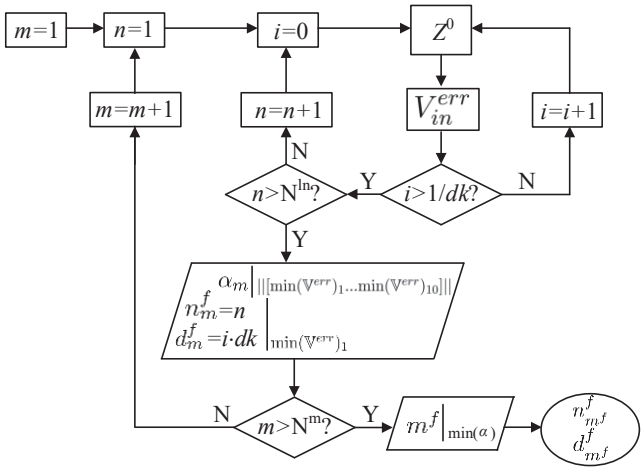

Figure 4.29: Algorithm of the earth fault locator.

point). Here, N^{ln} is a number of lines in the system. For each m, line number n_m^f and fault distance on this line d_m^f are determined on the basis of the first minimum voltage error, and α_m is also calculated using the first ten voltage error minima. N^m is a number of available measuring points. m^f is a reference measuring point number determined on the basis of condition $\min(\alpha)$, whicht gives the best precision for faulty line detection $n_{m^f}^f$ and distance $d_{m^f}^f$. [Paper V] presents calculation of I_f^0 and V_{in}^{err} for a general case.

4.3.8 PSCAD/EMTDC tests of the exact fault location method [Paper V]

The paper demonstrates application of the fault locator for fast anti-islanding protection and prevention of unnecessary DG disconnection. The locator is best adapted to permanent faults with stable signals and it is not a reliable solution for intermittent faults. *Fig.6* demonstrates that precision of the locator is worst during the transient period, better during the steady-state, and at its best for higher fault currents (caused by low-ohmic faults or adjusting of the inductance of the Petersen coil). Faults in side branches cannot be located with sufficient accuracy without additional measurements, as illustrated in *Fig.7a*. Nevertheless, as was demonstrated in the previous section, a group of voltage error minima can indicate the faulty branch without measurements from this branch, *Fig.7b*. It can be used for branch disconnection and decreasing of a search area saving time (even though exact point is not found precisely). Finally, the utilisation of measurements from

several points helps to increase the precision of the locator. *Fig.9* shows fault location errors on the correctly determined faulty lines for different fault impedances and coil inductances. To summarise, application of the locator for persistent faults utilising multi-point measurements is recommended for better performance.

4.3.9 A new transient-based method for faulty feeder or section selection [Paper VI]

The paper presents a new method capable of zero sequence current direction identification without the involvement of the parallel resistor. It is based on low-frequency transients: the first period of the cosine function of an angle between zero sequence current and voltage after fault inception is analysed using 50-Hz phasors. The paper proposes a new algorithm for making decisions about fault position: whether they are front of the relay or behind it. The algorithm is based on the integration of $\cos(\phi_0)$ after fault recognition upon exceeding a threshold of zero sequence voltage, *Fig.4*. The integration process allows the handling of high frequency transients, improving selectivity and simplifying settings. This can be seen in *Fig.5* – the negative value after integration indicates the faulty feeder. The algorithm does not require zero sequence current operation settings, making it universal and independent of network configuration.

The similar theory presented in section 4.3.1 based on differential equations *(1)* (in the paper) is used to justify the application of $\cos(\phi_0)$: *Fig.3b* demonstrates considerable differences in the transient period for the faulty and healthy feeder. The same approach can be used for sensitivity and security evaluation of the method in practice.

4.3.10 Laboratory verification of the transient-based method [Paper VI]

Algorithm performance, in comparison with the commercially available ground relay, is demonstrated experimentally by applying the Monte Carlo approach [147]. The tests are conducted for variable capacitive imbalances in the network, different fault locations (place in the network and phase), variable fault resistances (low and high) and inception angles, permanent and intermittent faults. Additionally, failure of the parallel resistor is modelled. The results presented in *Tables II,III,IV* show an excellent dependability (always 100%) of the proposed algorithm and shorter operation time than the standard method, which is prone to malfunction during resistor failures or intermittent faults.

Additionally, the algorithm is tested on the real fault records, *Fig.11*. The appearance of the tripping signal for all presented fault cases demonstrates the algorithm's applicability for the existing measuring facilities. Nevertheless, its fast operation is not desirable for temporary faults that are cleared after hundreds of milliseconds; therefore, it is considered as a part of a more complex tripping logic including other algorithms and operation time delays.

Finally, the tests have revealed several cases of security violation of the method caused by pre-fault displacement of $\cos(\phi_0)$, as illustrated in *Fig.9*.

4.3.10.1 Security improvement of the transient-based method

Performance of the method can be affected by switching transients, an issue which is not studied in the paper, but can be a problem in practice. Moreover, the paper also reveals a security problem for high impedance faults in the presence of a significant pre-fault angle displacement (analysis in *Fig.9*).

To illustrate the reasoning behind the improvement of algorithm security, the theory and data in section 4.3.1 are used. The high impedance fault (20 kOhm) is applied in the background network in Fig.4.19, and the characteristics obtained with the help of the solver in Fig.4.20 are illustrated in Fig.4.30.

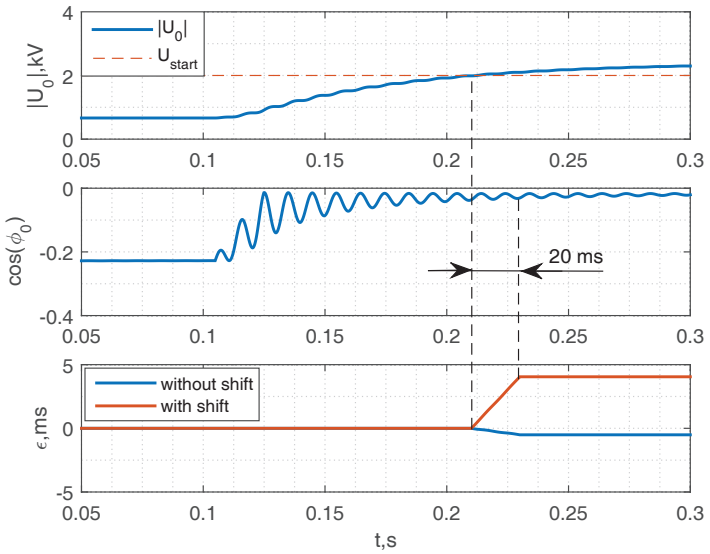

Figure 4.30: Integration of transient $\cos(\phi_0)$ during one period (with shift by its pre-fault value and without) during high impedance fault in the background network.

It is possible to see that the pre-fault steady-state $\cos(\phi_0)$ (at 0.05 s) has the negative displacement from zero, -0.25 (a strong active component of zero sequence current in the healthy conditions). As a result, after fault inception (at 0.1 s), the angle in the transient period and the faulty steady-state period is negative. The integration during one period (the start time of integration is a moment when zero sequence voltage exceeds the threshold) yields the negative value that, according to the algorithm logic (*Fig.4*), leads to the tripping signal. Since the fault is behind the measuring point (in the background network), security violation occurs.

In order to avoid misoperation, it is proposed to use for the integration $\cos(\phi_0)$ shifted by its pre-fault value $\cos(\phi_0)_{\text{pre}}$, i.e. $\cos(\phi_0) - \cos(\phi_0)_{\text{pre}}$ is used in the algorithm instead of $\cos(\phi_0)$. Fig.4.30 shows that in such cases, the integration gives a positive value and tripping does not occur. It does not affect the dependability of the algorithm and faults in front are still recognisable.

4.3.11 Application of the transient-based method for faulty section identification

The developed algorithm can be utilised for identification of a faulty section along the feeder using communication links between relays analogously as is presented in [Paper V] for the k-indicator. In such cases, information for exchange only contains a simple message about fault position - in front of or behind a relay.

This scheme requires such messages from all available substations on the faulty feeder. Depending on the combination of the received messages, different actions in the network can be initiated. Table 4.1 presents all possible combinations and the corresponding actions of the scheme applied for the feeder with the DG, Fig.3.1. It is assumed that the substations are equipped with reclosers. Zero denotes false output of the algorithm (earth fault is behind), one denotes true output (earth fault is in front).

The first row contains logical zeros, indicating that this feeder is healthy and no actions are required. If only relay 8 sees an earth fault in front (the second row), it means that it takes place in the zone bounded by relays 8, 9, 12 and 11. In this case, breaker 12 is opened (to avoid infeed current from the DG) and switch S is closed for connection of DG and unaffected customers to the upper feeder. Recloser at point 8 starts its operation. If relays 8 and 9 see an earth fault in front (the third row), then the fault occurs in the zone between relays 9 and 10. This fault can be cleared by reclosing at substation 9. Analogously, a recloser at 10 is operated if relay 10 sees a fault in front of it (similar logic for reclosers at 11 and 13). Either

Table 4.1: Combinations of transient method outputs registered by different relays in the system and the corresponding actions.

Relay						action
8	9	10	11	12	13	
0	0	0	0	0	0	-
1	0	0	0	0	0	open 12 and close S, reclosing at 8
1	1	0	0	0	0	reclosing at 9
1	1	1	0	0	0	reclosing at 10
1	0	0	1	0	0	reclosing at 11
1	0	0	0	1	0	trip DG 1 and 2, reclosing at 12
1	0	0	0	0	1	reclosing at 13

an earth fault is cleared by a recloser or a breaker isolates a corresponding faulty section if it is persistent. In all these cases, disconnection of the DG is not required. Nevertheless, it is necessary if a fault occurs in the zone between relays 12 and 13 (the sixth row).

Thus, the protection scheme can be used for fast disconnection of DG to initiate reclosing procedure and avoid unintentional islanding formation (if recloser is not used). Furthermore, nuisance tripping is prevented (only one combination allows DG tripping). This scheme also allows the avoidance of manual fault location (successively opening-closing breakers); accelerating and facilitating fault location, as well as minimising the number of affected customers. Combinations different from those given in the table would indicate security violation of the transient algorithm in practice.

Chapter 5

Conclusion

This chapter summarises the research work presented in the thesis. It also outlines recommendations for future work.

The thesis covers the most typical fault types that might take place in distribution networks with DG and grounded by a suppression coil, that is phase-to-phase and phase-to-the-ground faults. The main challenges for conventional protection in these cases are presented and analysed. A solution depending on a fault type is proposed that is capable of improving protection dependability.

Firstly, phase-to-phase faults are examined and it is shown that the conventional overcurrent protection is prone to misoperation due to the presence of the DG (upstream power flows). Moreover, presence of the DG imposes special requirements on its internal protection, and nuisance tripping or unintentional islanding must be avoided. Impedance relaying is considered a promising alternative to overcurrent protection and could assist with DG protection.

Utilisation of impedance measurements is verified in the model of the real network. The results demonstrate the usefulness of this type of protection both for feeders and for DG of a small capacity. Furthermore, impact of high fault resistances (higher than arc resistances) on impedance measurements is considered in the current research work since it is the main disrupting factor for distance relays. Despite this, remote infeed currents from the DG might also have a negative influence. Such problems are typically studied for transmission networks, and the current work fills the gap for distribution systems where these issues are more likely and challenging.

A new method is proposed that is capable of eliminating underreaching problems caused by DG currents and non-zero fault impedances. The method utilises information from several substations in the system. The

method considerably improves the dependability of impedance protection and preserves fault location capabilities. Precision of the latter is mainly influenced by load currents. Performance of the method is affected by communication link impairments; therefore, this imposes specific requirements for telecommunication quality in future Smart Grids.

Secondly, phase-to-ground faults are examined and the key issue here is location of earth faults in the compensated systems. Detection of the earth fault is done using the zero sequence overvoltage criterion, and the problem of undetectable high impedance faults is not studied. It is shown that conventional ground fault protection is highly dependent on operation of the parallel resistor, whereas it can malfunction. Moreover, full reliability is still not guaranteed, especially in the case of intermittent faults. Additional challenges might arise in networks which use underground cables.

The current thesis proposes two new methods for the identification of faulty sections in the systems (or a feeder) and one method for exact earth fault location. The first two are associated with DG presence because its fast disconnection (or vice versa) is required in case of earth fault, depending on its position. The fault locator is developed to increase power supply reliability.

The first faulty section selection method uses zero sequence currents and voltages from two substations to judge whether the earth fault is between them or not. This method, requiring two-end measurements, can determine fault location without the parallel resistor. It can handle permanent or intermittent faults utilizing the transient periods or the steady-state periods of the signal (this is the main advantage of the method). Nevertheless, its operation depends on remote measurements and, therefore, requires attention to quality of communication links.

The second method for identifying a faulty section uses only local measurements and is based on the first transients after fault inception; therefore, it does not require parallel resistor operation. At the same time, it is fast and especially useful for locating intermittent faults. Moreover, it can also be applied to isolated networks. However, with this method, involvement of communication links is necessary for the organisation of reliable fast anti-islanding protection. Requirements to telecommunication quality is less than for the two-end method since a simple message is transmitted without need of synchronisation.

Finally, the study proposes a method for exact fault location. Its precision depends on network topology and a number of available measurements (zero sequence voltages and currents from substations), as well as on fault type. It is shown that transient faults with unstable signals demonstrate

the worst accuracy. Nevertheless, accuracy can be enhanced: fault current can shortly be increased changing a compensation rate in the system using variable inductance of the Petersen coil. The locator can be utilised for post-fault data processing to minimise outage time.

Efficient utilisation of measurements or various information obtained from several points in the distribution network becomes an important topic during development of protection schemes for future Smart Grids. The current research work provides insight into this area; presenting new methods and schemes, as well as clarifying the type of information needed for exchange. Each presented method attempts to reduce the size of transmitted data packets: the compensation method for impedance protection requires interphase currents and voltages (differences in the affected phases), the two-end method for feeder/section selection during earth fault utilises only zero sequence measurements (the same signals are used for precise location), the protection scheme based on the one-end method uses logical true or false (section 4.3.11). Reduction of data in communication links might increase the reliability of communication networks and avoid big data issues.

In connection with the foregoing, the current PhD thesis also demonstrates the significance of the co-simulation platform. With its help, the development and validation of protection schemes involving communication networks is possible, as well as identification of possible problems in the early stages before deployment in future Smart Grids.

5.1 Recommendations for future work

- The method for impedance compensation is tested on a simplified network with DG of a small capacity in one location; therefore, the next step is to utilise a model with more complex topology and with dispersed penetration of DG of various rates of power.

- The compensation method for impedance relaying can be further developed to include a load current compensation algorithm in order to enhance fault location capabilities. Development of a test prototype and validation of real fault records would also be advantageous.

- The methods for earth fault protection requires further verification on intermittent faults simulated for a system with large cable sections (the most frequent and challenging fault type in such systems) and/or obtained from real networks.

- The transient-based method for earth fault location should be studied for situations where switching transients are present in the sys-

tem. Research on discrimination of abnormal transients and improvement of method dependability/security might be the next step for the creation of an independent and new protection function for future microprocessor-based ground relays.

- Tests of the prototypes in real networks.

References

[1] Joint Working Group B5/C6.26/CIRED. (2015) *Protection of Distribution Systems with Distributed Energy Resources.*

[2] K. Mäki. (2007) *Novel Methods for Assessing the Protection Impacts of Distributed Generation in Distribution Network Planning.* Dr. phil. dissertation, Tampere University of Technology.

[3] F. Coffele, C. Booth, A. Dysko, G. Burt. (2012) Quantitative analysis of network protection blinding for systems incorporating distributed generation, *IET Generation, Transmission & Distribution*, 6(12), pp. 1218-1224.

[4] K. I. Jennett, C. D. Booth, F. Coffele, A. J. Roscoe. (2015) Investigation of the sympathetic tripping problem in power systems with large penetrations of distributed generation, *IET Generation, Transmission & Distribution*, 9(4), pp. 379-385.

[5] M. Lukac, Z. Matisic. (2017) Anti-islanding protection of distributed generators with regard to sensitivity in a balance and power system stability, *CIRED - Open Access Proceedings Journal*, 2017(1), pp. 943-946.

[6] K. A. Wheeler, M. Elsamahy, S. O. Faried. (2018) A Novel Reclosing Scheme for Mitigation of Distributed Generation Effects on Overcurrent Protection, *IEEE Transactions on Power Delivery*, 33(2), pp. 981-991.

[7] F. Coffele, C. Booth, A. Dysko. (2015) An Adaptive Overcurrent Protection Scheme for Distribution Networks, *IEEE Transactions on Power Delivery*, 30(2), pp. 561-568.

[8] H. Wan, K. K. Li, K. P. Wong. (2010) An Adaptive Multiagent Approach to Protection Relay Coordination With Distributed Generators in Industrial Power Distribution System, *IEEE Transactions on Industry Applications*, 46(5), pp. 2118-2124.

[9] H. J. Ashtiani, H. Samet, T. Ghanbari. (2017) Simple current-based algorithm for directional relays, *IET Generation, Transmission & Distribution*, 11(17), pp. 4227-4237.

[10] N. Perera, A. Rajapakse, T. Buchholzer. (2008) Isolation of faults in distribution networks with distributed generators, *IEEE Transactions on Power Delivery*, 23(4), pp. 2347-2355.

[11] A. Morandi. (2013) Fault Current Limiter: An Enabler for Increasing Safety and Power Quality of Distribution Networks, *IEEE Transactions on Applied Superconductivity*, 23(6), pp. 1-8.

[12] E. Casagrande, W. L. Woon, H. H. Zeineldin, D. Svetinovic. (2014) A Differential Sequence Component Protection Scheme for Microgrids With Inverter-Based Distributed Generators, *IEEE Transactions on Smart Grid*, 5(1), pp. 29-37.

[13] A. Sinclair, D. Finney, D. Martin, P. Sharma. (2014) Distance Protection in Distribution Systems: How It Assists With Integrating Distributed Resources, *IEEE Transactions on Industry Applications*, 50(3), pp. 2186-2196.

[14] J. I. Marvik. (2011) *Fault Localization in Medium Voltage Distribution Networks with Distributed Generation.* Dr. phil. dissertation, Norwegian University of science and Technology.

[15] S. Voima, K. Kauhaniemi. (2014) Using distance protection in smart grid environment, *IEEE PES Innovative Smart Grid Technologies*, pp. 1-6.

[16] L. K. Kumpulainen, K. T. Kauhaniemi. (2005) Aspects of the effects of distributed generation in single-line-to-earth faults, *International Conference on Future Power Systems*, pp. 1-5.

[17] J. H. Sumner. (1947) The theory and operation of Petersen coils, *Electrical Engineers - Part II: Journal of the Institution of Power Engineering*, 94(40), pp. 283-298.

[18] Standard Norge. (2015) *REN-blad NR 7505 VER 1.0, Stasjonsanlegg - Retningslinjer for spolejordet distribusjonsnett* .

[19] E. Määttä. (2015) *Earth Fault Protection Of Compensated Rural Area Cabled Medium Voltage Networks*, Mr. Sc. dissertation, University of Vaasa.

[20] H. Mortazavi, H. Mehrjerdi, M. Saad, S. Lefebvre, D. Asber, L. Lenoir. (2015) Application of distance relay for distribution system monitoring, *IEEE Power & Energy Society General Meeting*, pp. 1-5.

[21] V. C. Nikolaidis, C. Arsenopoulos, A. S. Safigianni, C. D. Vournas. (2016) A distance based protection scheme for distribution systems with distributed generators, *Power Systems Computation Conference (PSCC2016)*, pp. 1-7.

[22] D. Uthitsunthorn, T. Kulworawanichpong. (2010) Distance protection of a renewable energy plant in electric power distribution systems, *International Conference on Power System Technology*, pp. 1-6.

[23] C. Jecu, R. Caire, P. Alibert, O. Chilard, B. Raison, S. Grenard. (2013) Protection scheme based on non communicating relays deployed on MV distribution grid, *22nd International Conference and Exhibition on Electricity Distribution (CIRED 2013)*, pp. 1-4.

[24] I. Chilvers, N. Jenkins, P. Crossley. (2005) Distance relaying of 11 kV circuits to increase the installed capacity of distributed generation, *IEE Proceedings - Generation, Transmission and Distribution*, 152(1), pp. 40-46.

[25] H. Shateri, S. Jamali. (2008) Measured impedance at source node of a distribution feeder with DG unit for inter phase faults, *IEEE Canada Electric Power Conference*, pp. 1-7.

[26] H. Shateri, S. Jamali. (2008) Measured impedance at source node of a distribution feeder with Dispersed Generation unit, *TENCON 2008 - IEEE Region 10 Conference*, pp. 1-6.

[27] S. Mirsaeidi, D. M. Said, M. W. Mustafa, M. H. Habibuddin. (2015) A protection strategy for micro-grids based on positive-sequence component, *IET Renewable Power Generation*, 9, pp. 600-609.

[28] T. Dao Van, S. Chaitusaney. (2011) Maintaining the reach of protective devices in distribution system with penetration of distributed generation, *the 8th Electrical Engineering/Electronics, Computer, Telecommunications and Information Technology (ECTI) Association of Thailand - Conference*, pp. 696-699.

[29] V. C. Nikolaidis, A. M. Tsimtsios, A. S. Safigianni. (2018) Investigating Particularities of Infeed and Fault Resistance Effect on Distance Relays Protecting Radial Distribution Feeders With DG, *IEEE Access*, 6, pp. 11301-11312.

[30] V. P. Mahadanaarachchi, R. Ramakuma. (2008) Impact of distributed generation on distance protection performance - A review, *IEEE Power and Energy Society General Meeting - Conversion and Delivery of Electrical Energy in the 21st Century*, pp. 1-7.

[31] K. El-Arroudi, G. Joys. (2018) Performance of Interconnection Protection Based on Distance Relaying for Wind Power Distributed Generation, *IEEE Transactions on Power Delivery*, 33, pp. 620-629.

[32] M. Jing, L. Jinlong, W. Zengping. (2010) An adaptive distance protection scheme for distribution system with distributed generation, *5th International Conference on Critical Infrastructure (CRIS)*, pp. 1-4.

[33] R. Sirsi, S. Dasarathan. (2014) Application of fault current limiter to limit distributed generation effect on distance relay coordination, *Annual IEEE India Conference (INDICON)*, pp. 1-6.

[34] S. Voima, K. Kauhaniemi. (2012) Benefits of using telecommunication based protection with DG, *CIRED Workshop – Lisbon*, Paper 236, pp. 1-6 p.

[35] S. Voima, H. Laaksonen, K. Kauhaniemi. (2014) Adaptive protection scheme for smart grids, *12th IET International Conference on Developments in Power System Protection (DPSP 2014)*, pp. 1-6.

[36] A. Hooshyar, M. A. Azzouz, E. F. El-Saadany. (2015) Distance Protection of Lines Emanating From Full-Scale Converter-Interfaced Renewable Energy Power Plants 2014; Part I: Problem Statement, *IEEE Transactions on Power Delivery*, 30, pp. 1770-1780.

[37] A. Hooshyar, M. A. Azzouz, E. F. El-Saadany. (2015) Distance Protection of Lines Emanating From Full-Scale Converter-Interfaced Re-

newable Energy Power Plants 2014; Part II: Solution Description and Evaluation, *IEEE Transactions on Power Delivery*, 30, pp. 1781-1791.

[38] M. Xu, G. Zou, C. Xu, W. Sun, S. Mu. (2016) Positive sequence differential impedance protection for distribution network with IB-DGs, *IEEE International Conference on Power System Technology (POWERCON)*, pp. 1-5.

[39] W. Huang, T. Nengling, X. Zheng, C. Fan, X. Yang, B. J. Kirby. (2014) An Impedance Protection Scheme for Feeders of Active Distribution Networks, *IEEE Transactions on Power Delivery*, 29, pp. 1591-1602.

[40] W. Huang, N. Tai, L. Ke, X. Zheng, C. Shi. (2015) Protection scheme for active distribution networks using positive-sequence components, *IEEE Power & Energy Society General Meeting*, pp. 1-5.

[41] S. Biswas, V. Centeno. (2017) A communication based infeed correction method for distance protection in distribution systems, *North American Power Symposium (NAPS)*, pp. 1-5.

[42] S. Mirsaeidi, D. M. Said, M. W. Mustafa, M. H. Habibuddin. (2015) A protection strategy for micro-grids based on positive-sequence component, *IET Renewable Power Generation*, 9, pp. 600-609.

[43] H. Lin, C. Liu, J. M. Guerrero, J. C. Vasquez. (2014) Distance protection for microgrids in distribution system, *IECON 2015 - 41st Annual Conference of the IEEE Industrial Electronics Society*, pp. 731-736.

[44] M. E. Elkhatib, A. Ellis. (2017) Communication-assisted impedance-based microgrid protection scheme, *IEEE Power & Energy Society General Meeting*, pp. 1-5.

[45] L. Jin, M. Jiang, G. Yang. (2014) Fault analysis of microgrid and adaptive distance protection based on complex wavelet transform, *International Power Electronics and Application Conference and Exposition*, pp. 360-364.

[46] M. M. Saha, J. Izykowski, E. Rosolowski, M. Bozek. (2008) Adaptive Line Distance Protection with Compensation for Remote End Infeed, *IET 9th International Conference on Developments in Power System Protection (DPSP2008)*, pp. 1-6.

[47] J. Ma, X. Xiang, P. Li, Z. Deng, J. S. Thorp. (2017) Adaptive distance protection scheme with quadrilateral characteristic for extremely high-voltage/ultra-high-voltage transmission line, *IET Generation, Transmission & Distribution*, 11(7), pp. 1624-1633.

[48] Q. K. Liu, S. F. Huang, H. Z. Liu, W. S. Liu. (2008) Adaptive Impedance Relay With Composite Polarizing Voltage Against Fault Resistance, *IEEE Transactions on Power Delivery*, 23(2), pp. 586-592.

[49] V. H. Makwana, B. R. Bhalja. (2012) A New Digital Distance Relaying Scheme for Compensation of High-Resistance Faults on Transmission Line, *IEEE Transactions on Power Delivery*, 27(4), pp. 2133-2140.

[50] M. M. Eissa. (2006) Ground distance relay Compensation based on fault resistance calculation, *IEEE Transactions on Power Delivery*, 21(4), pp. 1830-1835.

[51] Y. Zhong, X. Kang, Z. Jiao, Z. Wang, J. Suonan. (2014) A Novel Distance Protection Algorithm for the Phase-Ground Fault, *IEEE Transactions on Power Delivery*, 29(4), pp. 1718-1725.

[52] Z. Y. Xu, G. Xu, L. Ran, S. Yu, Q. X. Yang. (2010) A New Fault-Impedance Algorithm for Distance Relaying on a Transmission Line, *IEEE Transactions on Power Delivery*, 25(3), pp. 1384-1392.

[53] M. H. Idris, M. S. Ahmad, A. Z. Abdullah, S. Hardi. (2013) Adaptive Mho type distance relaying scheme with fault resistance compensation, *IEEE 7th International Power Engineering and Optimization Conference (PEOCO)*, pp. 213-217.

[54] T. G. Bolandi, H. Seyedi, S. M. Hashemi, P. S. Nezhad. (2015) Impedance-Differential Protection: A New Approach to Transmission-Line Pilot Protection, *IEEE Transactions on Power Delivery*, 30(6), pp. 2510-2518.

[55] C. J. Lee, J. B. Park, J. R. Shin, Z. M. Radojevie. (2006) A new two-terminal numerical algorithm for fault location, distance protection, and arcing fault recognition, *IEEE Transactions on Power Systems*, 21(3), pp. 1460-1462.

[56] A. D. Filomena, R. H. Salim, M. Resener, A. S. Bretas. (2008) Ground Distance Relaying With Fault-Resistance Compensation for Unbalanced Systems, *IEEE Transactions on Power Delivery*, 23(3), pp. 1319-1326.

[57] S. Sarangi, A. K. Pradhan. (2015) Adaptive Direct Underreaching Transfer Trip Protection Scheme for the Three-Terminal Line, *IEEE Transactions on Power Delivery*, 30(6), pp. 2383-2391.

[58] V. D. Andrade, E. Sorrentino. (2010) Typical expected values of the fault resistance in power systems, *Transmission and Distribution Conference and Exposition: Latin America (T&D-LA)*, pp. 1-8.

[59] N. I. Elkalashy, M. Lehtonen, H. A. Darwish, M. A. Izzularab, A. I. Taalab. (2007) Modeling and experimental verification of high impedance arcing fault in medium voltage networks, *IEEE Transactions on Dielectrics and Electrical Insulation*, 14(2), pp. 1-9.

[60] P. C. Pietramala, M. Alla, B. K. Johnson. (2016) Distance element corrective biasing during remote infeed conditions, *North American Power Symposium (NAPS)*, pp. 1-6.

[61] M. Singh, V. Telukunta. (2014) Adaptive distance relaying scheme to tackle the under reach problem due renewable energy, *Eighteenth National Power Systems Conference (NPSC)*, pp. 1-6.

[62] N. A. Al-Emadi, A. Ghorbani, H. Mehrjerdi. (2016) Synchrophasor-based backup distance protection of multi-terminal transmission lines, *IET Generation, Transmission & Distribution*, 10(13), pp. 3304-3313.

[63] K. J. Sagastabeitia, I. Zamora, A. J. Mazon, Z. Aginako, G. Buigues. (2011) Phase Asymmetry: A New Parameter for Detecting Single-Phase Earth Faults in Compensated MV Networks, *IEEE Transactions on Power Delivery*, 26, pp. 2251-2258.

[64] K. J. Sagastabeitia, I. Zamora, A. J. Mazon, Z. Aginako, G. Buigues. (2012) Low-current fault detection in high impedance grounded distribution networks, using residual variations of asymmetries, *IET Generation, Transmission & Distribution*, 6, pp. 1252-1261.

[65] T. Schinerl. (2005) A new sensitive detection algorithm for low and high impedance earth faults in compensated MV networks based on the admittance method, *18th International Conference and Exhibition on Electricity Distribution (CIRED2005)*, pp. 1-4.

[66] Z. Chen, W. Li, J. Huang. (2012) Single-phase grounding fault identification and fault line selection for compensation grid, *proceedings of the 7th International Power Electronics and Motion Control Conference*, pp. 2290-2293.

[67] A. Nikander, P. Järventausta. (2017) Identification of High-Impedance Earth Faults in Neutral Isolated or Compensated MV Networks, *IEEE Transactions on Power Delivery*, 32, pp. 1187-1195.

[68] I. Zamora, A. J. Mazon, K. J. Sagastabeitia, J. J. Zamora. (2007) New Method for Detecting Low Current Faults in Electrical Distribution Systems, *IEEE Transactions on Power Delivery*, 22, pp. 2072-2079.

[69] K. Jia, Z. Ren, T. Bi, Q. Yang. (2015) Ground Fault Location Using the Low-Voltage-Side Recorded Data in Distribution Systems, *IEEE Transactions on Industry Applications*, 51, pp. 4994-5001.

[70] T. Velayudham, S. Ganesh, R. Kanimozhi. (2017) Locating ground fault in distribution systems using smart meter, *International conference of Electronics, Communication and Aerospace Technology (ICECA)*, pp. 104-109.

[71] D. Topolanek, M. Lehtonen, M. R. Adzman, P. Toman. (2015) Earth fault location based on evaluation of voltage sag at secondary side of medium voltage/low voltage transformers, *IET Generation, Transmission & Distribution*, 9, pp. 2069-2077.

[72] P. Wang, B. Chen, H. Zhou, T. Cuihua, B. Sun. (2018) Fault Location in Resonant Grounded Network by Adaptive Control of Neutral-to-Earth Complex Impedance, *IEEE Transactions on Power Delivery*, 33, pp. 689-698.

[73] Z. Qi, Z. Zheng, Y. Yang. (2010) Study on method of single-phase-to-earth fault section location in neutral point resonant grounded system, *5th International Conference on Critical Infrastructure (CRIS)*, pp. 1-4.

[74] C. Raunig, L. Fickert, C. Obkircher, G. Achleitner. (2010) Mobile earth fault localization by tracing current injection, *proceedings of the Electric Power Quality and Supply Reliability Conference*, pp. 243-246.

[75] G. Druml, C. Raunig, P. Schegner, L. Fickert. (2013) Fast selective earth fault localization using the new fast pulse detection method, *22nd International Conference and Exhibition on Electricity Distribution (CIRED2013)*, pp. 1-5.

[76] G. Druml, C. Raunig, P. Schegner, L. Fickert. (2014) Comparison of restriking cable-earth faults in isolated and compensated networks,

Electric Power Quality and Supply Reliability Conference (PQ2014), pp. 75-80.

[77] A. Wahlroos, J. Altonen. (2009) Performance of novel neutral admittance criterion in MV-feeder earth-fault protection, *20th International Conference and Exhibition on Electricity Distribution – Part 1*, pp. 1-8.

[78] W. Y. Huang, R. Kaczmarek. (2007) SLG Fault Detection in Presence of Strong Capacitive Currents in Compensated Networks, *IEEE Transactions on Power Delivery*, 22, pp. 2132-2135.

[79] L. Jian, H. Jianjun, Z. Hongwei, Y. Hua, Z. Jie, L. Lei, W. Rui. (2006) Fault Line Selection Based on Zero Sequence Power Direction of Transient Fundamental Frequency in MV Network Grounded with Arc Extinguishing Coil, *International Conference on Power System Technology*, pp. 1-4.

[80] Y. Chollot, J. Mecreant, D. Leblond, P. Cumunel. (2017) New solution of fault directional detection for MV fault passage indicators, *CIRED - Open Access Proceedings Journal*, 2017, pp. 1326-1329.

[81] X. H. Zhang, H. X. Ha, Z. C. Pan, B. Y. Xu. (2007) Grounding faulty line selection in non-solidly grounded systems using transient energy, *International Power Engineering Conference (IPEC2007)*, pp. 1147-1150.

[82] Y. Xue, B. Xu, Y. Chen, Z. Feng, P. Gale. (2002) Earth fault protection using transient signals in non-solid earthed network, *proceedings of International Conference on Power System Technology*, 3, pp. 1763-1767.

[83] Y. Wang, Y. Huang, X. Zeng, G. Wei, J. Zhou, T. Fang, H. Chen. (2017) Faulty Feeder Detection of Single Phase-Earth Fault Using Grey Relation Degree in Resonant Grounding System, *IEEE Transactions on Power Delivery*, 32, pp. 55-61.

[84] L. Bin, S. Hongchun. (2009) A method for fault line detecting based on cluster in resonant grounded systems, *International Conference on Sustainable Power Generation and Supply*, pp. 1-4.

[85] L. Hua, Z. Jiran, G. Fangliang, Z. Zhidan. (2017) Fault Location Based on Correlative Characteristic Values in Resonant Grounded System,

10th International Conference on Intelligent Computation Technology and Automation (ICICTA), pp. 255-259.

[86] M. Loos, S. Werben, M. Kereit, J. C. Maun. (2013) Detection of single phase earth fault in compensated network with C0 estimation, *22nd International Conference and Exhibition on Electricity Distribution (CIRED013)*, pp. 1-4.

[87] M. Lukac. (2009) Determination of earth faulted line with transient method, *20th International Conference and Exhibition on Electricity Distribution (CIRED2009), Part 1*, pp. 1-4.

[88] T. Henriksen, A. Petterteig. (2008) Faulty feeder identification based on charge-voltage relation, *8th Nordic Electricity Distribution and Asset Management Conference*, pp. 1-10.

[89] C. Huang, T. Tang, Y. Jiang, L. Hua, C. Hong. (2018) Faulty feeder detection by adjusting the compensation degree of arc-suppression coil for distribution network, *IET Generation, Transmission & Distribution*, 12, pp. 807-814.

[90] X. Lin, J. Huang, S. Ke. (2011) Faulty Feeder Detection and Fault Self-Extinguishing by Adaptive Petersen Coil Control, *IEEE Transactions on Power Delivery*, 26, pp. 1290-1291.

[91] J. Berggren, L. Hammarson. (2005) Novel method for selective detection of earth faults in high impedance grounded distribution networks, *18th International Conference and Exhibition on Electricity Distribution (CIRED2005)*, pp. 1-4.

[92] P. Balcerek, M. Fulczyk, J. Izykowski, E. Rosolowski, P. Pierz. (2012) Centralized substation level protection for determination of faulty feeder in distribution network, *IEEE Power and Energy Society General Meeting*, pp. 1-6.

[93] J. Altonen, A. Wahlroos, S. Vähäkuopus. (2017) Application of multi-frequency admittance-based fault passage indication in practical compensated medium-voltage network, *CIRED - Open Access Proceedings Journal*, 2017, pp. 947-951.

[94] D. Toader, P. Ruset, S. Haragua, C. Blaj, I. Hategan, N. Pinte, I. Cata. (2010) Selective detection of simple grounding faults in medium voltage power networks with resonant earthed neutral system, *12th*

International Conference on Optimization of Electrical and Electronic Equipment, pp. 1285-1293.

[95] M. F. Abdel-Fattah, M. Lehtonen. (2012) Transient algorithm based on earth capacitance estimation for earth-fault detection in medium-voltage networks, *IET Generation, Transmission & Distribution*, 6, pp. 161-166.

[96] Y. Li, X. Meng, X. Song. (2016) Application of signal processing and analysis in detecting single line-to-ground (SLG) fault location in high-impedance grounded distribution network, *IET Generation, Transmission & Distribution*, 10(2), pp. 382-389.

[97] E. Bjerkan, T. Venseth. (2005) Locating Earth-Faults in Compensated Distribution Networks by means of Fault Indicators, *International Conference on Power System Transients (IPST2005)*, pp. 1-6.

[98] S. Hong-Chun, P. Shi-Xin, L. H. Ai-Bo, Z. Wen-Yuan. (2009) A new approach to detecting fault line in resonant earthed system using energy ratio in short-window, *International Conference on Sustainable Power Generation and Supply*, pp. 1-5.

[99] Y. Zhou, L. Zhu, S. Dong, W. He, F. Zhang. (2010) Grounding Failure Detection Based on Wavelets Method in Resonant Grounded Power Distribution System, *Second WRI Global Congress on Intelligent Systems*, pp. 239-242.

[100] X. D. Zeng, M. F. Guo, D. Y. Chen. (2017) Machine-learning-based single-phase-to-ground fault detection in distribution systems, *IEEE Conference on Energy Internet and Energy System Integration (EI2)*, pp. 1-6.

[101] M. F. Guo, X. D. Zeng, D. Y. Chen, N. C. Yang. (2018) Deep-Learning-Based Earth Fault Detection Using Continuous Wavelet Transform and Convolutional Neural Network in Resonant Grounding Distribution Systems, *IEEE Sensors Journal*, 18, pp. 1291-1300.

[102] H. Shu, S. Sun, G. Qiu, S. Peng. (2010) A new method to detect single-phase fault feeder in distribution network by using S-transform, *IEEE 11th International Conference on Probabilistic Methods Applied to Power Systems*, pp. 277-282.

[103] Y. Yuan, X. Chen, L. Yang, X. Zeng, J. Cai, M. Yu. (2017) A novel fault line selection method of resonant grounding system, *IEEE Conference on Energy Internet and Energy System Integration (EI2)*, pp. 1-5.

[104] K. Zhong-Jian, L. Dan-Dan, Z. Chao, L. Xiao-Lin. (2010) Research on the Fault Characteristic in Non-effectively Grounding Distribution Network with a Single-Phase-to-Earth Fault Based on Hilbert-Huang Transform, *International Conference on Intelligent System Design and Engineering Application*, pp. 276-279.

[105] K. Musierowicz, J. Lorenc, Z. Marcinkowski, A. Kwapisz. (2005) A fuzzy logic-based algorithm for discrimination of damaged line during intermittent earth faults, *IEEE Russia Power Tech*, pp. 1-5.

[106] H. Ji, Y. Yang, H. Lian, S. Cong. (2006) Effect on earth fault detection based on energy function caused by imbalance of three-phase earth capacitance in resonant grounded system, *International Conference on Power System Technology*, pp. 1-5.

[107] T. Welfonder, V. Leitloff, R. Fenillet, S. Vitet. (2000) Location strategies and evaluation of detection algorithms for earth faults in compensated MV distribution systems, *IEEE Transactions on Power Delivery*, 15, pp. 1121-1128.

[108] M. Loos, S. Werben, J. C. Maun. (2012) Multiple measurements to locate single phase earth fault in compensated network, *3rd IEEE PES Innovative Smart Grid Technologies Europe (ISGT Europe)*, pp. 1-6.

[109] J. Orsagova, D. Topolanek, P. Toman, V. Wasserbauer. (2014) Localization method for the resistive earth faults in compensated network based on simultaneous earth faults evaluation, *12th IET International Conference on Developments in Power System Protection (DPSP2014)*, pp. 1-6.

[110] J. Altonen, A. Wahlroos. (2013) Novel algorithm for earth-fault location in compensated MV-networks, *22nd International Conference and Exhibition on Electricity Distribution (CIRED2013)*, pp. 1-4.

[111] A. M. Dan, D. Raisz. (2010) Towards a more reliable operation of compensated networks in case of single phase to ground faults, *proceedings of 14th International Conference on Harmonics and Quality of Power - ICHQP 2010*, pp. 1-4.

[112] P. Toman, J. Orsigova, D. Topolanek. (2008) Location of the Earth Faults in MV Compensated Networks, *9th International Conference on Developments in Power System Protection (DPSP2008)*, pp. 327-331.

[113] B. Jiang, S. Shi, X. Dong, B. Wang. (2011) Single phase grounding fault location based on frequency domain characteristics of fault current, *International Conference on Advanced Power System Automation and Protection*, pp. 2405-2409.

[114] S. Zhang, H. Gao, M. Hou, Y. Sun, Z. Shao, J. Li. (2015) Frequency spectrum characteristic analysis of single-phase ground fault in a Petersen-coil grounded system, *5th International Conference on Electric Utility Deregulation and Restructuring and Power Technologies (DRPT)*, pp. 369-374.

[115] S. Zhang, W. J. Shang, Z. Y. He. (2012) A Fault Locating Algorithm for the Resonant Grounding System Based on the Parameter Identification under Charge Transient, *Asia-Pacific Power and Energy Engineering Conference*, pp. 1-4.

[116] T. Jin, H. Li. (2016) Fault location method for distribution lines with distributed generators based on a novel hybrid BPSOGA, *IET Generation, Transmission & Distribution*, 10, pp. 2454-2463.

[117] A. Tian, W. Li, Z. K. R. Liu. (2016) A fault feature matching-based fault location for distribution network with DGs, *IEEE Industrial Electronics and Applications Conference (IEACon2016)*, pp. 167-172.

[118] T. D. Le, M. Petit. (2013) Performance of directional relays without voltage sensors: Impact of distributed generation technologies, *22nd International Conference and Exhibition on Electricity Distribution (CIRED2013)*, pp. 1-4.

[119] Y. Wang, G. Wei, H. Yang, H. Chen, Z. Ouyang. (2018) Novel Protection Scheme of Single-Phase Earth Fault for Radial Distribution Systems With Distributed Generators, *IEEE Transactions on Power Delivery*, 33, pp. 541-548.

[120] H. Laaksonen, P. Hovila. (2017) Enhanced MV microgrid protection scheme for detecting high-impedance faults, *IEEE Manchester PowerTech*, pp. 1-6.

[121] J. Gao, Q. Cheng, X. Wang, F. Tan, Y. Zhang, D. Yu. (2016) Fault line detection based on cross correlation coefficient for distribution network with DG, *China International Conference on Electricity Distribution (CICED)*, pp. 1-5.

[122] G. Celli, F. Pilo, F. Pilo. (2008) An Innovative Transient-Based Protection Scheme for MV Distribution Networks with Distributed Generation, *IET 9th International Conference on Developments in Power System Protection (DPSP2008)*, pp. 285-290.

[123] Q. Fan, K. Huang, Y. Xiao, M. M. Xu, J. G. Chen, W. Gu. (2015) The Algorithm Reseach of Detecting Single-Phase-to-Ground Fault Line on Distribution Network with Distributed Generation, *International Conference on Computer Science and Applications (CSA2015)*, pp. 99-104.

[124] IEEE Standards Coordinating Committee 21. (2009) *IEEE Std 1547 Interconnecting Distributed Resources with Electric Power Systems.*

[125] PSCAD/EMTDC *software start page.* Available at: https://hvdc.ca/pscad/

[126] *Introduction to M-files.* Available at: http://ctms.engin.umich.edu/CTMS/index.php?aux=Extras_Mfile

[127] MATLAB/SIMULINK *software start page.* Available at: https://se.mathworks.com/products/simulink.html

[128] RT-LAB *real-time software start page.* Available at: https://www.opal-rt.com/software-rt-lab/

[129] OPAL-RT *product page.* Available at: https://www.opal-rt.com/

[130] ABB *relay* RED670 *product page.* Available at: https://new.abb.com/substation-automation/products/protection-control/line-differential-protection/red670

[131] STM32F407VGT6 *product page.* Available at: https://www.st.com/en/microcontrollers/stm32f407vg.html

[132] OMICRON CMC356 *product page.* Available at: https://www.omicronenergy.com/en/products/cmc-356/

[133] J. A. Martinez-Velasco, A. I. Ramirez, M. Davila. (2010) Overhead Lines, in J. A. Martinez-Velasco (ed.) *Power System Transients, Parameter Determination*. Boca Raton: CRC Press pp. 17-136.

[134] P. L. D. Peres, C. R. de Souza, I. S. Bonatti. (2003) ABCD Matrix: A Unique Tool for Linear Two-Wire Transmission Line Modelling, *International Journal of Electrical Engineering Education*, 40(3), pp. 220-229.

[135] P. Kundur. (1993) Excitation Systems, in N. J. Balu, M. G. Lauby (ed.) *Power System Stability and Control*. MacGraw-Hill, Inc. 315-373.

[136] IEC Technical Committee 57. (2003) *IEC 61850 Communication networks and systems in substations*.

[137] C. M. Adrah,Ø. Kure, Z. Liu, H. Kr. Høidalen. (2017) Communication network modeling for real-time HIL power system protection test bench, *IEEE PES Power Africa*, pp. 1-6.

[138] A. S. Tanenbaum. (1996) *Computer Networks*. Prentice Hall.

[139] *USART protocol used in the STM32 bootloader*. Available at: https://www.st.com/resource/en/application_note/cd00264342.pdf

[140] *USR-TCP232-T2 User Manual*. Available at: https://www.usriot.com/download/M0/USR-TCP232-T2-User-Manual-V1.1.pdf

[141] *Waijung Blockset software start page*. Available at: http://waijung.aimagin.com/

[142] *Discrete FIR Filter* MATLAB/SIMULINK *model page*. Available at: https://se.mathworks.com/help/simulink/slref/discretefirfilter.html

[143] *Fourier* MATLAB/SIMULINK *model page*. Available at: https://se.mathworks.com/help/physmod/sps/powersys/ref/fourier.html

[144] I. G. Kulis, A. Marusic, S. Zutobradic. (2014) Insufficiency of wattmetric protection in resonant grounded networks, *8th IEE International Conference on Developments in Power System Protection (DPSP)*, 2, pp. 486-489.

[145] Norsk elektroteknisk komite. (2006) *Forskrift om elektriske forsyningsanlegg : med veiledning*. Available at: https://www.nb.no/nbsok/nb/3ead05688da39baee717f99d20b98a11.nbdigital?lang=no#0

[146] *Ode45* MATLAB *solver page*. Available at: https://se.mathworks.com/help/matlab/ref/ode45.html

[147] *Monte Carlo theory, methods and examples*. Available at: http://statweb.stanford.edu/ owen/mc/

[148] *Newton-Raphson Method*. Available at: https://onlinelibrary.wiley.com/doi/pdf/10.1002/0471458546.app1

Appendices

Appendix A

Calculation of solver parameters for earth fault analysis

The required network parameters for the solver in Fig.4.20 can be calculated from fault records obtained through simulations (steady-state zero sequence quantities are needed). If the relay at point 4 (see Fig.3.1) is considered for analysis, high impedance earth faults at busbar B1 and B2 are simulated, and the following measurements are required :

- during fault at busbar B2: phasors of zero sequence current and voltage at point 4 (I_{04}, U_{0B2}).
- during fault at busbar B1: phasors of zero sequence current and voltage at points 1, 2 and 3 (I_{01}, I_{02}, I_{03}, U_{0B1}).

From these measurements, zero sequence admittance of the whole network Y_{net}, of the faulty part Y_f and of the background healthy part Y_h can be determined as:

$$Y_{net} = \frac{I_{01} + I_{02} + I_{03}}{U_{0B1}} = 105.7 + j2395.95 \ \mu S \tag{A.1}$$

$$Y_f = \frac{I_{04}}{U_{0B2}} = 8.2 + j217.1 \ \mu S \tag{A.2}$$

$$Y_h = Y_{net} - Y_f = 97.5 + j2178,85 \ \mu S \tag{A.3}$$

Yielding

$$\mathrm{G_f} = \mathrm{real}(\mathrm{Y_f}) = 8.2\ \mu\mathrm{S} \tag{A.4}$$

$$\mathrm{C_f} = \frac{\mathrm{imag}(\mathrm{Y_f})}{100\pi} = 0.7\ \mu\mathrm{F} \tag{A.5}$$

$$\mathrm{G_h} = \mathrm{real}(\mathrm{Y_h}) = 97.5\ \mu\mathrm{S} \tag{A.6}$$

$$\mathrm{C_h} = \frac{\mathrm{imag}(\mathrm{Y_h})}{100\pi} = 7\ \mu\mathrm{F} \tag{A.7}$$

Electrostatic asymmetry in the faulty part $\Delta\mathrm{C_f}$ and in the background healthy $\Delta\mathrm{C_h}$ are expressed as

$$\Delta\mathrm{C_f} = 3k_{\mathrm{cf}}\mathrm{C_f} \tag{A.8}$$

$$\Delta\mathrm{C_h} = 3k_{\mathrm{ch}}\mathrm{C_h} \tag{A.9}$$

Parameter k_{cf} is used in the solver and it can be calculated directly from pre-fault measurements $\mathrm{I_{04pre}}$ and $\mathrm{U_{0B2pre}}$. For this purpose, equation (4.15) is used:

$$3\mathrm{i_{0f}} = 3\mathrm{G_f u_0} + 3\mathrm{C_f}\frac{\mathrm{du_0}}{\mathrm{dt}} + \Delta\mathrm{C_f}\frac{\mathrm{d(e_b + u_0)}}{\mathrm{dt}} + \frac{\mathrm{e_a + u_0}}{\mathrm{R_f}} \tag{A.10}$$

It is used to describe the pre-fault ($\mathrm{R_f} = \infty$) steady-state period; therefore, it can be written in the frequency domain:

$$3\mathrm{I_{04pre}} = 3\mathrm{U_{0B2pre}}\mathrm{Y_f} + (\mathrm{E_b} + \mathrm{U_{0B2pre}})j100\pi\Delta\mathrm{C_f} \tag{A.11}$$

From this expression, $\Delta\mathrm{C_f}$ can be found as:

$$\Delta\mathrm{C_f} = \frac{3\mathrm{I_{04pre}}/\mathrm{U_{0B2pre}} - 3\mathrm{Y_f}}{j100\pi(1 + \frac{|\mathrm{E_b}|}{|\mathrm{U_{0B2pre}}|}\mathrm{e}^{j\alpha})} \tag{A.12}$$

The Newton-Raphson method [148] is used for finding angle α such that $\angle\Delta\mathrm{C_f} = 0$. Having this angle, a value of $\Delta\mathrm{C_f}$ can be computed, and then k_{cf} is calculated using equation (A.8).

The parameter k_{ch} is also determined from the pre-fault ($\mathrm{R_f} = \infty$) steady-state period. Equations (4.16) and (4.17)

$$3\mathrm{i_{0h}} = 3\mathrm{G_h u_0} + 3\mathrm{C_h}\frac{\mathrm{du_0}}{\mathrm{dt}} + \Delta\mathrm{C_h}\frac{\mathrm{d(e_b + u_0)}}{\mathrm{dt}} \tag{A.13}$$

$$\mathrm{i_L} = -3\mathrm{i_{0f}} - 3\mathrm{i_{0h}} \tag{A.14}$$

are written in the frequency domain:

$$3\mathrm{I}_{0\mathrm{h}} = 3\mathrm{U}_{0\mathrm{B2pre}}\mathrm{Y}_{\mathrm{h}} + (\mathrm{E}_{\mathrm{b}} + \mathrm{U}_{0\mathrm{B2pre}})j100\pi\Delta\mathrm{C}_{\mathrm{h}} \tag{A.15}$$

$$\mathrm{I}_{\mathrm{L}} = -3\mathrm{I}_{04\mathrm{pre}} - 3\mathrm{I}_{0\mathrm{h}} \tag{A.16}$$

Together with the expression for $3\mathrm{I}_{04\mathrm{pre}}$ (A.11), these equations yield:

$$\mathrm{I}_{\mathrm{L}} = \frac{\mathrm{U}_{0\mathrm{B2pre}}}{j100\pi L} = -3\mathrm{U}_{0\mathrm{B2pre}}\mathrm{Y}_{\mathrm{f}} - (\mathrm{E}_{\mathrm{b}} + \mathrm{U}_{0\mathrm{B2pre}})j100\pi\Delta\mathrm{C}_{\mathrm{f}} - 3\mathrm{U}_{0\mathrm{B2pre}}\mathrm{Y}_{\mathrm{h}} - (\mathrm{E}_{\mathrm{b}} + \mathrm{U}_{0\mathrm{B2pre}})j100\pi\Delta\mathrm{C}_{\mathrm{h}} \tag{A.17}$$

Here, $\mathrm{U}_{\mathrm{L}} = \mathrm{U}_{0\mathrm{B2pre}}$ because $\mathrm{u}_{\mathrm{L}} = \mathrm{u}_0$ from equation (4.14). As a result:

$$\mathrm{U}_{0\mathrm{B2pre}} = -\frac{\mathrm{E}_{\mathrm{b}}j100\pi(\Delta\mathrm{C}_{\mathrm{f}} + \Delta\mathrm{C}_{\mathrm{h}})}{3\mathrm{Y}_{\mathrm{net}} + 1/(j100\pi\mathrm{L}) + j100\pi(\Delta\mathrm{C}_{\mathrm{f}} + \Delta\mathrm{C}_{\mathrm{h}})} \tag{A.18}$$

Finally, the expression for $\Delta\mathrm{C}_{\mathrm{h}}$ is:

$$\Delta\mathrm{C}_{\mathrm{h}} = -\Delta\mathrm{C}_{\mathrm{f}} - \frac{3\mathrm{Y}_{\mathrm{net}} + 1/(j100\pi\mathrm{L})}{j100\pi(1 + \frac{|\mathrm{E}_{\mathrm{b}}|}{|\mathrm{U}_{0\mathrm{B2pre}}|}\mathrm{e}^{j\alpha})} \tag{A.19}$$

As for k_{cf}, α is determined such that $\angle\Delta\mathrm{C}_{\mathrm{h}} = 0$, and then $\Delta\mathrm{C}_{\mathrm{h}}$ is calculated along with k_{ch} using expression (A.9).

Appendix B

Papers

[Paper I]

K. Pandakov, H. Kr. Høidalen, J. I. Marvik. (2016) Implementation of distance relaying in distribution network with distributed generation, *13th International Conference on Development in Power System Protection (DPSP 2016)*, p. 1-7.

Implementation of Distance Relaying in Distribution Network with Distributed Generation

K. Pandakov[*]*, H.Kr. Høidalen*[†]*, J.I. Marvik*[‡]

[*]*NTNU, Norway, Trondheim, konstantin.pandakov@ntnu.no,* [†]*NTNU, Norway, Trondheim, hans.hoidalen@elkraft.ntnu.no,*
[‡]*SINTEF Energy Research, Norway, Trondheim, jorun.irene.marvik@sintef.no*

Keywords: distance protection, distributed generation, distribution network.

Abstract

The article discusses issues related to application of distance protection schemes in a nonstandard environment – distribution networks with dispersed generation. This type of relay is considered as a reasonable alternative to overcurrent devices susceptible to presence of upstream power flows and replacement for voltage protection of distributed generation (DG) units restricting their fault ride through (FRT) capability. The study method is performed through analyses of relay responses to different fault types and locations, and coordination between them during various scenarios. It has disclosed adequacy of security provided by impedance relays during normal and abnormal events in the system, and it has also been revealed limitations for their application. Conclusions provide general recommendations and establish fields for further investigations.

1 Introduction

Utilization of renewable sources is getting more extensive inducing rise of distributed generation penetration into power networks, especially of low and medium voltage (MV) levels. Presence of DG in power systems impacts its performance because it creates various difficulties described, for instance, in [1, 2] especially for regularly used overcurrent protection schemes with fuses [3]. Hence, an additional study of new protection methods are of interest.

A number of technical papers have been published dealing with misoperation of securing devices. The problem of sympathetic tripping is examined in [2] and it requires directional relays. The reasons of blinding effect were comprehensively studied in [4], and reference [5] proposes using of fault current limiters. Other problems, such as unwanted tripping of production units, unwanted islanding, unsuccessful reclosing, selectivity violations have also been documented in [1–3]; however, reliable solutions do not still exist. Authors of [6–13] argued that using of impedance (or distance as an interchangeable term) relays in distribution networks with DG can help to cope with these issues. Furthermore, it is currently recommended or already applied in several countries [14].

Research on new protection schemes involving impedance relays has been done in [6–8] for cases with DG. The obtained results show malfunction of the overcurrent relays and benefits of the distance protection application in either the IEEE standard or simple networks with several buses. Using of impedance relaying to increase the installed capacity of DG in the MV system described in [9]; however, this study does not consider DG connection along a feeder that has influence on impedance measurements. For several years great effort has been devoted to the study of adaptive settings for future smart grids, and references [10–12] report general aspects and advantages of distance protection. Paper [10] discusses the intentional islanding, [11] considers topology changing and performance of the impedance relays for these cases; however, the simple network configurations and balanced faults were investigated. Reference [12] solves the problems with output power variation of the inverter interfaced DG, but the study focuses only on Zone 2 settings because the first is not affected. Moreover, a key limitation of these methods is a requirement of communication technologies. Although authors of [13] tested the methods on the real network in the non-communicating environment, the impedance measurements were utilized for discrimination of the fault locations assisting the overcurrent protection.

Thus, study of the most realistic approach – replacement of overcurrent relays by an impedance type in distribution networks is still lacking; therefore, the main objective of this paper is an analysis of distance relaying in a real network without involvement of communication links. The main findings show feasibility, benefits and limitations of its implementation under system normal operation and various fault situations.

2 Test case network

In this paper we deal with an actual 22 kV distribution network depicted in Fig. 1. It has two DG units connected to Feeder 2: *DG1* is an induction generator (0.623 MVA) and *DG2* is a synchronous (1.395 MVA) driven by the hydro-turbines. The main utility transformer has *YY* connection and resonance grounding. Secure operation of this network is provided by standard overcurrent relays *R1-R13* protecting transmission lines *TL1-TL21*.

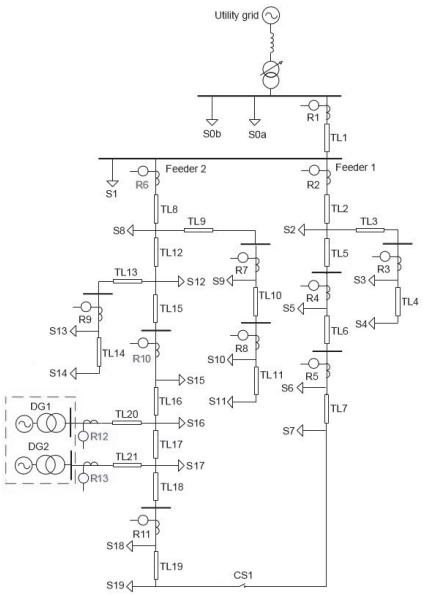

Fig. 1: 22 kV network with distributed generation.

Replacement of all overcurrent relays by the impedance type is inexpedient and, in reality, economically onerously; therefore, only the relays endured to power flow direction changes are considered – *R6* and *R10*. Moreover, undervoltage relays included in the standard DG protection set might restrict FRT capability; therefore, devices *R12* and *R13* securing infeed lines *TL20,TL21* will also be the impedance type in order to examine if the distance relays can prevent unwanted tripping of the DG.

3 Investigation methodology

The network in Fig. 1 is modeled in PSCAD/EMTDC based on the data provided by the system operator. Passive branches concentrated at the beginnings and ends of the transmission lines replace distributed loads. A number of the used real parameters is large to be listed in this paper.

The results of the transient electromagnetic simulations in terms of electrical quantities $U_{a,b,c}$, $I_{a,b,c}$ measured by the relays are processed in MATLAB/MathWorks.

The main approach is analysis of impedance transient trajectories calculated by a specific relay, in the text referred to as measured. For study of abnormal situations, two types of faults are addressed – three-phase and one-phase-to-ground. The first type can be detected observing, for example, z_{ab} [15]:

$$z_{ab} = \frac{U_a - U_b}{I_a - I_b} = kZ_1, \tag{1}$$

where Z_1 is a positive sequence line impedance. Hereafter, k expresses a fraction of a line length between a relay and fault location. This expression is true in case of absence of infeed/outfeed currents along a line. The second type of faults is organized for phase a and it involves ground resistance; therefore, a measured current requires a compensation in order to get kZ_1 as follow [15]:

$$kZ_1 = \frac{U_a}{I_a + I_0 \frac{Z_0 - Z_1}{Z_1}}, \tag{2}$$

where Z_0 is a zero sequence line impedance, and $3I_0 = I_a + I_b + I_c$. These equations are only valid for a zero fault impedance. The next sections presents the most demonstrative simulated results with their discussions.

4 Results and discussions

4.1 Effect of load variation and DG power production on impedance measurements.

An impedance seen by a distance relay can be affected by several factors and the most significant are variations of load in power systems and infeed current from DG, especially if it is located between a relay and a fault point. Indeed, the impedance calculations of relay *R10* (hereinafter, if it is not specified, variables imply a positive sequence) can be performed for a downstream power flow as:

$$\frac{U_{10}}{I_{10}} = Z_{sum} - \frac{I_L}{I_{10}} Z_{eq1} + \frac{I_{DG1} Z_{eq2} + I_{DG2} Z_{dw}}{I_{10}}, \tag{3}$$

where U_{10}, I_{10} – the voltage and current measured by the relay, $Z_{sum} = Z_{TL16} + Z_{TL17} + Z_{dw}$ is the feeder impedance without infeed/outfeed effects, $Z_{TL16,17}$ – the impedances of the lines, Z_{dw} is the impedance of the downward section of the feeder (after relay *R11*) including line *TL18*; $Z_{eq1} = Z_{TL16} + 2Z_{TL17} + 2Z_{dw}$, $Z_{eq2} = Z_{TL17} + Z_{dw}$; $I_{S17} = 0$ and $I_{S15} = I_{S16} = I_L$ – the load currents, $I_{DG1,DG2}$ are the currents from the generators.

Analysis of (3) shows that the presence of the generators (associated with infeed currents) causes the increase of the measured impedance, whereas the load current (outfeed) leads to the decrease. Hence, they can initiate over- or underreaching problems. An upstream power flow will emerge as a negative impedance (it will be in the left-half plane of a *R-X* diagram) seen from relays *R6*, *R10* towards the utility grid.

The simulations have revealed that the power flow through relay *R6* is in the normal direction and through *R10* – reverse for

the high load in the system, and for both devices the upstream flow is identified for the low load. Thus, according to (3), the closest to the origin impedance trace occurs during the high load and zero DG production in the system. Nevertheless, it is far from the impedance circles of the corresponding lines under protection. Hence, the settings of these relays are not affected by these events and there is no need in special means, such as load encroachment blinders [16]. Analogous conclusions are valid for relays *R12* and *R13* located at the DG units.

To sum up, inherent directionality of distance relays performed as a measured negative impedance is used to cope with sympathetic tripping issues: during faults in the system a downstream power flow is established on account of the DG small capacity, therefore the settings do not require tripping zones in the left-half plane of the *R-X* diagram. Finally, a calculated impedance does not depend on a short circuit current level therefore the blinding effect is not observed.

4.2 DG commutation operations and production variation.

Here dynamic change of impedance trajectories due to variation of system operation conditions is examined in order to ensure that they do not cross the tripping zones. The most interesting events for feeder relays *R6*, *R10* are commutation operations of the DG (e.g. due to internal faults or maintenance works) and changing of its output power (intermittent nature).

The simulations have disclosed the large traces for both relays. As an example, Fig. 2 illustrates changing of the DG production from 0 to 100% during the high load. The loci do not cross the tripping zones performed as the *Mho* circles [17]. Hereafter, red circles denote departure points and asterisks – ends of trajectories. It is seen how relay *R10* detects the change of the power flow direction – Fig. 2b. The tripping characteristics of the relays also stay intact during the low load in the system.

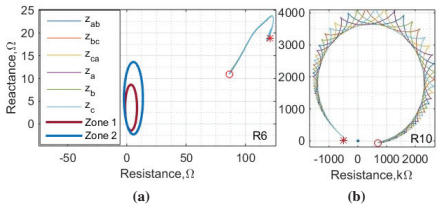

Fig. 2: Impedances measured by *R6*, *R10* for DG production variation.

Thus, the settings of these relays do not require special means preventing inadvertent operation (e.g. blinding zones, power swing blocking logic [18]) because of the planned changes of operation states of the system, as distinct from the overcurrent protection. The further study relates to abnormal events in the network and relay performance during them.

4.3 Faults close to DG location.

In this section faults occurring in *TL16-TL18,TL20,TL21* are investigated; designations in all further plots as *3ph* for a three-phase and *1ph-g* for an one-phase-to-ground type are held. Abnormal currents must be tripped by *R10*, and relay *R6* should serve as a backup protection. Initially, the settings for the tripping zones of relay *R10* have been chosen as the *Mho* circles with [17]: Zone 1 – 90% from the sum of the positive sequence impedances of lines *TL16,TL17,TL18*; Zone 2 reaches 50% of *TL19*; Zone 3 – 100% of this line. As an example, Fig. 3 illustrates the simulated results for the faults in *TL18* with a location at 90% of the summing length, i.e. $k = 0.9$.

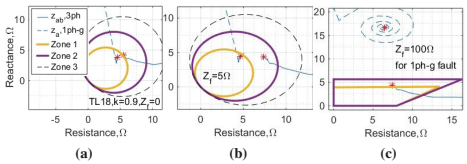

Fig. 3: Impedances measured by relay *R10* for faults in *TL18*.

Fig. 3a demonstrates the cases with zero fault impedance Z_f that are efficiently detected by the given relay settings. However, considering that the fault location in this situation coincides with the Zone 1 settings, it is possible to notice that the end points of the trajectories are slightly differ from the circle of Zone 1 because for the three-phase type the underreaching effect is observable. The reason is the infeed current from the DG described by expression (3). However, due to the small capacity of the generators, the error is less than 5%. For the ground fault, the reason of the overreaching is the load current because the level of the short circuit current is comparable.

Zone 1 does not normally have a time delay to ensure fast tripping; however, it might be necessary in special cases (some of them are presented later) and to guarantee selectivity with downstream fuses (fuse-blowing strategy). Zone 2 and 3 require a coordination time interval (CTI) in order to provide selectivity with neighboring relays. A CTI_2 (the index implies belonging to the corresponding zone) is normally $0.25 - 0.4$, and $\text{CTI}_3 = 0.4 - 1$ s [17].

Fig. 3b shows effect of the nonzero fault impedance. It is observable that the small fault impedance (existing due to an arc) shifts the end points from Zone 1 to 2 deteriorating fast tripping capability of the relay. To cope with this concern, the quadrilateral characteristics can be applied as it is shown in Fig. 3c. They are calculated on the basis of a fault impedance which can be represented as a pure arc resistance R_f estimated, for instance, with the help of Warrington's equation [17].

At the same time, Fig. 3c shows the ground fault locus for the high impedance – 100 Ω. It leads to the underreaching problem even if applying a new quadrilateral zone. To eliminate this error, compensation of Z_f is required during calculations that

demands auxiliary equipment or communication links between adjacent protective devices.

4.3.1 Coordination of feeder relays with DG protection.

For faults at this location it is necessary to trip the generators according to the safety requirements [14]; therefore, the further examples focus on the DG relays. Let us consider a fault in *TL21*. As the location is in the infeed line, relay *R13* must detect and clear it as fast as possible, then feeder relay *R10* should act to separate the damaged line from the system. Thus, Zone 2 reaches the generator locations in term of an apparent impedance. For the generator relay, it is possible to derive the following expressions of the impedance measurements:

$$\frac{U_{13}}{I_{DG2}} = kZ_{TL21} + R_f\Big(\frac{I_s}{I_{DG2}} + 1\Big), \tag{4}$$

where U_{13}, I_{DG2} are the voltage and current measured by the relay, Z_{TL21} – the infeed line impedance, I_s is the current from the utility grid. Analyzing equation (4), it is possible to deduce that an error caused by I_s/I_{DG2} (if $R_f \neq 0$) will be significant due to the large current from the utility grid. Thus, the expected fast reaction of the DG relay cannot be achieved – fault detection will occur only after relay *R10* trips the system current.

The feeder faults must be recognized by Zone 1 of relay *R10* and a clearing time is mainly determined by breaker operation – 100 ms [17]. After that the generators must be decoupled and it is normally provided by the undervoltage relays [19] that are supposed to be replaced by the impedance type. For these purposes Zone 2 of relays *R12*,*R13* reaches the highest apparent impedance for faults in *TL16*-*TL18*. It requires a CTI_2 higher than a corresponding time delay of Zone 2 for relay *R6* and the pickup time of relay *R11* in order to preserve selectivity.

Fig. 4a demonstrates the loci seen by *R13* during the three-phase faults in *TL16*-*TL18* before a feeder breaker acts ($t <$ 100 ms). As it is possible to notice, almost all locations are not detected by relay *R13*. The reasons of these phenomena depend on a fault location.

For the upward faults (in *TL16*) the error is caused by an additional voltage drop at the fault resistance similarly to the described above situation with the damaged infeed line; therefore, only the case with $R_f = 0$ is recognized by Zone 2 (the yellow curve). For the ground faults this problem does not exist due to the small short circuit current level – the violet curve in Fig. 4c.

For the downward faults (in *TL18*) the error (Fig. 4a, the blue and orange curves) is induced by the system current that is the infeed current in the generator relay point of view. The ground faults are detected by Zone 1 due to the overreaching caused by the load current, Fig. 4c.

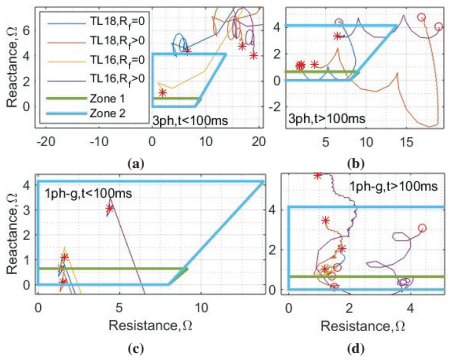

Fig. 4: Impedances measured by relay *R13* for faults in *TL16* and *TL18*.

Fig. 4b and Fig. 4d show the situation after the feeder breaker disconnect the rest of the network ($t > 100$ ms). For the three-phase faults it provokes elimination of the errors associated with the system current, for the ground type – with the load. Now the end points are inside the zones excepting the ground fault in *TL16* (Fig. 4d, the violet curve). The reason is the infeed current from the asynchronous generator that does not exist during the three-phase faults because of a significant drop of phase voltages and, consequently, lack of reactive power. Hence, impedance relay *R12* cannot detect tree-phase faults in the feeder (as well as in the own line) and provide reliable protection.

Summarizing this section, the generator distance relays require compensation of a fault impedance error (4) in order to provide the fast protection for the infeed lines. Zone 2 of the ground units should be extended considering all possible infeed currents in advance; moreover, to avoid misoperation, compensation of load current should be accomplished or a CTI_1 can be used if it is acceptable for the generator. Despite these means, a fault impedance can exceed an anticipated value and the distance protection cannot guarantee the reliable decoupling functions.

4.4 Distant faults from DG location.

This study case is related to unwanted tripping of the generators because of faults outside the intertie location. Operation of the production units during such events depends on locations in feeders. During faults in Feeder 1 the DG is allowed to stay connected to the main grid because the protection of Feeder 2 must not react to abnormal currents in the system. Nevertheless, voltage collapse might violate the given limits and the DG will be inadvertently decoupled by the undervoltage relays. Response of the generator relays to faults in Feeder 2 are completely identical to the studied above feeder faults at

the intertie location, Fig. 4. Any fault is detected and cleared by local protection facilities; then the DG continues to work if a downward breaker acts (controlled by *R11*), and must be disconnected in case of tripping of any upward feeder breaker (governed by *R6*,*R10*).

Fig. 5a demonstrates the calculated impedances by relay *R13* for the three-phase faults in the beginnings of *TL8,TL2* and end of *TL19* (the extreme locations) after the local breakers clear them. As it is possible to see, Zone 2 and 3 detect the faults in Feeder 2 (the blue and orange curves), whereas the fault in Feeder 1 is out of their reach (the yellow curve). It should be noticed that the fault in *TL19* (the blue curve) is cleared by relay *R10* (failure of relay *R11*), otherwise the end point would not fall into the tripping zones. Here, Zone 3 is chosen to reach an apparent impedance for a fault close to the common busbar; such approach can help to discriminate faults in the adjacent feeders.

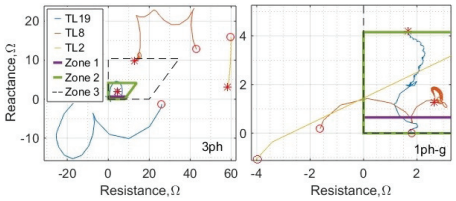

Fig. 5: Impedances measured by relay *R13* for faults in *TL2,8,19*.

Analyzing the trajectories of the ground faults in Fig. 5b, it is possible to see again that the uncompensated load current can lead to misoperation for the downward faults (the blue curve) and for the faults in Feeder 1. In general, it should be compensated as it is proposed, for instance, in [20]. Thus, the distance protection of the DG can block the undervoltage relay preventing false tripping. Nevertheless, there is risk of malfunction for high fault impedances; therefore, the undervoltage protection plays still a vital role in cases where communication links are not used, and the impedance relays should only assist it.

4.4.1 Protection of lateral lines.

This section is referred to the settings of relay *R6*. For the first zone it is used the standard calculations – 90% of the summing impedance of lines *TL8,TL12,TL15*. Zone 2 must provide a backup protection for relay *R10*, therefore it reaches the end of *TL16*. Finally, Zone 3 can cover the impedance up to relay *R11*. Fig. 6 shows the calculated impedance trajectories for the faults at the beginnings of lines *TL8,TL16,TL10,TL14*. The main purpose of this study is to make sure that the relay provides protection for lateral outfeed lines *TL9* and *TL13*.

Fig. 6a presents the cases for the three-phase faults: the selectivity requirements between relay *R6* and *R9,10* are met. At the same time, the end point for the fault in *TL10* (the yellow curve) falls into Zone 1 that means violation of the time coordination with relay *R7* – relay *R6* might pick up faster. Thus, to preserve selectivity, Zone 1 must have a time delay greater than the pickup time of relay *R7*.

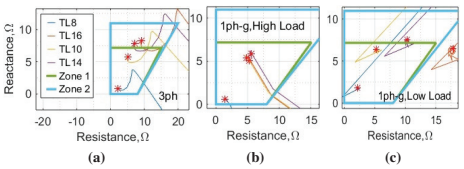

Fig. 6: Impedances measured by relay *R6* for different fault locations.

Fig. 6b represents the following complications for the ground faults: all end points are inside Zone 1 because of the load current influence. Decreasing of the zones cannot resolve this issue because, as it is possible to see from Fig. 6c, shifting of the load from the high to low leads to the loci relocation. Thus, this example also illustrates a need in load compensation for the ground units of the feeder relays.

5 Conclusion

This work has demonstrated the performance of the distance protection in the specific distribution network with the DG. The results show that the impedance relays can eliminate the issues caused by power flow changes and unwanted tripping of the DG. To sum up, the main conclusion from the executed study are:

- The impedance measurements are affected by infeed/outfeed connections along a protected line. The phase units of the feeder distance protections are not subjected to these effects but susceptible to a fault impedance – it causes underreaching problems. The ground units require compensation of load current for better performance. This compensation is needed only for power flows in the forward directions; for the backward, in turn, the logic of the relays can block a tripping signal (an impedance trajectory will come from the left half-plane) preserving directionality capability.

- The distance protection of the DG has the same problems and, additionally, it requires compensation of fault impedances. Hence, without communication technologies, reliable functionality cannot be provided.

- If an accurate compensation of a fault impedance and load current is accomplished, the distance relays can replace

the undervoltage protection of the DG. It provides decoupling functions for faults in Feeder 2 and discriminations of other abnormal events improving FRT capability.

- Special attention deserves time coordination between the relays. For the feeder relays the general recommendation is to set a CTI_2 and CTI_3 greater than the pickup times of all overcurrent protection locating in the zone reaches. For the DG relays, the time delays have to exceed these intervals in order to prevent anticipatory tripping of the generation units.

- The feeder distance protection can secure several outfeed lateral lines. Depending on a network configuration, it can require an additional CTI_1. A time delay for Zone 1 might also be needed for coordination with downstream equipment.

These findings are valid for the generators of the comparably small capacity and for their remote location from the main busbar. Therefore, further research works also require derivation of generalized results by means of consideration of different types of distribution networks, sources of energy for DG, their ratings, locations and conversion technologies. Furthermore, under/overreaching effects brought in by a high fault impedance and loads must be compensated in order to increase competitive ability of distance relays for application in distribution networks. The approaches to accomplish this task will also be presented in the future studies.

With utilization of communication technologies many concerns become effortless [21] because pilot protection can be implemented that gives reliable solutions for MV networks. The presented results help to recommend design guidelines for the most appropriate protection schemes in distribution networks with DG.

Acknowledgements

The authors would like to thank the system operator of Norwegian distribution network "Eidsiva Nett" for provision of the necessary information to build and verify the model.

References

[1] K. Kauhaniemi, L. Kumpulainen, "Impact of Distributed Generation of the Protection of Distributed Networks", *Eighth IEE International Conference on Developments in Power System Protection*, **volume 1**, pp. 315-318, (2004).

[2] G. Antonova, M. Nardi, A. Scott, M. Pesin, "Distributed Generation and Its Impact on Power Grids and Microgrids Protection", *65th Annual Conference for Protective Relay Engineers*, pp. 152-161, (2012).

[3] Y. Pan, I. Voloh, W. Ren, "Protection Issues and Solutions for Protecting Feeder with Distributed Generation", *66th Annual Conference for Protective Relay Engineers*, pp. 92-111, (2013).

[4] F. Coffele, C. Booth, A. Dyśko, G. Burt, "Quantitative analysis of network protection blinding for systems incorporating distributed generation", *Generation, Transmission & Distribution, IET*, **volume 6**, **issue 12**, pp. 1218-1224, (2011).

[5] R. Sirsi, S. Dasarathan, "Application of Fault Current Limiter to Limit Distributed Generation Effect on Distance Relay Coordination", *2014 Annual IEEE India Conference (INDICON)*, pp. 1-6, (2014).

[6] D. Uthitsunthom, T. Kulworawanichpong, "Distance Protection of a Renewable Energy Plant in Electric Power Distribution Systems", *International Conference on Power System Technology (POWERCON)*, pp. 1-6, (2010).

[7] F. A. Viawan, D. Karlsson, A. Sannino, J. Daalder, "Protection Scheme for Meshed Distribution Systems with High Penetration of Distributed Generation", *Power Systems Conference: Advanced Metering, Protection, Control, Communication, and Distributed Resources*, pp. 99-104, (2006).

[8] H. Mortazavi, H. Mehrjerdi, M. Saad, S. Lefebvre, D. Asber, L. Lenoir, "Application of Distance Relay for Distribution System Monitoring", *IEEE Power & Energy Society General Meeting*, pp. 1-5, (2015).

[9] I. Chilvers, N. Jenkins, P. Crossley, "Distance relaying of 11 kV circuits to increase the installed capacity of distributed generation", *IEE Proceedings-Generation, Transmission and Distribution*, **volume 152**, **issue 1**, pp. 40-46, (2005).

[10] S. Voima, K. Kauhaniemi, "Using Distance Protection in Smart Grid Environment", *IEEE PES Innovative Smart Grid Technologies Conference Europe (ISGT-Europe)*, pp. 1-6, (2014).

[11] S. Voima, H. Laaksonen, K. Kauhaniemi, "Adaptive Protection Scheme for Smart Grids", *12th IET International Conference on Developments in Power System Protection (DPSP 2014)*, pp. 1-6, (2014).

[12] J. Ma, J. Li, Z. Wang, "An Adaptive Distance Protection Scheme for Distribution System with Distributed Generation", *5th International Conference on Critical Infrastructure (CRIS)*, pp. 1-4, (2010).

[13] C. Jecu, B. Raison, R. Caire, P. Alibert, P. Deschamps, O. Chilard, S. Grenard, "Protection scheme based on non communicating relays deployed on MV distribution grid", *IEEE Grenoble PowerTech (POWERTECH)*, pp. 1-6, (2013).

[14] "Protection of Distribution Systems with Distributed Energy Resources", *International Conference on Electricity Distribution, CIGRE-CIRED Joint Working Groups, Final Report C6.26/B5*, (2015).

[15] P. M. Anderson, "Power System Protection", New York: IEEE Press, A John Wiley & Sons, (1999).

[16] A. Sinclair, D. Finney, D. Martin, P. Sharma, "Distance Protection in Distribution Systems: How It Assists With Integrating Distributed Resources", *Rural Electric Power Conference (REPC), IEEE*, pp. B3-1 – B3-12, (2013).

[17] J. L. Blackburn, T. J. Domin, "Protective relaying. Principles and applications", 4th ed., New York: CRC Press, Taylor & Francis Group, (2014).

[18] J. Mooney, P.E. and N. Fischer, "Application Guidelines for Power Swing Detection on Transmission Systems", *Power Systems Conference: Advanced Metering, Protection, Control, Communication, and Distributed Resources, PS '06*, pp. 159-168, (2006).

[19] IEEE Standard for Interconnecting Distributed Resources with Electric Power Systems, IEEE Standard 1547-2003, Approved 12 June 2003.

[20] J. I. Marvik, "Fault Localization in Medium Voltage Distribution Networks with Distributed Generation", Ph.D. dissertation, Dept. of Electric Power Engineering, Norwegian University of Science and Technology, Trondheim, June 2011.

[21] S. Voima, K. Kauhaniemi, "Benefits of using telecommunication based protection with DG", *Integration of Renewables into the Distribution Grid, CIRED Workshop*, pp. 1-4, (2012).

[Paper II]

K. Pandakov, H. Kr. Høidalen. (2017) Distance protection with fault impedance compensation for distribution network with DG, *IEEE PES Innovative Smart Grid Technologies Conference Europe (ISGT-Europe 2017)*, p. 1-6.

Distance Protection with Fault Impedance Compensation for Distribution Network with DG

Konstantin Pandakov
NTNU, Norway, Trondheim
Email: konstantin.pandakov@ntnu.no

Hans Kristian Høidalen
NTNU, Norway, Trondheim
Email: hans.hoidalen@elkraft.ntnu.no

***Abstract*—Impedance type relays are a promising alternative to overcurrent protection in distribution networks with dispersed generation (DG) due to their inherent directionality and fault current independence. At the same time, the biggest problem in their application is underreaching issues caused by non-zero fault impedances. This work proposes a universal compensation strategy aiming at eliminating errors produced by fault impedances and infeed currents from DG. The method is tested on a model of an actual network in PSCAD™/EMTDC™. It demonstrates good performance for interphase faults and gives possibilities for fault location. The developed approach helps to improve dependability of impedance relaying in distribution networks with DG and overall quality of power supply.**

***Index Terms*—distance relay, distribution network, DG, fault impedance**

I. Introduction

Impedance type protection can be a suitable solution for distribution networks against issues arising due to presence of distributed generation (DG): mainly sympathetic tripping, blinding and miscoordination between devices. Application of distance relays in the real system with DG has been discussed in [1] with pointing at the main challenge: non-zero fault impedance causing underreaching effect. The current paper offers a solution to this problem.

The work is only focused on low-ohmic (up to 100 Ω) interphase faults (to ground) because single-line-to-ground faults are challenging for impedance relays in compensated and isolated networks and require special attention.

Fault impedance and distance calculations for a multiterminal transmission network are extensively studied. The methods are mainly based on a known topology, line impedance information and multi-point synchronized measurements, for example [2]. They cannot however be implemented in distribution networks due to numerous load taps between measuring points that produce errors. Moreover, topology of a system and line parameters are not always available.

Presence of DG complicates the situation further: impedance measurements are affected by remote infeed currents. Reference [3] shows that three different methods on fault location suitable for distribution networks become inadequate in case of presence of DG. Thus, for compensation purposes it is necessary to determine additional voltage drops from infeed currents on lines (if there is a common path with the main power flow) and on a fault impedance.

For this purpose, determining of a fault position can be required. The developed fault location methods for distribution networks with DG, for example [4], require prefault input information (line impedances, loads, topology, multi-point measurements) and extensive calculations. Nevertheless, precision of the methods is insufficient for protection purposes.

More accurate results in location and fault impedance calculations can be achieved with application of multi-agent systems as it is proposed in [5]. [6] demonstrates utilization of PMU technologies for these purposes. Authors of [7] perform the impedance differential protection method with fault impedance evaluation.

Studies on fault impedance compensation in presence of DG are still lacking. The main drawbacks of the performed methods are a need of information about line impedances and network configuration, as well as absence of load taps between a registering and a faulty point.

The current work offers a method for compensation of the fault impedance and errors associated with DG for distance relays in distribution networks. The method is universal since it utilizes an equivalent line (or a network if infeed currents are present) approach and independent of topology or load conditions; however, it requires multi-point synchronized measurements. After compensation and selective fault clearance, a measured impedance can be used for fault location with the object of restoration time reduction.

II. Theoretical background

For compensation of an error only caused by fault impedance Z_f, synchronized two-point measurements are utilized: voltages and currents of phases involved into a fault. Let us consider a simple network with three sections terminated by relays R_{1-3} illustrated in Fig.1a. Compensation is performed for distance relay R_1.

A pair of relay is chosen (either $R_1 - R_2$ or $R_1 - R_3$) in order to wrap the system with all load taps and sections into a simple equivalent line with series impedance Z calculated as:

$$Z = \frac{V_s - V_r}{I_s}, \tag{1}$$

where $V_s = V_{ph1} - V_{ph2}$ is voltage between two faulty phases ($ph1$ and $ph2$) measured by R_1 (index "s" stands for sending) and similarly for current $I_s = I_{ph1} - I_{ph2}$; V_r is

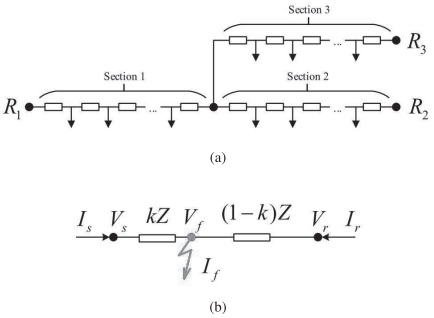

Fig. 1: Wrapping of the system (a) into its equivalent line split by the fault (b).

analogous interphase voltage measured by R_2 or R_3 (index "r" denotes receiving); as a result, series impedance Z corresponds to a positive sequence quantity [1]. At this step, prefault measurements are utilized.

Then, the equivalent line is split by the faulty point as it is shown in Fig.1b. At this stage, all measurements are after fault inception. Parameter k is a relative distance from the sending end. Hereafter, V_f is voltage at the faulty point and I_f is current in a fault impedance. Faulty voltage V_f can easily be determined having the following system of equations:

$$\begin{cases} V_f = V_s - kZI_s \\ V_f = V_r - (1-k)ZI_r \end{cases} \tag{2}$$

Here $I_r = I_{ph1} - I_{ph2}$ is current at the receiving end. Then compensation is realized as follows:

$$Z_{R_1} = \frac{V_s - V_f}{I_s} = kZ \tag{3}$$

The value will be smaller than an actual line impedance between the measuring and the faulty point because of the load outfeeds (overreaching).

Nevertheless, depending on a chosen pair of relays, the equivalent line approach can serve as a fault locator based on measured impedance Z_{R_1}. This point is summarized in Table I.

TABLE I: Compensated impedance Z_{R_1} obtained through the equivalent line approach

Fault location	R_1–R_2	R_1–R_3
Section 1	kZ_1	kZ_1
Section 2	$Z_1 + (1-k)Z_2$	Z_1
Section 3	Z_1	$Z_1 + (1-k)Z_3$

Z_{1-3} are the summed line impedances (in positive sequence) in the corresponding section. It is seen that, for example for pair R_1–R_2, if $Z_{R_1} < Z_1$, then a fault is in section 1; if $Z_{R_1} > Z_1$ – section 2; if $Z_{R_1} = Z_1$, a fault takes place at the intersection point or in any place of section 3. In order to find this place, pair R_1–R_3 is employed.

If a fault is neither in section 1 nor in section 2 or 3 (out of the protection zone), a real part of a calculated fault impedance V_f/I_f will be negative and underreaching will take place $Z_{R1} > Z_{\text{Zone1}}$ (Zone 1 settings of R_1).

Loads will not significantly affect calculations due to negligibility comparing with high fault current. The method can be extended to more measuring points.

A. Compensation of infeed currents from DG

The equivalent line approach is inadequate in case of presence of DG in the protection zone. In order to compensate infeed curents, an equivalent network is determined: a part of a system between relays R_1 and R_2 is wrapped into $N+1$ equivalent lines, where N is a number of additional measuring points at interconnected generators. Fig.2 shows the example with two generators (R_{DG1} and R_{DG2}) in order to generalize the approach.

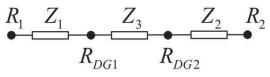

Fig. 2: The equivalent network with measuring points at DGs.

Now, prefault four-point synchronized measurements are exploited in order to find series impedances Z_{1-3} in positive sequence:

$$\begin{aligned} Z_1 &= \frac{V_{R_1} - V_{R_{DG1}}}{I_{R_1}} \\ Z_2 &= \frac{V_{R_2} - V_{R_{DG2}}}{I_{R_2}} \\ Z_3 &= \frac{V_{R_{DG1}} - V_{R_{DG2}}}{I_{R_1} + I_{R_{DG1}}}, \end{aligned} \tag{4}$$

where $V_{R_{1,2}}$ and $V_{R_{DG1,2}}$ are interphase voltages at the measuring points; $I_{R_{1,2}}$ and $I_{R_{DG1,2}}$ are analogously interphase currents. After that, utilizing measurements during fault, a fault location procedure is introduced:

1) It is initially supposed that fault takes place in one of the equivalent line. Then, $V_{s,r}$, $I_{s,r}$ can be calculated.
2) Fault parameters k, V_f are calculated according to (2), additionally fault current as $I_f = I_s + I_r$, and fault impedance as $Z_f = V_f/I_f$.
3) Additional voltage drop ΔV on the equivalent lines due to presence of the DGs is calculated:

$$\begin{aligned} \Delta V &= 0, \text{ if line 1 is chosen} \\ \Delta V &= Z_3 I_{R_{DG1}} + (1-k)Z_2(I_{R_{DG1}} + I_{R_{DG2}}), \text{ if line 2} \\ \Delta V &= kZ_3 I_{R_{DG1}}, \text{ if line 3} \end{aligned} \tag{5}$$

4) V_f, Z_f and ΔV are saved.

5) All these steps are repeated for the next line.

As a result, vectors $\mathbf{V_f}$, $\mathbf{Z_f}$ and $\mathbf{\Delta V}$ (size of all is 3×1, in general case is $(N+1) \times 1$) are accumulated. A minimal value in $\mathbf{Z_f}$ (that is without added errors) points out the true faulty equivalent line and associated V_f and ΔV from the corresponding vectors can be extracted. Then, compensation is performed as:

$$Z_{R_1} = \frac{V_s - V_f - \Delta V}{I_s} \tag{6}$$

Utilizing this approach, the same logic for fault location as in Table I can be applied. Let us assume that all DGs are located in section 3 (Fig.1a), then the first two rows in the table are valid for both pairs of relays. For pair R_1–R_3 and fault in Section 3, Z_{R_1} stays the same at it is given in the table (infeed currents are compensated). For pair R_1–R_2 and fault in Section 3, calculated Z_{R_1} is not equal to Z_1 anymore and becomes greater due to infeed currents.

The performed approaches are tested on the real network with DG described in the next section.

III. Test case network

The distribution network illustrated in Fig.3 is an actual 22 kV grid with DG: a synchronous (1.6 MVA) and an induction generator (0.6 MVA). Main distribution transformer *T1* is 20 MVA, the utility grid is 66 kV and has 250 MVA of short circuit capacity. The network has overhead transmission lines *TL1-TL22* together with extensive cable sections (specially marked lines *TL10_1,TL10_3,TL11_1,TL22_2*). Numerous load points are connected with the main trunks by short cables; detailed modeling of this configuration is bulky, therefore represented as concentrated loads *S0-S19*. Protection functions are accomplished by relays *R1-R13*. Relays *R2*, *R6* and *R10* are impedance type.

The model is built in PSCAD™/EMTDC™: the transmission lines are represented as the PI-equivalent models (electrostatic asymmetry is taken into account), the loads are delta-connected constant impedances, the utility grid is an ideal voltage source with inductive short circuit impedance, the transformers and the generators can be found in the standard libraries of the simulation program. All parameters were provided by the system operator and cannot be disclosed.

To cover extreme cases, high load is modeled. Since interphase measurements are utilized, only three-phase-faults are performed (two-phase have the same results) at line ends. Arcing faults with a low fault impedance (~10 Ω) can be handled by quadrilateral characteristics of the impedance relays as it was shown in [1]; therefore, a considerable fault impedance is used (100 Ω) to introduce underreaching problems. As the compensation is applied, mho characteristics for the impedance relays are used. For illustrative purposes, Zone 1 is equal to 100 %. All line impedances are given for positive sequence.

Simulated voltages and currents are processed through the Discrete Fourier Transform with anti-aliasing filter in order to extract magnitudes and angles of the fundamental components only. Impedances are calculated during 50 ms after fault inception according to requirements about protection speed [8]. The compensation is started when an impedance falls below 50 % from a prefault value.

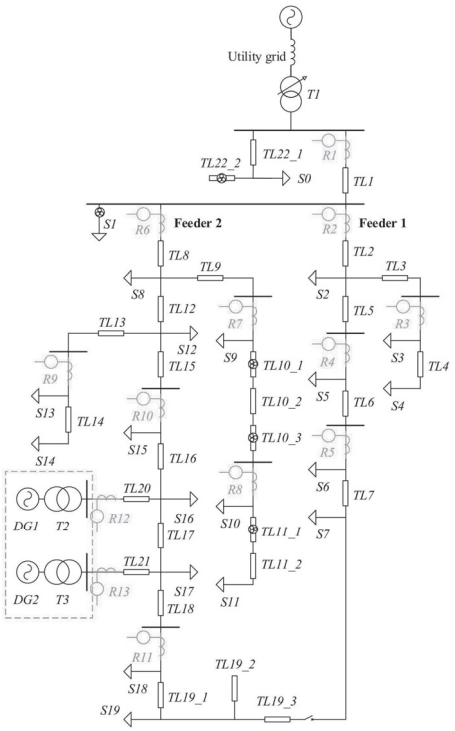

Fig. 3: 22 kV distribution network with DG.

IV. Results and discussions

Fig.4 and Fig.5 show application of the equivalent line approach. Fig.4a shows the impedance trajectories measured by relay *R2* for the fault in *TL2*. Relay pairs *R2 – R3* and *R2 – R4* for identification of equivalent lines are utilized. The compensation is performed according to (3) for relay *R2*. The compensated impedances (hereafter, an end point of an impedance trajectory marked by a circle is implied) falls into Zone 1, whereas the uncompensated (notation "w/o cmp" is used) does not. For both pairs, the compensated impedances are the same according to Table I and equal to the impedance of *TL2* (Z_{TL2}).

Fig.4b illustrates the fault in *TL6*. The compensation with pair *R2 – R3* gives the same result as before (Z_{TL2}) according

to Table I, whereas pair *R2* – *R4* leads to underreaching – the compensated impedance is precisely equal to the impedance between relay *R2* and the faulty point ($Z_{TL2} + Z_{TL5} + Z_{TL6}$). Such result of the compensation is possible for feeders without DG.

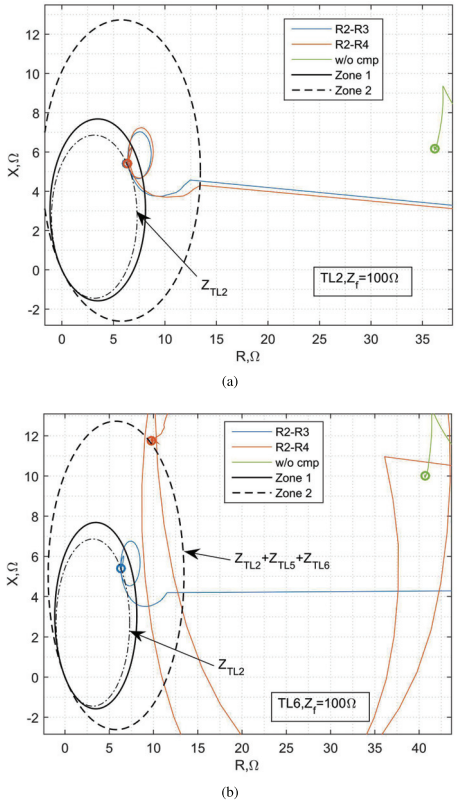

Fig. 4: The impedance trajectories measured by relay *R2* for the fault in a) *TL2* and b) *TL6*. Measurements of relays *R3* and *R4* are used for the compensation strategy.

Fig.5 demonstrates the uncompensated (measured by relay *R6*) and the compensated loci (obtained by the means of pair *R6* – *R10*) for the faults in Feeder 2: *TL8*, *TL10_2*, *TL13*, *TL16*, and *TL18*. The compensation start points corresponding to 50 % of prefault impedance values are also presented. As it is possible to see, the compensated impedances for *TL8* and *TL10_2* are the same and equal to the impedance circle corresponding to *TL8*. For *TL13*, it is close to the circle reflecting the impedances of *TL8* and *TL12* ($Z_{TL8} + Z_{TL12}$). The small discrepancy (overreaching) is caused by the loads. The compensated impedances for *TL16* and *TL18* are equal and situated inside Zone 2; they are not linked to the line impedances between relay *R6* and the actual faulty points as in the previous case due to presence of the DGs.

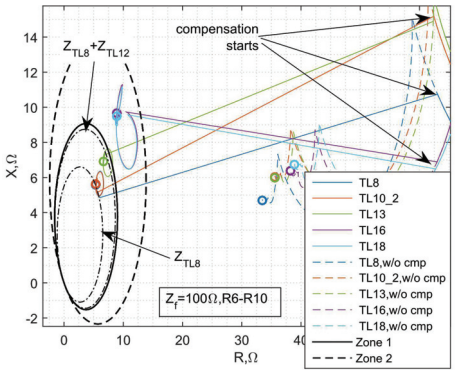

Fig. 5: The uncompensated impedance trajectories measured by relay *R6* for the faults in *TL8*, *TL10_2*, *TL13*, *TL16*, *TL18* and their compensation by the mean of relay *R10*.

In order to identify a faulty position in the side branche (*TL13*) measurements of relays *R7* and *R9* are utilized. In such case, due to presence of the DG in the protection zone, the equivalent network depicted in Fig.2 is used. Fig.6 shows the result of the compensation accomplished according to (6).

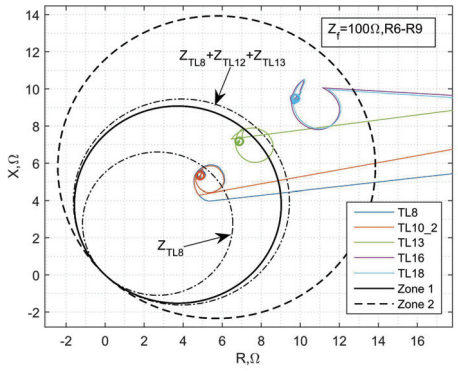

Fig. 6: The compensated with the help of relay *R9* impedance trajectories measured by relay *R6* for the faults in *TL8*, *TL10_2*, *TL13*, *TL16*, and *TL18*.

Since infeed currents are compensated, the impedances for the faults in *TL8* and *TL10_2* are equal and close to circle

Z_{TL8} according to Table I as in the previous case. It is also noticeable that the overreaching errors for *TL8*, *TL10_2*, and *TL13* (the compensated impedance does not end on circle $Z_{TL8} + Z_{TL12} + Z_{TL13}$) are higher than in the previous case.

For low fault impedances, this error is smaller due to significant fault currents in the system. Although this circumstance provides inaccuracies for evaluation of the fault locations, it does not have negative influence on protection functionality. Fig.7 illustrates the compensated impedances for the faults outside the protection zone: Feeder 1 (*TL2*) and Zone 2 of relay *R6* (*TL14*).

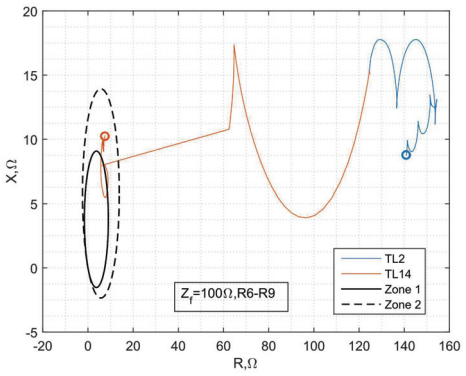

Fig. 7: The compensated with the help of relay *R9* impedance trajectories measured by relay *R6* for the faults in *TL2* and *TL14*.

The fault in the adjacent feeder is unambiguously discriminated. Despite overreaching errors during the compensation, the compensated impedance for the fault in *TL14* cannot fall into Zone 1 provoking miscoordination with downstream relay *R9*; however, the locus crosses Zone 1, therefore Zone 1 must not initiate instantaneous tripping (at least 50 ms delay is required).

At the same time, an end point of a locus of a fault close to relay *R6* will be near the origin and can be outside Zone 1 because of errors; hence, the mho characteristics must have safety margins in other quadrants in order to guarantee dependability.

In order to distinguish the faults in *TL16* and *TL18*, measurements of relays *R10* and *R11* must be involved. The compensation is realized for relay *R10* according to (6). Fig.8 demonstrates the results.

It is seen that the uncompensated impedances are significantly affected by the presence of the DG: the real parts are higher than expected (three-phase-fault with interphase impedance 100 Ω must have position around 35 Ω, see Fig.5), the imaginary are negative due to injection of reactive power by the synchronous generator. The compensated loci are close to the corresponding circles (the fault in *TL16* to Z_{TL16}, and

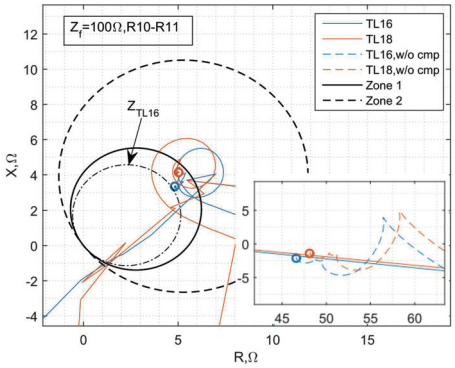

Fig. 8: The impedance trajectories measured by relay *R10* for the faults in *TL16*, *TL18* and their compensation by the mean of relay *R11*.

TL18 to Zone 1 as it is anticipated according to Table I) with the small errors. The same conclusion about close-in faults is valid.

These examples show applicability of the compensation strategy base on the equivalent line or the network in case of presence of infeed currents. In addition, it must be noted that relay *R10* is exposed to reverse power flow due to the DG; however, this fact does not affect results of the compensation either it is a master or a slave unit.

It is worth mentioning that the faults located outside the protective zone give the compensated impedances significantly beyond Zone 1 of relay *R10*, see Fig.9. This peculiarity hampers unnecessary tripping even if reverse power flow occurs and assists coordination with the downstream relay.

V. Conclusion

This work presents a fault impedance compensation strategy for distance relays based on multi-point synchronized measurements in distribution networks. The performed approaches do not require information about detailed multitapped system topology and loads. It has demonstrated sufficient performance for high impedance faults in the system with the DG.

In reality, the compensation can be initiated based on two conditions: an impedance falls below 50 % from a prefault value; rate of change of impedance is comparable with several tens of Ohms per millisecond.

In case of communication failure (losing of compensation capability), an impedance relay can continue to perform protection functions, however dependability is threatened. For end sections, when two-point measurements are not available, single-end methods can be applied [3], [9] in order to improve reliability.

As an advantageous outcome, the method allows fault location in side branches using multi-point measurements.

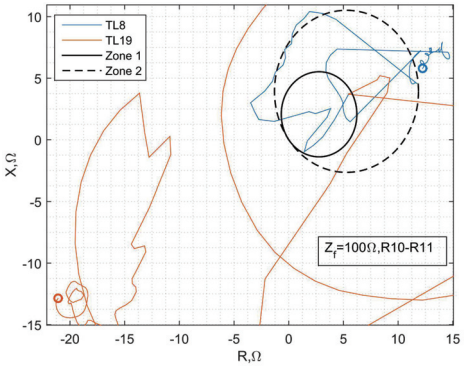

Fig. 9: The compensated with the help of relay *R11* impedance trajectories measured by relay *R10* for the faults in *TL8* and *TL19*.

Utilization of the equivalent line or the network allows to identify faulty sections and to estimate line impedance from a relay to a faulty point. An error for the equivalent line is below 3 % and for the network can be 20 % (the worst case with a short side line, a high fault impedance and high load in the system). It is affected by simplicity of the representation and ways to improve it is a topic for further research.

The main drawback of the method is economical issues of realization in practice since a number of synchronized measurements is required. Despite this fact, application of the proposed approach in the real system will benefit as follows:

- Elimination of underreaching issues caused by non-zero impedance interphase faults and presence of DG.
- Fault location capability enabling improvement of power supply reliability.
- Discrimination of fault location can help to avoid unintentional islanding and nuisance tripping of dispersed generators.

Acknowledgment

The authors would like to thank the system operator of Norwegian distribution network Eidsiva Nett for provision of the necessary information to build and verify the model.

References

[1] K. Pandakov, H. Kr. Høidalen, J. I. Marvik, "Implementation of distance relaying in distribution network with distributed generation", in *Proc. 2016 13th International Conference on Development in Power System Protection*, pp. 1-7.

[2] P. C. Pietramala, M. Alla, B. K. Johnson, "Distance element corrective biasing during remote infeed conditions", in *Proc. 2016 North American Power Symposium*, pp. 1-6.

[3] B. D. S. Jose, P. A. H. Cavalcante, F. C. L. Trindade, M. C. de Almeida, "Analysis of distance based fault location methods for Smart Grids with distributed generation", in *Proc. 2013 IEEE PES ISGT Europe*, pp. 1-5.

[4] S. M. Brahma, "Fault Location in Power Distribution System with Penetration of Distributed Generation", *IEEE Transactions on Power Delivery*, vol. 26, issue 3, pp. 1545-1553, 2011.

[5] T. Zheng, H. Jia, "Application of Multi-Agent and impedance-based algorithm for fault location in power distribution systems with DG", in *Proc. 2011 International Conference on Advanced Power System Automation and Protection*, pp. 1044-1049.

[6] M. Zhang, Y. Wang, Z. Zhou, Z. Li, "Research on fault location based on PMU for multi-source distribution network", in *Proc. 2016 IEEE PES Asia-Pacific Power and Energy Engineering Conference*, pp. 1877-1882.

[7] W. Huang, T. Nengling, X. Zheng, C. Fan, X. Yang, B. J. Kirby, "An Impedance Protection Scheme for Feeders of Active Distribution Networks", *IEEE Transactions on Power Delivery*, vol. 29, issue 4, pp. 1591-1602, 2014.

[8] J. L. Blackburn, T. J. Domin, *Protective relaying. Principles and applications*, 4th ed., New York: CRC Press, Taylor & Francis Group, 2014.

[9] M. M. Saha, R. Das, P. Verho, D. Novosel, "Review of Fault Location Techniques for Distribution Systems", in *Proc. 2002 Power Systems and Communications Infrastructures for the future*, 6 p.

[Paper III]

K. Pandakov, C. M. Adrah, H. Kr. Høidalen, Ø. Kure. Experimental validation of a new impedance based protection for networks with distributed generation using co-simulation test platform, *Journal to be decided*.

Experimental validation of a new impedance based protection for networks with distributed generation using co-simulation test platform

Konstantin Pandakov, Charles M Adrah, Hans Kristian Høidalen, Øivind Kure

***Abstract*—Combined real-time hardware-in-the-loop simulations and modeling of communication networks (co-simulation platforms) is a powerful testbed for development and validation of relay protection schemes utilizing communication links especially for applications in Smart Grids. This paper introduces laboratory tests in such environment of a new protection scheme for medium voltage networks with distributed generation. It is based on impedance measurements with compensation of remote infeed currents and high fault resistances. Since the scheme utilizes multi-terminal measurements, a communication network emulator has been developed to model Ethernet network impairments. The test method uses Monte-Carlo approach for evaluation of protection dependability. The results demonstrate enhancement of impedance relay performance compared to the conventional protection. Moreover, fault location capability is preserved with sufficient accuracy. Nevertheless, communication network imperfections, such as jitters and data loss, deteriorate scheme functionality.**

***Index Terms*—co-simulation testbed, distributed generation, HIL, IEC 61850, impedance relaying**

I. Introduction

EXTENSIVE penetration of distributed generation (DG) into distribution networks creates problems for correct operation of the conventional protection mainly based on overcurrent relays. It requires development of new schemes to provide secure network operation.

Impedance (or distance) protection in such case can be an advantageous solution as showed in [1]. Nevertheless, it is prone to malfunctioning due to underreaching in presence of remote infeed currents from DG and high impedance faults.

Single-end methods developed for transmission systems, e.g. [2]–[7], might not be reliable for application in medium voltage (MV) networks with complex topology. In such case, dependability can be enhanced utilizing two-end [2], [8]–[12] or multi-terminal [13] measurements requiring communication links.

A necessary stage before real deployment of a new protective scheme is its laboratory validation. The most typical approaches are standalone tests using relay test sets and real-time (RT) hardware-in-the-loop (HIL) tests [14]. Advantages of the latter have been discussed and demonstrated in [15]. Moreover, RT HIL tests can be useful for development and verification of new protection methods for Smart Grids involving communication networks [16].

Application of a co-simulation platform that combines the RT HIL testbed and a communication network emulator allows thorough investigation of impact of communication network imperfections on protection performance, as e.g. in [17], avoiding consequent malfunctioning in real applications.

The current paper presents laboratory verification with a RT HIL testbed of the new protection scheme developed in [18] for distance relays in the multitapped distribution network with DG. The method compensates under-reaching errors of impedance measurements caused by remote infeeds and high fault impedances during interphase faults (with ground path as well if high impedance system grounding is used). Since the compensation strategy in this scheme uses multi-terminal measurements (required, at least, from DG locations), a communication emulator has been developed and used in the RT HIL tests to evaluate overall performance in close to real-life conditions.

The rest of the paper is organized as follows: Section II briefly outlines the developed compensation strategy (2 particular cases); Section III presents the laboratory co-simulation platform for testing of the protection scheme that includes the real time simulator OPAL-RT®, ABB impedance relay RED 670® and the communication network emulator; the network model with several load points and DG is described in subsection III-A; functionalities and model algorithms of the network emulator are listed in subsection III-B; Section IV introduces the test method including Monte-Carlo simulations for evaluation of method dependability for different conditions; Section V contains the test results with discussions.

II. Overview of compensation strategy

The compensation strategy previously developed in [18] consists of two similar approaches depending on if infeed currents are present between two measuring points.

A. Equivalent line approach (ELA)

For two point measurements in a part of a network without infeed currents (Fig.1), the following method of compensation has been proposed:

$$Z_{\text{cps}} = \frac{U - U_{\text{err}}}{I}, \tag{1}$$

K. Pandakov is with Department of Electric Power Engineering, Norwegian University of Science and Technology (NTNU), Trondheim, NO-7491 Norway, e-mail: konstantin.pandakov@ntnu.no

C. M. Adrah is with Department of Information Security and Communication Technology at NTNU, e-mail: charles.adrah@ntnu.no

H. Kr. Høidalen is a professor in NTNU at Department of Electric Power Engineering, e-mail: hans.hoidalen@elkraft.ntnu.no

Ø. Kure is a professor in NTNU at Department of Information Security and Communication Technology, e-mail: okure@ntnu.no

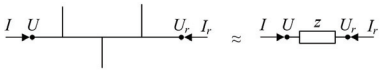

Fig. 1: Exemplary network topology for application of ELA (to the left) and its equivalent (to the right).

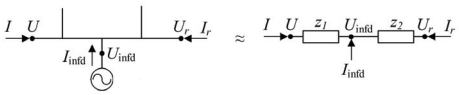

Fig. 2: Exemplary network topology for application of ENA with one infeed source (to the left) and its equivalent (to the right).

where Z_{cps} is the compensated phase-to-phase impedance calculated by the relay and used for tripping decision. As in the standard approach, U is the interphase voltage and I is the interphase current measured at relay location. Hereafter, phasor quantities are implied. Voltage error U_{err} is equal to zero during normal conditions in the network, whereas it is nonzero during fault situation recognized upon fulfillment of three conditions together:

1) impedance magnitude measured at relay location falls below a threshold: 80% of what was measured 40 ms ago (two periods). It is expressed as $|U/I| < 0.8|U^{\text{pre}}/I^{\text{pre}}|$, where 'pre' stands for prefault conditions.
2) rate of change of this impedance $\frac{\delta|U/I|}{\delta t}$ over the last 5 samples is less than -1 Ohm/ms. Fast collapse indicates a fault.
3) the real part of the impedance is positive that indicates downstream fault (a directional element), real$(U/I) > 0$.

U_{err} is calculated utilizing interphase measurements from the remote end U_r and I_r as:

$$U_{\text{err}} = \frac{UI_r + U_r I - zII_r}{I + I_r}, \tag{2}$$

where $z = (U^{\text{pre}} - U_r^{\text{pre}})/I^{\text{pre}}$ is a prefault equivalent impedance of the network's part between two measuring points. Current directions are towards the network, Fig.1.

Hereafter, it is assumed that Z_{cps} is separately calculated for phases a-b, b-c, and c-a.

B. Equivalent network approach (ENA)

The current paper experimentally verifies a particular configuration when one source of infeed current (one measuring point) is present in a part of a network between two other measuring points, Fig.2. General situation with several sources is described in [18]. Then, voltage error in equation (1) is equal to $U_{\text{err}} = \min[U_{\text{err1}},\ U_{\text{err2}}] + U_{\text{err3}}$, where:

$$U_{\text{err1}} = \frac{U(I_r + I_{\text{infd}}) + U_{\text{infd}} I - z_1 I(I_r + I_{\text{infd}})}{I + I_r + I_{\text{infd}}} \tag{3}$$

$$U_{\text{err2}} = \frac{U_r(I + I_{\text{infd}}) + U_{\text{infd}} I_r - z_2 I_r(I + I_{\text{infd}})}{I + I_r + I_{\text{infd}}}, \tag{4}$$

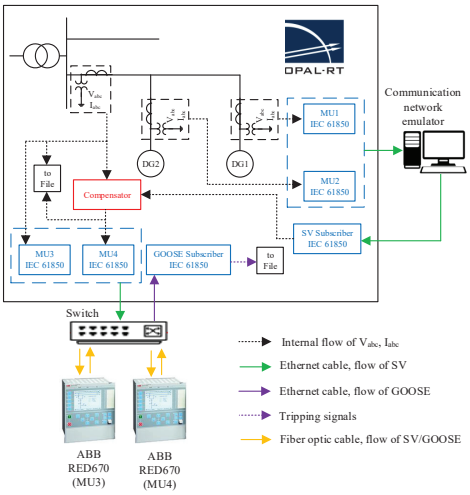

Fig. 3: Laboratory co-simulation testbed: the hardware-in-the-loop testing platform with emulator of communication links.

and minimum is determined upon phasor magnitudes. Here $z_1 = (U^{\text{pre}} - U_{\text{infd}}^{\text{pre}})/I^{\text{pre}}$, $z_2 = (U_r^{\text{pre}} - U_{\text{infd}}^{\text{pre}})/I_r^{\text{pre}}$, U_{infd} and I_{infd} are measured voltage and current at the infeed source.

If U_{err1} is chosen from the minimum condition, then $U_{\text{err3}} = 0$. If U_{err2}, then

$$U_{\text{err3}} = U_{\text{infd}} - U_{\text{err2}} - \frac{I}{I_r}\Big(U_{\text{err2}} - U_r + I_r z_2\Big) \tag{5}$$

This expression is a voltage drop on equivalent line z_2 caused by only infeed current. It is zero on z_1.

Equally, measurements at the infeed source can be taken as U_r and I_r in equations (3)-(5), then the remote measurements become U_{infd} and I_{infd}. Having possibility of such swap, two voltage errors U_{err} for compensation (1) appear. A minimum value (upon magnitude) must be chosen to avoid overcompensation and to increase fault location precision.

III. Laboratory Test Setup

Fig.3 shows the full laboratory setup for verification of the proposed method. The previously developed hardware-in-the-loop testing platform [19] is expanded with a communication network emulator [20]. Real time simulations of the network with the DG are executed in OPAL-RT® with 50 μs time step.

Detailed description of the model with 2 embedded generators and fault scenarios are given in the next subsection.

Three-phase voltage and current measurements at the generators and the substation are formed as sample values (SV) in the merging units (MU) using the standard IEC 61850. SV measured at the substation are directly sent to ABB relay RED 670® via MU3 in order to examine impact of

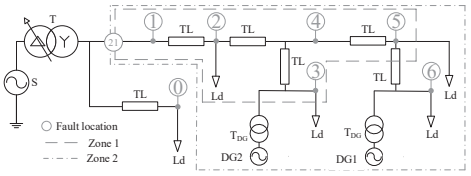

Fig. 4: The test case network.

the DG on impedance measurements. SV measured at the generators (MU1-2) are sent to the communication network emulator. It models constant time delays, jitters, data loss and background traffic in the SV flows imitating real time communication links (more details are given in subsection III-B). The emulator sends the obtained SV back to the real time simulator (SV Subscriber). The MUs and the subscribers have 4 kHz sampling rate, quality of SVs is set as good.

The compensator accomplishes calculations described in section II, namely: it determines phasors utilizing the obtained SV from the substation and both generators, calculates $U - U_{\text{err}}$ and converts it into an instantaneous signal. This signal together with the measured current at the substation are formed as SV in MU4 and sent to another impedance relay with the same configuration.

In this work, time stamp on SV is not applied assuming unavailability of GPS signal (non-synchronized measurements). Thus, the compensator takes into account known permanent latencies t_d of the remote measurements superimposed by the emulator: $t_d = 3$ ms for DG1 and $t_d = 2$ ms for DG2 have been chosen based on DG remoteness.

Thus, responses (missing or presence of the tripping signals) of the relays with and without compensation are compared: they send GOOSE messages back to the real time simulator (GOOSE Subscriber). The tripping signals and the SV are written to file for further off-line analysis.

The relay settings have Zone 1 not reaching the DG units to allow keeping the feeder alive during DG internal faults and Zone 2 covering the whole feeder and providing backup protection. Zone 1 has positive sequence impedance 13.5+13.5i Ohm with 20 ms time delay for coordination with load fuses; Zone 2 has 20.5+20.5i Ohm. Its time delay must be bigger than breaking operation at the DG units; however, for simplicity and test quickness, 40 ms is set. The zones' boundaries are depicted in Fig.4. The quadrilateral relay characteristics have forward direction and preset fault resistance 10 Ohm because expected maximal arc resistance estimated on Warrington's formula [21] is 7.5 Ohm.

A. Test case network

The test case network is illustrated in Fig.4. Its model has been realized in Matlab Simulink®, and all model parameters are described in Table I.

Lines 'TL' are modeled as PI-equivalents because studied frequency wavelengths much larger than transmission line lengths.

TABLE I: Network parameters.

	Matlab Simulink model name: parameters
S	Three-Phase Source: 66 kV, 50 Hz, 0.055 H (source inductance)
T, T_{DG}	Three-Phase Transformer (Two Windings): 50 Hz, Rm=500 pu, Lm=500 pu (ideal model) T: 20 MVA, Winding 1 [66 kV 0.0045 pu 0.09739 pu], Winding 2 [22·1.05 kV 0.0045 pu 0.09739 pu] T_{DG}: 3 MVA, Winding 1 [6.6 kV 0.0066 pu 0.06336 pu], Winding 2 [22 kV 0.0066 pu 0.06336 pu]
TL	Three-Phase PI Section Line: 50 Hz, [r1 r0]=[0.36 0.5] Ohms/km, [l1 l0]=[1.146 5.093] mH/km, [c1 c0]=[10.137 4.794] nF/km, length 10 km
Ld	Three-Phase Parallel RLC Load: Delta configuration, 22 kV, 50 Hz, power factor 0.98, Qc=0, total active power is randomly set as 1 MW, 2 MW or 3 MW, 80% imbalance (see description below)
DG1,2	Synchronous Machine: 3 MVA, 6.6 kV, 50 Hz, [Xd Xd' Xd" Xq Xq" Xl]=[2 0.22 0.2 1.4 0.2 0.18] pu, [Tdo' Tdo" Tqo"]=[4 0.025 0.1] s (open circuit), Rs=5e-3 pu, [H(s) F(pu) p]=[1 0 2] Excitation System: IEEE type 1 (default parameters), Hydraulic Turbine and Governor: default parameters

Loads 'Ld' have a random level of active power P and imbalance. Load imbalance at the given load point is modeled as interphase loads with values equal to 100%, 80% and 120% (between randomly determined phases) from $P/3$. Each load point is independently determined. Thus, overall load profile and imbalance on the feeder alternates. Randomness is realized using block 'Random Source' with uniform distribution and not repeatable automatic initial seed.

The interconnected generators are operated with zero reactive power production (unit power factor).

Phase-to-phase permanent faults are applied in 7 different locations as shown in Fig.4 with detectable low resistance (an arc with 10 Ohm) and undetectable high resistance (an extraneous object with 50 Ohm causing intentional relay underreach).

B. Communication network emulator

Testing of protection algorithms utilizing inter-substations or even wide area networks requires modeling of communication network impairments to study their impact on overall performance. At the same time, OPAL-RT® has limited capabilities for these purposes. Thus, the communication emulator is proposed to be used together with the RT simulator to mirror behavior and characteristics of communication network properties that tend to have effects in the real-world applications.

The core functionality is to emulate topologies between several relays exchanging GOOSE/SV packets or messages so that the communication properties between source relays and destination relays can be varied. These properties are regarded as impairments in the network and include delays, jitters, packet losses, packet corruptions, bandwidth restriction. Additionally, the emulator as a software router can direct packets to actual existing routers and other network elements such as switches, bridges and hubs for integration into real networks. Hence, the emulator is also used to achieve different queuing schemes with different priorities, as well as different router scheduling algorithms.

Network impairments applied in the current work are as follows:

1) Random delay emulator element: It is used to emulate jitters and the input is a specific range for random delays expressed further in the paper using DG permanent latency t_d. Two jitter levels are used in the tests: 1) the low level when an actual delay is between t_d and $1.5t_d$); 2) the high level when an actual delay is between t_d and $2t_d$. Normal distribution is used.

2) Burst packet drop emulator element: It is used to emulate packet losses. It drops a consecutive number of packets with a given probability. The input is a number of consecutive packets to drop and a probability. Similarly, two data loss levels are used: 1) the low level where 10% on average of packets sending during 1 s are lost; 3) the high level where 20% on average of packets are lost during the same period.

3) Influence of background traffic and network dimension: The generated SV of MU1 and MU2 is sent through the emulator combined with a VLAN enabled switch network (HPE 1920) to the OPAL-RT® simulator. A separate background traffic generated as a User Datagram Protocol (UDP) video source is added to the network traffic mix. The network configurations utilizes the IEEE 802.1Q and IEEE 802.1p priority tagging to investigate how prioritizing the background traffic will affect the performance of the received SV from MU1 and MU2.

IV. Test method

In order to evaluate dependability and security of the tested protection scheme, a Monte Carlo simulation approach is used that applies several consecutive faults in arbitrary set conditions. The following repeatable sequence with a three-seconds period is utilized for each new fault:

- A random source sets load power P and a separate source with its own seed determines phases where load imbalance takes place. Settings are applied to all load points independently with their own random sources.
- After end of the transient period caused by load variation (2 s), a fault is initiated with random selection of faulty phases. A different random source determines fault resistance: 10 Ohm or 50 Ohm.
- After another 100 ms the fault is cleared followed by a relaxation period of 900 ms.

Thus, the performed compensation techniques can be applied for different fault parameters and network conditions.

In equations (1) - (5), U and I are always measured at the main substation for device number 21 in Fig.4. U_r, I_r, U_{infd}, I_{infd} can belong to either DG1 or DG2 depending on a case below.

The following scenarios are studied:

- Case 1: no communication impairments are introduced. DG permanent latencies are taken into account by the compensator.
  - Case 1a: test of equivalent network approach (ENA, section II-B). U_{infd} and I_{infd} are measured at DG1 (the source of infeed), U_r and I_r are at DG2 (a remote end). 100 consecutive faults are simulated.
  - Case 1b: ENA where U_{infd} and I_{infd} are measured at DG2, and U_r and I_r are at DG1 (100 faults).
  - Case 1c: equivalent line approach (ELA, section II-A). U_r and I_r are measured at DG2, and DG1 is disconnected from the grid (100 faults).
  - Case 1d: ELA where U_r and I_r are measured at DG1, and DG2 is disconnected (100 faults).

  Cases 1a-d are repeated for all 7 fault locations, in total 2800 faults for Case 1 have been simulated. Cases 1c and 1d are used to analyze impact of network configuration on ELA fault location precision. Cases 1a and 1b are used for the same purpose for ENA, as well as to verify validity of the criterion for infeed source selection discussed in subsection II-B.
- Case 2 simulates communication link imperfections – the low and the high level of either jitters or data losses. The compensator still applies the predefined DG permanent latencies.
  - Case 2a: ENA with the low (50 faults) and the high (50 faults) jitter level. Infeed source either DG1 or DG2 is automatically specified using the criterion discussed in subsection II-B.
  - Case 2b: ENA with the low (50 faults) and the high (50 faults) data loss level.
  - Case 2c: ELA with disconnected DG1 for the low (50 faults) and the high (50 faults) jitter level.
  - Case 2d: the same as in 2c, but for the low (50 faults) and the high (50 faults) data loss level.
  - Case 2e: repeats 2c, but with disconnected DG2 instead of DG1.
  - Case 2f: repeats 2d, but with disconnected DG2 instead of DG1.

  For analysis, three extreme fault location have been chosen - 1, 3, and 6. In total 1800 faults for Case 2 have been simulated.
- Case 3 studies impact of background traffic on SV delays and packet losses. Faults are not simulated because impact on protection is seen from Case 2. The practical Ethernet switch used in tests has a priority mapping of class of service queues (denoted with 'pcp' in the text) that is selected 1, 2, and 3 categorizing traffic types as background, best effort and critical applications respectively. Since SV are the time critical traffic, they were tagged with pcp 3. The background traffic was then varied in the network with pcp 1, 2 and 3. Two video files of 3MB and 10MB were used for the tests. Maximum sending speed for them through 1 Gbps Ethernet is 480 Mbps and 710 Mbps correspondingly.

Finally, percentage of successful tripping among all faults in a specific case can be calculated.

V. Results and discussions

A. Case 1

1) Case 1a and 1b: Firstly, Fig.5 demonstrates impedance loci of faults in the adjacent feeder (location 0) for test case 1a. $Z_{h,f}$ denotes steady-state healthy and faulty impedance correspondingly; upward power flow from the DG can be seen as the negative real part of Z_f. Sympathetic tripping during

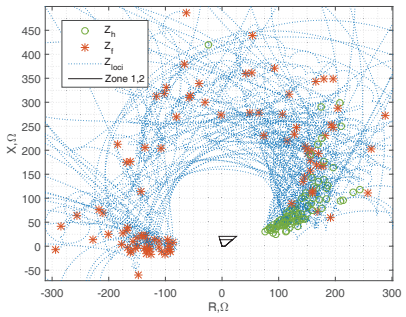

Fig. 5: The impedance loci of faults at location 0 (the adjacent feeder) in test case 1a.

TABLE II: Percentage of successful tripping in test case 1a and 1b.

FL[1]		Low-ohmic faults				High impedance faults			
		w/o cps[2]		with cps[3]		w/o cps		with cps	
		Z1[4]	Z2[5]	Z1	Z2	Z1	Z2	Z1	Z2
Case 1a	1	100	100	100	100	0	0	100	100
	2	100	100	100	100	0	0	100	100
	3	4	2	82	100	0	0	58	100
	4	100	100	100	100	0	0	100	100
	5	83,7	87,8	100	100	0	0	100	100
	6	0	15,7	74,5	100	0	0	65,3	100
Case 1b	1	100	100	100	100	0	0	100	100
	2	100	100	100	100	0	0	100	100
	3	22,9	10,4	100	100	0	0	96,2	100
	4	100	100	100	100	0	0	100	100
	5	96,4	100	96,4	100	0	0	95,6	100
	6	0	26,5	16,3	100	0	0	11,8	100

[1]fault location, [2]without compensation, [3]with compensation, [4]Zone 1, [5]Zone 2.

the tests has not been registered: all impedance loci are out of zones' reach.

Hereafter, this location is out of interest and excluded from the following analysis because tripping signal is not produced by the investigated relay. Security of the protection is not jeopardized because compensator cannot be initialized due to conditions 1 - 3 in section II.

Table II shows calculated percentages of successful tripping in test cases 1a and 1b for fault location 1-6 and two different fault resistances compared to relay performance without the compensation strategy.

The colored cells highlight indices indicating problems: red (relay without compensation) or pink (with) shows decreased dependability (less than 100%), orange - decreased security (higher than 0).

It is seen that low-ohmic fault in location 1,2,4 is reliably detected without compensation in both test cases; however, blinding is observed for high impedance fault because all locations and cases have 0. At the same time, application of the compensation methods resolves this issue.

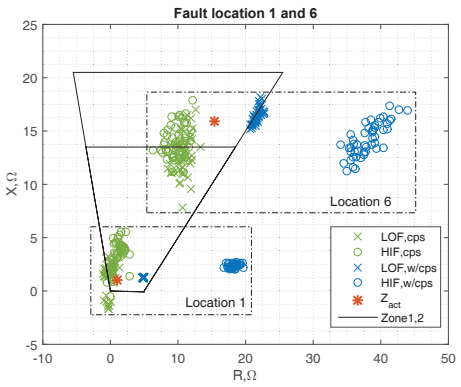

Fig. 6: The measured steady-state fault impedances for low-ohmic (LOF) and high impedance faults (HIF) at location 1 and 6 with compensation (cps) and without (w/cps).

We can clearly observe from Table II that relay dependability without compensation is significantly decreased at locations next to the generators (3,5,6). Dependability with compensation is 100% for Zone 2 in all cases, whereas it is not for Zone 1 due to compensation errors that leads to delayed tripping (location 3 for Case 1a and 3,5 for Case 1b).

It is worth noting two main outcomes: 1) Zone 1 must not see faults at location 6 (see Fig.4), whereas in both cases percentage with compensation is not 0 (the orange cells). In other words, the compensated impedance might become smaller than an actual. Since it can lead to a situation when internal faults in DG1 cause unnecessary feeder tripping, the compensator must be blocked to maintain protection selectivity. It can be checked with the same conditions 1 - 3 in subsection II-A applied to measurements at the DG locations: if they are not fulfilled (current is measured towards the monitoring zone), the compensation is not used for the feeder relay; 2) performance of the compensation method in Case 1a is slightly better than in Case 1b for location 5, whereas it is considerably worse for location 3 and 6. As it will be shown further, it is linked with fault location accuracy.

Finally, protection with compensation demonstrates faster operation time: mean value is 40 ms for Zone 1 and 60 ms for Zone 2 irrespectively of fault location and resistance. Without compensation, it can reach 90 ms for problematic locations 3, 5, and 6.

Fig.6 demonstrates the reason for poor relay dependability without compensation and improvements applying ENA (Case 1a is considered) for close-in fault location 1 and far-end location 6. It is seen from the figure that all high impedance faults (HIF) without compensation are out of the zones' reach. Zone 1 can handle all low-ohmic faults (LOF) at close-in location, whereas Zone 2 cannot detect all faults at far-end location due to impact of the DG. 'Z_{act}' denotes an actual fault impedance. The compensated impedances are inside the

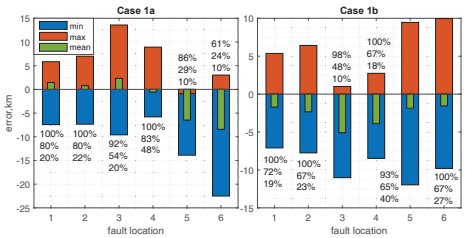

Fig. 7: Maximum, minimum and mean fault location errors for Case 1a and 1b (LOF). Indices reflect number of faults located with accuracy ±10 km (upper), ±5 km (middle), ±2 km (lower).

zones and they have inherent errors with bigger dispersion due to influence of variable network conditions that is the reason of dependability and security issues in Table II. Though for location 1 not all Z_{cps} are in Zone 1, a corresponding locus crosses it and, therefore, the tripping signal appears.

The main advantage of the strategy compared to differential protection is preserving of fault location capability. It is seen from Fig.6 that Z_{cps} for location 1 and 6 are distinguishable, and it is of interest to analyze impact of the compensation on fault location accuracy for all cases.

There are many different approaches for fault location calculation in distribution networks with distributed generation. In this paper, we use a simple one based on the imaginary part of the compensated impedance discussed in [22]. Combination of the compensation strategy with more complex locating algorithms is out of the scope of this paper.

Error in kilometers can be calculated as $\text{imag}(Z_{\text{cps}} - Z_{\text{act}})/\text{r1}$, where $\text{r1} = 0.36$ Ohm/km (Table I), and Z_{cps} is registered when the tripping signal from Zone 1 or 2 appears, or just a steady-state value if no response is present.

Fig.7 illustrates maximum, minimum and mean errors for 6 fault locations. LOF is considered because it has better precision. For better insight, number of fault incidents (in % from the total) that have a given precision are given alongside: the upper value is precision ±10 km, the middle is ±5 km and the lower is ±2 km.

It can be seen from the plots that the precision for remote locations 5 and 6 is better (compare corresponding indices and mean values) for Case 1b, whereas Case 1a demonstrates better accuracy for location 3. At the same time, average U_{err} for Case 1a is less than for Case 1b during fault at location 3, and it is less for Case 1b for fault at location 5 and 6. Thus, such criterion based on minimum U_{err} (discussed in subsection II-B) can be applied for infeed selection because it provides higher Z_{cps} and, consequently, better fault location accuracy.

To summarize, the presented results in Table II (the pink and orange cells) and in Fig.7 are in good agreement with theoretical expectations: if DG1 is a source of infeed (Case 1a), then locations 5 and 6 are seen as location 4 that gives better dependability and worse security because location 4 is in Zone 1. However, it leads to bigger fault location errors

TABLE III: Percentage of successful tripping in test case 1c and 1d.

FL		Low-ohmic faults				High impedance faults			
		w/o cps		with cps		w/o cps		with cps	
		Z1	Z2	Z1	Z2	Z1	Z2	Z1	Z2
Case 1c	1	100	100	100	100	0	0	100	100
	2	100	100	100	100	0	0	100	100
	3	74,4	67,4	100	100	0	0	100	100
	4	100	100	100	100	0	0	100	100
	5	100	100	100	100	0	0	100	100
	6	0	97,7	100	100	0	0	100	100
Case 1d	1	100	100	100	100	0	0	100	100
	2	100	100	100	100	0	0	100	100
	3	100	100	100	100	0	0	100	100
	4	100	100	100	100	0	0	100	100
	5	100	100	100	100	0	0	95,8	100
	6	0	5,7	45,3	100	0	0	36,2	100

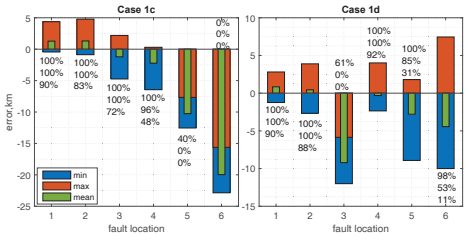

Fig. 8: Fault location errors for Case 1c and 1d (LOF).

with a negative sign. At the same time, location 3 is detected with some errors leading to the decreased dependability. The opposite is true if an infeed source is DG2 (Case 1b): location 3 is seen as 4 (therefore errors are higher and dependability is better), and 5 and 6 have better location precision (therefore worse dependability and better security).

2) Case 1c and 1d: Table III shows relay dependability in test cases 1c and 1d. Case 1c shows impact of DG2 (DG1 is disconnected) on relay performance without compensation. As a consequence, dependability reduction is seen for fault location 3,6 and HIF gives 0 as in the previous cases. Case 1d illustrates impact of DG1 seen for location 6. Compensation entirely improves indices for Case 1c, whereas HIF at location 5 has some difficulties for detection by Zone 1 in Case 1d. In both cases, relay security is deteriorated for location 6 (non zero indices for Zone 1). The same point about compensation blocking as in the previous cases is applied here. Finally, protection with compensation is also faster.

Fig.8 shows fault location errors. Case 1c has bigger errors for location 5,6 than Case 1d (zero indices mean large error), but better precision for location 3. This is in agreement with theory because if DG1 is disconnected, then locations 5,6 are seen as 4 (therefore large negative errors in Case 1c) and location 3 is correctly determined; therefore, in Table III, security at location 6 is completely disrupted. If DG2 is disconnected, then the opposite situation arises: location 3 is

TABLE IV: Percentage of successful tripping in test case 2a and 2b (ENA).

FL	Level	Case 2a (jitters)				Case 2b (data loss)			
		LOF		HIF		LOF		HIF	
		Z1	Z2	Z1	Z2	Z1	Z2	Z1	Z2
1	no[1]	100	100	100	100	100	100	100	100
	low	100	100	100	100	100	100	100	100
	high	81,8	100	85,7	100	95,5	100	100	100
3	no	100	100	96,2	100	100	100	96,2	100
	low	3,3	76,7	5	65	100	100	100	100
	high	0	15	0	10	20,8	83,3	26,9	76,9
6	no	16,3	100	11,7	100	16,3	100	11,8	100
	low	0	53,8	0	62,5	82,6	95,7	11,1	100
	high	0	20,7	0	23,8	18,8	75	14,7	55,9

[1]no impairments.

seen as 4 with large negative error (Case 1d), better security at location 6 and worse dependability for 5 is due to better location accuracy.

To summarize, LOF or HIF inside the zone of protection are reliably detected (at least by Zone 2) with application of the equivalent line or network approach. The main advantage compared to differential protection is preserved fault location capability since errors of impedance measurements can be compensated especially for HIF. For both approaches, the main source of location errors is load currents that are not directly compensated by the given method of equivalences. Accuracy can be improved applying the compensated measurements and the methods discussed in [22].

B. Case 2

This sections demonstrates impact of communication network imperfections, namely jitters and data packet loss, on performance of the compensation methods. Here, fault locations 1,3 and 6 are only considered as extreme points.

1) Case 2a and 2b: Table IV demonstrates performance of the compensation in test cases 2a and 2b compared to similar in Case 1 (without jitters and data loss). The pink colored cells show dependability deterioration compared with cases without communication network distortions, blue - affected security (location 6 only), and the green cells indicate improvements.

Jitter level rise (Case 2a) significantly aggravates relay dependability in locations 3 and 6. Analysis of fault location errors shows that it leads to compensated impedance increase (especially reactive part that deteriorates fault location accuracy) and, consequently, underreaching; therefore, for location 1, influence is not so prominent.

Data loss level rise (Case 2b) has also similar impact – relay dependability falls. Considerable influence is observed for location 3 and 6 for the highest probability.

Improvements are observed for protection security with jitter rise; however, worsening for data loss. At the same time, if the tripping signal appears, operation time is not affected by the communication impairments.

2) Case 2c and 2d: Table V shows results for impact of jitters and data loss in test cases 2c and 2d on the equivalent line approach with disconnected DG1. Comparison with the corresponding results in Case 1 are also present.

TABLE V: Percentage of successful tripping in test case 2c and 2d (ELA, DG1 disconnected).

FL	Level	Case 2c (jitters)				Case 2d (data loss)			
		LOF		HIF		LOF		HIF	
		Z1	Z2	Z1	Z2	Z1	Z2	Z1	Z2
1	no	100	100	100	100	100	100	100	100
	low	100	100	100	100	100	100	100	100
	high	100	100	71,4	100	100	100	100	100
3	no	100	100	100	100	100	100	100	100
	low	0	88,9	0	82,6	14,3	91,4	13,3	66,7
	high	0	50	0	0	42,9	100	41,4	96,6
6	no	100	100	100	100	100	100	100	100
	low	27, 3	100	0	94,1	78,6	100	77,3	90,9
	high	0	38,5	0	0	78,3	100	66,7	96,23

TABLE VI: Percentage of successful tripping in test case 2e and 2f (ELA, DG2 disconnected).

FL	Level	Case 2e (jitters)				Case 2f (data loss)			
		LOF		HIF		LOF		HIF	
		Z1	Z2	Z1	Z2	Z1	Z2	Z1	Z2
1	no	100	100	100	100	100	100	100	100
	low	100	100	100	100	100	100	100	100
	high	95,4	100	21,4	100	100	100	100	100
3	no	100	100	100	100	100	100	100	100
	low	14,8	92,6	0	69,6	69	100	9,5	85,7
	high	0	24,1	0	0	100	100	100	100
6	no	45,3	100	36,2	100	45,3	100	36,2	100
	low	0	38,9	0	3,1	34,5	93,1	23,8	90,5
	high	0	0	0	0	10,7	92,9	4,5	90,9

As it is possible to observe for location 1, dependability is less than 100% only for the high jitter level and HIF. Impact is less than in Cases 2a,b because only one communication channel is affected. More serious consequences from jitter and data loss level rise are seen for locations 3 and 6. At the same time, clear falling tendency is present with increase of jitter level (Case 2c); however, for data loss (Case 2d), this dependency is not revealed. Finally, location 6 has higher dependability indices due to the applied ELA: it is seen by the fault locating algorithm closer to location 4. In such case, communication network impairments have positive impact on security. Impact of communication link imperfections on location errors is the same as in the previous cases.

3) Case 2e and 2f: Table VI illustrates results for the same ELA as before but DG2 is disconnected. Here impact of the jitters on location 1 is seen even for LOF, and it is higher for HIF than in the previous case. The reason is that calculation errors increase with the distance between two measuring points.

Performance at location 3 is better (indices are higher) than in the previous case because location 3 is now seen as 4; however, impact of network impairments for location 6 is considerable compared to the previous case due to calculation errors of the applied ELA. Positive impact on security in such case is also higher.

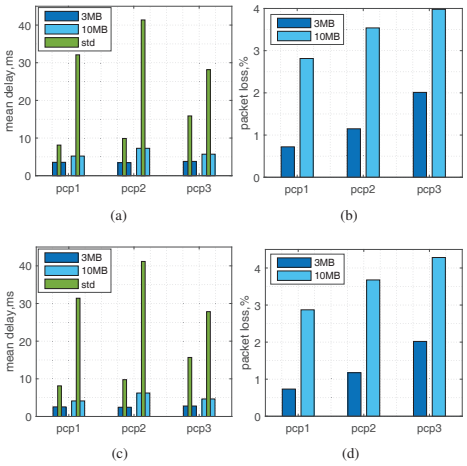

Fig. 9: Impact of 3MB and 10 MB background traffic set with priority (pcp) 1, 2 and 3 on a) end-to-end delays (MU1), b) percentage of lost packets (MU1), c) end-to-end delays (MU2), d) percentage of lost packets (MU2).

To summarize, the main reason of dependability issues in the considered cases is the presence of errors during calculation of the compensated impedance caused by non-synchronized remote measurements or information losses. The analysis of cases with jitter level variation (Case 2a,c,e) can be useful for utilities for evaluation of protective scheme dependability and security in case of sudden loss of synchronizing signal or its unavailability (e.g. underground substations). Data losses have overall adverse effect on the protective schemes increasing relay underreach (Case 2b,d,f); therefore, communication network reliability must be sufficient with minimal packet losses. Finally, comparing results in test Case 2 and Case 1, it is possible to see that even with unreliable communication, protection performance with compensation is superior than without especially for HIF and for LOF in case of low level impairments.

C. Case 3

Fig.9 shows results for test Case 3: end-to-end time delays as mean values over 400000 SV packets with the standard deviation (denoted as 'std') and percentage of lost packets measured between the substations for DG1 and DG2 merging units (MU1 and MU2 respectively) for the two background sources used in the tests, i.e. 3 MB (maximum 48% traffic occupancy) and 10MB (maximum 71% traffic occupancy) video file sizes, while varying the priority tags of the background traffic as previously explained.

It can be seen that the background traffic with different priority increases end-to-end delays because the mean values are higher than preset (3 ms for MU1 and 2 ms for MU2). Moreover, the 10MB video file as a background traffic source resulted in a generally higher increase in average network delays and standard deviation compared to the 3MB video file. Setting the background traffic with different priority tags has resulted in different packet delay variations; however, a strict regularity is not observed due to randomness nature of packet delays.

Influence of the background traffic on packet losses is seen from Fig.9b and Fig.9d: the 10MB video background traffic generally resulted in more packet losses compared to the 3MB video file. Unlike the previous case, a correlation between pcp and lost packets is prominent. Thus, setting the background traffic as critical messages with pcp = 3, same as the SV traffic for DG1 and DG2, has resulted in the highest percentage of lost packets in the network for both background traffic cases, i.e. MU1 (2.01%, 3.98%) and MU2 (2.01%, 4.28%).

VI. Conclusion

The current paper presents laboratory tests of a new communication assisted protective scheme for distribution grids with DG using the developed co-simulation platform that includes a real time hardware-in-the-loop testbed and a network emulator. The latter creates controlled network parameters for testing and measurement of protection applications in such environments.

The protection method consists of two approaches depending on a number of infeed current sources. It aims at elimination of underreaching errors during impedance measurements associated with DG and high impedance faults. It demonstrates promising results with ideal communication links improving dependability compared to the conventional distance relaying. Nevertheless, it has fault location errors due to impact of loads not fully compensated by the method.

Communication impairments introduced with the help of the emulator, such as uncompensated jitters or data losses, can threaten the protection method because they lead to underreaching errors especially for far end fault locations.

ELA can only be applied for a passive network between two-point measurements (Fig.1). As it is seen from the analysis, faults in lateral branches (when one DG is disconnected) are seen in false locations (on the feeder); therefore, additional measurements might be required for precise fault location. Utilization of multiple-point measurements in such case might require to use ENA if a network becomes active (Fig.2). In order to select a correct (i.e. that gives the best fault location precision) remote relay for calculation of Z_{cps} in both approaches, the criterion of minimum U_{err} or maximum Z_{cps} must be applied. Finally, the results reveal that ELA demonstrates better fault location accuracy than ENA and less susceptibility to communication network imperfections, therefore it must be prioritized.

References

[1] A. Sinclair, D. Finney, D. Martin, P. Sharma. (2014). Distance Protection in Distribution Systems: How It Assists With Integrating Distributed Resources. *IEEE Transactions on Industry Applications. 50(3)*, pp. 2186 – 2196.

[2] M. M. Saha, J. Izykowski, E. Rosolowski, M. Bozek, "Adaptive Line Distance Protection with Compensation for Remote End Infeed", *IET 9th International Conference on Developments in Power System Protection (DPSP)*, 2008, pp. 1 – 6.

[3] V.H. Makwana, B. Bhalja. (2012). New digital distance relaying scheme for phase faults on doubly fed transmission lines. *IET Generation, Transmission & Distribution. 6(3)*, pp. 265 – 273.

[4] V. H. Makwana, B. R. Bhalja. (2012). A New Digital Distance Relaying Scheme for Compensation of High-Resistance Faults on Transmission Line. *IEEE Transactions on Power Delivery. 27(4)*, pp. 2133 – 2140.

[5] Y. Zhong, X. Kang, Z. Jiao, Z. Wang, J. Suonan. (2014). A Novel Distance Protection Algorithm for the Phase-Ground Fault. *IEEE Transactions on Power Delivery. 29(4)*, pp. 1718 – 1725.

[6] Z. Y. Xu, G. Xu, L. Ran, S. Yu, Q. X. Yang. (2010). A New Fault-Impedance Algorithm for Distance Relaying on a Transmission Line. *IEEE Transactions on Power Delivery. 25(3)*, pp. 1384 – 1392.

[7] Q. K. Liu, S. F. Huang, H. Z. Liu, W. S. Liu. (2008). Adaptive Impedance Relay With Composite Polarizing Voltage Against Fault Resistance. *IEEE Transactions on Power Delivery. 23(2)*, pp. 586 – 592.

[8] M.M. Eissa. (2006). Ground distance relay Compensation based on fault resistance calculation. *IEEE Transactions on Power Delivery. 21(4)*, pp. 1830 – 1835.

[9] T. G. Bolandi, H. Seyedi, S. M. Hashemi, P. S. Nezhad. (2015). Impedance-Differential Protection: A New Approach to Transmission-Line Pilot Protection. *IEEE Transactions on Power Delivery. 30(6)*, pp. 2510 – 2518.

[10] Z.Li, X. Lin, H. Weng, Z. Bo. (2012). Efforts on Improving the Performance of Superimposed-Based Distance Protection. *IEEE Transactions on Power Delivery. 27(1)*, pp. 186 – 194.

[11] C. J. Lee, J. B. Park, J. R. Shin, Z. M. Radojevie. (2006). A new two-terminal numerical algorithm for fault location, distance protection, and arcing fault recognition. *IEEE Transactions on Power Systems. 21(3)*, pp. 1460 – 1462.

[12] W. Huang, T. Nengling, X. Zheng, C. Fan, X. Yang, B. J. Kirby. (2014). An Impedance Protection Scheme for Feeders of Active Distribution Networks. *IEEE Transactions on Power Delivery. 29(4)*, pp. 1591 – 1602.

[13] N. A. Al-Emadi, A. Ghorbani, H. Mehrjerdi. (2016). Synchrophasor-based backup distance protection of multi-terminal transmission lines. *IET Generation, Transmission & Distribution. 10(13)*, pp. 3304 – 3313.

[14] M. S. Almas, L. Vanfretti, "Methodologies for Power Protection Relay Testing: From Conventional to Real-Time Hardware-in-the-Loop (HIL) Simulation Approaches", *10th International Conference on Power System Transients*, 2013, pp. 1 – 7.

[15] V. A. Papaspiliotopoulos, G. N. Korres, V. A. Kleftakis, N. D. Hatziargyriou. (2017). Hardware-In-the-Loop Design and Optimal Setting of Adaptive Protection Schemes for Distribution Systems With Distributed Generation. *IEEE Transactions on Power Delivery. 32(1)*, pp. 393 – 400.

[16] C. Dufour, J. Belanger. (2014). On the Use of Real-Time Simulation Technology in Smart Grid Research and Development. *IEEE Transactions on Industry Applications. 50(6)*, pp. 3963 – 3970.

[17] A. C. Adewole, R. Tzoneva. (2017). Co-simulation platform for integrated real-time power system emulation and wide area communication. *IET Generation, Transmission & Distribution. 11(12)*, pp. 3019 – 3029.

[18] K. Pandakov, H. Kr. Høidalen. "Distance Protection with Fault Impedance Compensation for Distribution Network with DG", *IEEE PES Innovative Smart Grid Technologies Conference Europe (ISGT-Europe)*, 2017, pp. 1-6.

[19] Z. Liu, H. K. Høidalen. "An adaptive inverse time overcurrent relay model implementation for real time simulation and hardware-in-the-loop testing", *13th International Conference on Development in Power System Protection 2016 (DPSP)*, 2016, pp. 1-6.

[20] C. M. Adrah, Ø. Kure, Z. Liu, H. Kr. Høidalen. "Communication network modeling for real-time HIL power system protection test bench", *IEEE PES PowerAfrica*, 2017, pp. 1-6.

[21] V. D. Andrade, E. Sorrentino. "Typical expected values of the fault resistance in power systems", *Transmission and Distribution Conference and Exposition: Latin America (T&D-LA), 2010 IEEE/PES*, 2010, pp. 1-8.

[22] B. D. S. Jose, P. A. H. Cavalcante, F. C. L. Trindade, M. C. de Almeida. "Analysis of distance based fault location methods for Smart Grids with distributed generation", *IEEE PES ISGT Europe*, 2013, pp. 1-5.

[Paper IV]

K. Pandakov, H. Kr. Høidalen, J. I. Marvik. (2017) Misoperation analysis of steady-state and transient methods on earth fault locating in compensated distribution networks, *Sustainable Energy, Grids and Networks*. Available at: https://doi.org/10.1016/j.segan.2017.12.001 (accessed: 15 December 2017).

Misoperation analysis of steady-state and transient methods on earth fault locating in compensated distribution networks

Konstantin Pandakov, Hans Kristian Høidalen, and Jorun Irene Marvik

***Abstract*—Earth fault detection and location are very important issues in distribution networks. Current methods for faulty feeder selection are based on measurements of steady-state or transient signals. The work presented here identifies and gives analyses of scenarios when ground protection based on these methods is prone to misoperation in resonance grounded systems. It is shown that the traditional watt-metric approach can malfunction depending on network and fault parameters. The admittance methods help to eliminate many issues, however they might have complex settings depending on network configurations. Special attention is paid to approaches based on transient signals as the most promising alternative solution. The current work considers methods utilizing zero sequence current, angle, power, energy and admittance transients. The paper reveals limitations for their application mainly due to presence of electrostatic asymmetry, cables in a network, fault resistance and inception angle. Nevertheless, dependability of these methods is higher than the steady-state especially for intermittent faults. It is also found that analysis of prefault information is important both for the steady-state and the transient methods. The obtained results can be used to enhance reliability of protective schemes and as drivers for further developments of new algorithms.**

***Index Terms*—ground fault protection, resonant grounding, transient method, watt-metric**

I. Introduction

From the current operation practice of medium voltage (MV) networks, it is well known that the vast majority of faults are single-line-to-earth type. In order to decrease fault current, a system can be operated as an isolated or a non-solidly earthed. In this work, the special type of grounding of the main distribution transformer is considered – through a Petersen coil that is quite common in Nordic countries. In resonance grounded systems, ground faults are easily detected (apart from high impedance faults) by measuring the zero sequence voltage magnitude $|\bar{U}_0|$ (exceeds thresholds at a substation), and fault current is suppressed facilitating self-extinguishing of the arc.

For permanent faults, in order to affect as few customers as possible, it is necessary to find the faulty point in the system and isolate it. Measured $|\bar{U}_0|$ does not significantly depend on fault location in a network; moreover, fault current is comparable with load currents that also jeopardizes selectivity of the protection. Typically, problem of faulty feeder selection is considered and X. Zhang et al. [1] provide comprehensive review on the developed methods for this purpose. They can be divided into three groups: injection of additional signals in a substation (voltage, current with frequencies equal to fundamental or higher), usage of steady-state signals, and utilization of transients arising during faults. The injecting methods require additional equipment and they are out of the scope of this paper.

The traditional way of faulty feeder selection based on steady-state signals is the watt-metric approach [1]: detection of a magnitude and direction of zero sequence current $\bar{I}_0$ with respect to $\bar{U}_0$ – normally, healthy feeders and a faulty have different quadrants and magnitudes. In other words, $|\bar{I}_0|\cos(\phi_0)$ (where zero sequence angle ϕ_0 is between $\bar{U}_0$ and $\bar{I}_0$) will have a different sign for a faulty feeder comparing to a healthy. Thus, directionality of the ground protection is tuned according to this fact.

Paper [2] describes insufficiency of the watt-metric approach and a need for a resistor connected in parallel to a Petersen coil. Such operation leads to increase of fault current, produces transient overvoltages in a grid and it requires additional equipment; therefore, it is of interest to find new approaches. In case of sufficient line-to-ground conductance and arcing faults (small impedances), $|\bar{I}_0|\cos(\phi_0)$ can be applied without the resistor. Nevertheless, reference [3] reports the special cases when the sign of $|\bar{I}_0|\cos(\phi_0)$ in both a healthy and a faulty feeders are opposite compared to the prescribed polarity that can lead to misoperation of relays. It is also worth mentioning that a magnitude of zero sequence current by itself is not a reliable indicator for high impedance faults or presence of cables in a system. A new steady-state solution, in contrast to the watt-metric approach, based on zero sequence admittance is proposed in [4]. It copes with lose of sensitivity and other issues.

As an alternative, transient methods are becoming a promising solution. In addition to what was given in [1], authors of [5], [6] suggest to utilize the shape of the charge-voltage curves. In [7], [8] deviation of the feeder capacitance to the ground is estimated. Paper [9] suggests to measure only phase current with further detection of its relative change with respect to the previous periods. Besides the wavelet analysis, other approaches are also performed, such as the Hilbert-Huang [10] and the S-transform [11] investigations. Authors of [12] describe research on the frequency spectrum.

K. Pandakov is with Department of Electric Power Engineering, Norwegian University of Science and Technology, Trondheim, NO-7491 Norway, e-mail: konstantin.pandakov@ntnu.no

H. Kr. Høidalen is a professor in the same department, e-mail: hans.hoidalen@elkraft.ntnu.no

J. I. Marvik is a research scientist at SINTEF Energy Research, Norway, Trondheim 7034, Sem Sælands vei 11 e-mail: jorun.irene.marvik@sintef.no

The artificial intelligence algorithms involving the fuzzy-logic [13], application of the analytic hierarchy process [14] and the small-world network theory [15] can be found in literature as well.

The first-half-wave methods [1] based on low frequency transients deserve special attention due to suitability for compensated and isolated systems, and practical realization connected with limited sampling frequencies (few kilohertz) of used modern relays. High frequency transients might be contaminated by noise from measuring devices that makes application of associated methods difficult. The basic idea behind the first-half-wave methods is different polarity of instantaneous zero sequence current i_0 (with respect to voltage u_0) of a faulty feeder in comparison with other right after fault inception that helps to make decision in the first half of a period. Paper [16] illustrates this effect and proposes the algorithm calculating zero sequence impedance through averaged over a specified time window quantities. Authors of [17] utilize simple differential of i_0 (calculated at the first milliseconds) for faulty feeder selection. References [18], [19] present extraction of transient ϕ_0 and application of it as a main indicator. In order to enhance dependability, different summation and integration techniques are proposed. For instance, papers [20]–[22] calculate zero sequence active power over a quarter of the period, [23] – energy (integration time is not specified). In contrast, the Cumulative Phasor Summing (CPS) technique of zero sequence admittance for different moments of a transient period is used in [24].

To summarize, effect of difference between the prescribed and a factual sign of $\cos(\phi_0)$ in a faulty feeder illustrated in [3] is a key factor leading to inadequacy of ground protection based on the watt-metric approach. As the nature of this effect has not been analyzed in literature in details, the first contribution of the current paper is a deep analysis of it. Moreover, the paper shows how the effect might jeopardize the steady-state [4] and even transient methods. From the variety of the transient methods, the paper will substantially deal with the basic approaches utilizing transients of zero sequence current [16], angle [19], energy [23], and admittance [24]. As it is slightly mentioned in [1], the transient methods are vulnerable to network and fault parameters; therefore, several adverse effects deteriorating performance of the algorithms have not been revealed in the prior studies due to simplicity of the models (e.g. ideal symmetry) and lack of simulation cases. Hence, the next contribution of the paper is revealing what network nonidealities and fault origins can affect performance of ground relays based on these transient methods. The presented results might be valuable for estimation of the limitations of the methods both in relay planning in compensated distribution systems and as background for developments of new algorithms.

II. Theoretical analysis on fault locating utilizing steady-state signals

Let us consider a simple network depicted in Fig.1 with the ground fault in phase *b* of the upper feeder.

The network parameters: $\bar{Y}_{a,f} = \bar{Y}_{c,f} = k_f\bar{Y} = k_f(G + j\omega C)$, where $k_f\bar{Y}$ expresses the share of the faulty feeder in the total shunt admittance to the ground of the network per phase, $\bar{Y}$, that consist of conductance G and capacitance C of a phase. Similarly, $\bar{Y}_{a,h} = \bar{Y}_{c,h} = (1 - k_f)\bar{Y} = k_h\bar{Y}$. Indices *f* and *h* in the paper denote the faulty and the healthy feeder correspondingly. MV networks have capacitive imbalance $\Delta\bar{Y} = j\omega\Delta C$ that is normally 1-5% from $3\bar{Y}$ [25]. Let us assume that it takes place in phase *b*, then $\bar{Y}_{b,f} = k_f(\bar{Y} + \Delta\bar{Y})$ and $\bar{Y}_{b,h} = k_h(\bar{Y} + \Delta\bar{Y})$. The fault impedance is assumed to be pure resistive, $\bar{Y}_f = G_F$. In this work, only permanent resistive fault is studied.

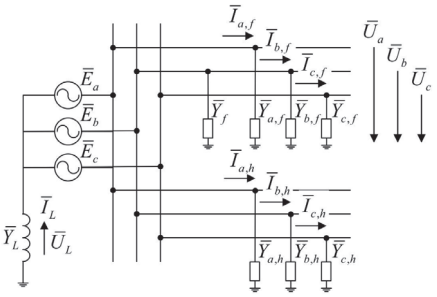

Fig. 1: Simplified network for analysis with two feeders.

For simplified steady-state analysis of ground faults, series impedances of transmission lines and loads can be neglected in comparison with large shunt impedances of lines. Taking this into account, the following set of equations can be written to describe the system in steady-state conditions:

$$\begin{cases} 3\bar{I}_{0,h} = 3\bar{U}_0 k_h\bar{Y} + \bar{U}_b k_h\Delta\bar{Y} \\ 3\bar{I}_{0,f} = 3\bar{U}_0 k_f\bar{Y} + \bar{U}_b k_f\Delta\bar{Y} + \bar{U}_b G_F \\ \bar{I}_L = 3\bar{I}_{0,f} + 3\bar{I}_{0,h} \\ \bar{E}_{ph} = \bar{U}_{ph} + \bar{U}_L \\ \bar{I}_L = \bar{Y}_L\bar{U}_L = -\bar{Y}_L\bar{U}_0 \end{cases}, \qquad (1)$$

where index ph stands for phases *a*, *b* and *c*; $\bar{U}_{ph}$ – phase voltage; $\bar{E}_{ph}$ – the balanced source of voltage; $\bar{I}_L$ and $\bar{U}_L$ are current and voltage of the Petersen coil, and $\bar{Y}_L = (j\omega L)^{-1}$ its admittance; zero sequence voltage and currents are determined as $3\bar{U}_0 = \sum \bar{U}_{ph}$ and $3\bar{I}_{0,f/h} = \sum \bar{I}_{ph,f/h}$.

Let us assume for simplicity that $k_f = k_h$, then the second equation in (1) is turned to $3\bar{I}_{0,f} = 3\bar{I}_{0,h} + \bar{U}_b G_F$. The phasor diagram for this case can be found in Fig.2a ($\Delta\bar{Y}$ is 1%, direction of zero sequence current is from the substation).

As it is possible to see, ϕ_0 of the healthy feeder is less than 90^0 ($|\bar{I}_{0,h}|\cos(\phi_{0,h}) > 0$) and vice versa for the faulty feeder ($|\bar{I}_{0,f}|\cos(\phi_{0,f}) < 0$). The traditional ground protection is based on this fact. It should also be noticed that such systems in Norway are overcompensated, therefore in further analyses $|\bar{Y}_L| > 3|\bar{Y}|$. After fault identification, a resistor can be connected in parallel with the coil that increases ϕ_0 in the faulty feeder and helps to facilitate the selection if watt-metric contribution is scarce.

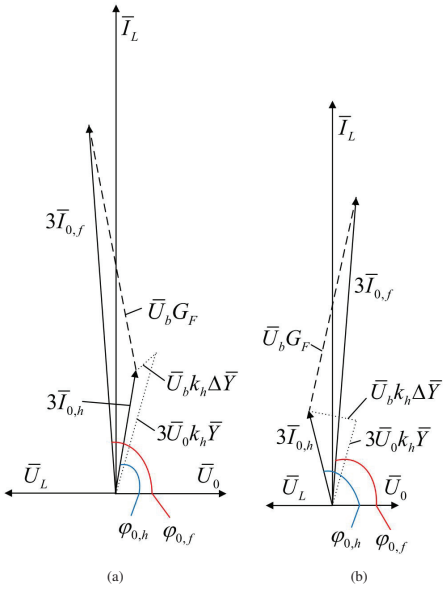

Fig. 2: Phasor diagram of the simplified network for fault in phase b and a) $\Delta\bar{Y} = 1\%$, b) $\Delta\bar{Y} = 5\%$.

Now, let us assume that $\Delta\bar{Y}$ is 5% in the network (it provokes decrease of $\bar{U}_L$ and $\bar{I}_L$ to preserve the same compensation rate). The phasor diagram for this case is illustrated in Fig.2b. The zero sequence currents for both feeders change the quadrants: apart from the previous case, $|\bar{I}_{0,f}|\cos(\phi_{0,f}) > 0$ and $|\bar{I}_{0,h}|\cos(\phi_{0,h}) < 0$. The protection can misjudge the healthy feeder as the faulty that is referred to as polarity disruption of ground relays. A parallel resistor will aggravate the situation. Authors of [3] showed through simulations that such situation appears for faults in a phase with the biggest capacitance. As a matter of fact, it can also occur in other phases depending on network and fault parameters, therefore this effect requires more thorough investigation.

A. Analysis of the polarity disruption

Finding of dependencies of the performed effect on network and fault parameters can be derived analytically through solution of (1) and decompositions of an angle of $\bar{I}_{0,h/f}/\bar{U}_0$ into real and imaginary parts. Here, numerical sensitivity analysis is performed with the following parameters (the base is 22 kV and 20 MVA): $|\bar{E}_{ph}| = 1$ p.u., $\bar{Y} = (0.24 + j6.64) \cdot 10^{-3}$ p.u. and $k_f = k_h$.

It is possible to get from (1) that

$$\bar{U}_0 = \frac{\bar{E}_b \Delta\bar{Y} + \bar{E}_b G_F}{-\bar{Y}_L - 3\bar{Y} - \Delta\bar{Y} - G_F} \tag{2}$$

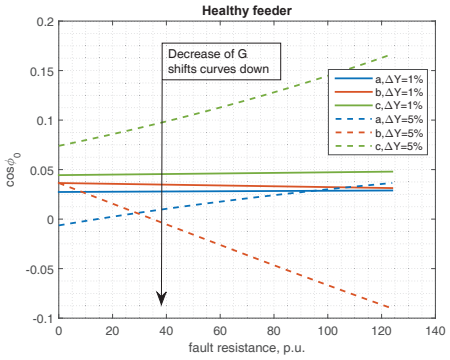

Fig. 3: Dependency of $\cos(\phi_0)$ on fault resistance in healthy feeder for fault in different phases, $\Delta\bar{Y} = 1\%$ and 5%, fixed compensation rate.

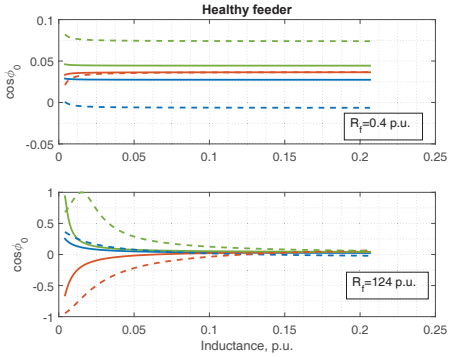

Fig. 4: Dependency of $\cos(\phi_0)$ on inductance of the Petersen coil in healthy feeder for fault in different phases, $\Delta\bar{Y} = 1\%$ and 5%, two fixed fault resistances $R_f = 0.4$ p.u. and 124 p.u. The legend is the same as in Fig.3.

Assuming $G_F = 0$ as prefault conditions and choosing overcompensation rate $K = |\bar{U}_0/\bar{E}_b|$ as 5% [25] (hereafter, such definition is used), inductance of the coil can be calculated for different network parameters. Having $\bar{U}_0$ for fault conditions ($G_F \neq 0$), cosine of angle of $\bar{I}_{0,h/f}/\bar{U}_0$ can be determined.

Fig.3 shows the results of analysis for constant compensation rate: dependency of $\cos(\phi_0)$ on fault resistance for three phases and different capacitive imbalance (1% and 5%).

From the plot, it can be seen that dependencies are not prominent for the small $\Delta\bar{Y}$, whereas more evident for the high imbalance. It must be noted that insufficiency of watt-metric contribution (small G) shifts all curves down. Taking this fact and the dependencies into account, it is possible to conclude that probability of relay misoperation in the healthy

feeder ($\cos(\phi_{0,h}) < 0$) increases with rise of fault resistance for phase b and decreases for a and c. The same conclusions are valid for the faulty feeder.

Fig.4 demonstrates the results for variation of compensation rate. It is observable from the upper plot (the small fault resistance) that $\cos(\phi_{0,h}) < 0$ only occurs for phase a and $\Delta\bar{Y} = 5\%$. Nevertheless, all curves might fall into the negative half-plane in case of insignificant G. The dependencies are more nonlinear for the high fault resistance (the lower plot). As the curves are shifted down with decrease of G, then larger overcompensations (small L) might lead to misjudgment ($\cos(\phi_{0,h}) < 0$) for faults in phase b and increase dependability of ground protection for faults in phases a and c. It is seen that the opposite situation arises for higher L. Analysis for the faulty feeder demonstrates the same results.

From these conclusions, it is noticeable that reliability of the traditional steady-state approach is low for insignificant natural watt-metric contribution and high electrostatic imbalance. Moreover, dependency of the polarity disruption effect on network and fault parameters prejudices application of $|\bar{I}_0|\cos(\phi_0)$ for faulty feeder selection without the parallel resistor. The effect also has impact on the alternative admittance method [4]; therefore, full analysis including lines (with $k_f \neq k_h$) and loads follows.

III. Theoretical Analysis of Fault Location Utilizing Transient Signals

In this paper, signals are only analyzed at the fundamental frequency and all high frequency components are filtered out. For the system in Fig.1, the following set of equations is valid for the instantaneous quantities:

$$\begin{cases} 3i_{0,h} = 3\frac{du_0}{dt}k_hC + 3u_0k_hG + \frac{du_b}{dt}k_h\Delta C \\ 3i_{0,f} = 3\frac{du_0}{dt}k_fC + 3u_0k_fG + \frac{du_b}{dt}k_f\Delta C + u_bG_F \\ i_L = 3i_{0,f} + 3i_{0,h} \\ e_{ph} = u_{ph} + u_L \\ u_L = L\frac{di_L}{dt} = -u_0 \end{cases} \quad (3)$$

Numerical solution of this set, based on the Runge-Kutta method with time discretization 10^{-5} s, with the same parameters used before and $G_F = 0.008$ p.u., $\Delta\bar{Y} = 0.02 \cdot 3\bar{Y}$, $K = 5\%$ ($L = 0.113$ p.u.) is demonstrated in Fig.5 as $u_0(t)$, $i_{0,f/h}(t)$. The initial conditions (in p.u.) corresponding to $u_b(0) = 0$: $e_a(0) = -1.222$, $e_b(0) = -0.006$, $e_c(0) = 1.228$, $u_0(0) = 0.006$, $i_L(0) = -1.98$.

The dynamic changes of the zero sequence currents in the faulty and the healthy feeder right after the fault ($t = 0$) are in opposite directions due to (dis)charging processes of the line capacitances. This peculiarities is used, for example, in the algorithm performed in [16]. Furthermore, considering the rest part of the transient period, it is seen that the zero sequence angle in the faulty feeder $\phi_{0,f}$ tends to values greater than 90^0. This phenomenon is used, for instance, in [19]. As a matter of fact, the transient period is significantly affected by network structures, parameters (including loads and line impedances), presenting nonidealities and fault origins; therefore, it requires further thorough investigation using an EMTDC-like software.

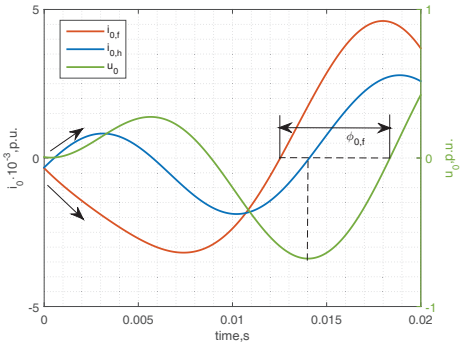

Fig. 5: Numerical solution of the differential equations in (3) for zero sequence voltage u_0 and currents in healthy $i_{0,h}$ and faulty feeder $i_{0,f}$.

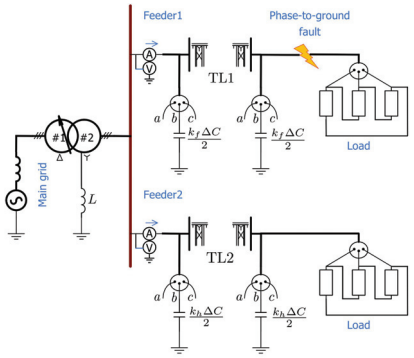

Fig. 6: Test case network.

IV. Test Case Network

The study is carried out based on the network depicted in Fig.6. The model is built in PSCAD™/EMTDC™. The main grid is modeled as an ideal voltage source with inductance (provides short circuit capacity). The distribution network consists of two feeders (transmission lines TL1, TL2 with variable lengths 10-50 km) with frequency dependent distributed parameters. For the given in Appendix A geometry, PSCAD calculates an admittance to the ground of each line per phase (per km) that gives possibility to determine the total network admittance per phase $\bar{Y}$. Electrostatic imbalance in the network $\Delta\bar{Y} = j\omega\Delta C$ is modeled as additional capacitors connected to phase b at the beginning and the end of each feeder; their values can be calculated as $k_{f/h}\Delta C/2$. Coefficients k_f and k_h will only depend on line lengths since their geometric parameters are the same, and $\Delta\bar{Y}$ is chosen as 1-5% from $3\bar{Y}$ to determine ΔC. The main distribution transformer has delta-wye connection and the secondary low voltage side

is grounded by the inductor. L is varied in accordance with $3\bar{Y}$ and so that to get compensation rate $K = 1 - 5\%$ from phase voltage of the transformer secondary side. In order to exclude influence of mutual inductances between phases, the lines are ideally transposed. Other parameters can be found in Appendix A.

The ground fault is always applied in Feeder 1 at the end (the location on the feeder is fixed because its change will not significantly alter the results). Simulated voltages and currents (as in Fig.5) are processed through the Discrete Fourier Transform (one-cycle at 50 Hz, sampling frequency is 4 kHz) with low-pass filtering (second order Butterworth with 1.5 kHz cut-off frequency) in order to extract magnitudes and angles of the fundamental components only. Consequently, apart from instantaneous quantities, we obtain dynamic variation of $\bar{U}_0$ and $\bar{I}_0$ (time-varying 50 Hz phasors) for further analysis.

Models of current transformers are not included into this study; however, it must be noted that their accuracy might be a concern for small fault currents and, as a consequence, for the locating methods.

V. Results and Discussions

A. Steady-state signals

Impact of variable network and fault parameters on the watt-metric approach has been studied using the performed model (for $k_f = k_h$). The results obtained through the simulations demonstrates similar dependencies of $\cos(\phi_{0,h})$ as in Fig.3 and Fig.4, and therefore are not presented. Additionally to the previous conclusions, it was found that load variation has indirect influence provoking changing of L in order to keep the same compensation rate; it can be regarded as the dependency on inductance in Fig.4. Finally, it was identified that ground resistivity does not have significant influence on performance of the steady-state methods.

The new admittance-based method described in [4] has been investigated for faulty feeder selection: the results are performed in Fig.7a ($k_f = k_h$, both lines are 50 km). Zero sequence admittances $\bar{Y}_0 = (\bar{I}_0 - \bar{I}_{0\text{pre}})/(\bar{U}_0 - \bar{U}_{0\text{pre}}) = G_0 + jB_0$ ("pre" stands for prefault) are calculated for the faulty (the red markers) and the healthy feeder (the blue) for different network and fault conditions. As it is possible to see, the faulty admittances fall into the operating area for the faulty feeder irrespectively of phase, compensation, electrostatic imbalance, fault impedance or watt-metric contribution of the network.

Fig.7b shows the admittances calculated for $k_f \neq k_h$, fault resistance $R_f = 3$ kΩ, $\Delta\bar{Y}$ is 2%, $K = 5\%$. If the faulty feeder is shorter than the healthy (10 km versus 50 km, that is $k_f = 1/6$ and $k_h = 5/6$), $\bar{Y}_{0,f}$ is in the operating area (the red o–marker). If it is longer (50 km versus 10 km, that is $k_f = 5/6$, $k_h = 1/6$), $\bar{Y}_{0,h}$ falls into the operating area, whereas $\bar{Y}_{0,f}$ is in the non-operating (the x–markers). Such situation is present due to two reasons: firstly, it is the polarity disruption effect; secondly, prefault ϕ_0 displacements caused by $|\bar{I}_{0,f}| > |\bar{I}_{0,h}|$ (prefault) because $k_f > k_h$. This issue requires individual settings for each feeder with more complex operating area in order to avoid misoperation.

It has been found that for cases with $k_f \neq k_h$, the same conclusions regarding postfault $\cos(\phi_0)$ are applicable (Fig.3, Fig.4). Displacement of ϕ_0 must be taken into account if a method utilizes prefault measurements. This phenomenon is typical for a network with cables and will be illustrated later.

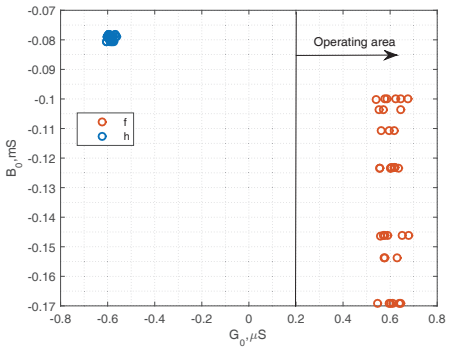

(a)

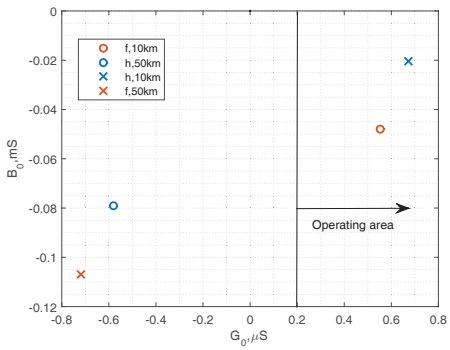

(b)

Fig. 7: Calculated zero sequence admittances for (a) equal feeder lengths of 50 km, $k_f = k_h = 0.5$ and (b) different feeder lengths: $k_f = 1/6$, $k_h = 5/6$ and $k_f = 5/6$, $k_h = 1/6$.

B. Transient signals

This section examines scenarios when the algorithms [16], [19], [23], [24] based on transient signals are prone to misoperation. Furthermore, two fault start times are applied: when phase voltage u_{ph} in faulty phase crosses 0 that is referred to as 0^0 inception angle (might occur when an extraneous object is in contact with a power line); when u_{ph} has a maximum value, that is 90^0 inception angle (can happen due to leakage ground current through an aged isolator). Below application of different quantities as an indicator of the faulty feeder is studied.

1) Indicators based on zero sequence angle: Fig.8a shows the typical behavior of $\cos(\phi_0)$ in case of fault ($K = 5\%$, $R_f = 3$ kΩ, $\Delta\bar{Y} = 1\%$, 0^0 inception angle, both lines are 50

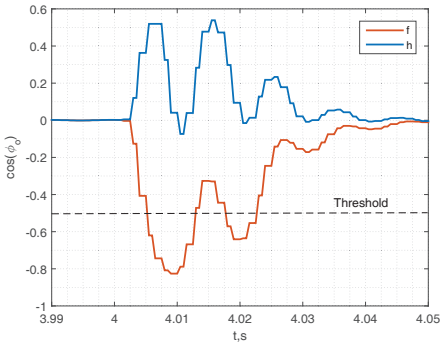

Fig. 8: Transient characteristics of $\cos(\phi_0)$ for high impedance fault ($\Delta\bar{Y} = 1\%$, 0^0 inception angle) in phase a) *a*, b) *b*.

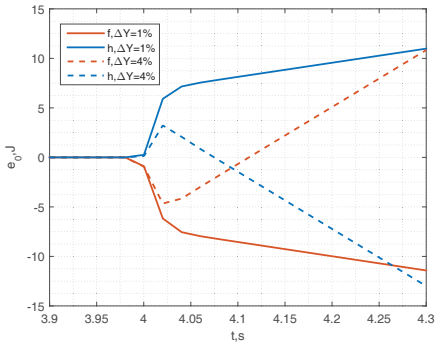

Fig. 9: Zero sequence energy e_0 for fault in phase a) *b* with $R_f = 3$ kOhm, b) *a* with $R_f = 10$ Ohm, and different $\Delta\bar{Y}$.

km) in the phase with small capacitance to the ground. The similar picture is observed for symmetrical systems regardless of a phase. Paper [19] suggests to use a simple threshold (the dashed line) to select the faulty feeder; however, it is not suitable solution in case of faults in the asymmetrical system: Fig.8b shows the transients for the same ground fault in phase *b* – $\cos(\phi_0)$ of the healthy and the faulty feeder cross the threshold.

Simulations have revealed that the transient process is not significantly affected by $\Delta\bar{Y}$, but extended penetration of $\cos(\phi_{0,h})$ into the negative half-plane mainly occurs for large K and phase *a* with 90^0 inception angle or *b* with 0^0 hindering the decision making procedure. Additionally, small fault resistances make the process faster (all important transients are only present during the first 5 ms) and oscillatory (change of the sign) that complicates signal acquisition and processing.

2) Indicators based on zero sequence energy: Paper [23] offers to use e_0 for feeder selection:

$$e_0 = \frac{1}{T}\int_{t_{inc}}^{t_{stop}}\int_{t\ \ T}^{t} i_0(\tau)u_0(\tau)\mathrm{d}\tau, \tag{4}$$

where t_{inc} is time of fault inception, t_{stop} – time of the end of integration, T is the period of the fundamental component.

Such parameter can help to avoid uncertainties caused by variation of $\cos(\phi_0)$ during the transient process. Fig.9a illustrates the application of it for the same fault in phase *b* (Fig.8b) – e_0 of the faulty feeder develops into the negative half-plane as shown in [23]. Nevertheless, due to the polarity disruption effect appearing for high $\Delta\bar{Y}$, e_0 for the healthy and the faulty feeder can change the half-planes (the dashed curves). This effect can also jeopardize other methods based on power, energy, impedance or admittance calculations. Proper choice of t_{stop} might not improve the situation because, as it is shown in Fig.9b for faults in phase *a* with 0^0 inception angle and $R_f = 10\ \Omega$, e_0 of the healthy feeder comes into the negative half-plane (and vice versa for he faulty) breaking the preset polarity. The reason was shown in the theoretical

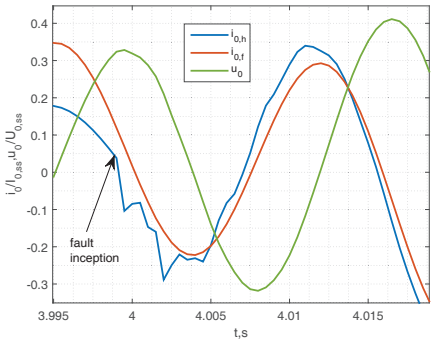

Fig. 10: Normalized by steady-state values instantaneous u_0 and i_0 for high impedance fault in feeder with cable.

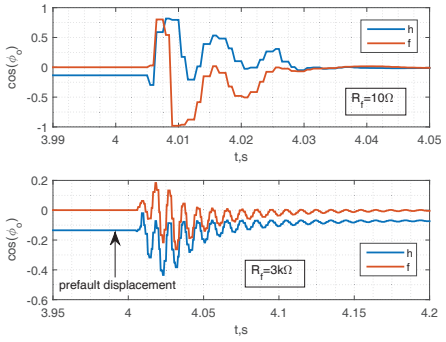

Fig. 11: Transient characteristics of $\cos(\phi_0)$ for fault (phase *a*, $\Delta\bar{Y} = 2\%$, 90^0 inception angle) in feeder with cable and two fixed fault resistances $R_f = 3$ kΩ and 10 Ω.

analysis (Fig.3, Fig.4): $\cos(\phi_{0,h}) < 0$ occurs for phase *a* and low fault resistances. Additionally, it was found that the method is highly sensitive to correct determination of t_{inc} (error in 1 ms is sufficient to get the wrong decision because of phase oscillations) and requires different settings for relays. It was also shown by [3] that the polarity disruption has negative influence on this method in the steady-state period.

3) Indicators based on polarity of instantaneous zero sequence current: The method based on polarity of i_0 described in [16] shows correct operation in all cases above. Nevertheless, the approach is compromised for the system with an underground cable. In order to demonstrate this, the model (Fig.6) is modified as follows: Feeder 1 has a 25 km overhead line and a 25 km underground cable (the parameters are given in Appendix A) connecting the load and the line, length of TL2 is 50 km.

Fig.10 shows the normalized by the steady-state values instantaneous zero sequence currents and voltage for high impedance fault in Feeder 1. It is possible to see that right after the fault inception $di_{0,h}/dt < 0$ and $du_0/dt < 0$ as well; from the theoretical analysis and previous studies, $di_{0,f}/dt > 0$ must be true (as in Fig.5), whereas it is not regardless of inception angle (or phase) due to large capacitance to the ground of the cable. However, this effect is not present during faults in Feeder 2 (without cables) or low R_f.

It is worth mentioning that e_0 is not the reliable indicator for high impedance faults occurring at 90^0 inception angle for the given system because of strong capacitive current from the cable.

4) Indicators based on zero sequence admittance: The Cumulative Phasor Sum proposed in [24] is calculated as:

$$\Sigma\bar{Y}_0 = \sum_{i=t_{inc}}^{t_{stop}} \bar{Y}_0(i), \tag{5}$$

where $\bar{Y}_0(i) = \bar{I}_0(i)/\bar{U}_0(i)$ is the zero sequence admittance (the fundamental frequency is considered) at specific time instant *i*.

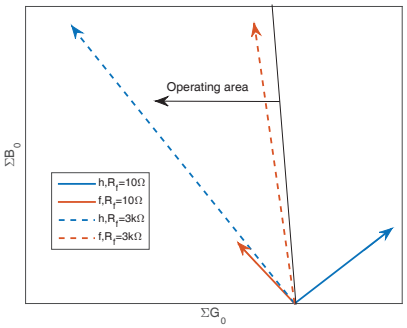

Fig. 12: Cumulative admittance phasors calculated using (5) for fault (phase *a*, $\Delta\bar{Y} = 2\%$, 90^0 inception angle, $R_f = 3$ kΩ and 10 Ω) in feeder with cable.

With proper t_{stop} (otherwise $\Sigma\bar{Y}_0$ will have an opposite sign due to the polarity disruption effect), this method analogously demonstrates good performance for cases in subsections V-B1 and V-B2. Moreover, it is fast (designed for intermittent faults) and does not require variety of settings – the decision is made on the ground of phasor positions. Nevertheless, an adverse effect appears for the system with the cable in subsection V-B3.

Fig.11 demonstrates extracted $\cos(\phi_0)$ for fault in phase *a*, $K = 3\%$, $\Delta\bar{Y} = 2\%$, 90^0 inception angle, $R_f = 10$ Ω and $R_f = 3$ kΩ. Presence of the cable leads to significant inequality of prefault zero sequence currents in the feeders, $|\bar{I}_{0,f}| \gg |\bar{I}_{0,h}|$; therefore, as can be seen from the plot, there is displacement of prefault $\cos(\phi_0)$ of the healthy feeder mentioned in section V-A. Due to this reason together with high $R_f = 3$ kΩ, faults in Feeder 1 will lead to $\cos(\phi_{0,h}) < 0$ during the transient and the steady-state periods. For $R_f = 10$

TABLE I: Summary on the analyzed methods.

Method	Network conditions of inadequacy	The worst fault conditions
SS[1], $\lvert\bar{I}_0\rvert\cos(\phi_0)$ [2]	$\downarrow^2 G$, $\uparrow^3 \Delta\bar{Y}$, $\downarrow L$	HIF[4] in phase with the highest $\bar{Y}$ (among three phases).
SS, $\bar{Y}_0$ [4]	$\uparrow \Delta\bar{Y}$, prefault $\lvert\bar{I}_{0,f}\rvert > \lvert\bar{I}_{0,h}\rvert$	HIF in phase with the highest $\bar{Y}$.
T[5], $\cos(\phi_0)$ [19]	$\Delta\bar{Y} \neq 0$, fault inception angle.	HIF at 0^0 inception angle.
T, e_0 [23]	$\downarrow G$, $\uparrow \Delta\bar{Y}$, $\downarrow L$, wrong detection of fault inception time.	LOF[6] in phase with the smallest $\bar{Y}$.
T, i_0 [16], $\Sigma\bar{Y}_0$ [24]	Prefault $\lvert\bar{I}_{0,f}\rvert \gg \lvert\bar{I}_{0,h}\rvert$ (especially in mixed networks).	HIF in the feeder with large penetration of cables.

[1] steady-state, [2]insufficient/small value, [3] excessive/big value, [4] high impedance fault, [5] transient, [6] low-ohmic fault.

Ω, $\cos(\phi_{0,h})$ is predominantly in the positive half-plane. Thus, the CPS method works correctly for low-ohmic faults, see Fig.12. However, for high impedance faults, both phasors fall into the operating area (the dashed arrows).

Dependability of the method is improved if displacement tends to zero (operation point is close to resonance) because angle transients fall into the positive half-plane (as for low-ohmic faults); therefore, careful analysis of prefault conditions is important as in the case with steady-state methods.

To summarize, the transient methods are prone to malfunctioning in case of high impedance faults in compensated systems with significant electrostatic imbalance of phases and presence of underground cables. Finally, simulations have revealed that ground resistivity and load imbalance will not have significant impact on transient methods.

To conclude this section, we shall note that similar results will be obtained for models of networks with more complex topologies because they can be wrapped into two-feeder model (Fig.6), where the healthy feeder will perform a background network as it is shown in [8]. Furthermore, many methods were theoretically illustrated on two-feeder models and tested on complex models or on real measurements, e.g. [4].

VI. Conclusion

The current work presents the most important methods (some of them can be founded in modern relays) for ground fault locating in distributed networks with resonant grounding and possible scenarios of their misoperations. The summary is presented in Table I. It indicates combination of the network parameters together with the worst fault conditions leading to inadequacy of the methods.

The protection based on steady-state signals is prone to the polarity disruption when a healthy feeder can be misjudged as a faulty. The obtained results clearly indicate how this effect depends on network and fault parameters. In many cases, this problem can be eliminated applying the parallel resistor; however, it provokes new challenges and finding of better solutions is still an ongoing process.

Utilization of transients to extract information is a more evident solution, however it requires more developed technologies (in terms of signal acquisition and processing) and careful analysis in order to avoid incorrect decisions. The results show that the network electrostatic asymmetry, phase, fault impedance and inception angle have significant impact on the transient period compromising the algorithms. Other challenges might appear for cumulative criteria in networks with extensive penetration of cables, however mainly for high impedance faults. All these circumstances imply a need for further development of algorithms applicable for different network and fault types, as well as independent of information about system parameters, complex signal processing tools or additional equipment. It is advantageous to have universal settings for all relays in a system and fast operation time.

The further work will be dedicated to finding of an algorithm meeting the described requirements and handling all adverse effects performed in the current paper.

Appendix A
Model parameters

TABLE II: Elements of the model and their description.

Element	Description
Main grid	66 kV (line-to-line), short circuit capacity 250 MVA, 50 Hz
Transformer	20 MVA, $66/22$ kV, leakage reactance 10%, copper losses 0.45%, tap 0.906 (primary side)
Overhead line (TL1 and TL2)	Hight 7.1 m, distance between 3 conductors (radius 10 mm, DC resistance 0.43 Ohm/km) 1.5 m (plane geometry), shunt conductance 10^{-8} S/km
Cable (part of TL1)	Depth 1 m, distance between phases 0.5 m (plane geometry); conductor: resistivity $4.2 \cdot 10^{-8}$ ohm·m, radius 5 mm; insulator: relative permittivity 5, radius 9 mm
Ground	resistivity 200 ohm·m
Load (100%)	interphase impedance $60 + j19$ Ohm

References

[1] X. Zhang, B. Xu, Z. Pan, P. Wei, "Study on single-phase earthed faulty feeder selection methods in non-solidly grounded systems", Third International Conference on Electric Utility Deregulation and Restructuring and Power Technologies, DRPT 2008, pp. 1836 – 1840, 2008.

[2] I. G. Kulis, A. Marusic, S. Zutobradic, "Insufficiency of watt-metric protection in resonant grounded networks", Eighth IEE International Conference on Developments in Power System Protection, DPSP 2004, volume 2, pp. 486 – 489, 2014.

[3] H. Ji, Y. Yang, H. Lian, S. Cong, "Effect on Earth Fault Detection Based on Energy Function Caused by Imbalance of Three-Phase Earth Capacitance in Resonant Grounded System", International Conference on Power System Technology, pp. 1 – 5, 2006.

[4] A.Wahlroos, J. Altonen, "Performance of novel neutral admittance criterion in MV-feeder earth-fault protection", 20th International Conference and Exhibition on Electricity Distribution – Part 1, CIRED, pp. 1 – 8, 2009.

[5] T. Henriksen, "Faulty feeder identification in high impedance grounded network using charge-voltage relationship", Electric Power Systems Research Journal, volume 81, issue 9, pp. 1832 – 1839, 2011.

[6] G. Druml, R. W. Klein, O. Seifert, "New adaptive algorithm for detecting low- and high ohmic faults in meshed networks", 20th International Conference and Exhibition on Electricity Distribution – Part 1, CIRED 2009, pp. 1 – 5, 2009.

[7] M. Loos, S. Werben, M. Kereit, J. C. Maun, "Detection of single phase earth fault in compensated network with C0 estimation", 22nd International Conference and Exhibition on Electricity Distribution (CIRED 2013), pp. 1 – 4, 2013.

[8] M. F. Abdel-Fattah, M. Lehtonen, "Transient algorithm based on earth capacitance estimation for earth-fault detection in medium-voltage networks", IET Generation, Transmission & Distribution, volume 6, issue 2, pp. 161 – 166, 2012.

[9] J. Berggren, L. Hammarson, "Novel method for selective detection of earth faults in high impedance grounded distribution networks", 18th International Conference and Exhibition on Electricity Distribution, pp. 1 – 4, 2005.

[10] K. Zhong-jian, L. Dan-dan, Z. Chao, L. Xiao-lin, "Research on the Fault Characteristic in Non-effectively Grounding Distribution Network with a Single-Phase-to-Earth Fault Based on Hilbert-Huang Transform", International Conference on Intelligent System Design and Engineering Application (ISDEA), volume 2, pp. 276 – 279, 2010.

[11] S. Hongchun, S. Shiyun, Q. Gefei, P. Shixin, "A new method to detect single-phase fault feeder in distribution network by using S-transform", IEEE 11th International Conference on Probabilistic Methods Applied to Power Systems (PMAPS), pp. 277 – 282, 2010.

[12] S. Zhang, H. Gao, M. Hou, Y. Sun, Z. Shao, J. Li, "Frequency spectrum characteristic analysis of single-phase ground fault in a Petersen-coil grounded system", 5th International Conference on Electric Utility Deregulation and Restructuring and Power Technologies (DRPT), pp. 369 – 374, 2015.

[13] K. Musierowicz, J. Lorenc, Z. Marcinkowski, A. Kwapisz, "A fuzzy logic-based algorithm for discrimination of damaged line during intermittent earth faults", IEEE Russia Power Tech, pp. 1 – 5, 2005.

[14] Y. Song, J. Liu, S. Yuan, C. Zhao, "Based on IAHP comprehensive evaluation method of the single-phase ground fault protection in cable distribution network", International Conference on Electrical and Control Engineering (ICECE), pp. 98 – 104, 2011.

[15] C. Zhongren, L. Weibo, H. Jian, "Single-phase grounding fault identification and fault line selection for compensation grid", 7th International Power Electronics and Motion Control Conference (IPEMC), volume 3, pp. 2290 – 2293, 2012.

[16] M. F. Abdel-Fattah, M. Lehtonen, "A transient fault detection technique with varying fault detection window of earth modes in unearthed MV systems", Power Quality and Supply Reliability Conference (PQ 2008), pp. 181 – 186, 2008.

[17] W. Y. Huang, R. Kaczmarek, "SLG Fault Detection in Presence of Strong Capacitive Currents in Compensated Networks", IEEE Transactions on Power Delivery, volume 22, issue 4, pp. 2132 – 2135, 2007.

[18] Y. Qi, Z. Wen, H. Jia, "Distribution Network Fault Location Algorithm Based on Zero-Sequence Current Phase", Spring Congress on Engineering and Technology (S-CET), pp. 1 – 4, 2012.

[19] P. Balcerek, M. Fulczyk, J. Izykowski, E. Rosolowski, P. Pierz, "Centralized substation level protection for determination of faulty feeder in distribution network", IEEE Power and Energy Society General Meeting, pp. 1 – 6, 2012.

[20] X. Yongduan, X. Bingyin, C. Yu, F. Zuren, P. Gale, "Earth fault protection using transient signals in non-solid earthed network", International Conference on Power System Technology (PowerCon 2002), volume 3, pp. 1763 – 1767, 2002.

[21] X. H. Zhang, H. X. Ha, Z. C. Pan, B. Y. Xu, "Grounding faulty line selection in non-solidly grounded systems using transient energy", International Power Engineering Conference (IPEC 2007), pp. 1147 – 1150, 2007.

[22] L. Jian, H. Jianjun, Z. Hongwei, Y. Hua, Z. Jie, L. Lei, W. Rui, "Fault Line Selection Based on Zero Sequence Power Direction of Transient Fundamental Frequency in MV Network Grounded with Arc Extinguishing Coil", International Conference on Power System Technology, pp. 1 – 4, 2006.

[23] M. Loos, S. Werben, M. Kereit, J. C. Maun, "Fault direction method in compensated network using the zero sequence active energy signal", IEEE EUROCON, pp. 717 – 723, 2013.

[24] A. Wahlroos, J. Altonen, "Application of novel multi-frequency neutral admittance method into earth-fault protection in compensated MV-networks", 12th IET International Conference on Developments in Power System Protection (DPSP 2014), pp. 1 – 6, 2014.

[25] Z. Chen, H. Wang, F. Chen, "Research on Damping Ratio and Off-Resonant Degree of Compensation Network", Asia-Pacific Power and Energy Engineering Conference (APPEEC), pp. 1 – 4, 2011.

[Paper V]

K. Pandakov, H. Kr. Høidalen, J. I. Marvik. (2017) Fast protection against islanding and unwanted tripping of distributed generation caused by ground faults, *CIRED - Open Access Proceedings Journal*, 2017(1), pp. 1126 - 1130.

FAST PROTECTION AGAINST ISLANDING AND UNWANTED TRIPPING OF DISTRIBUTED GENERATION CAUSED BY GROUND FAULTS

Konstantin Pandakov
NTNU – Norway
konstantin.pandakov@ntnu.no

Hans Kristian Høidalen
NTNU – Norway
hans.hoidalen@elkraft.ntnu.no

Jorun Irene Marvik
SINTEF – Norway
jorun.irene.marvik@sintef.no

ABSTRACT

Ground faults (GF) in a feeder with interconnected distributed generation (DG) might lead to overvoltages in healthy phases even after feeder disconnection from a substation, obstacles for reclosing schemes, and safety hazards. It requires urgent disconnection of DG to prevent islanding. On the other hand, fast location of GF in compensated networks is a difficult task and finding of the correct fault location is necessary in order to decrease a number of undesirable DG decoupling.

The current paper proposes a communication–based scheme preventing islanding forming in a system. The scheme utilizes a new fast and universal indicator revealing fault positions. A locating algorithm is also applied to restrict unwanted disconnection of DG. The method is tested on a model in PSCAD/EMTDC of an actual 22 kV multiterminal grid grounded by a Petersen coil and including DG.

The results show that the new indicator can reliably discriminate faults in the system. It has been found that precision of the locator utilizing two–point measurements is not sufficient and might lead to nuisance tripping of the DG. Using of multi–point measurements and the proposed indicator helps to solve this problem for a complex feeder topology. Finally, the same signals can be applied to enhance accuracy of the locator.

INTRODUCTION

Proliferation of distributed generation in power systems leads to several complications linked to dependability of the traditional protection schemes. Ground faults bring special issues in compensated and isolated networks. References [1] and [2] show that DG has no impact on performance of ground relays; however, for reliable and safe operation, it is necessary to disconnect interconnected generators as fast as possible. Undervoltage protection, used for this purpose, might lead to unnecessary decoupling of DG in case of faults in adjacent feeders or in downstream locations. On the other hand, relaxing of its settings and having proper fault right through capability can cause unintentional islanding in a system.

[3] describes the state–of–the–art methods on anti–islanding protection. The main purpose of such methods is to detect loss–of–main situation from DG point of view in a network a feeder circuit breaker is open. Taking into account that the vast majority of faults in distribution networks are single–line–to–ground and they have temporary character, it is advantageous for system reliability to disconnect DG as fast as possible and initiate reclosing procedures. It excludes application of complex schemes with check of synchronization and presence of an island if a fault is permanent.

For this purpose, a communication–assisted scheme [4] can be applied as the most reliable and fast approach. DG obtains measurements from a substation (or several depending on configuration) in order to determine a ground fault location:

- If it is inside of a potential island (a monitoring zone), DG must be decoupled.
- If it is outside, DG can continue operation (the standard undervoltage protection can be blocked).

Nevertheless, locating of ground faults in compensated (in this work, such type of grounding is only considered) distribution networks is a difficult task due to weak fault currents. The traditional approach based on steady–state signals with connection of a parallel resistor [5] is out of interest because such procedure leads to delays, switching transients, increase of fault current, and additional investments (for this reason, signaling methods are not considered here).

On the one hand, elimination of the resistor will accelerate operation, but on the other, it will decrease dependability of the methods based on comparison of residual current directions as it was shown in [6]. Therefore, phase–comparison schemes, for example in [7], can be compromised. Approaches based on variation of current magnitudes, for instance due to alternating of compensation rate presented in [8], might be inadequate in networks with cables or can lose sensitivity in case of high impedance faults. Alternative methods, for example based on calculation of zero sequence admittances [9], require pre–fault information, and settings depend on network configuration. Approaches utilizing low–frequency transients require careful study because they depend on network and fault parameters, whereas high–frequency are difficult to implement in practice due to susceptibility to measuring noise.

Incorrect determination of a fault position might lead to nuisance tripping of DG or, in the worst case, unexpected presence of the source. Thus, a new indicator not depending on network or fault parameters is needed to determine whether fault is in front or behind a ground relay. This paper proposes a simple and universal algorithm utilized in the fast communication–based protection in order to prevent potential islanding situations in a network or unwanted DG disconnection caused by ground faults, as well as to facilitate reclosing schemes in a feeder with DG. Furthermore, for decreasing of outage time, it is desirable to extract information from the same signals about a probable faulty area. The paper also offers an improved method, presented earlier in [10], on ground fault location

estimation demanding less computations and with possibility of precision enhancement.

DEVELOPMENT OF A NEW INDICATOR

Synchronized two–point measurements at a substation and DG are needed in order to find parameters of an equivalent line, Fig.1, through the following equation:

$$\begin{bmatrix} \frac{Y}{2}+\frac{1}{Z} & -\frac{1}{Z} \\ -\frac{1}{Z} & \frac{Y}{2}+\frac{1}{Z} \end{bmatrix} \begin{bmatrix} V_s \\ V_r \end{bmatrix} = \begin{bmatrix} I_s \\ I_r \end{bmatrix}, \tag{1}$$

where Z is the series impedance, Y is the shunt admittance, V and I are the voltage and the current at the sending (index s) and the receiving (r) end. All variables are zero sequence quantities.

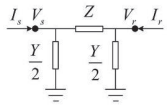

Figure 1: Equivalent line.

The next step is to change the real part of the calculated admittance as |real(Y)|+j·imaginary(Y) because, in most cases, it might be negative during ground faults. Finally, the line is split by the faulty point as shown in Fig.2.

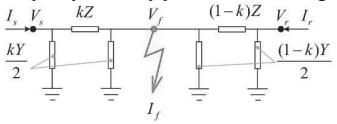

Figure 2: Splitting of the equivalent line by the fault.

Hereafter, V_f is the voltage at the faulty point and I_f is the fault current. Parameter k (a relative distance from the sending end) can be determined having the following system of expressions:

$$\begin{cases} V_f = V_s - kZ\left(I_s - V_s\frac{kY}{2}\right) \\ V_f = V_r - (1-k)Z\left(I_r - V_r\frac{(1-k)Y}{2}\right) \end{cases} \tag{2}$$

It yields the quadratic equation below that is solved for k.

$$k^2\frac{ZY}{2}\left(V_s - V_r\right) - kZ(I_s + I_r - V_rY) + V_s - V_r + Z\left(I_r - V_r\frac{Y}{2}\right) = 0 \tag{3}$$

The real part of the smallest root is taken as an indicator with the following condition applied in the algorithm:

- k≈0.5 – the fault is in front of the sending and the receiving relay.
- k≈0 – the fault is behind one of them.

Such k–indicator has simple universal settings for the whole system (even if the topology is changed) and immunity to fault origins because equation (3) does not contain V_f and I_f. Moreover, any prefault information is not needed. This method does not provide information about exact fault location, therefore the algorithm is supplemented by a locator utilizing the same measurements as outlined in the next section.

DESCRIPTION OF THE ALGORITHM FOR FAULT LOCATION

The same signals obtained from the sending and the receiving end together with prefault information about a zero sequence network are used in the locator. It is based on solution of the following matrix equation (in zero sequence quantities):

$$\left[\mathbf{Z}(k)\right]\begin{bmatrix} I_s \\ I_r \\ I_1 \\ \dots \\ I_n \\ I_f \end{bmatrix} = \begin{bmatrix} V_s \\ V_r \\ V_1 \\ \dots \\ V_n \\ V_f \end{bmatrix}, \tag{4}$$

In distribution networks there are many load outfeeds between the measuring points as it is illustrated in Fig.3.

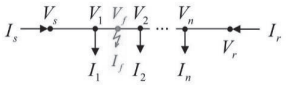

Figure 3: Multitapped network.

In (4) they are considered as voltages at load points $V_1 \dots V_n$ and load currents $I_1 \dots I_n$. In compensated systems loads are decoupled from the main trunk by the mean of YD transformers; therefore, for the zero sequence network $I_1 = \dots = I_n = 0$ is valid.

Equation (4) is nonlinear because zero sequence impedance matrix under fault conditions $\mathbf{Z}(k)$ is unknown and depends on a fault location. Thus, finding of $\mathbf{Z}(k)$ provides information about a possible faulty area. It is worth noting that number of measuring points N_m must be greater or equal to two due to the fact that: the number of the rows N in (4) is $N=N_m+N_{ld}+1$ (N_{ld} – the number of the load taps), and the amount of the unknowns is $N_{ld}+3$ ($V_1 \dots V_n$, V_f, I_f, k containing in $\mathbf{Z}$).

The current work proposes the following method for solution:

1. Linearization of $\mathbf{Z}(k)$: a fault is assumed to be at a specific position chosen arbitrary, then known $\mathbf{Z}^*$ can be formed.
2. Vector of currents $\mathbf{I}$ is determined. In fact, only I_f is unknown:

$$I_f = \frac{V_m - \mathbf{Z}^*_{m,1:N-1}\cdot\mathbf{I}_{1:N-1}}{\mathbf{Z}^*_{m,N}}, \tag{5}$$

   where m is a row that can be chosen among the rows containing the measured voltages and the currents. Notation m,N means an element in row m and column N. Notation 1:N-1 means all elements from 1 to N-1.
3. Calculation of a voltage error. The calculated

voltages can be compared with the measured in order to find the most probable fault location. For this purpose, norm of a relative voltage errors is evaluated:

$$\Delta V_{i,l} = \left\| \frac{|\mathbf{V}_{1:N_m} - \mathbf{Z}^*_{1:N_m,1:N} \cdot \mathbf{I}|}{|\mathbf{V}_{1:N_m}|} \right\| \quad (6)$$

where division is elementwise (voltage vector **V** is used), index i denotes an exact faulty point position on a chosen line l. Therefore, $k=i*dk$ with geometrical step dk and $i=0:1/dk$, and $l=1:N_l$ with the number of lines N_l.

4. The fault position is changed (i and l correspondingly) with fixed m, the matrix of errors is accumulated, $\Delta\mathbf{V}_{0:1/dk,1:Nl}$.
5. Finding of min($\Delta\mathbf{V}$) gives row $i^{\min}$ and column $l^{\min}$ with the minimal element. Values $k'_m = i^{\min}*dk$ and $l'_m = l^{\min}$ are memorized for fixed m.
6. Additionally, parameter α_m (for fixed m) is calculated as $\alpha_m = ||\Delta V^{\min}_1 \; \Delta V^{\min}_2 \; ... \; \Delta V^{\min}_5||$, where $\Delta V^{\min}_{1:5}$ the first five minimal errors from $\Delta\mathbf{V}$.
7. Row m for calculation of I_f is changed and all steps are repeated. Values of k'_m, l'_m and α_m are accumulated.
8. Finally, condition min($\alpha_{1:Nm}$) gives m that leads to better precision, denoted as m-f. After that, the most accurate $k'_{m\text{-}f}$ and $l'_{m\text{-}f}$ can be chosen.

Steps 6 – 8 differ the proposed approach from the previously developed in [10] and provide higher precision for the locator. Working with an impedance matrix requires fewer computations. Furthermore, in order to speed up calculations, parallel processing is possible (e.g. steps 1 – 6 can be executed simultaneously for different $m=1:N_m$). The performed algorithms have been tested on the model described below.

TEST CASE NETWORK

Several fault locations have been studied by means of the model of the distribution network illustrated in Fig.4. It is an actual 22 kV grid with DG: a synchronous and an induction generator. Main distribution transformer T1 is grounded through a variable inductor (the value and over compensation rate 3.5 % are provided by the system operator). The network has overhead transmission lines TL1 – TL22 together with extensive cable sections (specially marked lines TL10_1, TL10_3, TL11_1, TL22_2). Numerous load points are connected with the main trunks by short cables; detailed modelling of this configuration is bulky, therefore represented as concentrated loads S0 – S19. Protection functions are accomplished by relays R1 – R13.

The model is built in PSCAD™/EMTDC™: the transmission lines are represented as the PI–equivalent models (electrostatic asymmetry is taken into account), the loads are delta–connected constant impedances (that represents the YD distribution transformers), the utility grid is an ideal voltage source, the transformers and the generators can be found in the standard libraries of the simulation program. All parameters were provided by the system operator and cannot be specified.

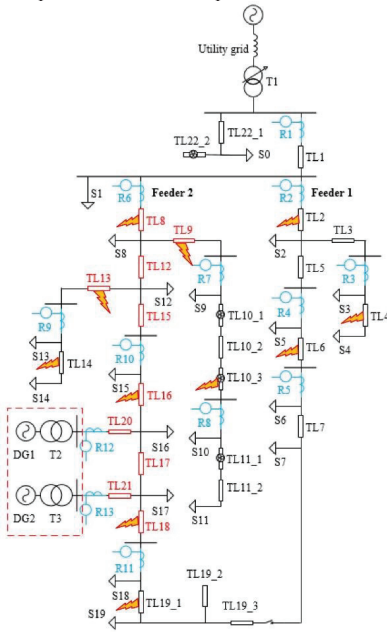

Figure 4: 22 kV distribution network.

Islanding situation will arise in case of faults in the lines marked by red colour in Fig.4 provided that relays R7, R9, R11 successfully clear the downstream faults.

RESULTS AND DISCUSSIONS

Fig.5 shows dynamic behaviour of the k–indicator for the faults (inception time is 4.45 s) in Fig.4. In addition to the lines specified above, a fault was applied for different phases (to handle network asymmetry) and fault resistances – 10 Ohm and 3 kOhm. Relays R6 and R13 are used to identify the equivalent line.

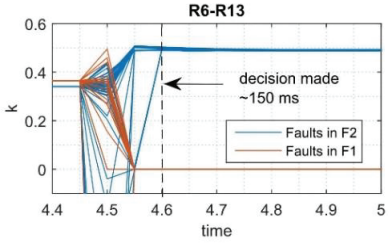

Figure 5: Dynamic performance of the k–indicator.

As it is possible to see, the faults in Feeder 1 are effectively discriminated regardless of fault origins.

Moreover, decision is made during the first few hundreds milliseconds (the transient period) that provides possibility for fast operation.

After the correct feeder selection, the faults in lines TL10_3, TL14, TL19_1 must be separated from the red–marked in Feeder 2 (Fig.4) in order to prevent nuisance tripping. For this purpose, the fault locator is used. Fig.6 shows the dynamic performance of the locator for the fault in line TL8. Here, post-fault processing of the recorded measurements is applied, step $dk = 0.01$ is used.

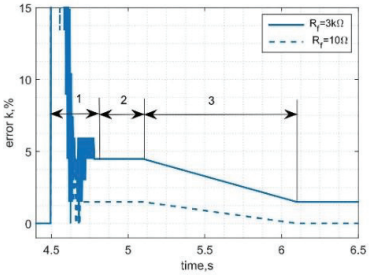

Figure 6: Dynamic performance of the fault locator.

In Fig.6, period 1 represents the transient period, and 2 – the steady–state; as it is possible to notice, stable solution for error of $k^f_{m\text{-}f}$ (the line is determined correctly), is achieved in the second period. It is also seen that the low–ohmic fault (higher fault current) leads to the better accuracy. Therefore, a parallel resistor or decrease of the Petersen coil inductance (period 3 reflects gradual process as an example) can be applied: it improves the precision of the locator.

Fig.7a illustrates the calculated results for the faults in phase A with resistance 3 kOhm in the locations mapped on the one–line diagram of Feeder 2. It can be seen that the maximal errors ($\Delta_{1,2,3}$) belong to lines TL10_3, TL14, TL19_1 that are the side branches from the main path between relays R6 and R13; in contrast, the more precise results are achieved for lines TL8, TL16. Errors $\Delta_{1,2,3}$ lead to nuisance tripping of the DG.

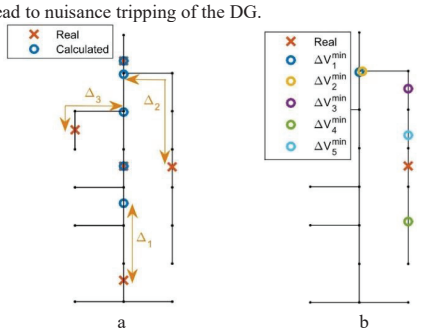

Figure 7: Fault location for (a) two–point measurements, (b) line TL10_3.

Fig.7b demonstrates that the several possible (calculated on the basis of the first five minimal voltage errors $\Delta V^{\min}_{1:5}$) locations for one fault, for example in line TL10_3, can identify that it is in the side brunch. Nevertheless, accuracy required for reliable prevention of nuisance tripping of the DG is still poor even for larger overcompensation.

Algorithm for four–point measurements

In order to avoid unintentional decoupling of DG because of locator error, measurements of relays R6, R7, R9, R11 must be involved. Hence, the *k*–indicator can be used to discard the lines downstream of these relays. Fig.8 illustrates this method for the faults in the system for all three phases in each line and two fault resistances – 10 Ohm and 3 kOhm (hence, six cases for each line).

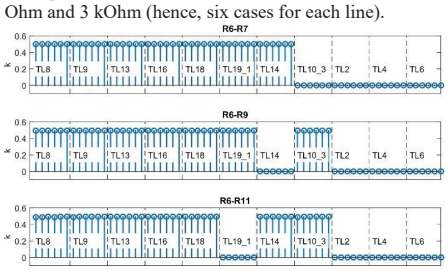

Figure 8: The *k*–indicator for four–point measurements.

Applying three pairs of relays (R6 – R7, R6 – R9 and R6 – R11), it is possible to construct the equivalent lines and find *k* for each pair. It is seen that relays R6 and R7 eliminate ($k \approx 0$) the faulty lines in Feeder 1 and in front of relay R7 (polarity is towards the substation). Analogously, relays R6 and R9 discriminate line TL14 and Feeder 1; relays R6 and R11 – Feeder 1 and TL19_1.

Applying AND logic between these three pairs, the final decision leave lines TL8, TL9, TL13, TL16, TL18 with $k \approx 0.5$. All these lines belong to the area of the potential island; therefore, the DG can be disconnected in a fast manner. Conversely, if $k \approx 0$, the DG continues operation with the grid with respect to its fault ride through capability. Numerous simulations with various network and fault parameters show high reliability of such approach.

Fig.9 illustrates performance of the locator for the faults inside the potential zone: all corresponding lines are correctly identified, and error of *k* depends on fault resistance and compensation rate (inductance L_1 is greater than L_2 in the plot). It is noticeable that the error is small or around zero for the long lines (e.g. TL8, ~15 km) and significant for the short (e.g. TL9, ~500 m).

CONCLUSION

This work has demonstrated the performance of the proposed *k*–indicator for ground fault position identification. It has the following advantages: simple settings coming to logical 1 or 0 (less information in data

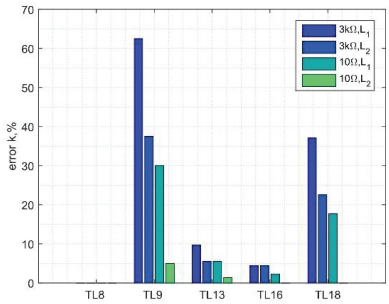

Figure 9: Fault location error for four–point measurements.

packages) and not depending on (variable) system configurations, immunity to fault parameters (locations, impedances), fast decisions during few hundreds milliseconds, no need in prefault information.

The improved fault locator based on the zero sequence network demonstrates sufficient usability for the multitapped distribution network. Accuracy can be enhanced by decreasing of a Petersen coil inductance at the substation or using more measurements and the smaller network size.

Application of the proposed algorithm in the real system will benefit as follows:

- Avoiding of unnecessary tripping of the DG caused by ground faults.
- Fast identification of potential islanding situation in case of ground faults in the network followed by disconnection of the DG and initiation of reclosing procedures.
- Accurate ground fault location that improves reliability of power supply.

It is worth mentioning that the basic indicator for ground fault identification and initialization of the performed algorithms can be zero sequence voltage. The further work requires studying of difficulties arising with presence of intermittent faults in cables (unstable signals).

REFERENCES

[1] L.K. Kumpulainen, K.T. Kauhaniemi, 2005, "Aspects of the effects of distributed generation in single–line–to–earth faults", *International Conference on Future Power Systems*, 5

[2] K. Mäki, S. Repo, P. Järventausta, 2007, "Impacts of Distributed Generation on Earth Fault Protection in Distribution Systems with Isolated Neutral", *19th International Conference on Electricity Distribution, CIRED*, 4

[3] S.C. Paiva, H.S. Sanca, F.B. Costa, B.A. Souza, 2014, "Reviewing of anti–islanding protection", *11th IEEE/IAS International Conference on Industry Applications, INDUSCON*, 1–8

[4] E.O. Schweitzer, D. Finney, M.V. Mynam, 2012, "Communications–assisted schemes for distributed generation protection", *IEEE PES Transmission and Distribution Conference and Exposition (T&D)*, 1–8

[5] I.G. Kulis, A. Marusic, S. Zutobradic, 2004, "Insufficiency of watt–metric protection in resonant grounded networks", *Eighth IEE International Conference on Developments in Power System Protection, DPSP 2004*, vol.2, 486–489

[6] H. Ji, Y. Yang, H. Lian, S. Cong, 2006, "Effect on Earth Fault Detection Based on Energy Function Caused by Imbalance of Three–Phase Earth Capacitance in Resonant Grounded System", *International Conference on Power System Technology*, 1–5

[7] D. Jiao, L. Yuping, Z. Guofang, L. Xia, 2009, "An asymmetrical fault location method based on communication system in distribution network with DGs", *IEEE/PES Power Systems Conference and Exposition (PSCE)*, 1–5

[8] M. Lehtonen, O. Siirto, M. F. Abdel–Fattah, 2014, "Simple fault path indication techniques for earth faults", *Electric Power Quality and Supply Reliability Conference (PQ 2014)*, 371–378

[9] A. Wahlroos, J. Altonen, 2009, "Performance of novel neutral admittance criterion in MV–feeder earth–fault protection", *20th International Conference and Exhibition on Electricity Distribution–Part 1, CIRE*, 1–8

[10] S. M. Brahma, 2011, "Fault Location in Power Distribution System with Penetration of Distributed Generation", *IEEE Transactions on Power Delivery*, vol. 26, issue 3, 1545–1553

[Paper VI]

K. Pandakov, H. Kr. Høidalen, S. Trætteberg. (2018) An additional criterion for faulty feeder selection during ground faults in compensated distribution networks, *IEEE Transactions on Power Delivery*, 33(6), pp. 2930 - 2937.

An additional criterion for faulty feeder selection during ground faults in compensated distribution networks

Konstantin Pandakov, Hans Kristian Høidalen, and Sidsel Trætteberg

***Abstract*—Identification of faulty feeders and sections during ground faults in compensated medium voltage systems is a complex task demanding development of new methods. Existing steady-state approaches, such as the watt-metric or the admittance based, can be compromised by various parameters of distribution lines or network configuration. Moreover, sensitivity might be threatened during high impedance faults. Transient methods (extensively studied in the recent literature) require thorough analysis before implementation due to their dependency on fault and system parameters. The current paper proposes a new approach for faulty feeder selection during ground faults. It has been tested in the laboratory utilizing EMTP simulations. Performance of the developed algorithm has been compared with the conventional steady-state method implemented in a modern feeder relay. The results show improved selectivity and robustness of the new proposed algorithm. Moreover, its applicability for real systems has been demonstrated on fault records obtained from an actual distribution network. The proposed approach can be used as an additional criterion to increase selectivity of the ground fault protection in compensated networks.**

***Index Terms*—ground fault protection, resonant grounding, transient**

I. Introduction

In compensated distribution systems the main transformer is grounded through an inductor (Petersen coil). This decreases earth fault current and thereby increases probability of a self-extinguishing arc. In case of permanent or longstanding intermittent faults, breaking operation is required that interrupts load current. In order to affect as few customers as possible, it is necessary to determine a faulty branch (or a feeder in general) and isolated it from the network.

The traditional method of earth fault detection is to measure zero sequence voltage magnitude at the substation and zero sequence currents in each feeder in order to compare them with thresholds. For identification of a faulty feeder, zero sequence current magnitude is not a reliable indicator (especially for long lines and cables), whereas its direction (that is phase with respect to zero or negative sequence voltage) is typically utilized.

As it was shown in [1], this standard approach of faulty feeder selection is jeopardized in case of high impedance faults. Reference [2] demonstrates that the direction can also be erroneously determined due to significant capacitive imbalance in the network. The main reason of adverse effects in compensated networks related to this is the large reactive component of zero sequence current compared to the active. This insufficient natural watt-metric contribution of the grid is considered in [3]; therefore, in order to guarantee selectivity of ground protection, a parallel resistor is connected to the Petersen coil [3], [4].

Connection of a parallel resistor during faults leads to increase of fault current and switching transients; moreover, the ground protection can misoperate due to resistor malfunctioning or delayed operation during intermittent faults. Thus, development of a new protection scheme independent of such operation is important for utilities.

Reference [1] proposes a novel admittance method showing a good performance without the parallel resistor (due to the natural losses of the coil and the network). The main disadvantage is a need of prefault measurements and information about the network for calculation of individual settings for each relay. This method together with the standard approach is related to steady-state approaches that might be unreliable for intermittent faults [5]. At the same time, as it was stated above, methods based on only magnitude of zero sequence current, for instance [6], can be compromised by presence of cables in a network. Signaling methods, for example [7], are of less interest because they require additional equipment.

On the basis of these facts, transient algorithms deserve special attention as an alternative solution. Methods using fast transients and wavelet analysis, as in [8], have several obstacles for practical realization, such as high frequency sampling and sensitivity to noise during signal acquisition. Hence, approaches utilizing slow transients (up to 1 kHz) are of great importance due to suitability for isolated and compensated networks [9], simplicity of signal processing and measurement (frequency sampling is limited to some kHz).

Reference [9] uses earth capacitance estimation for feeder selection and it requires information about the feeding network. Charge-voltage characteristics are used in [10] and they require complex algorithms for pattern recognition. Paper [11] describes investigation of frequency spectrum, however such approach requires better models taking into account frequency dependency of transmission line parameters. Paper [12] demonstrates that polarity of instantaneous zero sequence current in a faulty feeder is differed from healthy ones during the first milliseconds after fault inception. This observation

K. Pandakov is with Department of Electric Power Engineering, Norwegian University of Science and Technology, Trondheim, NO-7491 Norway, e-mail: konstantin.pandakov@ntnu.no

H. Kr. Høidalen is a professor in the same department, e-mail: hans.hoidalen@elkraft.ntnu.no

S. Trætteberg is with company Eidsiva Nett AS, Norway, e-mail: sidsel.traetteberg@eidsivaenergi.no

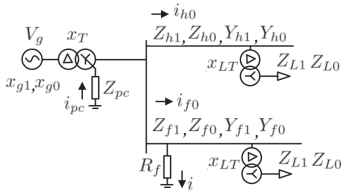

Fig. 1: Two-feeder compensated system with fault for analysis.

gives a basis for development of algorithms based on transients of current phase as it is performed in [13].

Transient methods are subjected to many adverse effects. They can partially be eliminated applying integrating criteria, such as zero sequence power in [14] or energy in [15]. Additionally, reference [16] presents application of zero sequence impedance and [5] – admittance. Nevertheless, transient power and energy algorithms tend to malfunction for asymmetrical systems as it was shown in [17]. Moreover, these methods have not been extensively studied for mixed networks, i.e. having both cables and overhead transmission lines, and various fault conditions (impedance, inception angle, phase in presence of electrostatic imbalance).

To summarize, the proposed paper aims to develop a new transient faulty feeder selection algorithm that is capable of reliable operation without the parallel resistor. Section II outlines the proposed algorithm justified by an initial analytical analysis. Its applicability is tested in the laboratory using simulated and actual fault records. Section III details the complete Monte Carlo simulations in PSCAD/EMTDC. Algorithm performance is also compared with the standard steady-state method described above implemented in a modern feeder relay. Section IV explains the laboratory test setup for these purposes. Section V contains the test results with discussions. Finally, real fault records from a 22 kV distribution network are utilized in subsection V-D in order to examine suitability of the algorithm for the existing measuring facilities.

II. Theoretical background

A simple network depicted in Fig.1 is used to describe physics behind the standard steady-state method and the new transient criterion for faulty feeder selection. It has: utility grid with positive sequence voltage V_g, positive (denoted as 1) and zero sequence (denoted as 0) reactance x_{g1} and x_{g0} correspondingly; a step-down transformer with positive sequence reactance x_T grounded through a Petersen coil with impedance Z_{pc} represented as inductor (L_{pc}) with resistive losses (R_{pc} in parallel); a healthy feeder (denoted as h) having series impedance $Z_{h1,0}$ and shunt admittance $Y_{h1,0}$; a faulty feeder (denoted as f) with similar parameters $Z_{f1,0}$ and $Y_{f1,0}$ and fault resistance R_f at the beginning of the feeder; a load transformer (x_{LT}) and load impedance $Z_{L1,0}$.

In order to detect and locate a single-line-to-the-ground (SLG) fault, zero sequence voltage u_0 measured at the common busbar and zero sequence currents in the feeders (i_{h0} and i_{f0} in Fig.1) are required.

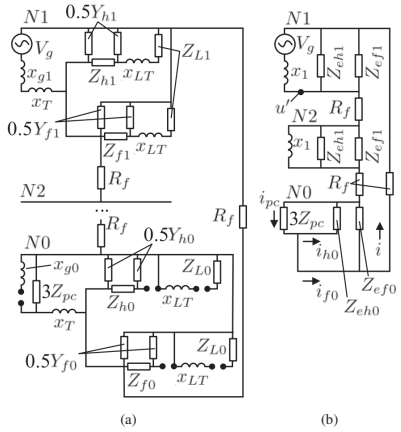

Fig. 2: a) Decomposition of the system into the positive, negative (not shown) and zero sequence network, b) the simplified network with the equivalent impedances.

The faulty system can be represented as series connection of the sequence networks shown in Fig.2a: the negative sequence network is the same as the positive (only source V_g is shorted) and, therefore, omitted. Fig.2b demonstrates its simplified version. Here equivalent healthy feeder zero sequence impedance is $Z_{eh0} \approx 1/Y_{h0}$ because typically $Z_{h0} \ll 1/Y_{h0}$. Y_{h0} consists of shunt conductance G and capacitance C. For simplicity, $Y_{f0} = Y_{h0}$ is assumed and, therefore, $Z_{ef0} = Z_{eh0}$.

Equivalent positive sequence impedance $Z_{eh1} = Z_{ef1} \approx Z_{L1}$ because again $Z_{h1} \ll 1/Y_{h1}$, and $Z_{L1} \gg Z_{h1},\ x_{LT}$. Equivalent reactance x_1 includes both x_{g1} and x_T.

For the system in Fig.2b, the following equations can be written:

$$\begin{cases} i_{h0} = -u_0 G - C\frac{du_0}{dt} \\ i_{f0} = i_{h0} + i = i_{pc} - i_{h0} \\ i_{pc} = i_{L_{pc}} + \frac{u_0}{3R_{pc}} = \frac{1}{3L_{pc}}\int u_0 + \frac{u_0}{3R_{pc}} \\ u_0 = V_g - 3R_f i - \frac{x_1}{\omega}\frac{di}{dt} \\ i = i_{pc} - 2i_{h0} \end{cases} \quad (1)$$

Here i is current in fault resistance and i_{pc} is in the Petersen coil. The fourth equation is derived assuming that potential $u' \approx V_g$ because x_1 is much smaller than equivalent impedance of connected in parallel Z_{eh1}, Z_{ef1}, and the rest part of the scheme with prevailing zero sequence impedances. Additionally, an equivalent impedance of parallel connection of x_1, Z_{eh1}, and Z_{ef1} (the negative sequence network) is roughly equal to x_1 because $x_1 \ll Z_{L1}/2$ (see above). Angular frequency is ω.

System (1) is solved for u_0, i_{h0}, i_{f0} using the numerical method with time step 0.1 ms and the following parameters: $V_g = 12.7$ kV, $x_1 = 17.3\ \Omega$, $\omega = 314.16$ rad/s, $C = 1\ \mu$F,

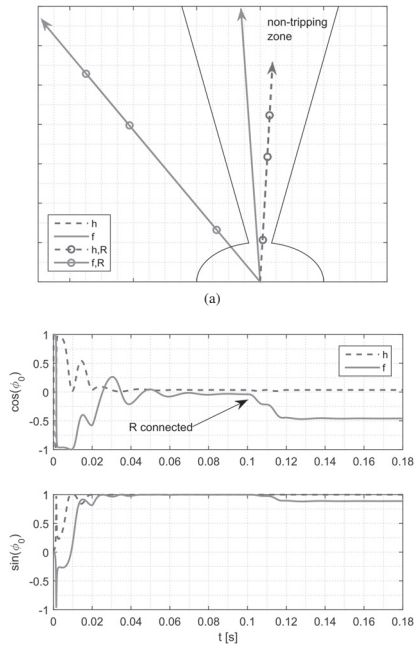

Fig. 3: a) The standard stead-state approach for faulty feeder selection, b) the transient period of time-varying angle ϕ_0 between zero sequence voltage and current.

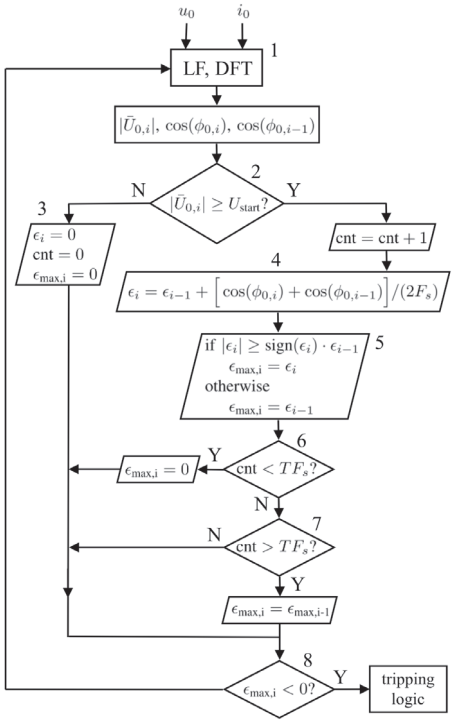

Fig. 4: The block diagram of the algorithm.

$G = 6.3$ μS, $L_{pc} = 1.5$ H, $R_{pc} = 23.6$ kΩ, $R_f = 100$ Ω. All initial conditions are zero.

The obtained instantaneous signals are processed using Discrete Fourier Transform (DFT with sliding window of one period $T = 2\pi/\omega = 20$ ms) [18] in order to derive 50 Hz time-varying phasors $\bar{U}_0$, $\bar{I}_{h0}$, $\bar{I}_{f0}$.

Fig.3a illustrates the standard approach for faulty feeder selection: both steady-state phasors $|\bar{I}_{h0}|e^{j\phi_{h0}}$ and $|\bar{I}_{f0}|e^{j\phi_{f0}}$ (ϕ_0 is angle between $\bar{U}_0$ and $\bar{I}_0$) are in the non-tripping region (insufficient natural watt-metric contribution from the system); in order to shift the faulty phasor into the tripping region, a parallel resistor (denoted as R, chosen 1.8 kΩ) is connected to the Petersen coil (resulting in the dashed arrows). The healthy phasor almost preserves its position after such operation.

This approach has several disadvantages mentioned in the introduction; therefore, we propose to utilize the transient period of $\cos(\phi_0)$ right after fault inception: Fig.3b shows that during the first period, $\cos(\phi_{h0})$ and $\cos(\phi_{f0})$ are explicitly distinguishable: the first one is mainly situated in the positive half plane, the second - in the negative; unlike the sine function that develops in the same direction for both. It allows selection of the faulty feeder before connection of the parallel resistor and avoiding relay misoperation associated with this.

The block diagram of the proposed logic is presented in Fig.4 and it includes:

- Block 1 realizes signal processing with DFT (one period sliding window) and LF (low-pass filter) of u_0 and i_0 in order to extract $|\bar{U}_{0,i}|$, $\phi_{0,i}$, and $\phi_{0,i-1}$ (i denotes current sample, $i-1$ is previous). Sampling frequency $F_s = 2$ kHz is used in this work for laboratory experiments.
- Condition 2 checks fault presence if zero sequence voltage magnitude exceeds threshold U_{start}.
- Block 3 zeros all initial conditions used during calculations (reset function) and the output in order to avoid tripping when fault is absent.
- Block 4 accomplishes calculation of parameter ϵ_i as trapezoidal integration of $\cos(\phi_0)$ samples (with zero initial conditions):

$$\epsilon_i = \epsilon_{i-1} + \Big[\cos(\phi_{0,i}) + \cos(\phi_{0,i-1})\Big]/(2F_s) \qquad (2)$$

Integration improves selectivity handling undesirable angle oscillations and thereby allows application of simple

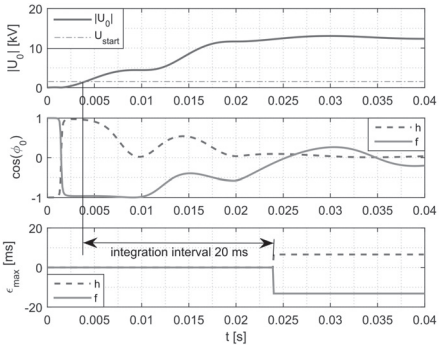

Fig. 5: $|\bar{U}_0|$ with U_{start} and $\cos(\phi_0)$ as the solution of system (1), and corresponding time running ϵ_{max} from the integration applied in the new proposed algorithm.

settings because $\cos(\phi_{f0})$ is predominantly in the negative half plane and vice versa for $\cos(\phi_{h0})$ (see Fig.3b).

- Block 5 looks for maximum of $|\epsilon_i|$ (either for positive or negative ϵ_i) because during integration, $\cos(\phi_{0,i})$ might change sign and shift ϵ_i closer to zero where selection procedure can be problematic (less certainty due to oscillations and measurement errors).
- Condition 6 limits the extreme point search by one period $T = 2\pi/\omega$ where all necessary information is contained (seen from Fig.3b). For this purpose, each new sample $\cos(\phi_{0,i})$ utilized after fault inception is counted by variable 'cnt'. If this condition is true, the output of the algorithm $\epsilon_{\text{max,i}}$ is set to zero and a new sample is taken.
- Condition 7 holds $\epsilon_{\text{max,i}}$ after integration of one period. This condition can be false only when cnt $= TF_s$, then the output of the algorithm is $\epsilon_{\text{max,i}}$ calculated by block 5.
- Block 8 sends logical one to the relay tripping logic if $\epsilon_{\text{max,i}}$ is strictly negative during fault (illustrated below). Then, the loop is repeated with the new samples of voltage and angle.

The relay tripping logic includes outputs from other algorithms; therefore, the performed one is considered as an additional criterion improving selectivity. Further in tests, presence of this logical one (the tripping signal from the algorithm) is examined; its application in the relay tripping logic is out of the scope of this paper.

Fig.5 shows time-varying $|\bar{U}_0|$ (solved system (1)) with $U_{\text{start}} = 1.5$ kV, faulty and healthy $\cos(\phi_0)$ from Fig.3b, and corresponding time running ϵ_{max} for them. It is possible to see the start time of the integration and the end when ϵ_{max} becomes negative for the faulty and positive for the healthy. Hence, inherent operation time of the algorithm is 20 ms (one period).

To sum up, the algorithm in Fig.4 produces the tripping signal only if fault occurs in front of the relay ($\epsilon_{\text{max,i}} < 0$) and it lasts longer than one period (otherwise, $|\bar{U}_{0,i}| < U_{\text{start}}$ and block 3 resets initial condition of the integration and the counter of samples).

Thus, universal settings for all relays at the substation can be applied regardless of feeder parameters and zero sequence current magnitude.

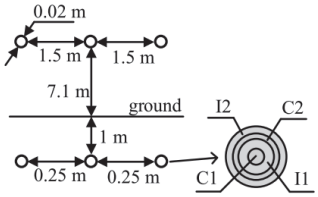

Fig. 6: Geometry of the overhead line and the cable applied in the EMTP model.

TABLE I: Elements of the model and their parameters.

Element	Parameters
Main grid	66 kV, 50 Hz, $x_{g1} = 17.3\ \Omega$
Main transformer	20 MVA, 50 Hz, D/Y(Lags), $x_T = 0.1$ pu, unideal, no load losses, copper losses 0.0045 pu, 66kV/22kV, no saturation, tap 0.97
Overhead line	$G = 3 \cdot 10^{-11}$ S/m, DC resistance 0.43 Ω/km, ideal transposition, $\mu = 1$, sag 0, length 50 km, geometry in Fig.6
Underground cable	$G = 2.6 \cdot 10^{-9}$ S/m, conductor C1: resistivity $4.2 \cdot 10^{-8}$ Ωm, $\mu = 1$, diameter 0.01 m; insulator I1: $\epsilon = 5$, $\mu = 1$, diameter 0.018 m; C2: $2.2 \cdot 10^{-7}$ Ωm, $\mu = 1$, diameter 0.022 m; I2: $\epsilon = 2.3$, $\mu = 1$, diameter 0.026 m; length 10 km, geometry in Fig.6
Load	$Z_{L1} = 500 + 78.5i\ \Omega$
Petersen coil	$Z_{pc} = 4 + 200i\ \Omega$ (overcompensation +3 A), parallel resistor $R = 760\ \Omega$ (according to Norwegian regulations [19])

III. Test case network and Monte Carlo simulations

To study the transient phenomena during ground faults in a systematic way, the network in Fig.1 is realized in PSCAD™/EMTDC™. One of the feeder is an underground cable, the other is an overhead line (see Fig.6). Both are line models with frequency dependent distributed parameters. All model parameters can be found in Table I.

Such topology is used to create extreme conditions for a conventional ground fault protection: the cable has dominant uncompensated capacitive earth-fault current (94.4% from the total) compared to the overhead line. In this network, feeder active earth-fault current only constitutes 2% from capacitive; therefore, application of the parallel resistor is required to ensure reliable protection operation.

Three fault types have been introduced: permanent low-ohmic (250 cases in each feeder, 500 in total) and high impedance fault (250 cases in each feeder, 500 in total), as well as low-ohmic intermittent faults (250 cases in each feeder, 500 in total). In total, 1500 fault scenarios have been simulated. Faults have been simulated consecutively as self-clearing with

on time 0.5 s and relaxation time 0.5 s. Each fault (of each type) has arbitrarily determined parameters in order to examine performance of the algorithm under different conditions.

The following parameters are randomly changed: faulty phase (a, b or c), fault location (beginning and end of the feeder). Additionally, according to [2], it is important to introduce electrostatic asymmetry for the overhead line: an additional capacitor is arbitrarily connected to one phase (a, b or c). Its value is varied between 0 and 5% from the total ground capacitance of the line [20]. At the same time, parameters are randomly changed for:

- Permanent low-ohmic faults: $R_f = 0...500\ \Omega$, inception angle $0...90^0$ (important for transient methods).
- Permanent high impedance faults: $R_f = 0.5...3$ kΩ, inception angle $0...90^0$.
- Low-ohmic intermittent faults: $R_f = 10...100\ \Omega$, number of strikes, their inception times and durations.

Randomness of the parameters in PSCAD is realized using block 'Random Number Generator' with uniform distribution and automatic initial seed. For permanent faults, it produces a new random number every 1 s that is used to determine fault parameters above (phase, location, size and position of the capacitor, fault resistance, inception angle) for each new fault.

For intermittent fault modeling, this block produces a random value (between 0 and 1) every 50 ms during 0.5 s on time – if it is greater than 0.5, a strike is initiated (50% probability). Fault resistance is varied with the same frequency. Other parameters (phase, location, size and position of the capacitor) are only changed every 1 s.

The parallel resistor is connected after 100 ms as fault is detected (exceeding of U_{start}) and disconnected without delay if $|\bar{U}_0| < U_{\text{start}}$. Its malfunctioning is also modeled: it is not connected if the random number generator produces a value (between 0 and 1) less than 0.05 (5% probability).

In the simulations, U_{start} has been chosen equal to 1.5 kV to guarantee detection of far-end high impedance faults ($R_f = 3$ kΩ) at the substation.

IV. Laboratory test setup

Simulated instantaneous u_0 and i_0 (for each feeder in order to check sympathetic tripping) are saved in .csv files and played back with $F_s = 2$ kHz in OMICRON CMC356 using advanced transient play functionality. Analog signals are sent to a modern microprocessor based ground relay (vendor and product cannot be disclosed) and binary tripping signals are registered during the tests, see Fig.7. The relay utilizes the standard steady-state method (see Fig.3a) with the following settings: Operate current – 8 A (cable) and 2.5 A (overhead line), operate voltage – 1.5 kV, forward/reverse angle – 80^0, reset delay time – 0 s, minimum operate time – 40 ms.

The algorithm in Fig.4 is realized by means of a programmable microcontroller STM32F4 Discovery. Since it cannot accept large analog signals and scaling leads to poor precision, u_0 and i_0 are played back with $F_s = 2$ kHz in the OPAL-RT real time simulator in order to compare algorithm performance with the relay for the same signals in equal

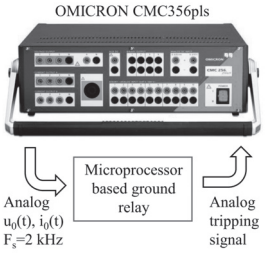

Fig. 7: The laboratory setup for testing of a modern microprocessor based ground relay.

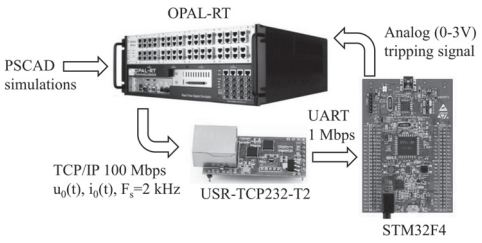

Fig. 8: The laboratory setup for testing of the developed algorithm.

conditions. The signals are sent using TCP/IP protocol trough interface transformer USR-TCP232-T2 to the microcontroller (embedded UART interface). Binary tripping signals are sent back to the simulator as analog voltage signals, see Fig.8. Thus, we verify algorithm applicability in situations close to reality (presence of communication latencies, hidden or neglected factors not appearing in off-line simulations) and estimate operation time.

Current and voltage transformers in the model are assumed ideal.

V. Results and discussions

In this section the following indices are used for the faulty feeder (i_{f0} is used in the test setups):

- successful (S) operation (presence of tripping signal):
  - $S_{\text{R}} = T_{\text{R}}/N_{\text{R}} \cdot 100\%$, where N_{R} is the number of faults when the parallel resistor properly operates, T_{R} is the number of cases among N_{R} when the tripping signal appears.
  - $S_{\text{noR}} = T_{\text{noR}}/N_{\text{noR}} \cdot 100\%$, where N_{noR} is the number of faults when the parallel resistor fails to connect, T_{noR} is the number of cases among N_{noR} when the tripping signal appears.

  Obviously, $N_{\text{R}} + N_{\text{noR}} = 250$, and 100% for both S_{R} and S_{noR} shows that misoperation of the method is not registered during the tests.

TABLE II: Indices for permanent faults in the cable.

Index	Low-ohmic (0…500 Ω) faults		High impedance (0.5…3 kΩ) faults	
	Ground relay	Algorithm in Fig.4	Ground relay	Algorithm in Fig.4
S_{R}	100	100	100	100
S_{noR}	0	100	0	100
U_{noR}	100	–	100	–
t_{op}	160.8	44.1	169.5	44.1
t_{st}	2.4	6.4	4.4	6.9

- unsuccessful (U) operation (no tripping signal):
  - $U_{\mathrm{noR}} = M_{\mathrm{noR}}/(250 - T_{\mathrm{R}} - T_{\mathrm{noR}}) \cdot 100\%$, where M_{noR} is number of missed tripping signals when the parallel resistor fails to connect (over the total number of missed tripping signals).

  A value less than 100% indicates that there is an another reason of protection misoperation different from failure of the parallel resistor. If $T_{\mathrm{R}} + T_{\mathrm{noR}} = 250$ (no missed tripping signals), then U_{noR} cannot be computed (denoted as '–' in the tables below).
- t_{op} - mean operation time in ms and t_{st} is its standard deviation in ms.

A. Permanent cable faults

Table II shows results for permanent faults in the cable. The row with S_{noR} indicates that the ground relay cannot recognize faults and U_{noR} shows that the reason is the parallel resistor malfunction. Thus, dependability of the relay depends on resistor operation due to presence of high capacitive current from the cable. At the same time, the new proposed algorithm demonstrates good performance in all cases (no missed tripping signals). Smaller than 100 ms operation time (44.1 ms includes 20 ms operation time of the algorithm and communication latencies) means that it makes decision before operation of the parallel resistor.

In these tests, the signal from the healthy feeder (the overhead line) i_{h0} sent to the ground relay does not lead to tripping signals. In other words, sympathetic tripping does not occur. However, it happens when the new algorithm is tested during a specific fault scenario: $R_f > 2.5$ kΩ and significant electrostatic imbalance (∼5%) in the phase adjacent to the faulty. In such cases, the algorithm tends to disconnect, together with the cable, the healthy overhead line. Fig.9 shows $\cos(\phi_0)$ in such fault scenario and clearly demonstrates predominantly negative values for both feeders in the transient period (in contrast to Fig.3b).

Though security of the ground relay is guaranteed in such case by minimum operating current (2.5 A for the overhead line), sympathetic tripping arises for more sensitive settings (for example, 0.5 A if the system operator requires detection of 10 kΩ faults). This point has been verified through separated tests not demonstrated in this paper.

B. Permanent overhead line faults

Table III shows results for permanent faults in the overhead line. For low-ohmic faults, we can observe similar results as in the previous case. For high impedance faults, the ground relay produces tripping signal even when the parallel resistor fails ($S_{\mathrm{noR}} = 100\%$) because uncompensated capacitive earth-fault current in the overhead line much less than in the cable. Performance of the algorithm is similar to the previous case; furthermore, sympathetic tripping does not occur for any of the test cases.

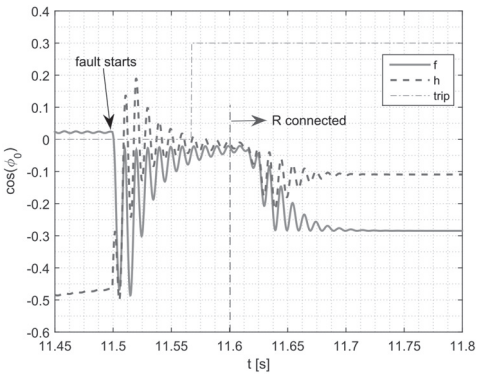

Fig. 9: The transient period of $\cos(\phi_0)$ and the trip signal in the healthy feeder during high impedance fault in the cable in the highly asymmetrical system.

TABLE III: Indices for permanent faults in the overhead line.

Index	Low-ohmic (0…500 Ω) faults		High impedance (0.5…3 kΩ) faults	
	Ground relay	Algorithm in Fig.4	Ground relay	Algorithm in Fig.4
S_{R}	100	100	100	100
S_{noR}	0	100	100	100
U_{noR}	100	–	–	–
t_{op}	164.7	44.2	44.7	45.2
t_{st}	3.8	6.7	1.4	6.9

C. Intermittent low-ohmic faults

Table IV shows results for low-ohmic intermittent faults. The row with S_{R} indicates that the ground relay cannot guarantee reliable operation even if the parallel resistor properly works (indices are less than 100%). It happens because of unstable faulty signals and inherent operation times of the relay algorithm. For faults in the cable, the relay can initiate tripping in a few cases when the parallel resistor misoperates (non-zero S_{noR}).

In Table IV, index U_{noR} is less than 100% in all cases showing that the reason of relay misoperation is not only parallel resistor failure. Indeed, Fig.10 shows zero sequence magnitude and $\cos(\phi_0)$ for such case. It can be observed that, after connection of the resistor, fault disappears (from relay point of view because voltage magnitude is below the threshold until the second strike occurs); if this time span is less than relay operation time, it cannot detect the fault. In

TABLE IV: Indices for low-ohmic (10...100 Ω) intermittent faults.

Index	Fault in cable		Fault in overhead line	
	Ground relay	Algorithm in Fig.4	Ground relay	Algorithm in Fig.4
S_{R}	83.7	100	86.4	100
S_{noR}	4.3	100	0	100
U_{noR}	37.3	–	32	–
t_{op}	212.8	44.3	211.4	44.3
t_{st}	92.7	6.9	93.2	6.37

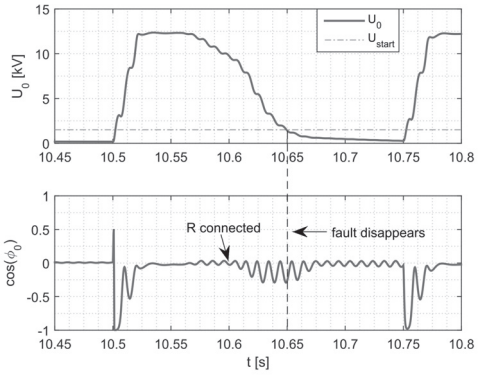

Fig. 10: Zero sequence voltage magnitude and angle during restriking fault on the feeder.

this test set, the new proposed algorithm does not miss any tripping signal.

It is necessary to mention that the presented indices for the ground relay can be improved if the resistor is disconnected with a sufficient time delay or it is constantly connected to the Petersen coil (such operation is sometimes used by utility companies, however not widespread).

D. Real fault records

The system operator of an actual 22 kV distribution network in Norway (total capacitive current is about 80 A) provided oscillograms of 21 ground faults that occurred in the autumn 2016 - winter 2017. Ground relays in this network are capable of recording only if they initiate start (ready to trip) or tripping signal. The recordings consists of measured zero sequence current and phase voltages that are used to calculate zero sequence voltage. The sampling frequency is 600 Hz. Fig.11 demonstrates the registered magnitudes of zero sequence voltages (the real settings of U_{start} is 1.5 kV for the primary side), extracted $\cos(\phi_0)$ and tripping signals obtained using the laboratory setup in Fig.8 for 9 the most interesting faults (repetitive cases are not included):

- Row 1 (depicted time range is 0–2 s): low-ohmic temporary (self-extinguishing) fault.

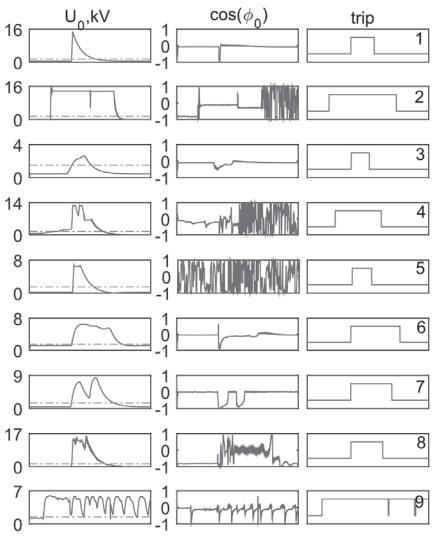

Fig. 11: Zero sequence voltage magnitude (left, the dash-dot horizontal line is U_{start}) and angle (middle) for 9 fault records from an actual distribution grid, and response of the new proposed algorithm (right) as the tripping signal.

- Row 2 (0–4 s): low-ohmic fault cleared by the breaker. It makes extracted $\cos(\phi_0)$ unstable due to uncertainties because of feeder disconnection and, consequently, current disappearance.
- Row 3 (0–2 s): temporary high impedance (∼5 kΩ) fault (the voltage magnitude is close to the threshold).
- Row 4 (0–2 s): cleared low-ohmic restriking fault (the voltage magnitude has 2 spikes).
- Row 5 (0–2 s): cleared medium-ohmic (∼1 kΩ) fault with prefault current close to zero (unstable $\cos(\phi_0)$).
- Row 6 (0–2 s): temporary medium-ohmic fault.
- Row 7 (0–2 s): temporary restriking medium-ohmic fault (2 spikes).
- Row 8 (0–2 s): self-extinguishing short-time low-ohmic intermittent fault.
- Row 9 (0–6 s): cleared medium-ohmic intermittent fault.

We can observe that precision of the existing measuring facilities is sufficient for algorithm implementation and $\cos(\phi_0)$ can be extracted even with the lower sampling frequency. Regardless the fault conditions, it initiates the tripping signals (especially in row 5); however, since it is quite fast (∼40 ms), it requires inclusion of operation time delay in the tripping logic (Fig.4) in order to avoid unnecessary operation during self-extinguishing faults.

VI. Conclusion

The paper proposes a new faulty feeder selection algorithm. Though it utilizes zero sequence voltage and current angle as the standard approach, the work introduces novelty distinguishing it from the previously developed methods: 1) the time-varying current angle is utilized (transient approach); 2) the first transient period after fault onset is considered (it contains the most indicative information); 3) integration criterion has been developed to improve selectivity.

The developed algorithm has demonstrated good selectivity compared to the existing method in laboratory tests for permanent and transient faults with various parameters. Its performance is not affected by number of feeders; therefore, it can equally be applied in more complex systems. The main advantages are simplicity in signal processing, no need of additional equipment (application for the real fault records shows its usability), universality of algorithm settings for all relays in the network, and reset delay time settings that can be challenging are not required; moreover, the decision can be made in a fast manner without involvement of the parallel resistor. Nevertheless, it is not an universal solution because of a few identified sympathetic tripping cases; therefore, it can be used as an additional criterion improving selectivity together with more complex tripping logic typically involving pickup current to guarantee security. Finally, algorithm application is limited by high impedance faults when zero sequence voltage does not exceed U_{start} and the algorithm is not initialized.

The future work requires deeper study of algorithm performance for real systems and fault records, finding limitations and improvements.

Acknowledgment

The authors would like to thank the system operator of Norwegian distribution network 'Eidsiva Nett' for provision of the fault records.

References

[1] A.Wahlroos, J. Altonen, "Performance of novel neutral admittance criterion in MV-feeder earth-fault protection", *20th International Conference and Exhibition on Electricity Distribution – Part 1 (CIRED)*, 2009, pp. 1 – 8.

[2] H. Ji, Y. Yang, H. Lian, S. Cong, "Effect on Earth Fault Detection Based on Energy Function Caused by Imbalance of Three-Phase Earth Capacitance in Resonant Grounded System", *International Conference on Power System Technology*, 2006, pp. 1 – 5.

[3] I. G. Kulis, A. Marusic, S. Zutobradic, "Insufficiency of watt-metric protection in resonant grounded networks", *Eighth IEE International Conference on Developments in Power System Protection (DPSP), volume 2*, 2014, pp. 486 – 489.

[4] T. Henriksen, A. Petterteig, "Detection of Earth Fault in a Medium Voltage Distribution Network", *International Conference on Power System Transients (IPST)*, 2007.

[5] A. Wahlroos, J. Altonen, "Application of novel multi-frequency neutral admittance method into earth-fault protection in compensated MV-networks", *12th IET International Conference on Developments in Power System Protection (DPSP)*, 2014, pp. 1 – 6.

[6] X. Lin, I. Kursan, J. Sun, Z. Li, R. Zheng, Z. Bo, J. Xu, Z. Wei, "Fault section identification based on per-unit zero sequence current", *12th IET International Conference on Developments in Power System Protection (DPSP)*, 2014, pp. 1 – 6.

[7] B. Yong, C. Wei, L. Jiansheng, D. Lei, L. Qingdong, Y. Ning, "Single phase to earth fault location method in distribution network based on signal injection principle", *4th International Conference on Electric Utility Deregulation and Restructuring and Power Technologies (DRPT)*, 2011, pp. 204 – 208.

[8] X. Dong, S. Shi. (2008). Identifying Single-Phase-to-Ground Fault Feeder in Neutral Noneffectively Grounded Distribution System Using Wavelet Transform. *IEEE Transactions on Power Delivery. 23(4)*, pp. 1829 – 1837.

[9] M. F. Abdel-Fattah, M. Lehtonen. (2012). Transient algorithm based on earth capacitance estimation for earth-fault detection in medium-voltage networks. *IET Generation, Transmission & Distribution. 6(2)*, pp. 161 – 166.

[10] T. Henriksen. (2011). Faulty feeder identification in high impedance grounded network using charge-voltage relationship. *Electric Power Systems Research Journal. 81(9)*, pp. 1832 – 1839.

[11] S. Zhang, H. Gao, M. Hou, Y. Sun, Z. Shao, J. Li, "Frequency spectrum characteristic analysis of single-phase ground fault in a Petersen-coil grounded system", *5th International Conference on Electric Utility Deregulation and Restructuring and Power Technologies (DRPT)*, 2015, pp. 369 – 374.

[12] W. Y. Huang, R. Kaczmarek. (2007). SLG Fault Detection in Presence of Strong Capacitive Currents in Compensated Networks. *IEEE Transactions on Power Delivery. 22(4)*, pp. 2132 – 2135.

[13] P. Balcerek, M. Fulczyk, J. Izykowski, E. Rosolowski, P. Pierz, "Centralized substation level protection for determination of faulty feeder in distribution network", *IEEE Power and Energy Society General Meeting*, 2012, pp. 1 – 6.

[14] L. Jian, H. Jianjun, Z. Hongwei, Y. Hua, Z. Jie, L. Lei, W. Rui, "Fault Line Selection Based on Zero Sequence Power Direction of Transient Fundamental Frequency in MV Network Grounded with Arc Extinguishing Coil", *International Conference on Power System Technology*, 2006, pp. 1 – 4.

[15] M. Loos, S. Werben, M. Kereit, J. C. Maun, "Fault direction method in compensated network using the zero sequence active energy signal", *IEEE EUROCON*, 2013, pp. 717 – 723.

[16] M. F. Abdel-Fattah, M. Lehtonen, "A transient fault detection technique with varying fault detection window of earth modes in unearthed MV systems", *Power Quality and Supply Reliability Conference (PQ)*, 2008, pp. 181 – 186.

[17] K. Pandakov, H. K. Høidalen, J. I. Marvik, "Misoperation analysis of steady-state and transient methods on earth fault locating in compensated distribution networks", *Sustainable Energy, Grids and Networks*. Accessed on: December 15, 2017, DOI: 10.1016/j.segan.2017.12.001, [Online].

[18] M. M. Saha, J. Izykowski, E. Rosolowski, "Fault Location on Power Networks", Springer London Dordrecht Heidelberg New York, 2010.

[19] *Stasjonsanlegg - Retningslinjer for spolejordet distribusjonsnett*, REN-blad NR 7505 VER 1.0, 2015.

[20] Z. Chen, H. Wang, F. Chen, "Research on Damping Ratio and Off-Resonant Degree of Compensation Network", *Asia-Pacific Power and Energy Engineering Conference (APPEEC)*, 2011, pp. 1 – 4.